To the Graduate Council:

I am submitting herewith a dissertation written by Donald L. Erdman entitled "The Mechanical Response of Cross-Ply Ceramic Matrix Composites." I have examined the final copy of this dissertation for form and content and recommend that it be accepted in partial fulfillment of the requirements for the degree of Doctor of Philosophy, with a major in Engineering Science.

Y. J. Weitsman

Y. J. Weitsman, Major Professor

We have read this dissertation and recommend its acceptance:

W. J. Swanson

Madhu S. Madhukar

John D. Landes

Marion G. Hansen

Accepted for the Council:

C W Minkel

Associate Vice Chancellor and Dean of The Graduate School

The Mechanical Response of Cross-Ply Ceramic Matrix Composites

A Dissertation

Presented for the

Doctor of Philosophy

Degree

The University of Tennessee, Knoxville

Donald Erdman

December, 1995

DEDICATION

This dissertation is dedicated to my wife and best friend Renee who unselfishly postponed her own education while I was completing mine.

Sometimes it's funny the way thing turn out, isn't it ?

ACKNOWLEDGMENTS

I want to express my gratitude to Dr. Weitsman for all of his help, advice, and extraordinary patience during the last four years. Dr. Weitsman's technical expertise and mentorship provided me with opportunities and experiences for which I am grateful.

I also want to thank my comittee members : Marion Hansen, John Landes, Madhu Madhukar, and Frank Swinson for all the advice, constructive criticism, and support they provided.

I want to acknowledge all the people at Oak Ridge National Laboratories for the support they provided through the use of their laboratories, fellowship funding, technical advice and friendship. In particular I need to thank Jim Corum and Rick Lowden for the support they provided through student fellowships while I completed this work. Additionally I would like to express my gratitude to Rick Battiste and Don Godwin for sharing their laboratory and wealth of experiences, making the mechanical testing possible. Finally I need to thank Ray Boeman, Dave Warren and all the people in the Composite Materials and Structures group for realizing my potential as a post-graduate research assistant. Their support and use of facilities was invaluable. I am very fortunate to be associated with one of the finest scientific organizations imaginable.

Finally, I have to thank my wife Renee, for all the support and encouragement she provided, especially during those times when it seemed as though my education would never come to this conclusion. The completion of this dissertation would not have been possible without her companionship and selfless dedication.

ABSTRACT

This work concerns the development of an analytic model to predict the stress-strain and damage behavior of ceramic matrix cross-ply laminates. The validity of the model is to be assessed by experimental observations. Major features of the analysis include : prediction of transverse matrix cracking in the 90° plies at each increment of applied stress utilizing a fracture criterion to determine the increase in crack density, prediction of interfacial slip zones between the 0° and 90° ply groups, and a bilinear constitutive formulation to account for the non-linear behavior of the 0° ply groups within the cross-ply composite.

This work presents a novel approach to analyze cross-ply ceramic composites in a rational manner, while most other analyses of ceramic composites are confined to the simpler case of unidirectional reinforcement. The analysis employs basic concepts of fracture mechanics to establish criteria for the complex process of multiple crack formation within the laminate. The incorperation of the non-linearity associated with the 0° plies along with interfacial slippage between the 0° and 90° ply groups in the damage prediction, leads to the stress-strain response of the cross-ply lay-up. In this manner, the current approach enables the prediction of both damage states and the stress-strain behavior of the laminate.

A comprehensive mechanical testing program which complements the analytical portion of this work, provides essential verification of stress-strain data for the unidirectional and cross-ply laminates, along with quantitative information concerning damage initiation, as well as interlaminar shear strength.

TABLE OF CONTENTS

LIST OF FIGURES

CHAPTER 1
INTRODUCTION

Ceramic Matrix Composite Description

Ceramic composite materials are potential candidates for structural components in a variety of applications, due to their ability to retain their properties in high temperature and aggressive environments as compared to most metals as well as polymeric and metal matrix composites. Additionally, ceramic composites demonstrate enhanced toughness and ductility, when compared to monolithic ceramics, due to the energy absorbing mechanisms that are associated with the damage evolution preceding the failure of the composite.

In polymeric composite material systems, desirable properties such as stiffness and strength are obtained by imbedding stiff, high strength fibers into relatively soft and weak matrix material. Generally the matrix provides a means to bond the fibers to each other and contributes little to the stiffness and strength of the composite. For example, in typical polymeric composites such as graphite/epoxy, the stiffness parallel to the fibers is approximately twenty times greater than that in the transverse direction. Similarly, the ratio of longitudinal to transverse strengths can be on the order of 30-40:1. It should also be noted, that since the strain to failure in polymeric matrix materials generally exceeds the failure strain of the fibers, and polymeric composites are strongly bonded at the fiber matrix interface, fiber fracture may precede matrix cracking. An example of this behavior is depicted in Figure 1.1(a), for unidirectional reinforcement with the loading direction parallel to the fibers. In this case, isolated fiber breaks occur without debond between the matrix and neighboring fibers.

In contrast, the stiffnesses of the fibers and matrix in ceramic matrix composites are approximately equal. Consequently, the ratio of longitudinal to transverse stiffness for a typical ceramic matrix material system is 1-2:1. However, the fibers are much more ductile than the matrix, and their primary role is to enhance the ductility and energy absorbing capacity of the inherently brittle ceramic matrix. Since the strain to failure of the fibers in a ceramic matrix composite largely exceeds that of the matrix material, failure of the matrix material precedes that of the fibers. This is depicted in Figure 1.1(b), where matrix cracks are spanned by intact fibers.

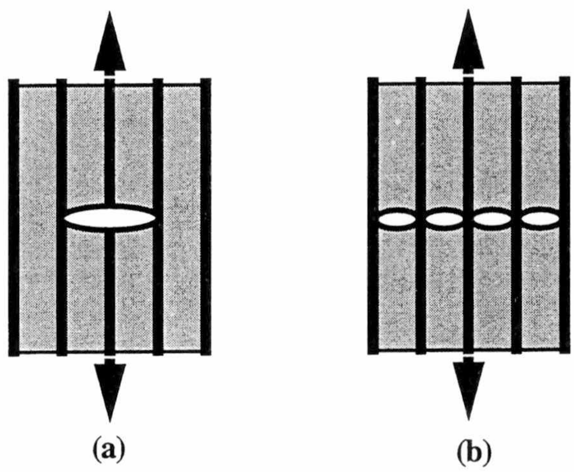

Figure 1.1. Comparison of (a) Ductile and (b) Brittle Matrix Composite Material Systems

Obviously, the aforementioned differences concerning strength and stiffness between polymeric and ceramic matrix composites can be readily extended to laminate lay-ups other than the unidirectional cases shown in Figure 1.1. Consider for example a cross-ply laminate with transverse ply groups (90° plies) sandwiched between longitudinal ply groups (0° plies) as shown in Figure 1.2. Under applied load, as transverse cracking of 90° plies takes place in both the ceramic and polymeric composites, the overall stiffness and strength of the laminate will decrease. However, in view of the nearly equal stiffness values for the 0° and 90° plies within the ceramic matrix laminate, it is apparent that cracks in the 90° plies will cause a significant reduction in the composite stiffness and strength. This stands in contrast with the case of a polymeric matrix cross-ply composite, where fracture of transverse plies will have only minor effects on the strength and stiffness of the laminate.

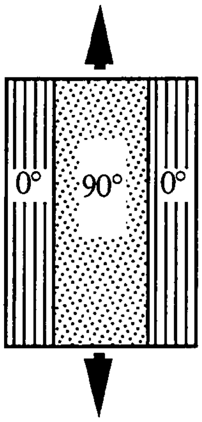

Figure 1.2. Typical Cross-Ply Laminate

In view of the foregoing differences between polymeric and ceramic matrix composites, it is evident that a clear understanding of the behavior of a particular material system is essential before initiating any type of predictive analysis. Hence, to model ceramic matrix material systems it is necessary to be aware of their characteristic features, instead of resorting to familiar approaches used in polymeric composites.

CHAPTER 2

LITERATURE REVIEW / PROBLEM STATEMENT

2.1 Overview

After reviewing the investigations available in literature it appears that, with the exception of unidirectional configurations, little work has been done with ceramic composites to model the stress-strain response of stacking sequences usually encountered in the study of continuous fiber composite laminates such as cross-ply, angle-ply, and quasi-isotropic lay-ups. Although a limited number of models exist that consider ceramic cross-ply laminates, none seem to correlate the experimentally observable damage with the prediction of stress-strain response in a comprehensive manner.

2.2 Publications Concerned with Unidirectional Ceramic Matrix Composites

Although the current work focuses on cross-ply ceramic matrix laminates, it incorporates information from earlier experimental and analytical studies of unidirectional laminates, since they provide some essential insights into the general mechanical behavior and damage mechanisms associated with ceramic composites. It turns out that a thorough understanding of unidirectional stress-strain behavior is most helpful in modeling the response of cross-ply ceramic matrix composites. An up-to-date compilation of publications related to the modeling and testing of unidirectional ceramic composites is provided by the list of references [1-32]. This listing is categorized in the following manner : references [1-13] consist of publications that deal primarily with modeling, references [14-20] include modeling supported by experimental work, while references [21-29] are mainly concerned with experimental material characterization. Selected key articles from these three groups concerning unidirectional ceramic composites will be discussed in more detail below. Additionally, references [30-32] are review articles dealing primarily with unidirectional ceramic composites.

Some of the earliest efforts to characterize the response of ceramic composites were made during the early to mid 1970's. One of the first articles concerning the behavior of brittle-matrix composites, where the fibers are more ductile than the matrix, was published in 1971 by Aveston, Kelly and Cooper [1]. Although this work was not specifically aimed at the study of modern advanced ceramic laminates (the authors consider fiber reinforced cement, plaster and glass), the analysis (referred to as the "ACK model") addresses the phenomenon of matrix failure preceding fiber fracture. This work established the need to distinguish between brittle and ductile matrices when modeling composite materials, and suggests a clear-cut distinction between ceramic and polymeric matrix composites.

In 1986, Schioler and Stiglich [32] published a literature review discussing the "current state of ceramic composites". This survey reviewed the various fiber/matrix systems available at that time, along with manufacturing techniques and material properties. The authors also pointed out that although the development of new materials systems was advancing, there was a significant lack of experimental data and appropriate modeling. In the same year, Budiankski, Hutchinson and Evans [4] published a key paper addressing the analysis of unidirectional ceramic composites. In this article which, as pointed out by the authors, was directly motivated by the earlier work of Aveston, Kelly and Cooper, they developed a shear-lag type model to explain the mechanism of load transfer from the cracked matrix material to surrounding intact fibers. The authors also addressed slippage at the fiber-matrix interface, and established an energy criterion to predict the critical stress levels for the inception of the first matrix crack. However, they did not extend their analysis to predict the evolution of subsequent cracks, and therefore did not attempt to predict crack densities or global stress-strain response. A large number of unidirectional shear-lag models followed the work of Budiankski *et. al.*, selected notable works are given in references [5-7,9-17]. Many of these papers extended the shear-lag model by incorporating detailed analysis of specific damage mechanisms. For instance, in references [5-7,9,10] the authors focus on the details of matrix cracks spanned by intact fibers, while in [13], the authors studied the relations between thermal expansion in the presence of interfacial slippage and matrix cracking. Another example of a very specific model, although not a shear-lag analysis, is presented in [8]. In this work, the details of the stress-field ahead of a crack as it grows between laminate plies is studied. In contrast, the shear-lag models in references [12,14-17] are modified versions of the basic model proposed by Budianski *et. al.* in [4] (reference [15] incorporated the model of [4] *ad hoc*). It seems that the main purpose of these works was to correlate the results of mechanical testing, such as the initiation of matrix cracks and stiffness reductions, with existing models, rather than extend the shear-lag analysis. References [12,16-17] consider matrix cracking and employ an energy criterion along with interfacial slippage, while the authors in [14] utilize a model that employs statistical fiber fracture analysis in conjunction with matrix cracking.

It should be noted that many of these models focus attention on specific failure mechanisms, which is of interest to material scientists, but they fail to provide overall stress-strain predictions to correlate with experimental results. In contrast, a detailed model that aims at predicting the observed "global" response of unidirectional ceramic composites was developed by Weitsman and Zhu in references [18-20]. This model utilized the energy criterion of Budianski, Hutchinson, and Evans [4] to predict the progression of matrix cracking along with interfacial slip between the fiber and matrix. Additionally, this work incorporated statistical aspects of fiber fragmentation and failure.

As mentioned previously, a listing of investigations that address the experimental characterization of unidirectional ceramic composites are given in [14-29]. Many of these works prove to be valuable sources for experimental data, such as material properties [15-17,20-22,29], stress-strain response [16-21,24,28,29], and observations of associated damage mechanisms [15-17,20-22,25-29]. Additionally some of these works have documented experimental techniques utilized by the authors to study the mechanical characteristics of the various ceramic composites under investigation [15-17,21,23,29]. The details of the specific contributions of these works are discussed below.

Some of the earliest experimental publications concerned with ceramic matrix composites were conducted by Prewo *et. al.*, starting in 1980 [24-28]. These works considered the basic mechanical response of various glass matrix ceramic laminates (mainly unidirectional lay-ups). These investigations revealed the presence of several damage mechanisms, namely, matrix cracking, fiber breakage, and fiber-matrix interfacial debonding and slip. Most of these observations were made during post-test examination of the fracture surfaces of the specimens. Additionally, these early works reported the non-linear stress-strain response associated with ceramic matrix laminates. Although detailed observations of damage were reported, little effort was made to associate the observed damage with stress-strain behavior.

References [15,21] are NASA technical memoranda by Bhatt *et. al.* which studied the experimental characteristics of SiC/RBSN (SCS-6, 140 micron silicon carbide fiber / reaction bonded silicon nitride). These works demonstrated new techniques to observe damage mechanisms employing *in situ* x-radiography during incremental loading, in real-time. Although it was shown that x-rays may provide accurate information about matrix crack initiation and progression, along with some details of the crack shape in the specimen interior, the technique lacks resolution (magnification), especially in the cases of smaller diameter fibers, such as Nicalon, which are typically 15 microns in diameter. Additionally, since these experiments dealt with large SCS-6 fibers, the authors were also able to achieve satisfactory observations with conventional microscopes. Detailed photographs of interfacial slip and fiber pullout, often difficult to obtain with other material systems were reported.

The work of Daniel *et. al.* [16,17] employed real-time observations of damage in unidirectional ceramic matrix composites by monitoring the specimen surface with an optical microscope during loading. Using magnifications of approximately 600-800 X, they were able to observe details of matrix crack initiation and progression between intact fibers (albeit on the specimen surface), along with fiber breakage and fiber crack opening displacements. Additionally, several micrographs in [17] suggest that it may be possible to identify interfacial failure zones between the fiber and matrix, although it would be difficult to assess the slip zone length from those photographs. It should also be noted that this investigation employed a manually operated loading device resulting in variable rates of displacement, hence affecting the reproducibility of stress-strain curves.

A publication by Davidson, Rousseau and Campbell in reference [22] successfully employed *in situ* mechanical testing of unidirectional ceramic matrix composites within a scanning electron microscope (SEM) to achieve real-time observations of damage progression during quasi-static and cyclic loading. Using this test set-up, they were able to record crack densities and measure crack opening displacements. It should be noted that this technique has several limitations. One of the greatest difficulties is due to the confined space available within the SEM, requiring very small specimens that must be loaded with devices built specifically to fit within the SEM enclosure. Additionally, use of the SEM requires metallic coating of the surface to be viewed, hence newly formed fracture surfaces that are not coated may not reveal the detailed images that are anticipated from the SEM.

To support the work conducted by Weitsman and Zhu in [18-20] the author of this dissertation constructed a traveling microscope system to be used in conjunction with standard load frames that can accommodate fixtures that minimize misalignment and bending, such as that discussed in [23]. This system, which includes a controller and digital function generator, combines the advantages of the aforementioned systems [16,17,23] (i.e. real time damage observation under load), along with carefully controlled loading of the specimen. This set-up results in reproducible stress-strain curves in addition to crack initiation and progression measurements. Additionally, in view of the lesser restrictions on specimen size with this system, there is more flexibility in making strain measurements.

2.3 Publications Concerned with Cross-Ply Ceramic Matrix Composites

The list of publications concerned with modeling and experimental characterization of cross-ply laminates is given in references [36-45]. References [36,37] are concerned exclusively with the modeling of cross-ply ceramic composites, while the articles in [38-42] contain analysis supported by mechanical testing. Articles [43-45] represent purely experimental investigations. As mentioned previously, it is clear that in the case of ceramic composites there is an obvious lack of models addressing the behavior of cross-ply laminates. Additionally, many of the models that do exist can be described as "preliminary" since they often omit characteristic damage mechanisms associated with ceramic cross-ply laminates, resulting in poor predictions of laminate stress-strain response. Most of the existing models are of a shear-lag type analysis [38-42], where a simplified analysis is employed to account for the transfer of stress is from the cracked 90° plies back to the intact 0° plies through shearing stress at the 0°/90° ply interface (For further details of this type of analysis, the reader is referred to Chapters 4-6 of this dissertation).

Before discussing the publications concerned with modeling of ceramic composites, it should be noted that several shear-lag analyses for polymeric composites are given in [33-35]. These articles are listed herein since their models are often utilized for the more complicated circumstance of ceramic cross-ply laminates. The authors in [33,34] developed predictions for matrix cracking utilizing an energy criterion along with laminate stiffness reduction, while in [35] the same type of analysis was extended to include "global" stress-strain response. Additionally, all three works reported reasonable agreement between predicted and experimental data for polymeric composites.

Turning attention to the articles related to shear-lag analysis of ceramic cross-ply laminates, Daniel in [38] presents a model to determine the stress distributions within the laminate and overall specimen stiffness for a fixed crack spacing. Since no attempt is made to predict the formation of new transverse crack, this analysis requires the introduction of experimental values for crack densities to predict the stress-strain response of the laminate. Additionally, neither slippage between plies, or the non-linear behavior of the 0° ply groups is addressed. Another attempt is presented in a series of papers authored by Chou *et. al.* [39-41]. They consider a somewhat more comprehensive shear-lag model that includes the effects of interfacial slip between the fibers and matrix in the 0° plies along with matrix cracking in both ply groups, but omits slip between the 0° an 90° ply groups. Due to some essential shortcomings this model also requires the introduction of experimentally determined crack densities and presumed slip zone lengths as *ad-hoc* quantities to predict the stress-strain behavior of the laminate. Their comparisons between the predicted stress-strain response and experimental results significantly overestimates the laminate stiffness. One source for the lack of correlation can be attributed to their omission of the non-linear behavior of the 0° ply groups.

In references [36,37], Xia *et. al.* consider distinct damage mechanisms in ceramic cross-ply laminates. In article [36] they consider the growth of transverse cracks in the 90° ply groups, while the second work [37] is concerned with the progression of the foregoing cracks into the 0° plies after reaching saturation density in the 90° ply groups. The resulting stress-strain predictions from these models have the typical features associated with the response of cross-ply laminates. However, the results are not compared with experimental data, which makes it difficult to assess the validity of these models. It should be noted that although these works include slip at the fiber-matrix interface in the 0° plies, they assume a perfectly bonded 0°/90° interface.

In summary, although the existing models for cross-ply ceramic laminates include some specific details of material response, they neglect to address the damage mechanisms associated with this lay-up in a thorough manner. Specifically, many of the models do not account for the progression of matrix cracking by means of a fracture criterion, and they overlook the interfacial slip at the 0°/90° interface, and in many cases fail to address the non-linearity of 0° ply groups. Additionally, few comparisons are made between the aforementioned analytical schemes and experimental data, making it difficult to evaluate the results. Since the main purpose of any type of model should be to predict the overall response of the material system, it is necessary to correlate its predictions with experimental results and explore the effects of various parameters on the predictions. Consequently, many of the above models are incomplete.

The publications concerned with the mechanical testing of cross-ply laminates are given in references [38-45]. As an overview, references [38-41,44] proved to be good sources for material properties, while [38-42,44,45] reported reasonable stress-strain data, and [38,39,42,44,45] included detailed observations of damage mechanisms. These investigations will be discussed in further detail below.

One of the earliest experimental investigations concerning modern ceramic laminates was conducted by Brennan and Prewo in [43]. They reported the flexural response of several glass-ceramics consisting of SiC fiber and lithium aluminosilicate (LAS) matrix material. It should be noted that their main goal was to develop a high temperature toughened material system, therefore these mechanical tests focused on comparative toughness measurements employing notched bend specimens along with charpy impact tests, while axial tensile tests were not conducted. In addition to toughness measurements, they presented detailed SEM photographs of fracture surfaces, and examples of fiber pullout.

Daniel in reference [38] studied the tensile response of SiC/CAS (15 micron silicon carbide fiber/calcium aluminosilicate), cross-ply laminates along with detailed observations damage progression employing *in situ* microscopy. The stress levels for the initiation and accumulation of transverse cracking in the 0° and 90° plies were recorded along with details of the micro-cracking sequence between fibers in the 90° plies that precedes fully developed transverse cracks. Additionally, observations were made of the tendency of transverse cracks to branch, forming a "delta" shape as they grew toward the 0°/90° interface.

Chou *et. al.* in [39-41] conducted tensile tests for SiC/CAS cross-ply specimens, and employed a replication technique to transfer surface features (transverse cracks in both the 0° and 90° plies) of the specimen edge at various applied stress levels. From the replicas, sequences of photo-micrographs were made to show the progression of matrix cracking with applied stress. To study the laminate response the authors conducted two types of tests. The first consisted of continuous loading up to failure, while monitoring strain to obtain the stress-strain response. In the second type of test, the specimen was loaded and unloaded in a cyclic manner, each time to a higher stress level, and the specimen stiffness was determined from the slopes of the stress-strain record during unloading.

Another notable investigation of SiC/CAS and SiC/LAS ceramic cross-ply laminates was conducted by Kim [44]. This investigation monitored acoustic emission (AE) activity emanating from the specimen during load application to detect the initiation and progression of damage conjointly with optical measurements of crack density. However, no attempt was made to correlate acoustic signatures with damage mechanisms.

It should also be mentioned that crack density measurements were made after removing the specimens from the test machine at predetermined stress levels for microscopic examinations, hence many of the finer cracks may have closed upon removal of the load, resulting in fewer observable cracks.

In summary, many of the aforementioned publications concerned with the experimental characterization of ceramic cross-ply laminates provide verifications for several of the experimental observations noted in this dissertation. However, they frequently lack essential data necessary as input parameters for modeling. Additionally, detailed information about damage evolution necessary for correlation with analytic stress-strain predictions is often incomplete. Specifically, none of the aforementioned works contain detailed *in situ* transverse crack density data as a function of applied stress, or information regarding the interfacial shear strength between the 0° and 90° ply groups. It will be shown that the above information is essential for the construction of a predictive model for ceramic cross-ply laminates.

Although information concerning the interface between laminate ply groups is virtually nonexistent, there is a wealth of articles related to the behavior of the fiber-matrix interface, for example [46-59]. At this time, there seems to exist only a single reference related to inter-ply shearing strength by Wu *et. al.* [60]. In this work the authors examined the interfacial shearing characteristics of SiC fiber reinforced zirconia titanate composites. Tests were conducted with a custom made shear fixture that "pushed-out" a number of plies from the composite to measure the interlaminar shearing strength. Although this investigation was concerned with a unidirectional configuration, the aforementioned fixture provided a guideline to the design of the apparatus employed to assess the interlaminar shearing strength of ceramic cross-ply laminates in the current study.

2.4 Problem Statement

Unidirectionally reinforced ceramic matrix composites are of limited use in structural applications due to their extremely low transverse ductility. For this reason, it is necessary to employ more versatile lay-ups in order to achieve acceptable multidirectional toughness values. The simplest such lay-up would be the cross-ply laminate, consisting of 0° and 90° ply groups. For obvious reasons, it is important to model and mechanically test the response of the cross-ply laminates in order to develop a rational predictive capability for their behavior.

Considering the state of the art in the study of cross-ply ceramic composites, it is apparent that investigations predicting the stress-strain response of this material system in a comprehensive manner are not available at the present time. Therefore, this dissertation will focus on the development of an analytical model to predict the behavior of ceramic cross-ply composites, accompanied by an appropriate mechanical test program to correlate stress-strain predictions and actual material behavior.

The purpose of the analytical model is to predict the stress-strain response of ceramic matrix cross-ply laminates, in correlation with the associated damage states. This approach will enable the modeling of material behavior without resorting to empirically prescribed damage parameters, such as transverse crack density and slip zone length, as often transpires in the current literature. The features of the current analysis not present in previous works include:

- Incorporation of the non-linear behavior of the 0° plies within the cross-ply composite into the analysis. It should be noted that this issue is not mentioned in any of the aforementioned works on cross-ply composites, although the non-linearity of unidirectional material is often reported in experimental investigations.

- Prediction of the evolution of transverse matrix cracking in the 90° plies based on a fracture criterion that accounts for the non-linear stress-strain response of the 0° plies. It should be noted that the few investigations that employ a fracture criterion to predict damage evolution consider only linear behavior.

- Evaluation of the length of interfacial slip zones between the 0° and 90° ply groups based on a shear strength criterion at the interface, along with its evolution with applied load. Other investigations which dealt with slip, such as references [37,39-41], confined their attention to slip at the fiber/matrix interface, but neglected slippage at the interface between the 0° and 90° ply groups.

The second aspect of this investigation consists of an extensive experimental program to verify the validity of the proposed model and provide essential material properties. Major elements of the experimental investigation include:

- Stress-strain data for cross-ply and unidirectional ceramic matrix material systems. While most of these data are available in the literature, detailed firsthand observations are necessary for model verification .

- Transverse crack density in the 90° plies data as a function of applied stress. Only scant information about this aspect of laminate damage is available in the current literature, and detailed experimental results are necessary for comparing with the crack densities predicted by the model.

- The development of a custom made test method to determine the interfacial shearing strength between the 0° and 90° ply groups in the cross-ply laminate. With the exception of reference [60], this subject was not considered in any other investigations.

CHAPTER 3

EXPERIMENTAL OBSERVATION OF THE MECHANICAL BEHAVIOR OF CERAMIC CROSS-PLY LAMINATES

3.1 Specimen Description

Two SiC/CAS (Nicalon fiber/Calcium alumino-silicate glass-ceramic matrix) ceramic cross-ply lay-ups, $[0_2/90_2]_s$ and $[0_2/90_4]_s$ were obtained from Corning. These laminates were manufactured using a hot press process resulting in square plates of approximately 6 x 6 inches with thicknesses of 0.065 and 0.095 inches respectively . The plates were machined with a water cooled diamond saw into specimens of approximate dimensions of 6 x 0.5 x 0.065 and 6 x 0.5 x 0.095 inches. Tapered glass/epoxy end tabs were employed to reduce stress concentrations near the grips, thus limiting the number of failures outside the gage section. The specimen edges were polished using standard diamond compounds to 3 micron to facilitate microscopic observation of damage mechanisms in real time.

3.2 Experimental Set-Up / Testing Procedures

Testing was conducted on a MTS 50 Kip servo-hydraulic test system with 442 controllers and a Microprofiler function generator. Instron "Supergrips" were used in conjunction with Instron mechanical wedge action grips to minimize the effects of bending and torsion on the specimen and provide clamping in a controlled manner. An Olympus BH2 optical microscope mounted on a XYZ platform was used in conjunction with a digital chip camera to record all activity on the specimen surface during applied load. This video system was connected to a VHS format video cassette recorder to save all test records in real time as load was applied. The final magnification of this video system was approximately 750X. A schematic representation of the test set-up is shown in Figure 3.1 below:

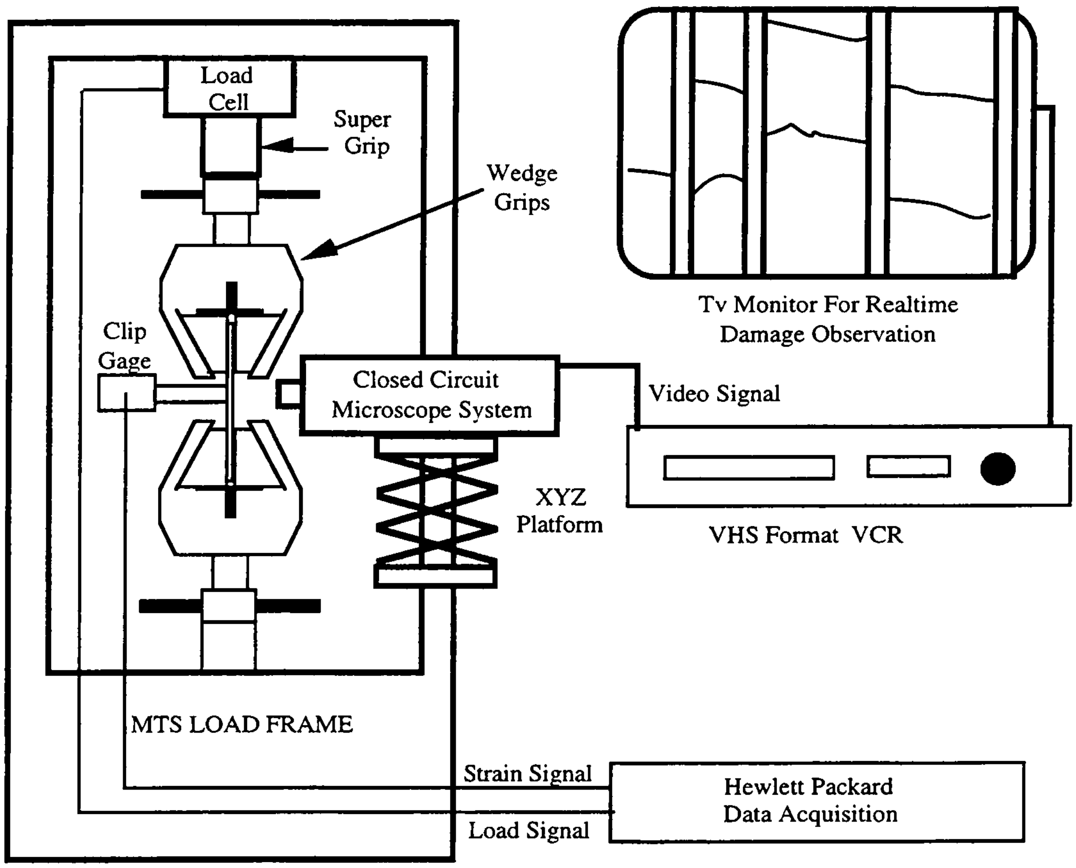

Figure 3.1 Experimental Set-Up

All tests were conducted in stroke (displacement) control at a loading rates from 0.003 to 0.010 inch/minute. An MTS 632 extensometer with a one inch gage length was used to monitor strain. To collect stress-strain data, the specimens were loaded continuously to failure while load and strain signals were recorded using an HP3497 data acquisition/control unit. To determine crack densities as a function of load/stress, it was necessary to interrupt the loading intermittently at pre-determined stress levels. During these stages, the surface of the specimen was scanned for evidence of damage. The stress and strain levels were then recorded to correlate observed damage with a specific points on the stress-strain curve. It should be noted that the stress-strain curves for both the continuous and intermittent tests were in close agreement.

3.3 Ceramic Matrix Cross-Ply Stress-Strain Behavior

A number of stress-strain curves were collected for the two aforementioned lay-ups. Although the curves are highly non-linear, they are nonetheless closely reproducible. Several examples for the $[0_2/90_2]_s$ are shown in Figure 3.2. below:

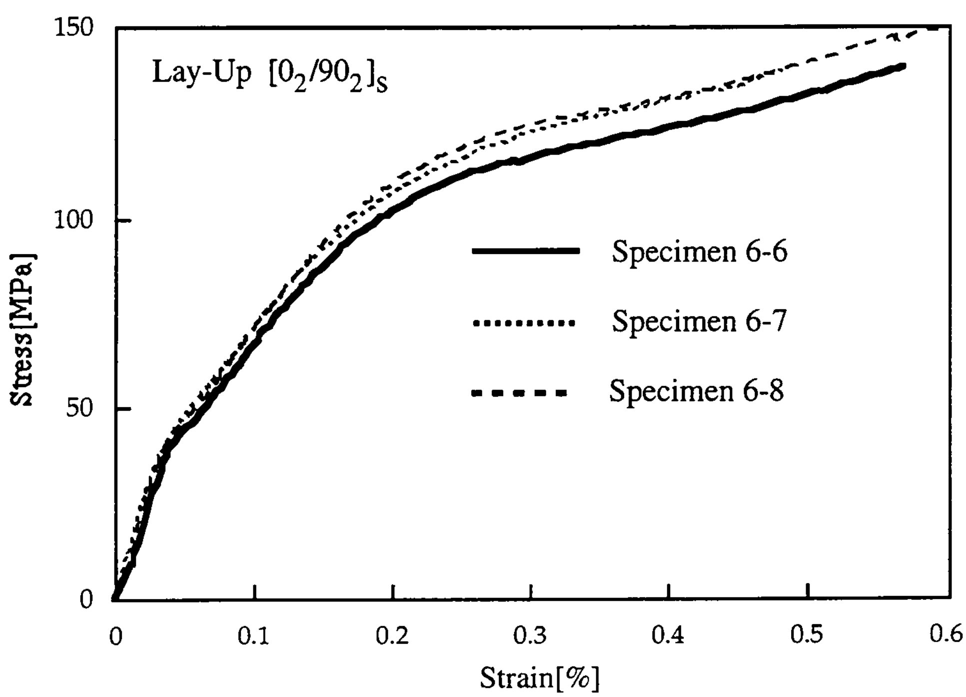

Figure 3.2 Stress-Strain Behavior of $[0_2/90_2]_s$ Laminate

It should be noted that these curves are for the continuous loading case. Additional examples of the cross-ply ceramic stress-strain behavior are given in Appendix A, Figures A1 through A7. Distinguishing features of these curves consist of an initial linear range followed by two basically linear regions, each with subsequent reductions in slope. The curves then terminate with a region of slightly increasing slope. Before discussing theories that account for this non-linear behavior, it is first necessary to identify the various damage mechanisms that occur during loading and distinguish the roles played by these mechanisms in the overall response of the material system.

3.4 Damage Mechanisms

There are basically three observable damage mechanisms associated with cross-ply ceramic composite at the ply level. These are : transverse matrix cracking in the 90° plies, interfacial slippage between the 0° and 90° plies, and the internal damage mechanisms within the 0° plies that account for the non-linearity of unidirectional ceramic matrix composites. The latter consist of the following mechanisms : transverse cracking in the unidirectional material spanned by intact fibers, fiber breakage, and fiber-matrix interfacial slippage. However for this investigation, analysis was conducted at the laminate ply level with the behavior of the unidirectional material taken as a "lumped" property to be used as an input to the cross-ply model. Therefore, the current analysis is not concerned with the detailed mechanisms at the fiber-matrix level, and focuses on the ply level behavior. For detailed modeling of the behavior of the 0° plies, the reader is referred to references [18-20].

Transverse matrix cracking is readily observable in this material system with the aid of an optical microscope. On the other hand, interfacial slippage is not easily detected in a direct manner. However, close inspection of the 0°/90° interface in the vicinities of transverse cracks in the 90° ply groups suggests the existence of an interfacial slip zone since there are noticeable discontinuities in the crack opening displacements at those locations.

3.4.1 Transverse Matrix Cracking

As mentioned before, the surface of the specimen was continuously monitored during the loading in real-time to observe damage mechanisms. Particular attention was paid to the edges of the specimen in anticipation of observing transverse matrix cracking and interfacial slippage between the plies.

Generally, the damage state consists of transverse cracks in the 0° and 90° plies with the latter spanning the 90° ply group in a nearly straight line. At the vicinity where a crack in the 90° ply impinges upon the 0° ply group, there is usually a clustering of parallel cracks in the 0° ply group as shown schematically in Figure 3.3 below. Moving along the interface away from this location, the crack density in the 0° ply decreases, indicating a reduction in the stresses borne by the 0° plies. Since the crack face is stress free, the 90° ply cannot support any load at this location, hence there is evidence of a shear-lag type behavior where the stress is being transferred back to the cracked 90° plies from the intact 0° plies through shearing stress at the ply interface. An example of actual transverse cracking, accompanied by a cluster of cracks in the 0° plies is given in Figure 3.4 below. It is also interesting to note the presence of a broken fiber in the 0° plies of Figure 3.4. Additional photographs of matrix cracking are given in Appendix B.

Scanning a 0.5 inch length of the specimen at each interval of loading, it is possible to observe the initiation and progression of the transverse cracks in the 90° ply group and obtain a reasonably accurate crack count, and thereby their density as a function of applied stress. The initiation and progression of transverse cracking occurs sequentially in the following manner : transverse cracks initiate in the 90° plies, and under increased load extend into the 0° plies where they are bridged by intact fibers. Upon further load increase,

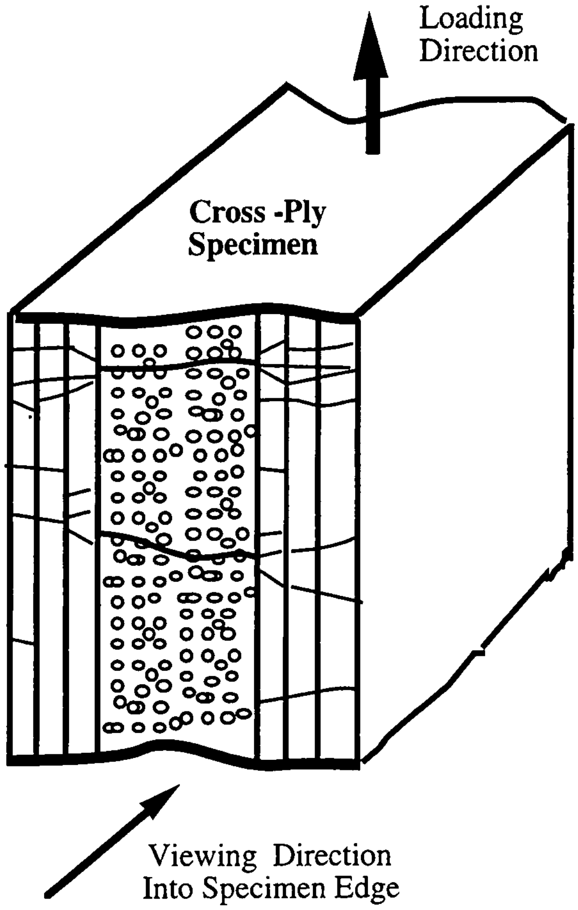

Figure 3.3 Transverse Matrix Cracking Schematic

the cracks in the 90° plies reach a saturation density while the crack density in the 0° plies rapidly exceeds that in the 90° plies, increasing until failure. An example of this crack accumulation and associated stress-strain response is shown in Figures 3.5a and 3.5b below. This crack progression process lends some insight to the mechanism that is partly responsible for non-linear stress-strain behavior of the cross-ply laminate.

Referring to Figures 3.2 and 3.5, the first "knee" in the stress-strain curve occurs at approximately 50 MPa and corresponds reasonably well with the initiation of transverse cracking in the 90° plies, while the second reduction in slope at around 100 MPa seems to agree with the saturation state of the foregoing cracks. Upon further loading the effects of transverse cracking in the 90° plies seem to be overshadowed by other mechanisms.

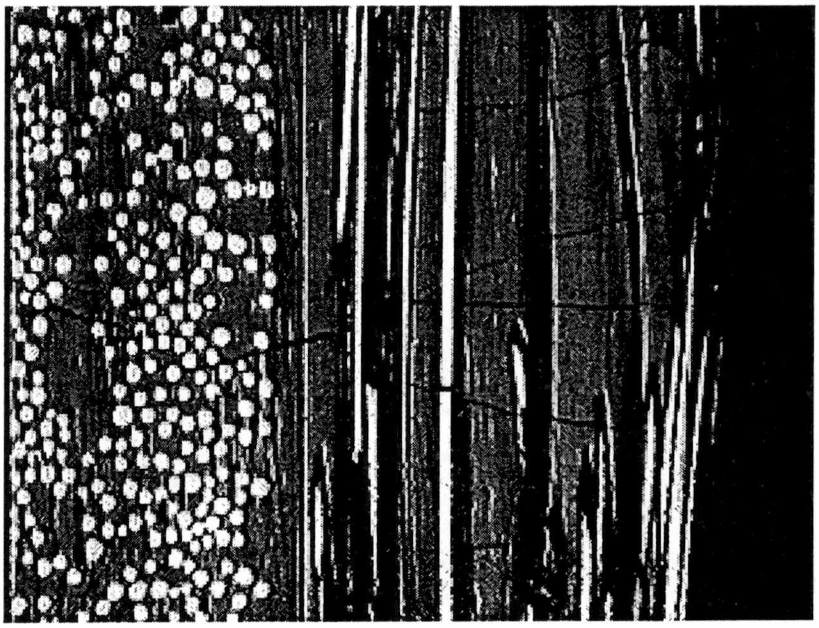

Figure 3.4 Typical Transverse Cracking in a Cross-Ply Laminate

Since one of the primary objectives of the experimental portion of this research was to provide data to correlate the predictions of matrix cracking from the analysis with mechanical tests, care was taken to record the sequence of damage progression simultaneously with the stress-strain behavior and ultimate strength. Specifically, the key damage parameters include the stress level of transverse crack initiation in the 0° and 90° plies as well as the final crack saturation densities. These data for the cross-ply specimens are summarized in Table 3.1.

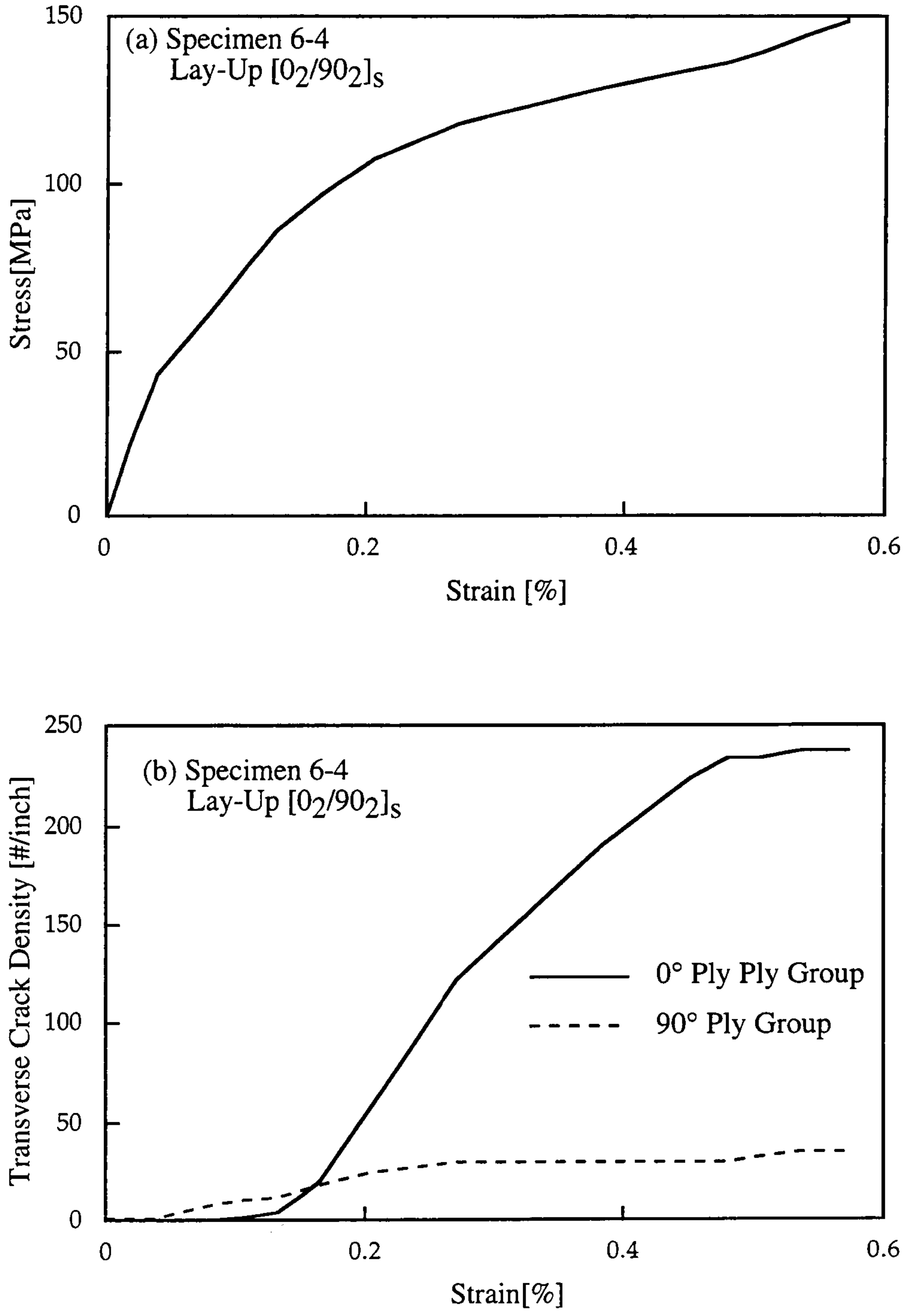

Figure 3.5 The Response of a Ceramic Cross-Ply Laminate: (a) Stress-Strain Behavior, (b) Crack Density Progression

TABLE 3.1 Cross-Ply Strength and Damage Data

Spec. Number	Lay-Up	σ_{ult} [MPa]	$\sigma_{initiation}$ [MPa] 90° Plies	$\sigma_{initiation}$ [MPa] 0° Plies	Saturation Density [#/in] 90° Plies	Saturation Density [#/in] 0° Plies
6-1	$[0_2/90_2]_s$	151.0	65	65	32	180
6-2	$[0_2/90_2]_s$	145.8	103	86	20	122
6-3	$[0_2/90_2]_s$	136.9	48	108	36	146
6-4	$[0_2/90_2]_s$	151.9	65	75	34	238
6-5	$[0_2/90_2]_s$	154.9	42	105	40	180
6-6*	$[0_2/90_2]_s$	139.0	NA	NA	NA	NA
6-7*	$[0_2/90_2]_s$	139.3	NA	NA	NA	NA
6-8*	$[0_2/90_2]_s$	149.0	NA	NA	NA	NA
5-3	$[0_2/90_4]_s$	134.7	72	50	20	186
5-4	$[0_2/90_4]_s$	136.6	51	51	24	192

*Continuous Loading Tests

It was mentioned at the beginning of this section that the stress-strain behavior for this material is highly reproducible. Additionally, from Table 3.1, it can be seen that the ultimate strength values, transverse crack initiation stress levels, and saturation density are also fairly consistent. There are some disparities in the crack initiation stress levels, however this is not unexpected since it is sometimes difficult to identify the initiation of a newly formed crack until the load level is increased, and the crack opens fully, enabling positive identification. Furthermore, it is well known that all cracking phenomena are inherently stochastic due to the randomness of the initial flaw distributions.

3.4.2 Interfacial Slippage Between the 0° and 90° Plies

As mentioned before, there is evidence of interfacial slippage between the 0° and 90° ply groups. This can be surmised from the photograph in Figure 3.4, noting that where the transverse crack in the 90° ply reaches the interface, there is a pronounced crack opening displacement. Hence, one may infer that there is a mismatch in the displacements at the interface between the 0° and 90° ply groups, which may be attributed to slip.

It should be noted that this slip zone does not necessarily result in a debond between the plies at the interface, and may simply constitute a region where the interfacial shear stress has overcome the resistance to relative motion between the two ply groups. Consequently, this region cannot support any increase in shear stress, akin to plastic yielding.

There are two interdependent parameters associated with the slip zone. The first being its length, l_s, being measured along the 0°/90° interface away from the location of the transverse crack in the 90° ply group. A schematic representation of the slip zone is shown in Figure 3.6 below. It should be realized that the actual slip region is not as clearly defined as the idealization in Figure 3.6, since in reality, the 0° and 90° ply groups are not delineated by a clearly defined boundary. It is believed that this entanglement of the 0° and 90° plies at the interface provides a more complex debonding mechanism as compared to the simpler case of the often studied fiber/matrix interface.

The second parameter associated with the slip zone is the interfacial shearing strength between the 0° and 90° plies, τ_s^*. Basically, this parameter is defined as the maximum shearing stress that can be sustained at the interface by the material system. In view of the preceding discussion it would be incorrect to assume that τ_s^* is the same as the fiber/matrix interfacial shearing strength. Therefore, it was necessary to develop a new experimental method to measure τ_s^*. A schematic diagram of the testing fixture used to estimate the inter-ply shearing strength shown in Figure 3.7.

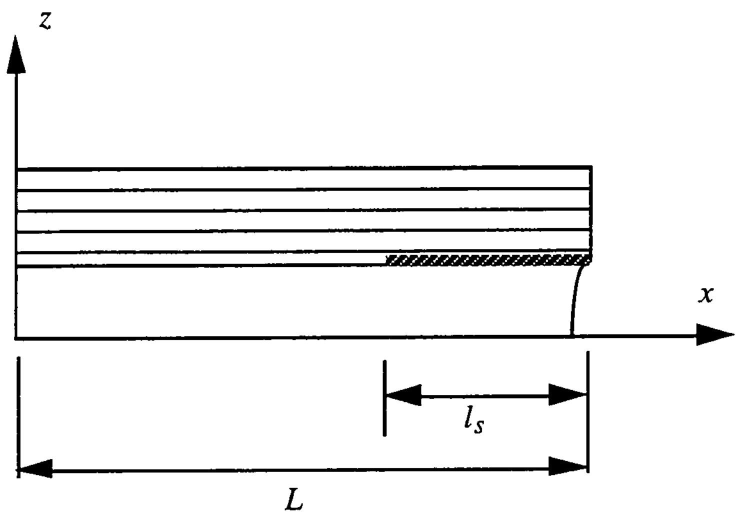

Figure 3.6 Schematic Slip Zone Length

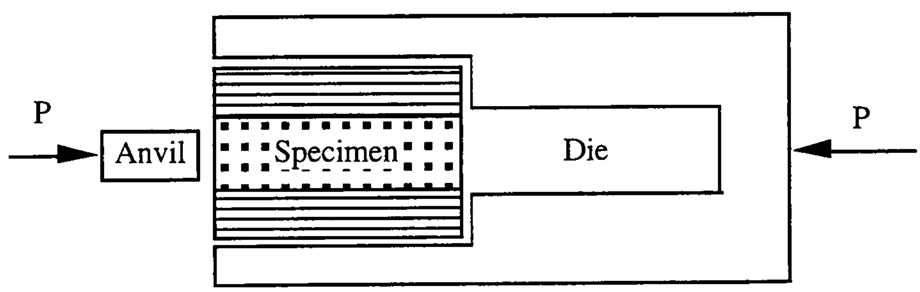

Figure 3.7 "Mini-Shear" Inter-Ply Strength Fixture

This fixture is designed to be installed between the actuator and the crosshead of any standard testing machine that can accommodate flat platens. The specimen, which consists of a $[0_n/90_m]_s$ lay-up, is inserted in the fixture, with the outer 0° plies constrained displacement of the anvil are then monitored throughout the test. It should be noted that a very small specimen is required to avoid buckling and reduce misalignment in order to minimize any uneven shearing stresses at the two 0°/90° interfaces. Since two cross-ply lay-ups were available in the current research, the dimensions of both the testing fixture and specimens were dictated by the available specimen thicknesses. This resulted in nominal specimen dimensions of 0.25 x 0.25 x 0.095 inches. Due to difficulty in maintaining specimen alignment, an alternative specimen, of 0.125 inch length in the axial loading direction was also employed. From the load-displacement record, an estimate of τ_s^* was calculated through a simple force balance relationship.

The tests were conducted in stroke control, using constant displacement rates. The first two tests were conducted at a loading rate of 0.05 in/min, which turned out to be too fast, making it difficult to observe the evolution of interfacial failure. Subsequently, the displacement rate was reduced to 0.005 in/min. A typical load displacement curve for a mini-shear specimen is shown in Figure 3.8 below:

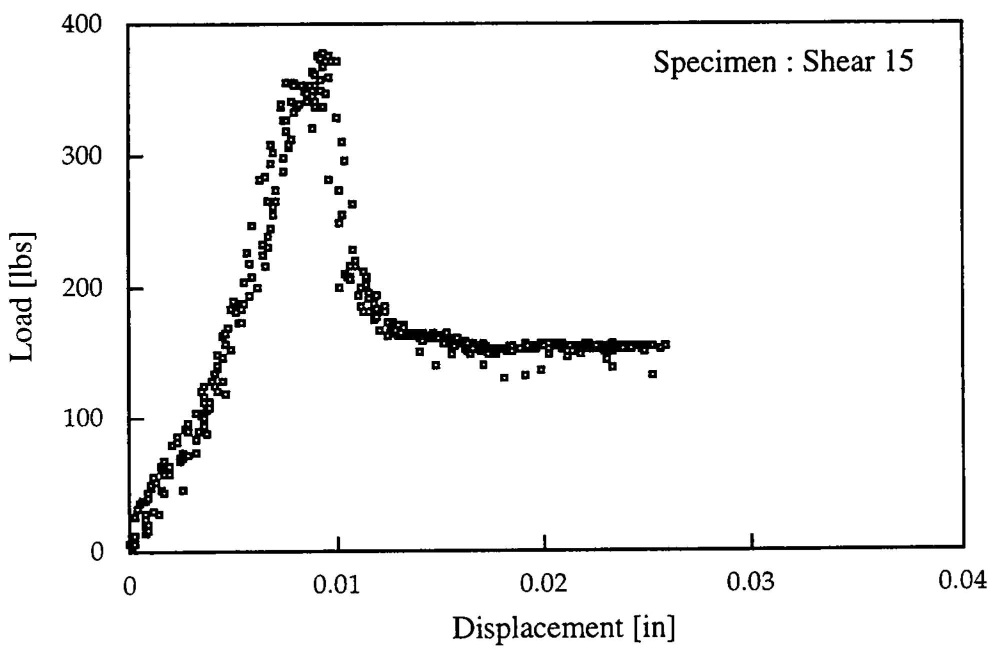

Figure 3.8 Load Displacement Response of the Mini-Shear Specimen

Additional load displacement curves are presented in Appendix C detailing the results of the seventeen additional tests that were conducted. It should be noted that Figures C1 contain the tests using 0.25 inch length specimen, while Figures C2 are for the shorter specimens with axial length of 0.125 inch. Additionally, Figures C1(a) and (b) were at the aforementioned exceedingly high loading rate, while the remaining tests were run at 0.005 inch/min. Although there is noticeable scatter in the load-displacement record given in Figure 3.8, the general characteristics of the mini-shear specimen response are discernible. It should be noted that the microscope video system used to detect transverse cracking in the cross-ply tensile tests was also employed for this series of experiments. Since a continuous video record of the specimen surface was recorded in real time and the displacement rate was constant, it was possible to correlate observable damage (i.e. interfacial slippage) with the corresponding location on the load-displacement curve.

From Figure 3.8 it can be seen that the load-displacement response of the mini-shear specimen is characterized by an initial nearly linear region up to a peak load level where the interfacial damage zone initiates (as observed through the microscope). This occurs at approximately 375 pounds. It should be noted that the observable damage is randomly distributed along the length of the interface region as the peak load is approached. Just prior to the peak load, the damage at the interface begins to "link up" resulting in a complete debond of the 0° and 90° ply groups. At this instability point, the load drops rapidly to a level of approximately 160 pounds, as the unbonded inner 90° ply group separates from the 0° plies. Then, as the 90° ply group continues its downward motion, it is forced into the cavity of the fixture. The observed sequence of damage initiation and slip zone growth leading to ply separation is shown in Figure 3.9 below for the specimen whose load-displacement curve is given in Figure 3.8. Figure 3.9(a) shows the state of damage as interfacial slippage initiates prior to attainment of the maximum load level. Note that the interfacial cracking on the left side of the 90° ply group extends from the interface into the 90° plies, indicating that the shear failure may deviate from the 0°/90° interface. On the other hand, this photograph reveals that there is also damage in the right side interfacial region, indicated by a fine crack running parallel to the 0°/90° boundary. In Figure 3.9(b), the specimen exhibits complete interfacial slippage on both sides of the 90° ply group. Notice that at this stage the anvil of the test fixture has penetrated the top of the specimen giving conclusive evidence of initiation of "push-in" of the 90° ply group. This circumstance is more pronounced in Figure 3.9(c). Note that both outer 0° ply groups remain supported by the fixture. Additional examples of the sequence of interfacial shear failure are Appendix D.

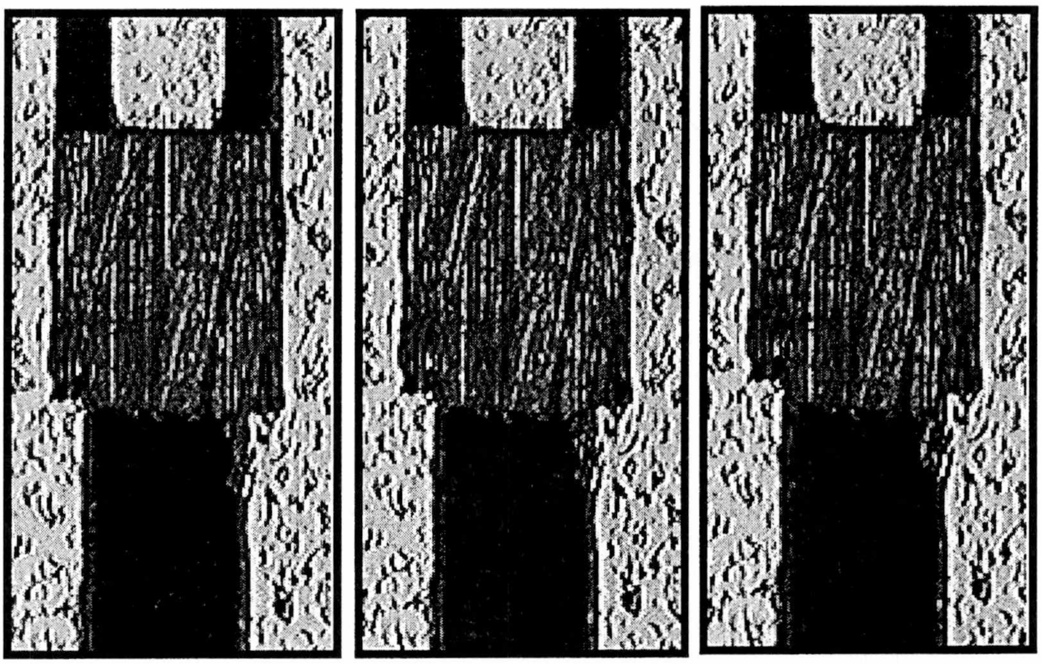

(a) **(b)** **(c)**

Figure 3.9 Damage Progression for the Mini-Shear Test

To estimate the 0°/90° interfacial shear strength, the load level where interface failure occurs is divided by the shear fracture area. After studying the sequence of the damage progression and the corresponding load-displacement curves for all the tests, it is believed that the interface failure occurs just prior to the maximum load level. Therefore, the shearing strength parameter, τ_s^* is calculated using this value. The results from all the interlaminar shear strength tests are given in Table 3.2 below :

TABLE 3.2 Mini-Shear Specimen Interlaminar Shear Strength Data

Specimen Number	Shear Area [in^2]	Failure Load [lbs]	Interfacial Strength [MPa]
2	0.0615	657	36.83
3	0.0603	592	33.85
4	0.0630	740	40.49
5	0.0600	522	29.99
6	0.0610	472	26.67
7	0.0605	483	27.52
8	0.0317	371	40.35
10	0.0312	331	36.57
11	0.0319	327	35.34
12	0.0315	375	41.04
13	0.0316	347	37.86
15	0.0312	355	39.23
16	0.0314	344	37.77
17	0.0309	303	33.80
18	0.0312	238	26.30
19	0.0318	408	44.23
20	0.0312	303	33.48
21	0.0306	479	53.96
		Average	36.40
		Stdev	6.75

Observing the strength data in Table 3.2, it can be seen that there is substantial scatter in the interfacial shearing strength values. These inconsistencies may be attributed to the inherent statistical characteristics of the interfacial failure phenomenon. For instance, the meandering of cracks in the damage zone between the random distribution of fibers and flaws most likely contributes to the scatter shown in Figure 3.2. Other sources of scatter are likely to be caused by slight variations in ply thickness of the laminate as well as variations in the 0°/90° interface leading to slight eccentricities of the loading. Additionally, another source of scatter in the shear strength data may be attributed to small inaccuracies associated with the test fixture, which in combination with variations in specimen thickness leads to specimen misalignment.

In Table 3.2, the average interfacial shear strength is given to be approximately 35 MPa. However, careful inspection of Figure 3.9 reveals that the anvil pushing down on the 90° plies is slightly thinner than the 90° ply group. This results in the formation of inclined cracks in the 90° plies below the corners of the anvil, in conjunction with the initiation of damage at the interface as depicted in Figure 3.10 below:

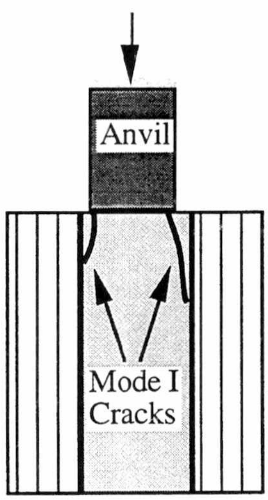

Figure 3.10 Mode I Cracks Accompanying Interfacial Shear Failure

These cracks have the tendency to open perpendicular to the loading direction, hence they can be classified as Mode I fracture. Since pure Mode II fracture toughness is several times greater than that of Mode I, it is possible that the drop in load preceding interfacial failure is partially a result of the formation of the Mode I cracks, and not entirely caused by the Mode II interfacial failure as intended. Consequently, the calculated values of the interfacial shearing strength, as recorded in Table 3.2 are likely to be lower than the actual value.

3.5 Non-Linearity of the 0° Ply Groups

As mentioned earlier, the non-linear behavior of the 0° outer plies plays a significant role in the overall response of the cross-ply laminate. This non-linearity, and the associated damage mechanisms causing it, have been addressed in great detail in other works [18-20], which include a comprehensive model that accounts for the evolution of damage mechanisms under load and prediction of the stress-strain response of the material. Several examples of unidirectional stress-strain tests conducted by the author in support the research in [18-20] are given in Figure 3.11 below. It should be noted that although these stress-strain curves exhibit some time dependency indicated by the different responses for the three loading rates, the characteristics of the curves are similar. Furthermore, replicate tests at a rate of 0.003 in/min. have shown remarkable reproducibility. From Figure 3.11, it can be seen that the stress-strain response of the unidirectional material is linear until the stress reaches approximately 200 MPa, becoming non-linear beyond that point. To understand the role this non-linearity plays in the behavior of the cross-ply consider the following : As may be inferred from Figures 3.5(a) and 3.5(b), the transverse cracking in the in the 90° ply group has reached the saturation density at an applied stress level of approximately 100 MPa. It stands to reason that since the stress in the 90° plies vanishes at the location of such transverse cracks, the 0° plies must support the entire far-field applied stress at these locations. Consequently, the stress in the 0° plies may exceed 200

MPa over some regions adjacent to the locations of the foregoing cracks. However, as noted from Figure 3.11, this stress level exceeds the "yield point" on the unidirectional stress-strain curve, thus contributing to a reduction in the overall laminate stiffness. Upon further increase in load, a larger region of the 0° ply material "yields", leading to a further reduction in global stiffness of the composite. This interaction between the cross-ply behavior and the non-linearity of the 0° plies will be discussed further in Chapters 5 and 6 when the analysis of the cross-ply ceramic matrix laminate is presented.

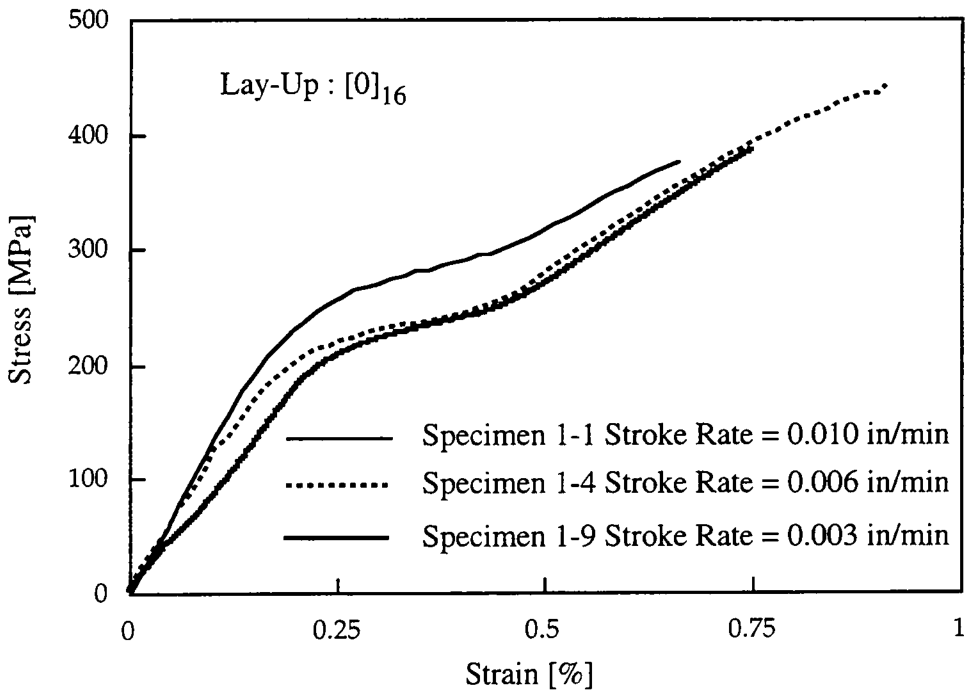

Figure 3.11 The Stress-Strain Response of a Unidirectional Ceramic Matrix Composite

CHAPTER 4

LINEAR SHEAR-LAG ANALYSIS

To introduce this chapter, it should be mentioned that the linear analysis presented herein follows that of R. J. Nuismer and S. C. Tan in references [33,34]. However, some modifications were made in the current formulation by considering a kinematically admissible displacement field which is shown to lead to the linear shear stress distributions assumed by Nuismer and Tan. Additionally, a more comprehensive method to determine the energy available for crack extension was formulated in the present analysis in order to accommodate the more general case of non-linear material behavior which will be considered in subsequent chapters.

4.1 Basic Considerations

Consider a ceramic cross-ply laminate as shown in Figure 4.1 below with exterior layers of 0° plies and interior 90° plies. An average axial stress, $\bar{\sigma}_x$, is applied resulting in the cracking of the 90° plies. The crack spacing, *2L*, is assumed to be uniform along the length of the specimen.

The analysis assumes the following displacement field with uniform transverse strain, $\bar{\varepsilon}_y$ in the y-direction:

$$\begin{aligned} u_i &= u_i(x,z) \\ v_i &= y\bar{\varepsilon}_y + v_i(x,z) \\ w_i &= w_i(x,z) \end{aligned} \qquad [4.1]$$

where the subscript i=1 corresponds to the 90° and i=2 to the 0° ply groups.

Due to the symmetry of the model about both the x and z axes, a quarter volume representation can be used as shown in Figure 4.2. The distances h_1 and h_2 refer to the thicknesses of the 90° and 0° ply groups, and $\bar{h}$ denotes half the thickness of the laminate.

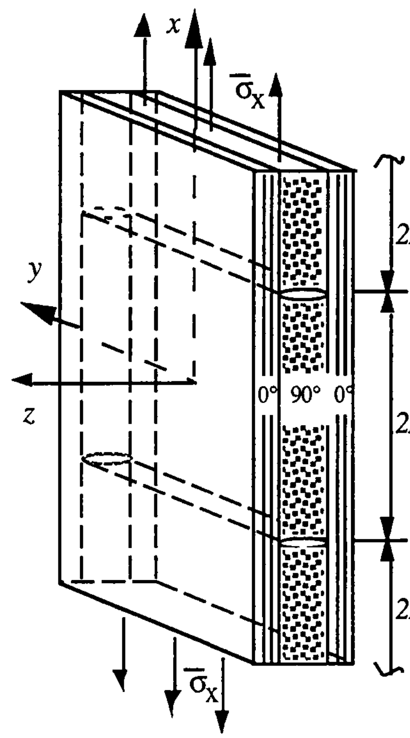

Figure 4.1 Cross-Ply Specimen Geometry

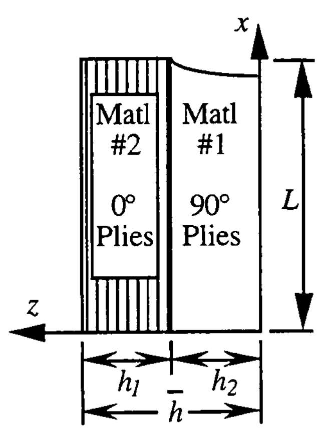

Figure 4.2 Quarter Volume Representative Element

For an orthotropic laminate, the following constitutive relation applies for the two ply groups :

$$\begin{Bmatrix} \sigma_x \\ \sigma_y \\ \sigma_z \\ \tau_{yz} \\ \tau_{xz} \\ \tau_{xy} \end{Bmatrix}^{(i)} = \begin{bmatrix} C_{11} & C_{12} & C_{13} & 0 & 0 & 0 \\ C_{12} & C_{22} & C_{23} & 0 & 0 & 0 \\ C_{13} & C_{23} & C_{33} & 0 & 0 & 0 \\ 0 & 0 & 0 & C_{44} & 0 & 0 \\ 0 & 0 & 0 & 0 & C_{55} & 0 \\ 0 & 0 & 0 & 0 & 0 & C_{66} \end{bmatrix}^{(i)} \begin{Bmatrix} \varepsilon_x \\ \varepsilon_y \\ \varepsilon_z \\ \gamma_{yz} \\ \gamma_{xz} \\ \gamma_{xy} \end{Bmatrix}^{(i)} \qquad [4.2]$$

Also define an average ply property through the thickness of i^{th} ply group, indicated with an overbar, namely:

$$\bar{t}^{(i)} = \frac{1}{h_i}\int_0^{h_i} t^{(i)} dz \qquad [4.3]$$

Based on geometry and applied loading, it is reasonable to make the following assumptions:

(i) Since the laminate is thin and stress free at the surfaces at $z = \pm\bar{h}$ the condition $\sigma_z(\pm\bar{h}) = 0$, suggests:

$$\sigma_z \approx 0 \qquad [4.4i]$$

(ii) To remain within the context of an essentially one dimensional analysis, we assume:

$$\frac{\partial w_i}{\partial x} = 0 \qquad [4.4ii]$$

Consider the "global" equilibrium of the two ply groups over an infinitesimal distance, *dx*, as shown in Figure 4.3 below. The overbars indicate the average axial stress in each ply, and τ^* is the interfacial shearing stress between the two ply groups.

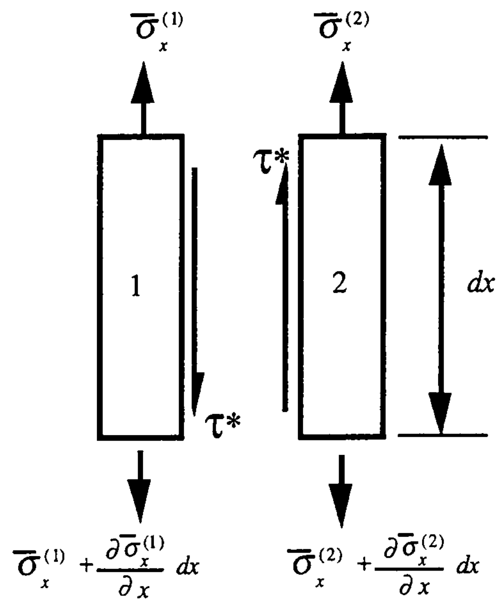

Figure 4.3 Equilibrium Force Balance

A straight forward force balance results in the following equilibrium equations relating normal stresses to interfacial shearing stresses:

$$\bar{\sigma}_x'^{(1)} = \frac{\tau^*(x)}{-h_1} \qquad [4.5i]$$

$$\bar{\sigma}_x'^{(2)} = \frac{\tau^*(x)}{h_2} \qquad [4.5ii]$$

Where primes indicate derivatives with respect to x. Additionally, the "global" force balance at any location $0 \leq x \leq L$ yields:

$$\bar{\sigma}_x^{(1)} h_1 + \bar{\sigma}_x^{(2)} h_2 = \bar{\sigma}_x \bar{h} \qquad [4.5iii]$$

Employing $\sigma_z^{(i)} = 0$, it is possible to eliminate ε_z from the first two equations in [4.2], then averaging the normal stresses over the thickness of the plies using [4.3] results in the following constitutive relations:

$$\begin{aligned} \bar{\sigma}_x^{(i)} &= Q_{11}^{(i)}\bar{u}_i' + Q_{12}^{(i)}\bar{\varepsilon}_y \\ \bar{\sigma}_y^{(i)} &= Q_{12}^{(i)}\bar{u}_i' + Q_{22}^{(i)}\bar{\varepsilon}_y \end{aligned} \qquad [4.6]$$

Next consider the axial displacements, $u_i(x,z)$ in the two ply groups. It is reasonable to assume parabolic displacement fields in the two ply groups as depicted in Figure 4.4 below:

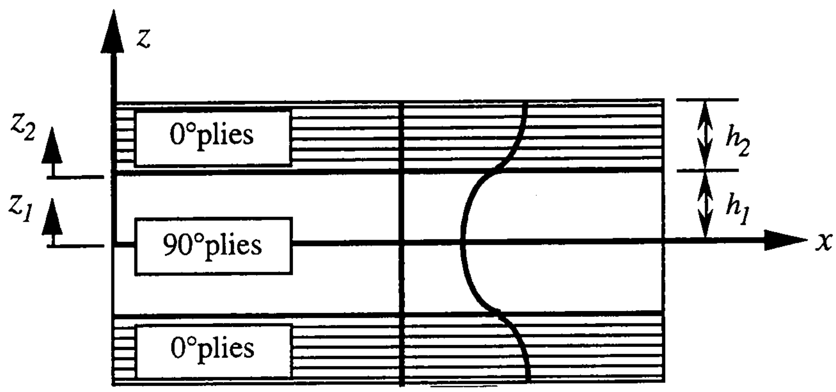

Figure 4.4 Assumed Displacement Field in the 0° an 90° Ply Groups

These displacements can be expressed as variations with respect to z_i given by second order polynomials as follows:

$$u_1(x,z_1) = f(x)\left[a_1 + c_1\left(\frac{z_1}{h_1}\right)^2\right] \qquad 0 \le z_1 \le h_1 \qquad [4.7a]$$

$$u_2(x,z_2) = f(x)\left[a_2 + b_2\left(\frac{z_2}{h_2}\right) + c_2\left(\frac{z_2}{h_2}\right)^2\right] \qquad 0 \le z_2 \le h_2 \qquad [4.7b]$$

where $\quad z_1 = z \quad , \quad z_2 = z - h_1$

Employing [4.3] to take averages of [4.7] with respect to z we get:

$$\bar{u}_1(x) = f(x)\left[a_1 + \frac{c_1}{3}\right] \tag{4.8a}$$

$$\bar{u}_2(x) = f(x)\left[a_2 + \frac{b_2}{2} + \frac{c_2}{3}\right] \tag{4.8b}$$

Using the fifth equation of [4.2], and employing the assumption given in [4.4ii], we obtain the following constitutive relation for the shearing stresses in each ply:

$$\tau_{xz}^{(i)} = C_{55}^{(i)} \frac{\partial u_i}{\partial z} \tag{4.9}$$

Substituting the displacement fields from [4.7], the shearing stresses in each ply can then be written as:

$$\tau_{xz}^{(1)} = f(x) C_{55}^{(1)} \left(\frac{z_1}{h_1}\right) \frac{2c_1}{h_1} \tag{4.10a}$$

$$\tau_{xz}^{(2)} = f(x) C_{55}^{(2)} \left(b_2 + 2c_2 \frac{z_2}{h_2}\right) \frac{1}{h_2} \tag{4.10b}$$

Note that the symmetry condition, $\tau_{xz}^{(1)}(x, z_1 = 0) = 0$, is automatically satisfied by the form of $u_1(x, z_1)$. On the other hand, for the stress free surface at $z_2 = h_2$ we have:

$$\tau_{xz}^{(2)}(x, z_2 = h_2) = 0 \tag{4.11}$$

Which in view of [4.10b] we get:

$$b_2 = -2c_2 \tag{4.12}$$

Continuity of displacements (no slip between ply groups) at the interface requires:

$$u_1(x, z_1 = h_1) = u_2(x, z_2 = 0) \tag{4.13}$$

Employing this relation in [4.7] yields:

$$a_1 + c_1 = a_2 \tag{4.14}$$

Since the shearing stresses in each ply group must match at the interface we have:

$$\tau_{xz}^{(1)}(x, z_1 = h_1) = \tau_{xz}^{(2)}(x, z_2 = 0) \equiv \tau^*(x) \tag{4.15}$$

Then from [4.10] along with the relation in [4.12] the following result is obtained:

$$\frac{2c_1}{h_1} C_{55}^{(1)} = \frac{b_2}{h_2} C_{55}^{(2)} = -\frac{2c_2}{h_2} C_{55}^{(2)} \tag{4.16}$$

Additionally, employing [4.12] in [4.8b] yields:

$$\bar{u}_2(x) = f(x)\left[a_2 - \frac{2}{3}c_2\right] \tag{4.8b'}$$

The results in [4.8a], [4.14], [4.16], and [4.8b]' consist of four linear equations in four unknowns, namely, a_1, a_2, c_1, and c_2 as shown below:

$$\begin{bmatrix} 1 & 0 & 1/3 & 0 \\ 0 & 1 & 0 & -2/3 \\ 1 & -1 & 1 & 0 \\ 0 & 0 & C_{55}^{(1)}/h_1 & C_{55}^{(2)}/h_2 \end{bmatrix} \begin{Bmatrix} a_1 \\ a_2 \\ c_1 \\ c_2 \end{Bmatrix} = \frac{1}{f(x)} \begin{Bmatrix} \bar{u}_1(x) \\ \bar{u}_2(x) \\ 0 \\ 0 \end{Bmatrix} \qquad [4.17]$$

Solving simultaneously yields:

$$c_1 = \frac{3}{2} C_{55}^{(2)} h_1 \left(\frac{\bar{u}_2 - \bar{u}_1}{h_2 C_{55}^{(1)} + h_1 C_{55}^{(2)}} \right) \frac{1}{f(x)} \qquad [4.18a]$$

$$c_2 = -\frac{3}{2} C_{55}^{(1)} h_2 \left(\frac{\bar{u}_2 - \bar{u}_1}{h_2 C_{55}^{(1)} + h_1 C_{55}^{(2)}} \right) \frac{1}{f(x)} \qquad [4.18b]$$

Employing the last result, the shearing stresses in equations [4.10] can be written as:

$$\tau_{xz}^{(1)} = \frac{3 C_{55}^{(1)} C_{55}^{(2)}}{C_{55}^{(1)} h_2 + C_{55}^{(2)} h_1} \frac{\bar{u}_2 - \bar{u}_1}{h_1} z_1 \qquad [4.19a]$$

$$\tau_{xz}^{(2)} = \frac{3 C_{55}^{(1)} C_{55}^{(2)}}{C_{55}^{(1)} h_2 + C_{55}^{(2)} h_1} \frac{\bar{u}_2 - \bar{u}_1}{h_2} (h_2 - z_2) \qquad [4.19b]$$

From [4.15] along with [4.19], the interfacial shearing stress becomes:

$$\tau^* = A_{55} \left(\frac{\bar{u}_2 - \bar{u}_1}{\bar{h}} \right) \quad \text{where} \quad A_{55} = \frac{3 \bar{h} C_{55}^{(1)} C_{55}^{(2)}}{h_1 C_{55}^{(2)} + h_2 C_{55}^{(1)}} \qquad [4.20]$$

Note that equation [4.20] is a constitutive relation for the interfacial shearing stress in terms of the average displacement over each ply group. Using the definitions for z_1 and z_2 with [4.19] and [4.20], the shearing stresses in the two ply groups can be expressed in terms of the interfacial shearing stress as:

$$\tau_{xz}^{(1)}=a(x)z \quad , \quad \tau_{xz}^{(2)}=a(x)h_1\left(\frac{\bar{h}-z}{\bar{h}-h_1}\right) \qquad [4.21]$$

where

$$a(x)=\frac{\tau^*(x)}{h_1}$$

The first two equations of [4.5], along with [4.6] and [4.20] can now be combined to form a second order homogeneous ordinary differential equation for $\tau^*(x)$ with constant coefficients. This is accomplished by taking two derivatives of [4.20] with respect to x, and substituting one derivative of [4.6] with respect to x into this expression. Terms involving derivatives of stresses are then eliminated by employing equations [4.5i] and [4.5ii], resulting in the following expression:

$$\tau''^{*}-\alpha_0^2\tau^* = 0 \qquad [4.22]$$

where

$$\alpha_0^2=\frac{A_{55}}{\bar{h}}\left(\frac{1}{h_1Q_{11}^{(1)}}+\frac{1}{h_2Q_{11}^{(2)}}\right)$$

The solution of [4.22] reads:

$$\tau^*(x) = A_0\sinh(\alpha_0 x) + B_0\cosh(\alpha_0 x) \qquad [4.23]$$

However due to symmetry about x=0, B_0=0 and we have:

$$\tau^*(x) = A_0\sinh(\alpha_0 x) \qquad [4.24]$$

To determine A_0, we utilize the fact that the crack surface at $x=L$ within the 90° ply group is traction free. Therefore:

$$\begin{aligned}&\bar{\sigma}_x^{(1)}(x=L)=0\\&\bar{\sigma}_x^{(2)}(x=L)=\frac{\bar{\sigma}_x\bar{h}}{h_2}\end{aligned} \qquad [4.25]$$

Where the second of equations [4.25] follows from the global equilibrium given in [4.5iii] and $\bar{\sigma}_x$ is the average applied stress on the laminate. Differentiation of [4.20] and evaluation both at $x=L$ gives:

$$\tau'^{*}(L) = A_{55}\left(\frac{\bar{u}_2'(L)-\bar{u}_1'(L)}{\bar{h}}\right) \qquad [4.26]$$

Upon recalling [4.6] we have:

$$\bar{u}_1'(L)=\frac{\bar{\sigma}_x^{(1)}(L)-Q_{12}^{(1)}\bar{\varepsilon}_y}{Q_{11}^{(1)}} \quad \text{and} \quad \bar{u}_2'(L)=\frac{\bar{\sigma}_x^{(2)}(L)-Q_{12}^{(2)}\bar{\varepsilon}_y}{Q_{11}^{(2)}}$$

Whereby, employment of the condition in [4.25] along with [4.5iii] results in:

$$\begin{aligned}&\bar{u}_1'(L)=\frac{-Q_{12}^{(1)}\bar{\varepsilon}_y}{Q_{11}^{(1)}}\\&\bar{u}_2'(L)=\frac{1}{Q_{11}^{(2)}}\left(\frac{\bar{\sigma}_x\bar{h}}{h_2}-Q_{12}^{(2)}\bar{\varepsilon}_y\right)\end{aligned} \qquad [4.27]$$

Substituting this result into [4.26] gives :

$$\tau'^{*}(L) = \frac{A_{55}}{\bar{h}Q_{11}^{(1)}}\left(\frac{\bar{\sigma}_x \bar{h} Q_{11}^{(1)}}{h_2 Q_{11}^{(2)}} + \bar{\varepsilon}_y\left(Q_{12}^{(1)} - \frac{Q_{12}^{(2)}}{Q_{11}^{(2)}} Q_{11}^{(1)}\right)\right) \qquad [4.28]$$

Note that differentiation of [4.24] and evaluation at x=L gives:

$$\tau'^{*}(L) = A_0 \alpha_0 \cosh(\alpha_0 L)$$

Consequently, A_0 can now be determined from the last two results:

$$A_0 = \frac{\tau'^{*}(L)}{\alpha_0 \cosh(\alpha_0 L)} \qquad [4.29]$$

Note that $\tau'^{*}(L)$ is given in [4.28] in terms of $\bar{\sigma}_x$ and the yet unknown transverse strain, $\bar{\varepsilon}_y$. With A_0 thus determined the interfacial shearing stress is given as a function of position, x.

The normal stress distributions now follow upon integration of equations [4.5i] and [4.5ii]. The constants of integration are evaluated with the aid of [4.5iii] and [4.25]. In summary, the resultant stress distributions are then given by:

$$\begin{aligned} \tau^{*}(x) &= A_0 \sinh(\alpha_0 x) \\ \bar{\sigma}_x^{(1)}(x) &= \frac{A_0}{h_1 \alpha_0}\left(\cosh(\alpha_0 L) - \cosh(\alpha_0 x)\right) \\ \bar{\sigma}_x^{(2)}(x) &= \frac{\bar{\sigma}_x \bar{h}}{h_2} - \frac{\bar{\sigma}_x^{(1)}(x) h_1}{h_2} \end{aligned} \qquad [4.30]$$

The value of $\bar{\varepsilon}_y$ is obtained from the condition that in the absence of transverse loading, N_y=0 we have the following expression for equilibrium in the y-direction:

$$\bar{\sigma}_y \bar{h} L = h_1 \int_0^L \bar{\sigma}_y^{(1)} dx + h_2 \int_0^L \bar{\sigma}_y^{(2)} dx = 0 \qquad [4.31]$$

Expressions [4.6] give the following relations for the transverse stresses in each ply group:

$$\bar{\sigma}_y^{(1)} = C_1\bar{\sigma}_x^{(1)} + C_2\bar{\varepsilon}_y$$
$$\bar{\sigma}_y^{(2)} = C_3\bar{\sigma}_x^{(2)} + C_4\bar{\varepsilon}_y \qquad [4.32]$$

where

$$C_1 = Q_{12}^{(1)} / Q_{11}^{(1)}$$
$$C_2 = Q_{22}^{(1)} - \left(Q_{12}^{(1)}\right)^2 / Q_{11}^{(1)}$$
$$C_3 = Q_{12}^{(2)} / Q_{11}^{(2)}$$
$$C_4 = Q_{22}^{(2)} - \left(Q_{12}^{(2)}\right)^2 / Q_{11}^{(2)}$$

Carrying out the integration in [4.31] results in the following expression for the transverse strain:

$$\bar{\varepsilon}_y = \frac{-\bar{\sigma}_x\left(C_3\bar{h}L + \beta_1 k_1 k_3\right)}{\beta_1 k_1 k_4 + L\left(C_2 h_1 + C_4 h_2\right)} \qquad [4.33]$$

where

$$\beta_1 = \frac{(C_1 - C_3)}{\alpha_0}\left(L\cosh(\alpha_0 L) - \frac{\sinh(\alpha_0 L)}{\alpha_0}\right)$$
$$k_1 = A_{55} / \left(\bar{h}\,\alpha_0 Q_{11}^{(1)} Q_{11}^{(2)} \cosh(\alpha_0 L)\right)$$
$$k_3 = \frac{\bar{h} Q_{11}^{(1)}}{h_2}$$
$$k_4 = Q_{12}^{(1)} Q_{11}^{(2)} - Q_{12}^{(2)} Q_{11}^{(1)}$$

Substitution of [4.33] into [4.28] results in a relation between $\tau'^*(L)$ and $\bar{\sigma}_x$, thereby determining A_0 in terms of $\bar{\sigma}_x$. The stress distribution predicted by the shear-lag model is sketched in Figure 4.5 below. The shear stress $\tau^*(x)$ is an odd function of x vanishing at x=0, while the normal stress in the 90° ply vanishes at x=L. Note that the stress in the outer plies, $\bar{\sigma}_x^{(2)}$ reaches a maximum at x=L.

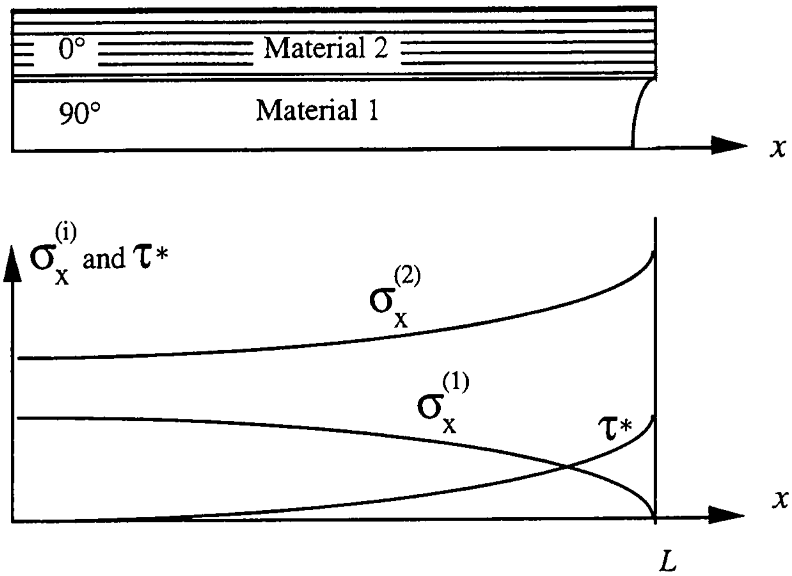

Figure 4.5 Linear Shear-Lag Analysis Stress Distributions

At this stage, it should be realized that the half crack spacing, L, is still an arbitrarily prescribed quantity, and to calculate the aforementioned stress distributions, L would have to be treated as an input to the analysis. Since one of the major goals of this dissertation is to develop a predictive failure model, a method to determine L will be presented in section 4.2.

To establish a stress-strain curve for the cracked laminate, it is necessary to calculate the global axial strain, $\bar{\varepsilon}_x$. To accomplish this, it should be realized that the outer plies remain intact during transverse crack formation in the interior 90° plies, thus the average global axial strain is given by :

$$\bar{\varepsilon}_x = \frac{\bar{u}_2(L)}{L} \qquad [4.34]$$

A straight forward integration of [4.6] over the region $0 \le x \le L$, yields the following expression:

$$\bar{\varepsilon}_x = \frac{1}{Q_{11}^{(2)}}\left(\frac{\bar{\sigma}_x \bar{h}}{h_2} - Q_{12}^{(2)}\bar{\varepsilon}_y - \frac{A_0}{h_2\alpha_0}\left(\cosh(\alpha_0 L) - \frac{\sinh(\alpha_0 L)}{\alpha_0 L}\right)\right) \qquad [4.35]$$

All terms in this equation are known for a given crack spacing and applied stress, hence a stress-strain curve for the composite can be generated as a function of the crack spacing.

4.2 Transverse Matrix Crack Progression / An Energy Criterion For the Determination of Transverse Crack Spacing

To correlate the crack spacing, *2L*, in a predictive manner with levels of applied stress, $\bar{\sigma}_x$, a fracture criterion is employed to compare available and required levels of energies at crack spacings L and $2L$. When, based on fracture considerations, it is energetically advantageous for a new crack to form, the crack spacing is updated by inserting a new crack between each pair of existing cracks while holding the applied stress constant. The new stress distribution is calculated from [4.30], with the global strain given in [4.35] providing the corresponding point on the stress-strain curve. This brings about an abrupt increase in global strain at some fixed levels of applied stress, resulting in a "softening" of the stress-strain curve.

The subdivision of crack spacing is depicted in Figures 4.6 below. Note that in Figure 4.6(a), the view is of the edge of the specimen normal to the *y*-coordinate (see Figure 4.1), while Figure 4.6(b) depicts the progression of a crack front being viewed normal to the *z*-coordinate as it propagates across the width of the specimen.

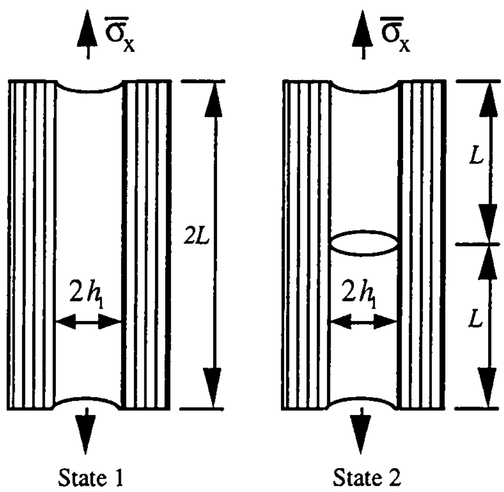

Figure 4.6(a) Progression of Transverse Matrix Cracks (Edge View)

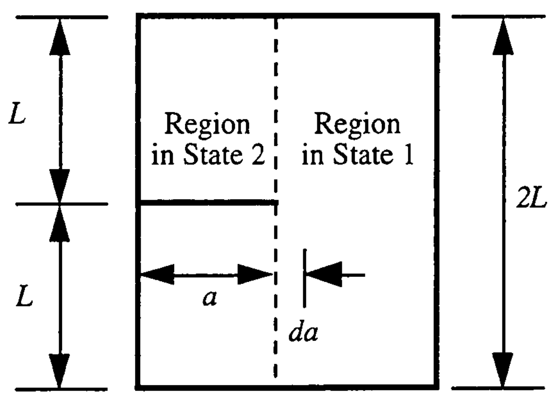

Figure 4.6(b) Progression of Transverse Matrix Cracks (Side View)

Consider now the energy criterion for the propagation of a new crack that is located midway between existing cracks spaced at a distance of $2L$. For this purpose consider a region in state 1, with crack spacing $2L$ and a region in state 2 with crack spacing L as depicted by the side view in Figure 4.6(a). It is assumed that an edge crack of length "a" exists in the region of state 2 as shown in the side view of Figure 4.6(b). The crack is assumed to propagate in a straight front spanning the entire thickness of the 90° ply group. The energy available for crack growth, J, is given by :

$$J=-\frac{d\Pi}{dA}\ ,\ \Pi=U-W \qquad [4.36]$$

Where Π is the total potential energy of the system, U is the elastic strain energy and W is the external work done on the system, while dA denotes the new fracture surface area. For the problem at hand, the crack of length "a" extends across the width of the cracked 90° plies and the incremental crack area, dA is then $2h_1 da$ (see Figure 4.2). State 2 is assumed to be established over the entire width of the coupon when:

$$J=J_{IC} \qquad [4.37]$$

where J_{IC}, the critical value, is a material property that can be determined experimentally for a given material system.

A typical load displacement curve that results from a crack formation in a body under applied load is shown in Figure 4.7 below. It is well known that the area under this curve is equal to the elastic strain energy, U, and the area above the curve is the complementary energy, U^*. The sum of these areas is then the work given by Pv, where P and v are the external load and displacement, respectively. Substituting $W=Pv$ back into [4.36] gives the following result:

$$\Pi=U-Pv=-U^*$$

whereby

$$J=\frac{dU^*}{2h_1 da} \qquad [4.38]$$

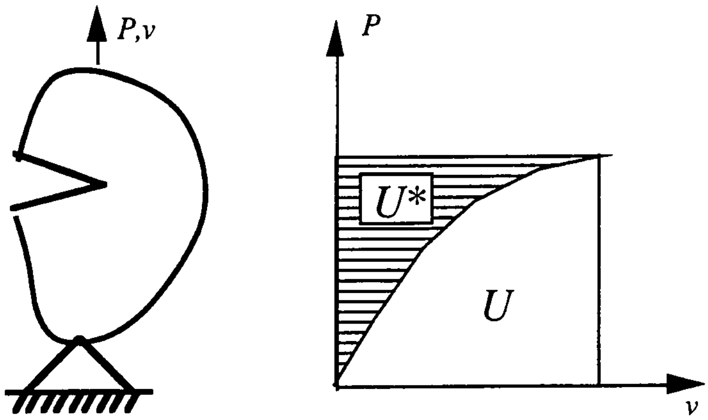

Figure 4.7 Cracked Body and Energy Content

For the linear elastic response case, $U^*= U$ and the areas above and below the curve are equal. Since the subsequent analysis will consider the non-linear stress-strain response of the laminate, the complementary energy will be used from here on to maintain consistency of presentation. Employing [4.38], the available energy for the formation of a new transverse crack between two existing cracks is then given by:

$$J = \frac{2U^*|_{L/2} - U^*|_L}{2h_1} \qquad [4.39]$$

Equation [4.39] expresses the change in energy between the two crack spacing configurations, and the factor 2 is used so that comparisons are made on the same material volume. Furthermore, assuming steady state crack growth, U^* in the above equation are evaluated per unit distance in the y-direction.

To evaluate the right hand side of [4.39], it is necessary to compute the energy at the two half crack spacings of L and $L/2$. This can be accomplished through integration of the stress distributions in equation [4.30]. For a crack spacing of L, the contribution due to normal stresses is given by:

$$U_\sigma^*(L) = 4h_1 \int_0^L \int_0^{\sigma_x^{(1)}} \tilde{\varepsilon}_x^{(1)}\left(\tilde{\sigma}_x^{(1)}\right) d\tilde{\sigma}_x^{(1)} dx + 4h_2 \int_0^L \int_0^{\sigma_x^{(2)}} \tilde{\varepsilon}_x^{(2)}\left(\tilde{\sigma}_x^{(2)}\right) d\tilde{\sigma}_x^{(2)} dx \qquad [4.40]$$

In addition, it is necessary to consider the contribution of the shearing stresses, $\tau_{xz}^{(i)}$ in both ply groups. The resulting equation is then :

$$U_\tau^*(L) = 4\int_0^L \int_0^{h_1} \int_0^{\tau_{xz}^{(1)}} \tilde{\gamma}_{xz}^{(1)}\left(\tilde{\tau}_{xz}^{(1)}\right) d\tilde{\tau}_{xz}^{(1)} dz dx + 4\int_0^L \int_{h_1}^{\bar{h}} \int_0^{\tau_{xz}^{(2)}} \tilde{\gamma}_{xz}^{(2)}\left(\tilde{\tau}_{xz}^{(2)}\right) d\tilde{\tau}_{xz}^{(2)} dz dx \qquad [4.41]$$

$$\text{Obviously,} \qquad U^* = U_\sigma^* + U_\tau^* \qquad [4.42]$$

To evaluate [4.40], it is necessary to express the strains in both ply groups in terms of stresses by means of the constitutive relation, [4.6]. In [4.41], the expression involves an additional integration since the shearing stress varies linearly with z as shown in equation [4.21]. Substitution of [4.6] into [4.40] gives:

$$U_\sigma^*(L) = 4h_1 \int_0^L \int_0^{\bar{\sigma}_x^{(1)}} \frac{\tilde{\sigma}_x^{(1)} - Q_{12}^{(1)}\bar{\varepsilon}_y}{Q_{11}^{(1)}} d\tilde{\sigma}_x^{(1)} dx + 4h_2 \int_0^L \int_0^{\bar{\sigma}_x^{(2)}} \frac{\tilde{\sigma}_x^{(2)} - Q_{12}^{(2)}\bar{\varepsilon}_y}{Q_{11}^{(2)}} d\tilde{\sigma}_x^{(2)} dx \qquad [4.43]$$

Carrying out the inner integration yields:

$$U_\sigma^*(L) = \frac{4h_1}{Q_{11}^{(1)}} \int_0^L \left(\frac{\left(\bar{\sigma}_x^{(1)}\right)^2}{2} - \bar{\sigma}_x^{(1)} Q_{12}^{(1)} \bar{\varepsilon}_y \right) dx + \frac{4h_2}{Q_{11}^{(2)}} \int_0^L \left(\frac{\left(\bar{\sigma}_x^{(2)}\right)^2}{2} - \bar{\sigma}_x^{(2)} Q_{12}^{(2)} \bar{\varepsilon}_y \right) dx \qquad [4.44]$$

The expressions for the stress distributions are then given in [4.30], and the final integration can be computed in a straightforward manner.

To compute the energy term due to shearing stresses, a similar approach is used, with an additional integration with respect to z. Recalling [4.21]:

$$\tau_{xz}^{(1)} = a(x)z \quad , \quad \tau_{xz}^{(2)} = a(x)h_1\left(\frac{\bar{h} - z}{\bar{h} - h_1}\right) \qquad [4.21]R$$

and noting the continuity of shearing stresses at the interface as given in equation [4.15]:

$$\tau_{xz}^{(1)}(x, z_1 = h_1) = \tau_{xz}^{(2)}(x, z_2 = 0) = \tau^*(x) \qquad [4.15]R$$

then, employing the known interfacial shearing stress $\tau^*(x)$ along with the first equation of [4.30] we have:

$$\begin{aligned} \tau_{xz}^{(1)} &= a(x)z = \frac{A_0 z \sinh(\alpha_0 x)}{h_1} \\ \tau_{xz}^{(2)} &= a(x)h_1\left(\frac{\bar{h} - z}{\bar{h} - h_1}\right) = A_0 \sinh(\alpha_0 x)\left(\frac{\bar{h} - z}{\bar{h} - h_1}\right) \end{aligned} \qquad [4.45]$$

Additionally, from the fifth of equations [4.2], we have:

$$\tau_{xz}^{(i)} = C_{55}^{(i)} \gamma_{xz}^{(i)} \qquad [4.9]R$$

Using these last two results in [4.41] and carrying out the integration gives:

$$U_\tau^* = \frac{2A_0^2}{3}\left(\frac{\sinh(2\alpha_0 L)}{4\alpha_0} - \frac{L}{2}\right)\left(\frac{h_1}{C_{55}^{(1)}} + \frac{h_2}{C_{55}^{(2)}}\right) \qquad [4.46]$$

4.3 Considerations of the Weak Fiber-Matrix Interface in Ceramic Matrix Composites

It is well known that the interface between the fiber and the matrix in ceramic composite materials is much weaker than that in polymeric composites. This characteristic feature of ceramic matrix composites is generally desirable since the weak interface gives rise to some of the energy absorbing mechanisms that contribute to the ductility of the composite. This weak interface has significant implications on the transverse toughness of ceramic matrix composites. For this purpose, consider the transverse crack in a cross-ply laminate as depicted in Figure 4.8 below.

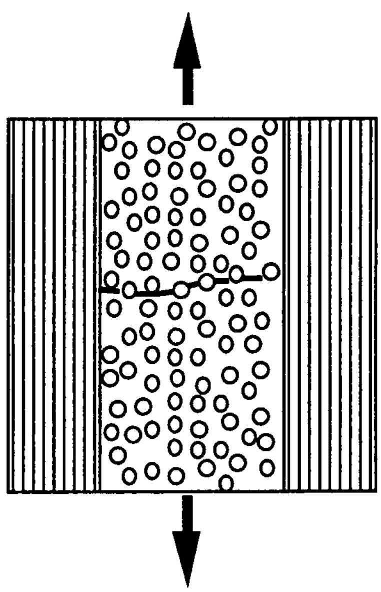

Figure 4.8 Transverse Crack and Fiber / Matrix Interface Interaction

This figure suggests that when a growing crack encounters a fiber, the weak interface provides a path that has less resistance to crack propagation than the matrix material without fibers. Hence, as the crack circumvents fibers, it expends less energy than it would growing through matrix material. This process of a crack growing around a fiber is idealized in Figure 4.9 below for the case of fibers evenly spaced at a distance, S :

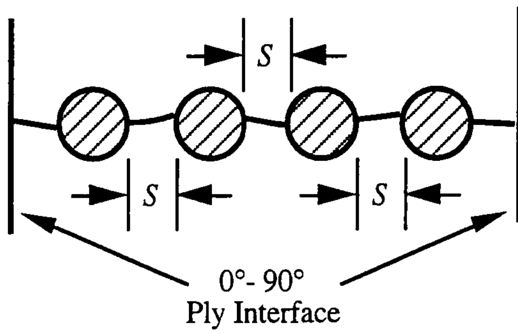

Figure 4.9 Detail of a Crack Growing Between Parallel Fibers

From simple geometric considerations, the relationship between the fiber spacing and radius can be related to the fiber volume fractions for various packing geometries, such as square and hexagonal arrays. For instance, for a square array the fiber spacing S is then given by:

$$S=2r\left\{\left(\frac{\pi}{4V_f}\right)^{\frac{1}{2}}-1\right\} \qquad [4.47]$$

Where r is the fiber radius and V_f is fiber volume fraction. Then for a typical fiber volume fraction of 40% for a Nicalon/CAS ceramic composite the fiber spacing is given as:

$$S=0.8025r\approx 0.4d \qquad [4.48]$$

Where d is the fiber diameter. Then if the fracture area is taken to be the distance between the fibers(assuming perfectly debonded fibers), the net fracture area becomes $S/(S+d) \approx 28\%$ of the original value, $2h_1$. This would imply that a lower bound on transverse toughness is given by $J_c^{90} = 0.28 J_c^m$, where J_c^{90} and J_c^m are the toughness of the 90° ply group and the neat matrix material respectively. It should be realized however that in reality the fibers are not aligned in a square array, and the interfacial strength at the fiber/matrix interface contributes to the transverse toughness, therefore it is reasonable to consider $J_c^{90} > 0.28 J_c^m$. Several values of fracture toughness will be employed in the subsequent parametric studies to explore this issue further.

4.4 Summary of Linear Analysis and Implementation

Equations [4.1] through [4.46] constitute the necessary expressions to determine the stress-strain response of the ceramic cross-ply laminate. These results are implemented by incrementing the far field applied stress , $\bar{\sigma}_x$, and carrying out simultaneous calculations for two crack spacings, $2L$ and L, at each fixed level of the applied stress $\bar{\sigma}_x$. This enables a comparison of energy at the two crack geometries. The analytical/computational scheme is as follows:

(1) Assume an initial crack spacing $2L$. This assumption may be guided by experimental observations, i. e., approximately one crack per inch.

(2) Consider some level of the far field stress, $\bar{\sigma}_x$, which is then incremented gradually. Increments of about one percent of the failure strength of the composite generate an acceptably dense stress-strain curve.

(3) Calculate the transverse strain from equation [4.33].

(4) Calculate the constants $\tau^{*}(L)$ and A_0 using equations [4.28] and [4.29].

(5) At this point the normal and the interfacial shearing stresses are known functions of x, given in equations [4.30]. Furthermore, the shearing stress component, $\tau_{xz}(x,z)$ is given by equations [4.21].

(6) Calculate the global strain for the composite using equation [4.35].

(7) It is now necessary to check if this applied stress can be sustained with the assumed crack spacing. This requires evaluating equations [4.43] and [4.46] with crack spacings of L and $2L$. The value of available energy is computed by equation [4.39] and compared against the transverse fracture toughness, J_{IC},, of the material.

(8i) If the available energy is less than the fracture toughness, then the assumed crack spacing of $2L$ is consistent with the applied stress. In this case, the global strain, which corresponds to the crack spacing, $2L$, as calculated in step 6, is valid and a new point on the stress-strain curve is obtained. At this stage it is necessary to increment the applied stress, $\overline{\sigma}_x$, and repeat the procedure to determine the next stress-strain value.

(8ii) If the available energy is equal to the fracture toughness, it is necessary to replace the current crack spacing, $2L$, by half its value, L, and repeat the process starting from step 1. The next comparison of energies will then involve geometries with crack spacings of L and $L/2$ for energy comparison.

(9) The analysis is terminated when the applied stress reaches the experimentally determined strength of the composite.

A case study is shown in Figure 4.10 below for a $[0_2/90_2]_s$ cross-ply lay-up:

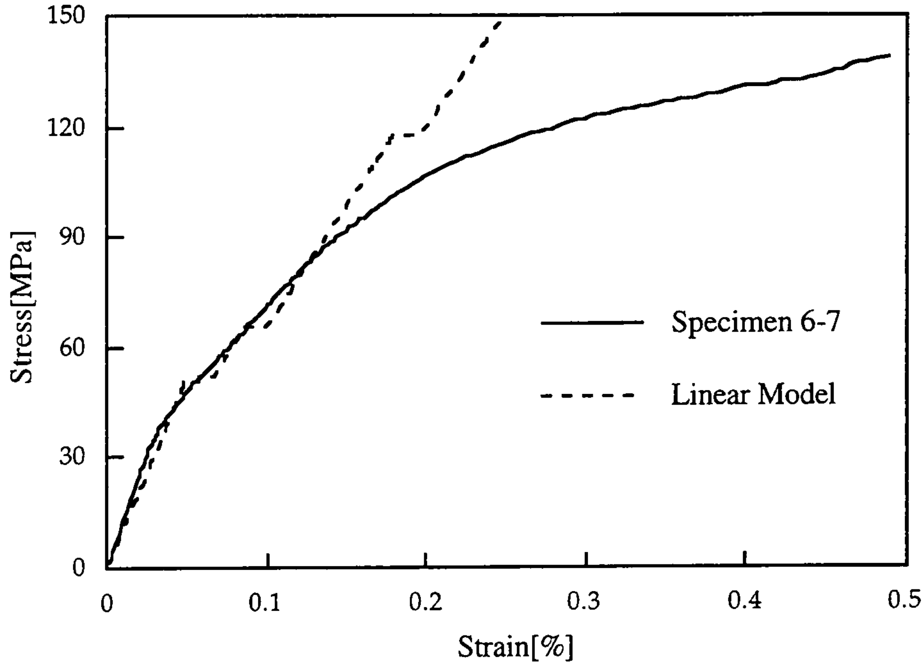

Figure 4.10 Comparison of Linear Model and Experimental Stress-Strain Response

It can be seen that at the earlier stages of loading the model predicts the stress-strain response of the laminate reasonably well. The first subdivision of transverse cracks occur at a stress level slightly above 50 MPa and there is a corresponding "jump" in the strain. After this point, there is a noticeable reduction of the slope of the curve, indicating that the overall stiffness of the laminate has been reduced due to the introduction of the transverse cracking in the 90° ply group. This process is repeated as the load is increased further, and the results from the model agree with the experimental data until the applied stress reaches about 100 MPa. At this point, the predicted and the experimental stress-strain curves diverge since the model predicts insufficient levels of available energy to introduce further cracks until $\overline{\sigma}_x$ reaches approximately 120 MPa. This discrepancy at the higher levels of loading demonstrates the inadequacy of the linear model in capturing the response of the laminate and the need to address the non-linearity in the 0° plies as discussed previously.

CHAPTER 5

MODIFIED SHEAR-LAG ANALYSIS FOR THE BILINEAR RESPONSE OF THE 0° PLIES

5.1 Introduction

Although the shear-lag analysis of Chapter 4 seems to show some prospect for correlating predicted stress-strain behavior with experimental results, it exhibits obvious shortcomings. The most noticeable discrepancy is the underestimation of the global strain at higher stress levels. This is not surprising considering that the linear analysis only addresses a single damage mechanism, transverse cracking in the 90° plies. Recalling the stress-strain response of the outer 0° ply group shown in Figure 3.11, it is obvious that the significant non-linearity in the response of those plies must be taken into account when trying to model the behavior of the cross-ply composite.

To simplify the formulation and computational work, the stress-strain curve for typical unidirectionally reinforced SiC/CAS is approximated by the bilinear behavior shown in Figure 5.1 below, where the bilinear stress-strain curve is indicated by the solid lines overlaying the experimental data. A "yield point", σ_0, is used to locate the onset of the nonlinear behavior, and a reduced modulus is then used then for stress levels above σ_0. A bilinear constitutive relation can then be defined in the following manner:

$$\begin{aligned} \bar{\sigma}_x^{(1)} &= Q_{11}^{(1)}\bar{u}_1' + Q_{12}^{(1)}\bar{\varepsilon}_y \\ \bar{\sigma}_y^{(i)} &= Q_{12}^{(i)}\bar{u}_i' + Q_{22}^{(i)}\bar{\varepsilon}_y \end{aligned} \qquad i=1,2$$

while

$$\begin{aligned} \bar{\sigma}_x^{(2)} &= Q_{11}^{(2)}\bar{u}_2' + Q_{12}^{(2)}\bar{\varepsilon}_y & (\bar{\sigma}_x^{(2)} \le \sigma_0) \\ \bar{\sigma}_x^{(2)} &= \tilde{Q}_{11}^{(2)}\bar{u}_2' + Q_{12}^{(2)}\bar{\varepsilon}_y + \hat{\sigma} & (\bar{\sigma}_x^{(2)} > \sigma_0) \end{aligned} \qquad [5.1]$$

and $$\hat{\sigma}=\sigma_0\left(1-\frac{\tilde{Q}_{11}^{(2)}}{Q_{11}^{(2)}}\right)$$

It should be noted that the stress in the outer plies is a function of x and may be greater than or less than σ_0, the "yield point", within the region $0 \le x \le L$. Considering conceivable stress distributions, it can be seen that three possibilities exist. This is demonstrated in the sequence of stress distributions sketched in Figure 5.2. The location where the stress, $\bar{\sigma}_x^{(2)}$, in the outer plies attains the level of σ_0 is given by x^*.

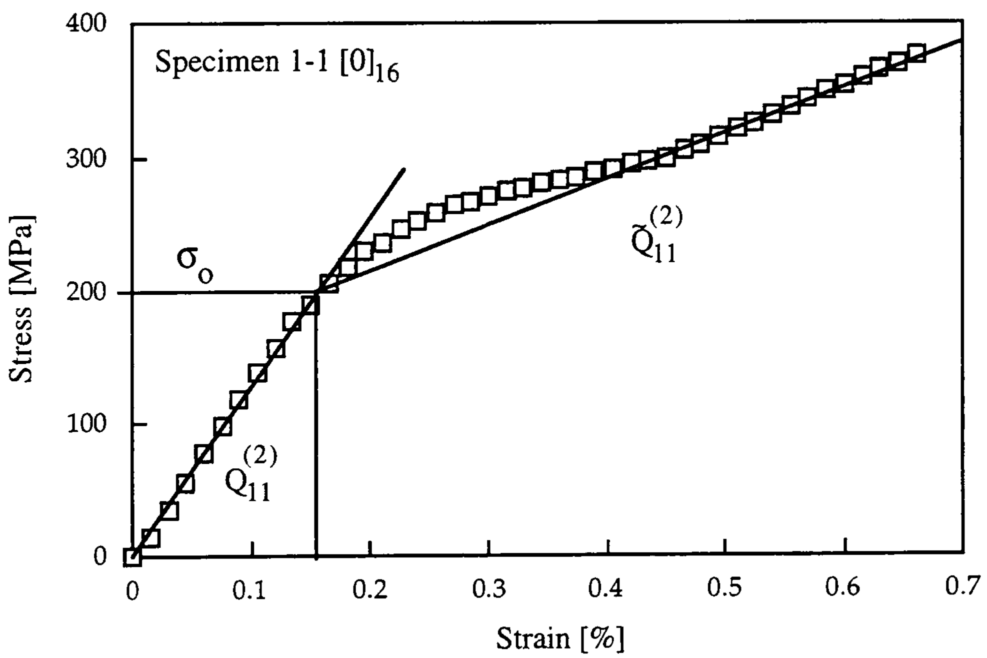

Figure 5.1 Bilinear Representation of the Unidirectional Stress-Strain Curve

Case (i) : $\bar{\sigma}_x^{(2)}$ is less than σ_0 throughout the domain, $(0 \le x \le L)$ and the first two equations in [5.1] will suffice.

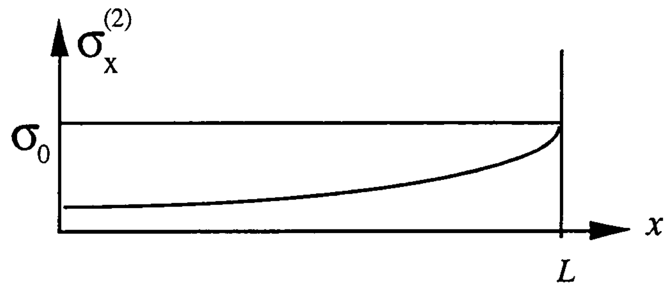

Case(i)

Case (ii) : $\bar{\sigma}_x^{(2)}$ is greater than σ_0 at $x{=}x^*$ and it is necessary to use the appropriate expression from [5.1] for $\bar{\sigma}_x^{(2)}$ to the left and right of the location, x^*.

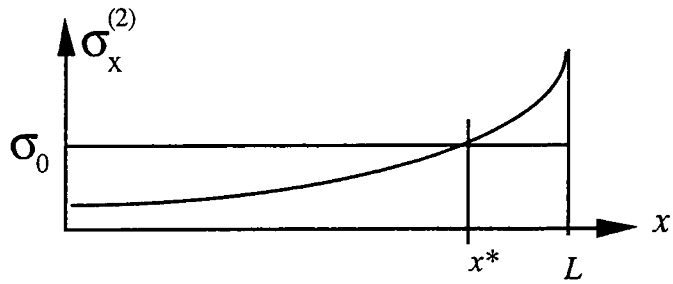

Case(ii)

Case (iii) : $\bar{\sigma}_x^{(2)}$ is greater than σ_0 for all x values, and only the second expression from [5.1] for $\bar{\sigma}_x^{(2)}$ needs to be considered.

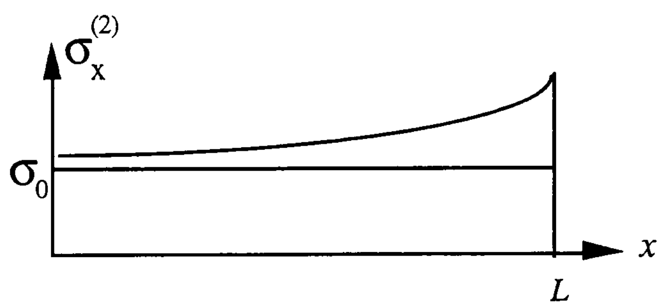

Case (iii)

Figure 5.2 Bilinear Stress Distributions

These three possible stress distributions depend on the level of the applied stress, $\bar{\sigma}_x$. It is thus necessary to consider three distinct solutions for the case of the bilinear behavior of the 0° plies. With these possible stress distributions in mind, it is advantageous to rewrite equations [5.1] in terms of position in the following manner :

$$
\begin{aligned}
&\bar{\sigma}_x^{(1)} = Q_{11}^{(1)}\bar{u}_1' + Q_{12}^{(1)}\bar{\varepsilon}_y && \\
&\bar{\sigma}_y^{(i)} = Q_{12}^{(i)}\bar{u}_i' + Q_{22}^{(i)}\bar{\varepsilon}_y && (0 \le x \le L) \\
&\bar{\sigma}_x^{(2)} = Q_{11}^{(2)}\bar{u}_2' + Q_{12}^{(2)}\bar{\varepsilon}_y && (0 \le x < x^*) \\
&\bar{\sigma}_x^{(2)} = \tilde{Q}_{11}^{(2)}\bar{u}_2' + Q_{12}^{(2)}\bar{\varepsilon}_y + \hat{\sigma} && (x^* \le x \le L)
\end{aligned}
\qquad [5.2]
$$

where $\hat{\sigma} = \sigma_0\left(1 - \dfrac{\tilde{Q}_{11}^{(2)}}{Q_{11}^{(2)}}\right)$

5.2 Case (i), $\bar{\sigma}_x^{(2)} < \sigma_0$, for all locations, $(0 \le x \le L)$

For this situation the stress in the outer plies is less than the yield stress throughout the entire domain and the linear analysis of Chapter 4 applies. Since the stress distribution, $\bar{\sigma}_x^{(2)}$, is calculated for each small increment in applied stress, and $\bar{\sigma}_x^{(2)}$ attains its maximum at $x{=}L$, it is a relatively simple matter to determine the applied stress level where the onset of non-linearity occurs and the linear analysis is no longer valid.

5.3 Case (ii), $\bar{\sigma}_x^{(2)} \ge \sigma_0$, $(0 \le x^* \le L)$

In this circumstance it is necessary to consider two separate solutions within the regions $0 \le x < x^*$ and $x^* \le x \le L$, respectively. The procedure to determine the governing differential equations parallels that for the linear analysis, however at each step involving the constitutive relation in the outer plies, the appropriate expression from equation [5.2] must be employed, providing the required modifications to the solution procedure.

The equilibrium equations remain unchanged since they are independent of the constitutive relations. Hence:

$$\bar{\sigma}_x'^{(1)} = \frac{\tau^*(x)}{-h_1} \qquad [4.5i]R$$

$$\bar{\sigma}_x'^{(2)} = \frac{\tau^*(x)}{h_2} \qquad [4.5ii]R$$

$$\bar{\sigma}_x^{(1)} h_1 + \bar{\sigma}_x^{(2)} h_2 = \bar{\sigma}_x \bar{h} \qquad [4.5iii]R$$

Since the shear response is assumed to remain linear, and since the condition of no interfacial slip between the plies still holds, we retain the relation :

$$\tau^* = A_{55}\left(\frac{\bar{u}_2 - \bar{u}_1}{\bar{h}}\right) \quad \text{where} \quad A_{55} = \frac{3\bar{h} C_{55}^{(1)} C_{55}^{(2)}}{h_1 C_{55}^{(2)} + h_2 C_{55}^{(1)}} \qquad [4.20]R$$

Differentiating [5.2] once with respect to x gives :

$$\begin{aligned} \bar{\sigma}_x'^{(1)} &= Q_{11}^{(1)} \bar{u}_1'' && (0 \le x < x^*) \\ \bar{\sigma}_x'^{(2)} &= Q_{11}^{(2)} \bar{u}_2'' && (0 \le x < x^*) \\ \bar{\sigma}_x'^{(2)} &= \tilde{Q}_{11}^{(2)} \bar{u}_2'' && (x^* \le x < L) \end{aligned} \qquad [5.3]$$

Upon differentiating [4.20] twice and employing [4.5] and [5.3] one obtains:

$$\begin{aligned} \tau''^* - \alpha_0^2 \tau^* = 0, &\quad \alpha_0^2 = \frac{A_{55}}{\bar{h}}\left(\frac{1}{h_1 Q_{11}^{(1)}} + \frac{1}{h_2 Q_{11}^{(2)}}\right) \quad (0 \le x < x^*) \\ \tau''^* - \alpha_1^2 \tau^* = 0, &\quad \alpha_1^2 = \frac{A_{55}}{\bar{h}}\left(\frac{1}{h_1 Q_{11}^{(1)}} + \frac{1}{h_2 \tilde{Q}_{11}^{(2)}}\right) \quad (x^* \le x \le L) \end{aligned} \qquad [5.4]$$

To solve these two equations, the following boundary conditions must be considered:

At $x=0, \tau^* = 0$ due to symmetry. [5.5i]

At $x=L, \bar{\sigma}_x^{(1)} = 0$ since the crack face must be stress free. [5.5ii]

At $x{=}x^*, \bar{\sigma}_x^{(2)} = \sigma_0$ defined as the point where yielding occurs. [5.5iii]

However, in view of [4.5iii], the last boundary condition can be expressed in terms of $\bar{\sigma}_x^{(1)}$ to read:

$$\bar{\sigma}_x^{(1)}(x^*) = \frac{\bar{\sigma}_x \bar{h} - \sigma_0 h_2}{h_1} \qquad [5.5iv]$$

Since the interfacial shearing stress, τ^*, should be continuous at $x{=}x^*$ (though the slope, τ'^*, may be discontinuous at x*) the following relation is utilized to match the shearing stresses when solving [5.4]:

$$\text{At } x{=}x^*,\ \tau^*(x^*{+}) = \tau^*(x^*{-}) \qquad [5.5v]$$

Solving the first differential equation in the region $(0 \le x < x^*)$ and using [5.5i]:

$$\tau^*(x) = A_0 \sinh(\alpha_0 x) \qquad [5.6]$$

Taking one derivative of [4.20] and evaluating at $x{=}x^*$:

$$\tau'^*(x^*) = A_{55}\left(\frac{\bar{u}_2'(x^*) - \bar{u}_1'(x^*)}{\bar{h}}\right) \qquad [5.7]$$

For $0 \le x < x^*$, the constitutive relation in [5.2] yields:

$$\bar{u}_1'(x^*) = \frac{1}{Q_{11}^{(1)}}\left(\bar{\sigma}_x^{(1)}(x^*) - Q_{12}^{(1)}\bar{\varepsilon}_y\right)$$
$$\bar{u}_2'(x^*) = \frac{1}{Q_{11}^{(2)}}\left(\bar{\sigma}_x^{(2)}(x^*) - Q_{12}^{(2)}\bar{\varepsilon}_y\right) \qquad [5.8]$$

Substituting this expression back into [5.7] and using the boundary conditions [5.5iii] and [5.5iv] we get :

$$\tau'^*(x^*) = \frac{A_{55}}{\bar{h}Q_{11}^{(1)}Q_{11}^{(2)}}\left(\sigma_0\left(Q_{11}^{(1)} + \frac{h_2}{h_1}Q_{11}^{(2)}\right) + \bar{\varepsilon}_y\left(Q_{12}^{(1)}Q_{11}^{(2)} - Q_{12}^{(2)}Q_{11}^{(1)}\right) - \frac{\bar{\sigma}_x\bar{h}Q_{11}^{(2)}}{h_1}\right) \qquad [5.9]$$

Now, differentiation of [5.6] and evaluating at $x=x^*$ upon comparison with [5.9] results in the following expression for A_0 :

$$A_0 = k_1\left(k_2 - k_3\bar{\sigma}_x + k_4\bar{\varepsilon}_y\right) \qquad [5.10]$$

where

$$k_1 = \frac{A_{55}}{\bar{h}\alpha_0 Q_{11}^{(1)}Q_{11}^{(2)}\cosh(\alpha_0 x^*)}$$
$$k_2 = \sigma_0\left(Q_{11}^{(1)} + \frac{h_2}{h_1}Q_{11}^{(2)}\right)$$
$$k_3 = \frac{\bar{h}Q_{11}^{(2)}}{h_1}$$
$$k_4 = \left(Q_{12}^{(1)}Q_{11}^{(2)} - Q_{12}^{(2)}Q_{11}^{(1)}\right)$$

With A_0 determined, an expression for $\tau^*(x)$ within the range $0 \le x < x^*$ is at hand. It is now possible to determine the normal stresses by integrating [4.5] with respect to x, and the constants of integration are found with the aid of the boundary conditions in [5.5iii] and [5.5iv]. Then the stress distribution in the region $\underline{0 \le x < x^*}$ is given by:

$$\tau^*(x)=A_0\sinh(\alpha_0 x)$$
$$\overline{\sigma}_x^{(1)}=\frac{\overline{\sigma}_x\overline{h}}{h_1}-\frac{\sigma_0 h_2}{h_1}+\frac{A_0}{h_1\alpha_0}\left(\cosh(\alpha_0 x^*)-\cosh(\alpha_0 x)\right) \qquad [5.11]$$
$$\overline{\sigma}_x^{(2)}=\frac{\overline{\sigma}_x\overline{h}}{h_2}-\frac{\overline{\sigma}_x^{(1)}h_1}{h_2}$$

It should be noted that at this stage, equations [5.11] still contain two unknown parameters namely, x* and $\overline{\varepsilon}_y$ (note that A_0 is given in terms of $\overline{\varepsilon}_y$ in [5.10]).

To determine the stress distributions in the region $x^* \le x \le L$, consider the second differential equation in [5.4], with the solution:

$$\tau^*(x)=A_1\sinh(\alpha_1 x)+B_1\cosh(\alpha_1 x) \qquad [5.12]$$

Note that in the absence of a symmetry condition as in the preceding solution, both constants A_1 and B_1 must be determined. These constants can be evaluated with the aid of the two remaining boundary conditions in [5.5], which were not used thus far :

At $x=L$, $\overline{\sigma}_x^{(1)}=0$, since the crack face must be stress free. [5.5ii]R

At $x=x^*$, $\tau^*(x^*+)=\tau^*(x^*-)$, due to continuity of $\tau^*(x)$. [5.5v]R

Upon matching the expressions in [5.12] and [5.6] at x^*, the condition of [5.5v] yields the following relation:

$$A_1\sinh(\alpha_1 x^*)+B_1\cosh(\alpha_1 x^*)=A_0\sinh(\alpha_0 x^*) \qquad [5.13]$$

To utilize [5.5ii], take one derivative of [4.20] with respect to x and evaluate at $x=L$:

$$\tau'^{*}(L) = A_{55}\left(\frac{\overline{u}_2'(L) - \overline{u}_1'(L)}{\overline{h}}\right) \qquad [5.14]$$

In view of [5.2] we have:

$$\begin{aligned} \overline{u}_1'(L) &= \frac{1}{Q_{11}^{(1)}}\left(\overline{\sigma}_x^{(1)}(L) - Q_{12}^{(1)}\overline{\varepsilon}_y\right) \\ \overline{u}_2'(L) &= \frac{1}{\tilde{Q}_{11}^{(2)}}\left(\overline{\sigma}_x^{(2)}(L) - Q_{12}^{(2)}\overline{\varepsilon}_y - \hat{\sigma}\right) \end{aligned} \qquad [5.15]$$

Substitution of [5.15] into [5.14] and employment of the boundary condition [5.5ii] yields:

$$\tau'^{*}(L) = \frac{A_{55}}{\overline{h}}\left\{\frac{\overline{\sigma}_x\overline{h}}{\tilde{Q}_{11}^{(2)}h_2} + \overline{\varepsilon}_y\left(\frac{Q_{12}^{(1)}}{Q_{11}^{(1)}} - \frac{Q_{12}^{(2)}}{\tilde{Q}_{11}^{(2)}}\right) - \frac{\hat{\sigma}}{\tilde{Q}_{11}^{(2)}}\right\} \qquad [5.16]$$

This expression can be written in a more compact form as:

$$\tau'^{*}(L) = k_5\overline{\sigma}_x + k_6\overline{\varepsilon}_y - k_7 \qquad [5.17]$$

where

$$k_5 = \frac{A_{55}}{\tilde{Q}_{11}^{(2)}h_2}$$

$$k_6 = \frac{A_{55}}{\overline{h}}\left(\frac{Q_{12}^{(1)}}{Q_{11}^{(1)}} - \frac{Q_{12}^{(2)}}{\tilde{Q}_{11}^{(2)}}\right)$$

$$k_7 = \frac{A_{55}}{\overline{h}}\frac{\hat{\sigma}}{\tilde{Q}_{11}^{(2)}}$$

Differentiation of [5.12] with respect to x evaluated at $x=L$, and comparison with [5.17] then results in:

$$A_1\alpha_1\cosh(\alpha_1 L) + B_1\alpha_1\sinh(\alpha_1 L) = k_5\overline{\sigma}_x + k_6\overline{\varepsilon}_y - k_7 \qquad [5.18]$$

Now note that equations [5.13] and [5.18] are a set of linear equations in A_1 and B_1 which can be written in matrix form. Upon inversion, we have:

$$\begin{Bmatrix} A_1 \\ B_1 \end{Bmatrix} = \frac{1}{D}\begin{bmatrix} \cosh(\alpha_1 x^*) & -\alpha_1 \sinh(\alpha_1 L) \\ -\sinh(\alpha_1 x^*) & \alpha_1 \cosh(\alpha_1 L) \end{bmatrix} \begin{Bmatrix} k_5\bar{\sigma}_x + k_6\bar{\varepsilon}_y - k_7 \\ A_0 \sinh(\alpha_0 x^*) \end{Bmatrix} \qquad [5.19]$$

where $\qquad D = \alpha_1 \cosh\left(\alpha_1 (L - x^*)\right)$

Thus A_1 and B_1 are given in terms of $\bar{\varepsilon}_y$ and x^*. Recall that A_0 in equation [5.10] is also given explicitly in terms of $\bar{\varepsilon}_y$ and x^*, hence there are four unknown parameters, A_1, B_1, $\bar{\varepsilon}_y$ and x^*, and two independent linear equations in [5.19]. To get a solution to this system of equations, two additional conditions are needed.

Before turning to the details, note that the stress distribution within the region $x^* \le x \le L$ can be calculated once the constants A_1 and B_1 are known. The stress distributions are determined by integrating [5.12] as indicated by the equilibrium conditions in [4.5]. Carrying out the integrations and using the stress free boundary condition in [5.5ii], the stress distributions in the region $\underline{(x^* \le x \le L)}$ read:

$$\begin{aligned} \tau^*(x) &= A_1 \sinh(\alpha_1 x) + B_1 \cosh(\alpha_1 x) \\ \bar{\sigma}_x^{(1)} &= \frac{1}{h_1 \alpha_1}\left\{A_1\left(\cosh(\alpha_1 L) - \cosh(\alpha_1 x)\right) + B_1\left(\sinh(\alpha_1 L) - \sinh(\alpha_1 x)\right)\right\} \qquad [5.20] \\ \bar{\sigma}_x^{(2)} &= \frac{\bar{\sigma}_x \bar{h}}{h_2} - \frac{\bar{\sigma}_x^{(1)} h_1}{h_2} \end{aligned}$$

Returning to the two additional conditions required for determining the foregoing four unknown parameters, note that the condition $\bar{\sigma}_x^{(2)} = \sigma_0$ at $x = x^*$ must also hold for the expression for $\bar{\sigma}_x^{(2)}$ in the region $x^* \le x \le L$ given in equation [5.20]. Furthermore, the global equilibrium condition in the y-direction, which remains the same as in [4.31], gives:

$$\bar{\sigma}_y \bar{h} L = h_1 \int_0^L \bar{\sigma}_y^{(1)} dx + h_2 \int_0^L \bar{\sigma}_y^{(2)} dx = 0 \qquad [4.31]R$$

Recall from equation [4.6] that the constitutive relation for the transverse stresses was given by:

$$\begin{aligned} \bar{\sigma}_y^{(1)} &= Q_{12}^{(1)} \bar{u}_1' + Q_{22}^{(1)} \bar{\varepsilon}_y \\ \bar{\sigma}_y^{(2)} &= Q_{12}^{(2)} \bar{u}_2' + Q_{22}^{(2)} \bar{\varepsilon}_y \end{aligned} \qquad [4.6]R$$

Substituting equation [5.2] into [4.6] it is possible to express the transverse stresses, $\bar{\sigma}_y^{(i)}$ in terms of the longitudinal stresses $\bar{\sigma}_x^{(i)}$. Note, however that $\bar{\sigma}_y^{(2)}$ will now be given by two distinct expressions over the two regions $0 \le x \le x^*$ and $x^* \le x \le L$. Carrying out the substitution, the following result is obtained:

$$\begin{aligned} \bar{\sigma}_y^{(1)} &= C_1 \bar{\sigma}_x^{(1)} + C_2 \bar{\varepsilon}_y \\ \bar{\sigma}_y^{(2)} &= C_3 \bar{\sigma}_x^{(2)} + C_4 \bar{\varepsilon}_y \qquad (0 \le x < x^*) \\ \bar{\sigma}_y^{(2)} &= C_5 \bar{\sigma}_x^{(2)} + C_6 \bar{\varepsilon}_y - C_7 \quad (x^* \le x \le L) \end{aligned} \qquad [5.21]$$

where

$$\begin{aligned} C_1 &= Q_{12}^{(1)} / Q_{11}^{(1)} \\ C_2 &= Q_{22}^{(1)} - \left(Q_{12}^{(1)}\right)^2 / Q_{11}^{(1)} \\ C_3 &= Q_{12}^{(2)} / Q_{11}^{(2)} \\ C_4 &= Q_{22}^{(2)} - \left(Q_{12}^{(2)}\right)^2 / Q_{11}^{(2)} \\ C_5 &= Q_{12}^{(2)} / \tilde{Q}_{11}^{(2)} \\ C_6 &= Q_{22}^{(2)} - \left(Q_{12}^{(2)}\right)^2 / \tilde{Q}_{11}^{(2)} \\ C_7 &= Q_{12}^{(2)} \hat{\sigma} / \tilde{Q}_{11}^{(2)} \end{aligned}$$

These expressions can now be substituted back into [4.31] to carry out the integration. It should be noted however that the integration must be split between the two ranges noted in [5.21] employing the appropriate expressions for $\bar{\sigma}_x^{(2)}$ from [5.11] and [5.20]. Further manipulations and regrouping of results give the following expression for $\bar{\varepsilon}_y$ in terms of x^*:

$$\bar{\varepsilon}_y = \frac{\left\{\begin{array}{l} h_2 C_7(L-x^*) + h_1\left[C_3\beta_6 + C_5\beta_9 - C_1(\beta_6+\beta_9)\right] \\ -\bar{\sigma}_x\left[h_1 C_1(\beta_4+\beta_7) - h_1 C_3\beta_4 + \bar{h}C_3 x^* + \bar{h}C_5(L-x^*) - h_1 C_5\beta_7\right] \end{array}\right\}}{\left\{h_1\left(C_2 L + C_1(\beta_5+\beta_8) - C_3\beta_5 - C_5\beta_8\right) + h_2\left(C_4 x^* + C_6(L-x^*)\right)\right\}} \qquad [5.22]$$

where

$$\beta_1 = x^*\cosh(\alpha_0 x^*) - \sinh(\alpha_0 x^*)/\alpha_0$$
$$\beta_2 = (L-x^*)\cosh(\alpha_1 L) - \sinh(\alpha_1 L)/\alpha_1 + \sinh(\alpha_1 x^*)/\alpha_1$$
$$\beta_3 = (L-x^*)\sinh(\alpha_1 L) - \cosh(\alpha_1 L)/\alpha_1 + \cosh(\alpha_1 x^*)/\alpha_1$$

and

$$\beta_4 = \frac{\bar{h}x^*}{h_1} - \frac{k_1 k_3 \beta_1}{h_1\alpha_0} \qquad \beta_7 = \frac{\gamma_1\beta_2 + \gamma_4\beta_3}{h_1\alpha_1}$$
$$\beta_5 = \frac{k_1 k_4 \beta_1}{h_1\alpha_0} \qquad \beta_8 = \frac{\gamma_2\beta_2 + \gamma_5\beta_3}{h_1\alpha_1}$$
$$\beta_6 = \frac{k_1 k_2 \beta_1}{h_1\alpha_0} - \frac{\sigma_0 h_2 x^*}{h_1} \qquad \beta_9 = \frac{\gamma_3\beta_2 + \gamma_6\beta_3}{h_1\alpha_1}$$

$$\begin{Bmatrix}\gamma_1\\ \gamma_2\\ \gamma_3\end{Bmatrix} = \frac{1}{D}\begin{bmatrix} k_5 & k_1 k_3 \alpha_1 \\ k_6 & -k_1 k_4 \alpha_1 \\ -k_7 & -k_1 k_2 \alpha_1 \end{bmatrix}\begin{Bmatrix}\cosh(\alpha_1 x^*)\\ \sinh(\alpha_1 L)\sinh(\alpha_0 x^*)\end{Bmatrix}$$

$$\begin{Bmatrix}\gamma_4\\ \gamma_5\\ \gamma_6\end{Bmatrix} = \frac{1}{D}\begin{bmatrix} -k_5 & -k_1 k_3 \alpha_1 \\ -k_6 & k_1 k_4 \alpha_1 \\ k_7 & k_1 k_2 \alpha_1 \end{bmatrix}\begin{Bmatrix}\sinh(\alpha_1 x^*)\\ \cosh(\alpha_1 L)\sinh(\alpha_0 x^*)\end{Bmatrix}$$

$$D = \alpha_1\cosh\left(\alpha_1(L-x^*)\right)$$

Examination of equation [5.23] reveals that all terms on the right hand side are constants or functions of x*, defined above. Therefore $\bar{\varepsilon}_y$ is given in terms of x^*, and all that remains at this stage to complete the solution is to determine x^*.

To determine x^*, an iterative root finding scheme is employed using the fact that at x^* the value of $\bar{\sigma}_x^{(2)}$ must equal the yield stress, σ_0. The following procedure is then employed:

step (1) Guess an x^* within the region $(0 \leq x^* \leq L)$.

step (2) Calculate all constant parameters listed subsequent to [5.22].

step (3) Calculate $\bar{\varepsilon}_y$ from [5.22].

step (4) Calculate A_0, A_1, B_1 in equations [5.10] and [5.19].

step (5) Calculate $\bar{\sigma}_x^{(2)}(x^*)$ employing [5.20].

step (6) Check if $\bar{\sigma}_x^{(2)}(x^*) = \sigma_0$. If so, then x^* has been located. If not, iterate by choosing another x^* location in step (1) and repeat the process.

It should be noted that a systematic iterative procedure employing a bisection algorithm is used to determine x^*, resulting in rapid convergence. This iterative method is discussed in detail in references [62,65].

To complete this solution, it is necessary to determine the global strain, $\bar{\varepsilon}_x$. This is done similarly to the linear case, however since there are now two constitutive relations on the region $(0 \leq x \leq L)$, it is necessary to split up the integral used to determine the global strain. Employing equation [5.2], the following result is obtained:

$$\bar{\varepsilon}_x = \frac{\bar{u}_2(L)}{L} = \frac{1}{L}\left\{\int_0^{x^*} \frac{\bar{\sigma}_x^{(2)} - Q_{12}^{(2)}\bar{\varepsilon}_y}{Q_{11}^{(2)}} dx + \int_{x^*}^{L} \frac{\bar{\sigma}_x^{(2)} - \bar{Q}_{12}^{(2)}\bar{\varepsilon}_y - \hat{\sigma}}{\tilde{Q}_{11}^{(2)}} dx\right\} \qquad [5.23]$$

Inserting the expressions for $\bar{\sigma}_x^{(2)}$, once again using the appropriate expressions in the two regions from equations [5.11] and [5.20], and carrying out the integration gives the following result:

$$\bar{\varepsilon}_x = \frac{1}{Q_{11}^{(2)} L}\left\{\sigma_0 x^* - \frac{A_0}{h_2\alpha_0}\left(x^*\cosh(\alpha_0 x^*) - \sinh(\alpha_0 x^*)/\alpha_0\right) - Q_{12}^{(2)}\bar{\varepsilon}_y x^*\right\} \qquad [5.24]$$

$$+\frac{1}{\tilde{Q}_{11}^{(2)} L}\left\{\begin{array}{l} \dfrac{\bar{\sigma}_x \bar{h}(L-x^*)}{h_2} - \dfrac{1}{h_2\alpha_1}\left[\begin{array}{l} A_1\left((L-x^*)\cosh(\alpha_1 L) - \sinh(\alpha_1 L)/\alpha_1 + \sinh(\alpha_1 x^*)/\alpha_1\right) \\ +B_1\left((L-x^*)\sinh(\alpha_1 L) - \cosh(\alpha_1 L)/\alpha_1 + \cosh(\alpha_1 x^*)/\alpha_1\right) \end{array}\right] \\ -(Q_{12}^{(2)}\bar{\varepsilon}_y + \hat{\sigma})(L-x^*) \end{array}\right\}$$

5.4 Case (iii), $\bar{\sigma}_x^{(2)} \geq \sigma_0$, $(0 \leq x \leq L)$

This case resembles the linear solution since the entire field between the cracks has yielded, and then x^* is effectively located at x=0. This results in solving a single differential equation, namely the second of equations [5.4] which gives:

$$\tau''^* - \alpha_1^2\tau^* = 0, \quad \alpha_1^2 = \frac{A_{55}}{\bar{h}}\left(\frac{1}{h_1 Q_{11}^{(1)}} + \frac{1}{h_2\tilde{Q}_{11}^{(2)}}\right) \quad (0 \leq x \leq L) \qquad [5.4]\text{R}$$

The boundary conditions are the same as for the linear case, the only departure from the linear solution is that the fourth equation of [5.2] must be employed for the response of the 0° plies, resulting in the following stress distribution:

$$\begin{aligned} \tau^*(x) &= A_1\sinh(\alpha_1 x) \\ \bar{\sigma}_x^{(1)}(x) &= \frac{A_1}{h_1\alpha_1}\left(\cosh(\alpha_1 L) - \cosh(\alpha_1 x)\right) \qquad [5.25] \\ \bar{\sigma}_x^{(2)}(x) &= \frac{\bar{\sigma}_x \bar{h} - \bar{\sigma}_x^{(1)} h_1}{h_2} \end{aligned}$$

where $\quad A_1 = k_1\left(k_2\bar{\sigma}_x + k_3\bar{\varepsilon}_y - k_4\right)$

with

$$k_1 = \frac{A_{55}}{\bar{h}\,\alpha_1 \cosh(\alpha_1 L)}$$

$$k_2 = \frac{\bar{h}}{h_2 \tilde{Q}_{11}^{(2)}}$$

$$k_3 = \frac{Q_{12}^{(1)}}{Q_{11}^{(1)}} - \frac{Q_{12}^{(2)}}{\tilde{Q}_{11}^{(2)}}$$

$$k_4 = \frac{\hat{\sigma}}{\tilde{Q}_{11}^{(2)}}$$

Once again, the constant A_1 is given in terms of transverse strain, which is determined from equilibrium in the y-direction, giving the following result:

$$\bar{\varepsilon}_y = \frac{C_7 h_2 L + k_1 k_4 \beta_1 - \bar{\sigma}_x (C_5 \bar{h} L + k_1 k_2 \beta_1)}{k_1 k_3 \beta_1 + L(C_2 h_1 + C_6 h_2)} \qquad [5.26]$$

where

$$\beta_1 = \frac{(C_1 - C_5)}{\alpha_1}\left(L\cosh(\alpha_1 L) - \sinh(\alpha_1 L)/\alpha_1\right)$$

and the constants C_i are given in [5.21].

The global strain is again determined according to the same procedure as in the previous cases. Upon integration of the constitutive relation for the 0° plies we get :

$$\bar{\varepsilon}_x = \frac{\bar{u}_2(L)}{L} = \frac{1}{\tilde{Q}_{11}^{(2)}}\left\{\frac{\bar{\sigma}_x \bar{h}}{h_2} - \frac{A_1}{h_2 \alpha_1}\left(\cosh(\alpha_1 L) - \frac{\sinh(\alpha_1 L)}{\alpha_1 L}\right) - (Q_{12}^{(2)} \bar{\varepsilon}_y + \hat{\sigma})\right\} \qquad [5.27]$$

5.5 Calculation of Available Energy for Crack Growth with Bilinear Response

Once the expressions for stress distributions are at hand, they can be incorporated within equations [4.40] and [4.41] to calculate levels of available fracture energy. However, since there are three solutions in the bilinear case, it is required to calculate the energy available for crack formation for each case separately. Recalling the solutions for the stress distributions in the bilinear case, the evaluation of the integrals in [4.40] and [4.41] becomes more complex than in the linear analysis of Chapter 4 due to the presence of multiple expressions for the stress distributions within the domain $0 \le x \le L$.

As noted earlier, sub-case(i) of the bilinear solution coincides with the linear case, and the procedure for the energy calculation is identical to that given in section 4.2.

5.5.1 Energy Calculation for Bilinear Response, Case(ii)

For this case, there are two distinct stress distributions within the intervals $0 \le x < x^*$ and $x^* \le x \le L$ (see Figure 5.2). To compute the complementary energy, recall equations [4.40], [4.41] and [5.2]:

$$U_{\sigma}^{*}(L) = 4h_1 \int_0^L \int_0^{\sigma_x^{(1)}} \tilde{\varepsilon}_x^{(1)}\left(\tilde{\sigma}_x^{(1)}\right) d\tilde{\sigma}_x^{(1)} dx + 4h_2 \int_0^L \int_0^{\sigma_x^{(2)}} \tilde{\varepsilon}_x^{(2)}\left(\tilde{\sigma}_x^{(2)}\right) d\tilde{\sigma}_x^{(2)} dx \qquad \text{[4.40]R}$$

$$U_{\tau}^{*}(L) = 4\int_0^L \int_0^{h_1} \int_0^{\tau_{xz}^{(1)}} \tilde{\gamma}_{xz}^{(1)}\left(\tilde{\tau}_{xz}^{(1)}\right) d\tilde{\tau}_{xz}^{(1)} dz dx + 4\int_0^L \int_{h_1}^{\bar{h}} \int_0^{\tau_{xz}^{(2)}} \tilde{\gamma}_{xz}^{(2)}\left(\tilde{\tau}_{xz}^{(2)}\right) d\tilde{\tau}_{xz}^{(2)} dz dx \qquad \text{[4.41]R}$$

$$\overline{\sigma}_x^{(1)} = Q_{11}^{(1)}\overline{u}_1' + Q_{12}^{(1)}\overline{\varepsilon}_y \qquad (0 \le x \le L)$$

$$\overline{\sigma}_x^{(2)} = Q_{11}^{(2)}\overline{u}_2' + Q_{12}^{(2)}\overline{\varepsilon}_y \qquad (0 \le x < x^*)$$

$$\overline{\sigma}_x^{(2)} = \tilde{Q}_{11}^{(2)}\overline{u}_2' + Q_{12}^{(2)}\overline{\varepsilon}_y + \hat{\sigma} \qquad (x^* \le x \le L) \qquad [5.2]R$$

$$\hat{\sigma} = \sigma_0\left(1 - \frac{\tilde{Q}_{11}^{(2)}}{Q_{11}^{(2)}}\right)$$

Focusing on the calculation of complementary energy due the normal stresses, split [4.40] as follows:

$$U_\sigma^*(L) = I_1 + I_2$$

where

$$I_1 = 4h_1\int_0^L\int_0^{\sigma_x^{(1)}} \tilde{\varepsilon}_x^{(1)}\left(\tilde{\sigma}_x^{(1)}\right)d\tilde{\sigma}_x^{(1)}dx \qquad [5.28]$$

$$I_2 = 4h_2\int_0^L\int_0^{\sigma_x^{(2)}} \tilde{\varepsilon}_x^{(2)}\left(\tilde{\sigma}_x^{(2)}\right)d\tilde{\sigma}_x^{(2)}dx$$

Note that I_1 and I_2 represent the energy contribution in the 90° and 0° plies, respectively. Since the integral I_1 relates to the linear, 90° ply group, the constitutive relation given in [5.2] remains unchanged throughout the region $0 \le x \le L$. Employing the first of equations [5.2] yields:

$$I_1 = \frac{4h_1}{Q_{11}^{(1)}}\int_0^L\int_0^{\sigma_x^{(1)}}\left(\tilde{\sigma}_x^{(1)} - Q_{12}^{(1)}\overline{\varepsilon}_y\right)d\tilde{\sigma}_x^{(1)}dx \qquad [5.29]$$

Which, upon carrying out the inner integration gives:

$$I_1 = \frac{4h_1}{Q_{11}^{(1)}}\int_0^L\left(\frac{\left(\overline{\sigma}_x^{(1)}\right)^2}{2} - \overline{\sigma}_x^{(1)}Q_{12}^{(1)}\overline{\varepsilon}_y\right)dx \qquad [5.30]$$

However, in view of the distinct expressions for $\bar{\sigma}_x^{(1)}$ within the two regions $0 \le x < x^*$ and $x^* \le x \le L$ as given in [5.11] and [5.20], it is necessary to split up the integration as shown below:

$$I_1 = \frac{4h_1}{Q_{11}^{(1)}}\left\{\int_0^{x^*}\left(\frac{\left(\bar{\sigma}_x^{(1)}\right)^2}{2} - \bar{\sigma}_x^{(1)}Q_{12}^{(1)}\bar{\varepsilon}_y\right)dx + \int_{x^*}^{L}\left(\frac{\left(\bar{\sigma}_x^{(1)}\right)^2}{2} - \bar{\sigma}_x^{(1)}Q_{12}^{(1)}\bar{\varepsilon}_y\right)dx\right\} \qquad [5.31]$$

Consider now the integral I_2, which represents the energy contribution of the 0° plies. Since the stress-strain relation changes at $x=x^*$ in the 0° plies, it is necessary to split the integral at this location:

$$I_2 = 4h_2\left\{\int_0^{x^*}\int_0^{\sigma_x^{(2)}}\tilde{\varepsilon}_x^{(2)}\left(\tilde{\sigma}_x^{(2)}\right)d\tilde{\sigma}_x^{(2)}dx + \int_{x^*}^{L}\int_0^{\sigma_x^{(2)}}\tilde{\varepsilon}_x^{(2)}\left(\tilde{\sigma}_x^{(2)}\right)d\tilde{\sigma}_x^{(2)}dx\right\} \qquad [5.32]$$

The appropriate expressions for the strains in terms of stresses from [5.2] must then be inserted into [5.32]. However, it should be realized that within the region $x^* \le x < L$, namely in the second integral of [5.32], the bilinear constitutive relation must be used since $\tilde{\sigma}_x^{(2)}$ will range from zero to a level that exceeds the yield stress, σ_0. This requires that the integration from x^* to L must be split again between values of $\tilde{\sigma}_x^{(2)}$ above and below σ_0, leading to the following result:

$$\begin{aligned} I_2 = {} & \frac{4h_2}{Q_{11}^{(2)}}\left\{\int_0^{x^*}\int_0^{\sigma_x^{(2)}}\left(\tilde{\sigma}_x^{(2)} - \bar{\varepsilon}_y Q_{12}^{(2)}\right)d\tilde{\sigma}_x^{(2)}dx\right\} \\ & + 4h_2\int_{x^*}^{L}\left\{\int_0^{\sigma_0}\frac{\tilde{\sigma}_x^{(2)} - \bar{\varepsilon}_y Q_{12}^{(2)}}{Q_{11}^{(2)}}d\tilde{\sigma}_x^{(2)} + \int_{\sigma_0}^{\sigma_x^{(2)}}\frac{\tilde{\sigma}_x^{(2)} - \bar{\varepsilon}_y Q_{12}^{(2)} - \hat{\sigma}}{\tilde{Q}_{11}^{(2)}}d\tilde{\sigma}_x^{(2)}\right\}dx \end{aligned} \qquad [5.33]$$

At this stage it is possible to carry out the inner integrations in [5.33] with respect to $\tilde{\sigma}_x^{(2)}$ and obtain the following expression:

$$I_2 = \frac{4h_2}{Q_{11}^{(2)}} \int_0^{x^*} \left(\frac{\left(\overline{\sigma}_x^{(2)}\right)^2}{2} - \overline{\sigma}_x^{(2)} \overline{\varepsilon}_y Q_{12}^{(2)} \right) dx + \frac{4h_2}{\tilde{Q}_{11}^{(2)}} \int_{x^*}^{L} \left(\frac{\left(\overline{\sigma}_x^{(2)}\right)^2}{2} - \overline{\sigma}_x^{(2)} \left(\overline{\varepsilon}_y Q_{12}^{(2)} + \hat{\sigma} \right) \right) dx$$
$$+4h_2(L - x^*) \left\{ \frac{1}{Q_{11}^{(2)}} \left(\frac{\sigma_0^2}{2} - \sigma_0 \overline{\varepsilon}_y Q_{12}^{(2)} \right) + \frac{1}{\tilde{Q}_{11}^{(2)}} \left(\sigma_0 (\overline{\varepsilon}_y Q_{12}^{(2)} + \hat{\sigma}) - \frac{\sigma_0^2}{2} \right) \right\} \quad [5.34]$$

The contribution of available energy for crack growth due to the normal stress distributions $\overline{\sigma}_x^{(i)}$ as indicated in equation [5.28] is then given by the sum of equations[5.31] and [5.34].

The evaluation of equation [4.41] is simplified by the fact that the shear response is assumed to be linear, independent of the level of applied stress, consequently it is only necessary to consider the variation of stress distributions within the two regions $0 \le x < x^*$ and $x^* \le x \le L$ to properly carry out the integrations in [4.41].

On the interval $0 \le x < x^*$ it is possible to employ the same procedure that led to equation [4.46], but with the upper limit of integration changed from x=L to x=x^*. Thus:

$$\left(U_\tau^*\right)^{0 \le x < x^*} = \frac{2A_0^2}{3} \left(\frac{\sinh(2\alpha_0 x^*)}{4\alpha_0} - \frac{x^*}{2} \right) \left(\frac{h_1}{C_{55}^{(1)}} + \frac{h_2}{C_{55}^{(2)}} \right) \quad [5.35]$$

For the region $\underline{x^* \le x \le L}$ the expression for the interfacial shearing stress is given by equation [5.20] :

$$\tau^*(x) = A_1 \sinh(\alpha_1 x) + B_1 \cosh(\alpha_1 x) \quad [5.20]R$$

As in the linear case, the shearing stresses in the 0° and 90° plies must match the interfacial shearing stress at z=h_1, namely:

$$\tau_{xz}^{(1)}(x,z_1=h_1)=\tau_{xz}^{(2)}(x,z_2=0)=\tau^*(x) \qquad [4.15]R$$

Utilizing [4.15] and [5.20], the expressions for the shear stress distributions in equations [4.21], within the region $x^* \le x \le L$ can be written as:

$$\begin{aligned}\tau_{xz}^{(1)} &= a(x)z = \frac{z}{h_1}\left(A_1\sinh(\alpha_1 x)+B_1\cosh(\alpha_1 x)\right)\\ \tau_{xz}^{(2)} &= a(x)h_1\left(\frac{\bar{h}-z}{\bar{h}-h_1}\right)=\left(A_1\sinh(\alpha_1 x)+B_1\cosh(\alpha_1 x)\right)\left(\frac{\bar{h}-z}{\bar{h}-h_1}\right)\end{aligned} \qquad [5.36]$$

These expressions can now be substituted into [4.41] to evaluate the integrals in a straightforward manner. The final result for the complementary energy due to shearing stress for $x^* \le x \le L$ becomes:

$$\begin{aligned}\left(U_\tau^*\right)^{x^*\le x\le L} &= \frac{2}{3}\left(\frac{h_1}{C_{55}^{(1)}}+\frac{h_2}{C_{55}^{(2)}}\right)\left\{\frac{\left(A_1^2+B_1^2\right)}{4\alpha_1}\left[\sinh(2\alpha_1 L)-\sinh(2\alpha_1 x^*)\right]\right.\\ &\left.+\frac{\left(B_1^2-A_1^2\right)(L-x^*)}{2}+\frac{A_1B_1}{2\alpha_1}\left[\cosh(2\alpha_1 L)-\cosh(2\alpha_1 x^*)\right]\right\}\end{aligned} \qquad [5.37]$$

Finally, the total complementary energy for the case(ii) bilinear solution is the sum of the contributions from the normal and the shearing stresses given in equations [5.31], [5.34], [5.35], and [5.36]. Or, using the notation for this section:

$$U^* = U_\sigma^* + U_\tau^* = I_1 + I_2 + \left(U_\tau^*\right)^{0\le x<x^*} + \left(U_\tau^*\right)^{x^*\le x\le L} \qquad [5.38]$$

5.5.2 Energy Calculation for Bilinear Response, Case(iii)

For the third case, the applied stress, $\bar{\sigma}_x$, has reached the level at which the stresses in the 0° have exceeded the yield point, σ_0 over the entire region $0 \le x \le L$ as shown in Figure 5.2. Consequently, the stress distributions are prescribed by the same expressions throughout the problem domain, namely equations [5.25], since a single constitutive relation applies to the stress-strain behavior of the 0° plies in this case.

Once again consider the complementary energy contribution due to the normal stresses, $\bar{\sigma}_x^{(i)}$ for $0 \le x \le L$. Equation [4.40] still applies, however since the fourth equation of [5.2] holds for all x, it is necessary now to split only the inner integrations with respect to $\bar{\sigma}_x^{(2)}$ similar to the energy computation in case(ii). This leads to the following expression:

$$
\begin{aligned}
U_\sigma^* &= \frac{4h_1}{Q_{11}^{(1)}} \int_0^L \int_0^{\sigma_x^{(1)}} \left(\tilde{\sigma}_x^{(1)} - \bar{\varepsilon}_y Q_{12}^{(1)} \right) d\tilde{\sigma}_x^{(1)} dx \\
&+ 4h_2 \int_0^L \left\{ \int_0^{\sigma_0} \frac{\tilde{\sigma}_x^{(2)} - \bar{\varepsilon}_y Q_{12}^{(2)}}{Q_{11}^{(2)}} d\tilde{\sigma}_x^{(2)} + \int_{\sigma_0}^{\sigma_x^{(2)}} \frac{\tilde{\sigma}_x^{(2)} - \bar{\varepsilon}_y Q_{12}^{(2)} - \hat{\sigma}}{\tilde{Q}_{11}^{(2)}} d\tilde{\sigma}_x^{(2)} \right\} dx
\end{aligned}
\qquad [5.39]
$$

Upon performing the inner integrations, the final expression for the complementary energy from the normal stresses becomes:

$$
\begin{aligned}
U_\sigma^* &= \frac{4h_1}{Q_{11}^{(1)}} \int_0^L \left(\frac{\left(\bar{\sigma}_x^{(1)}\right)^2}{2} - \bar{\sigma}_x^{(1)} \bar{\varepsilon}_y Q_{12}^{(1)} \right) dx + \frac{4h_2}{\tilde{Q}_{11}^{(2)}} \int_0^L \left(\frac{\left(\bar{\sigma}_x^{(2)}\right)^2}{2} - \bar{\sigma}_x^{(2)} \left(\bar{\varepsilon}_y Q_{12}^{(2)} + \hat{\sigma} \right) \right) dx \\
&+ 4h_2 L \left\{ \frac{\sigma_0^2}{2} \left(\frac{1}{Q_{11}^{(2)}} - \frac{1}{\tilde{Q}_{11}^{(2)}} \right) + \sigma_0 \left(\frac{\bar{\varepsilon}_y Q_{12}^{(2)} + \hat{\sigma}}{\tilde{Q}_{11}^{(2)}} - \frac{\bar{\varepsilon}_y Q_{12}^{(2)}}{Q_{11}^{(2)}} \right) \right\}
\end{aligned}
\qquad [5.40]
$$

Similarly, the energy contribution due to shearing stresses for this case is analogous to that of the linear case, however the expression for the interfacial shear stress is now given by equations [5.25] instead of [4.24]. The resulting contribution to the complementary energy then reads:

$$U_{\tau}^{*}=\frac{2A_1^2}{3}\left(\frac{\sinh(2\alpha_1 L)}{4\alpha_1}-\frac{L}{2}\right)\left(\frac{h_1}{C_{55}^{(1)}}+\frac{h_2}{C_{55}^{(2)}}\right) \qquad [5.41]$$

The total complementary energy available for crack growth for case(iii) is then given by the sum of [5.40] and [5.41].

5.6 Two Case Studies for the Shear-Lag Solution with Bilinear Response

It has been shown that in the circumstance of bilinear response, three solutions given in cases i, ii, and iii of the previous section must be considered to account for all possible stress distributions which depend on the level of the applied stress, $\bar{\sigma}_x$.

The bilinear analysis introduces a second mechanism, namely, a reduction in the stiffness of the 0° plies which contributes to the overall "softening" of the laminate stress-strain behavior. In a more subtle manner, the non-linearity of the 0° plies affects the formation of new transverse cracks in the 90° plies. This is due to the way the stress distributions influence the levels of available energy for crack formation in the 90° plies.

To illustrate this behavior, a case study employing the bilinear analysis is shown in Figures 5.3(a) and (b). The material properties and specimen geometry used for this preliminary study correspond to $[0_2/90_2]_S$ SiC/CAS laminate. They read as follows:

$Q_{11}^{(1)}=Q_{22}^{(2)}=110$	$C_{55}^{(1)}=52$	$J_{IC}=15$
$Q_{11}^{(2)}=Q_{22}^{(1)}=120$	$C_{55}^{(2)}=37$	$2L_0=25$
$Q_{12}^{(1)}=Q_{12}^{(1)}=30$	$\sigma_0=200$	$h_1=h_2=0.4$

The stiffness values are given in GPa, while the "yield stress", σ_0 has units of MPa. Ply thicknesses h_1, h_2 and initial crack spacing, L_o are in millimeters, and the fracture toughness is in J/m^2 .

From Figure 5.3(a), it is obvious that introduction of the nonlinear stress-strain behavior of the 0° plies has considerably improved the prediction of the cross-ply stress-strain response, compared to linear analysis of Chapter 4.

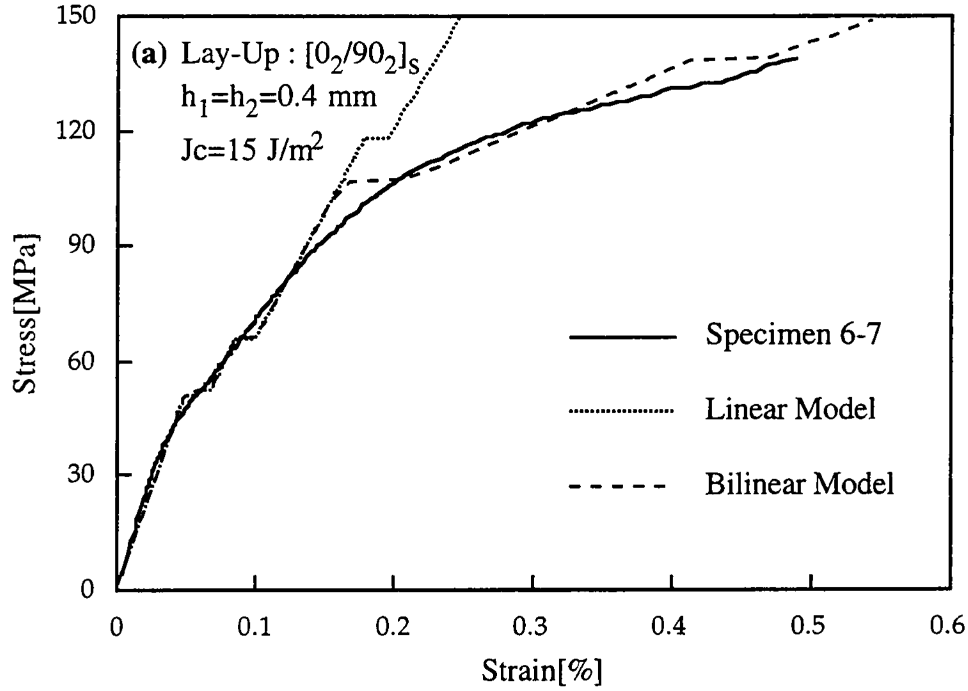

Figure 5.3 Comparison of Bilinear and Linear Models with Experimental Results (a) Stress-Strain Response

For this analysis, the "yield point", σ_0 , was taken to be 200 MPa. It turns out that a stress, $\overline{\sigma}_x^{(2)}$, in the 0° plies of 200 MPa corresponds to an applied stress of 100 MPa for the $[0_2/90_2]_S$ cross-ply laminate. At this stage, the influence of the reduced modulus of the 0° plies initiates "softening" of the cross-ply response. This mechanism results in an increase in global strain as the applied stress exceeds the foregoing level. This can be observed in Figure 5.3(a) by the location where the linear and bilinear results begin to diverge, which is just above 100 MPa.

In spite of the forgoing improvement in the stress-strain response, it is still necessary to compare predicted values for the crack density and experimental results. Such a comparison is shown in Figure 5.3(b) below:

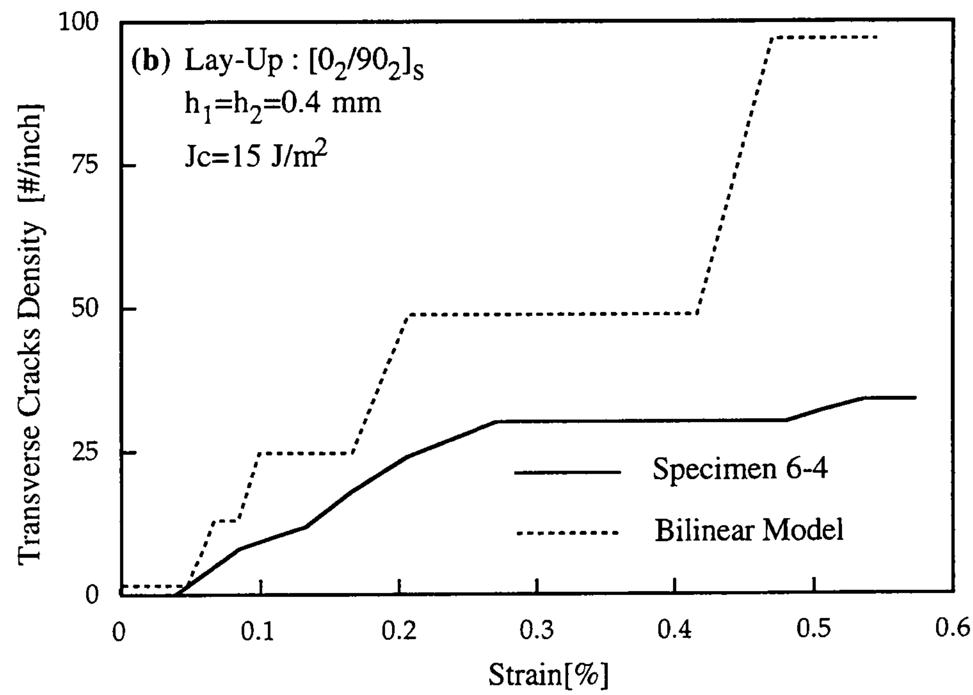

Figure 5.3 Cont. (b) Transverse Crack Density

Comparing the experimental and predicted crack densities, it is obvious that the transverse crack density predicted by the bilinear model significantly overestimates the experimental results.

Although the reasons for this discrepancy are not immediately obvious, some insight can be gained by studying the effect of the parameters used for this analysis. Since most of the material properties listed above have been experimentally verified, changing these values is not justified. However, recall that the fracture toughness is only known for the matrix material without fiber reinforcement. Therefore, in view of the weak fiber-matrix interface discussed in section 4.2, it is reasonable to vary J_{IC} parametrically and observe the effects on the cross-ply laminate response. The results for several values of J_{IC} ranging form 12 to 30 J/m^2 are shown in Figures 5.4(a) and (b) for $[0_2/90_2]_s$.

Recall, that as new transverse cracks are formed, there is a corresponding "jump" in the average laminate strain at the fixed applied stress level, $\overline{\sigma}_x$. With this in mind, it can be seen from Figures 5.4(a), that increasing the level of the fracture toughness, J_{IC} has the tendency to delay transverse crack initiation and progression. This is most noticeable at the earlier stages of applied stress in the test where the introduction of new transverse cracks has a more significant effect on the stiffness of the composite. Additionally, it should be noted that the corresponding stiffness of the laminate increases with higher fracture toughness values as indicated by the elevation of the stress-strain curves.

Turning attention to the Figure 5.4(b), the effect of J_{IC} on the transverse crack progression is more discernible. For J_{IC} = 30 J/m^2, it can be seen one less subdivision of transverse cracks occurs than for the other three cases, reducing the final crack density to approximately 50 cracks per inch. Nevertheless, this value is still about twice that of the experimental data. Furthermore, it should also be noted that a value of J_{IC} = 30 J/m^2 is unrealistically high, since the published values of fracture toughness for the unreinforced matrix material are approximately 25 J/m^2 .

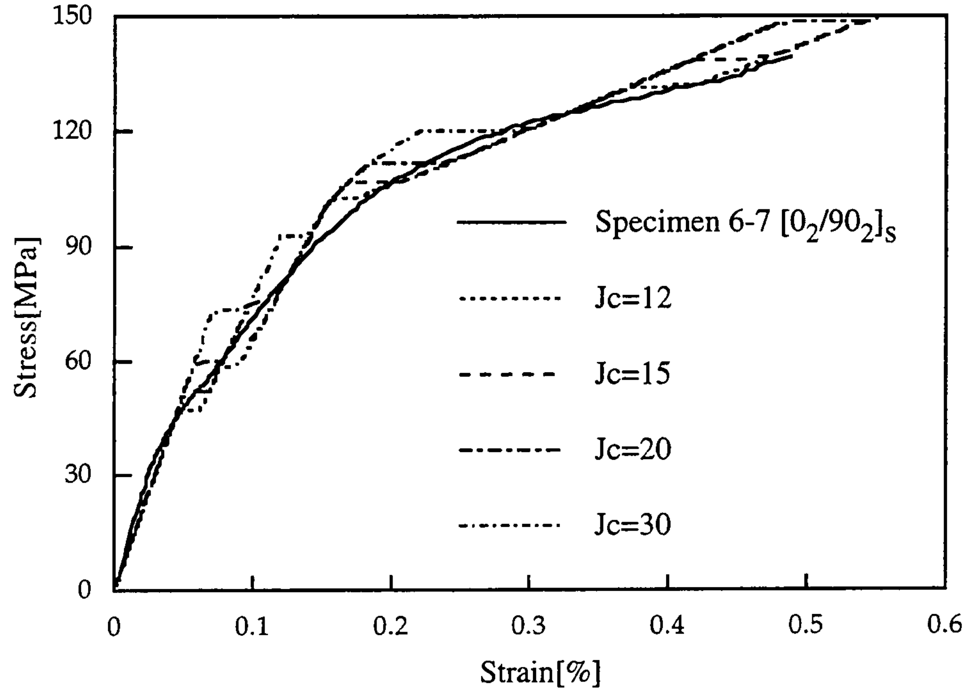

(a) Stress-Strain Response

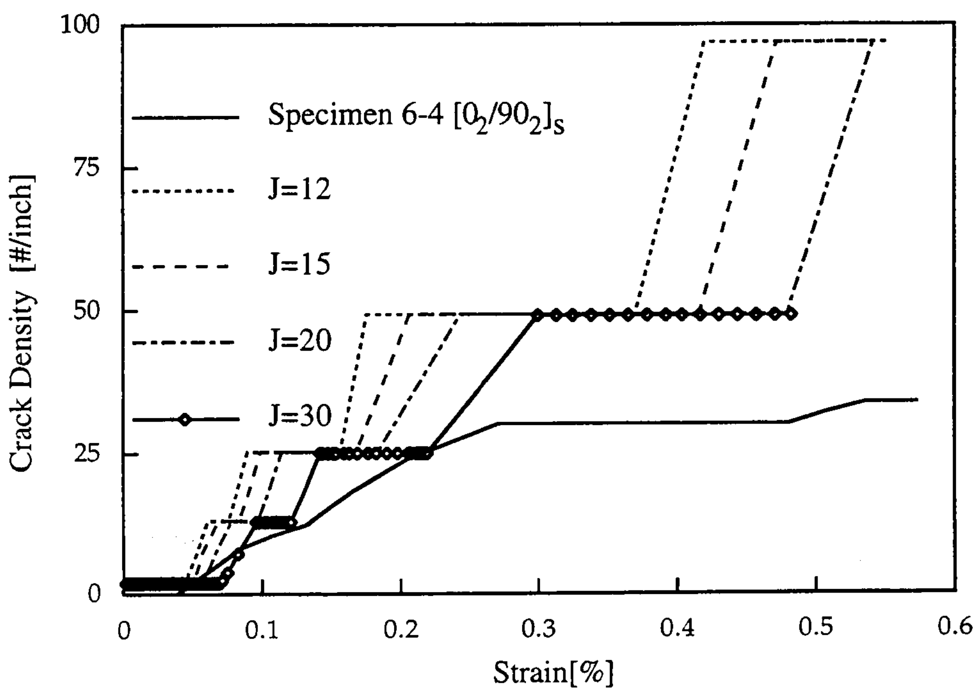

(b) Transverse Crack Density

Figure 5.4 Effect of J_{IC} On the Response of a $[0_2/90_2]_S$ Lay-Up

A second parametric study for a $[0_2/90_4]_S$ lay-up was conducted to see if the previous results remain consistent for this lay-up as well. It should be noted that for this lay-up, the material properties are the same as the previous case study, however, the 90° ply group thickness was doubled to h_1=0.8 mm. The stress-strain response and the crack density progression for this case is then give Figures 5.5(a) and (b). The results for the $[0_2/90_4]_S$ laminate follow trends that are similar to those for the $[0_2/90_2]_S$ case. In particular, in Figure 5.5, it should be noticed that similarly to the previous case study, there is elevation of the stress-strain curves accompanied by a delayed transverse matrix cracking with increased fracture toughness. Once again, for the largest fracture toughness value, J_{IC} = 30 J/m^2, the final transverse crack density attains a level that is about twice the experimental results.

The results from these two case studies demonstrate that, as may be expected, an increase in the fracture toughness reduces the progression of transverse cracks. However, even when unrealistically high levels for J_{IC} are prescribed, the predicted transverse crack density is still approximately twice as large as the experimental value. Therefore, it is necessary to consider the inclusion of slippage between the 0° and 90° ply groups as an additional mechanism to achieve reductions in overall laminate stiffness at lower transverse crack densities.

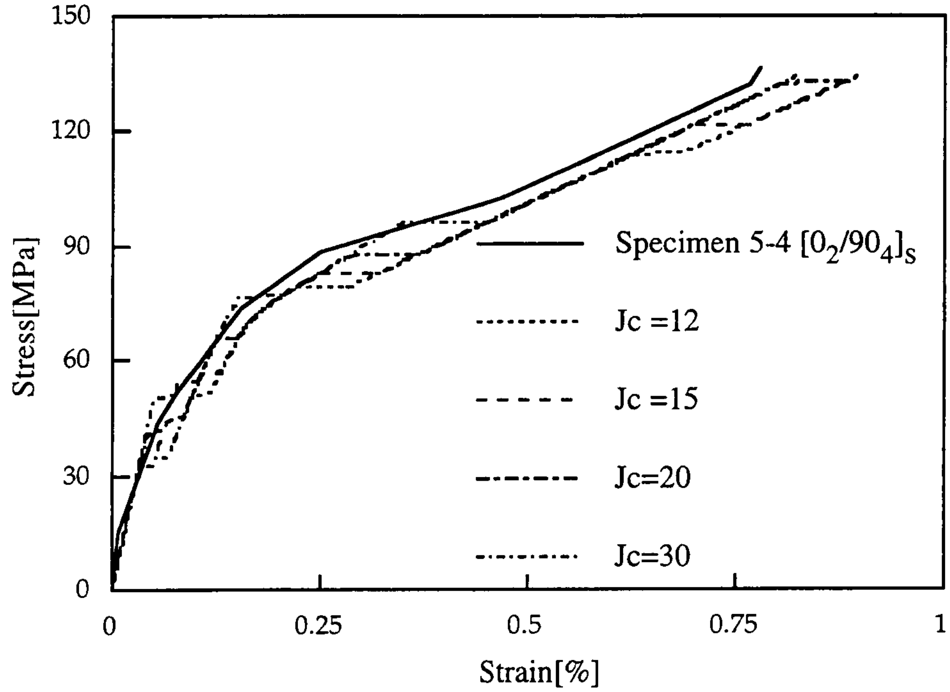

(a) Stress-Strain Response

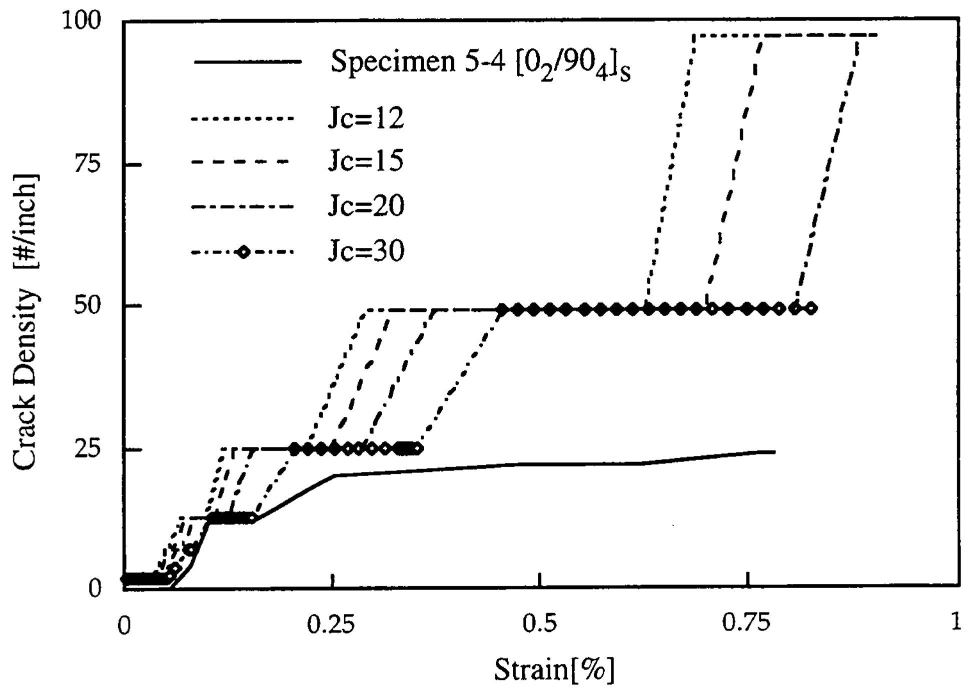

(b) Transverse Crack Density

Figure 5.5 Effect of J_{IC} On the Response of a $[0_2/90_4]_S$ Lay-Up

CHAPTER 6

MODIFIED SHEAR-LAG ANALYSIS WITH INTERLAMINAR SLIP

As discussed in Chapter 3, there is an indication of a slip zone at the interface between the 0° and 90° plies. This phenomenon was not included thus far, but must be considered on its own merits, as well as in view of the discrepancy between predicted and observed transverse crack densities noted at the end of Chapter 5.

It is obvious that introduction of an interfacial slip between the ply groups would result in a discontinuity between the displacements in the 0° and 90° plies within the slip region. This mismatch would then give rise to dissipative energy which has not been taken into account by the foregoing linear and bilinear analyses. Furthermore, this dissipative energy would result in a decrease in the available energy for crack formation, thus reducing the predicted values of crack density. At the same time, "slippage" between the plies would provide a softening mechanism that would contribute to additional global strain in the laminate.

This reasoning seems capable of yielding the desired result, namely a decrease in the transverse crack density leading toward more realistic values, yet preserving the overall stress-strain response of the model by introducing additional global strain via slip at the interface. The latter addition may compensate for the possible reductions in predicted strains stemming from fewer transverse cracks.

To generate the solution in the presence of slip, the simpler case of linear behavior will be addressed first. Subsequently, the more complicated cases that includes the non-linear behavior of the 0° plies along with interfacial slippage will be addressed.

6.1 Linear Response Coupled with Interlaminar Slip.

Consider a slip zone of length l_s shown in Figure 6.1 below, which is assumed to occur when the shearing stress, $\tau^*(x)$, at the interface between the 0° and 90° plies attains the level of the shear strength, τ_s^*. Typical stress distributions in the presence of a slip region are sketched in Figure 6.2 below.

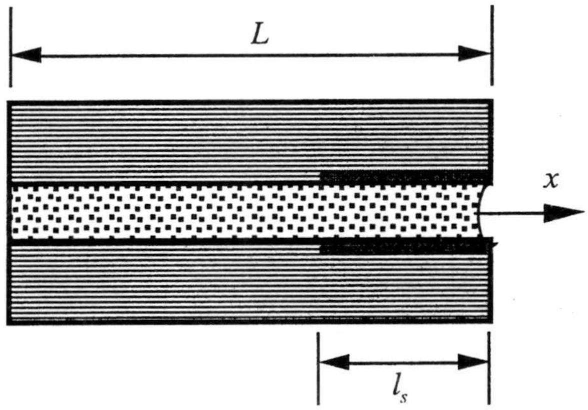

Figure 6.1 Schematic Slip Zone Geometry

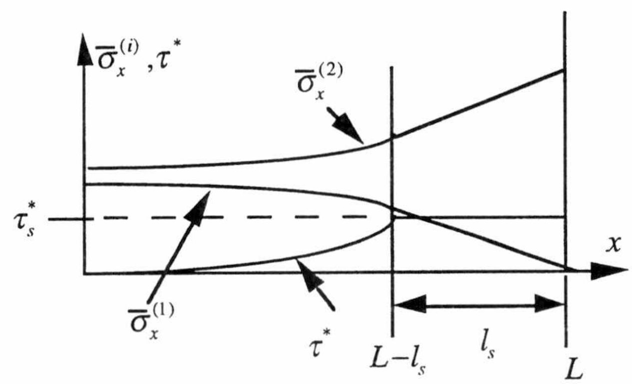

Figure 6.2 Schematic Stress Distributions in the Presence of Slip

Denoting a constant interfacial shearing stress within the slip zone by τ_s^* we have:

$$\tau^*(x) \equiv \text{constant} = \tau_s^* \quad (L - l_s \le x \le L) \qquad [6.1]$$

At the location of a transverse crack, the boundary conditions of [4.25] still apply:

$$\sigma_x^{(1)}(x=L)=0$$
$$\sigma_x^{(2)}(x=L)=\frac{\bar{\sigma}_x \bar{h}}{h_2} \qquad [4.25]R$$

Additionally, in view of the equilibrium equations [4.5] the stress distribution within this slip zone, $\underline{L - l_s \le x \le L}$ is then given by:

$$\tau^*(x) = \tau_s^*$$
$$\sigma_x^{(1)}(x) = \frac{\tau_s^*(L-x)}{h_1} \qquad [6.2]$$
$$\sigma_x^{(2)}(x) = \frac{\bar{\sigma}_x \bar{h}}{h_2} - \frac{\tau_s^*(L-x)}{h_2}$$

Consider now the contact zone $0 \le x < L - l_s$. For this region, the analysis is similar to the linear solution without slippage, with modified boundary conditions at $x=L\text{-}l_S$ obtained from force balance considerations at the inner edge of the slip region as depicted in Figure 6.3 below.

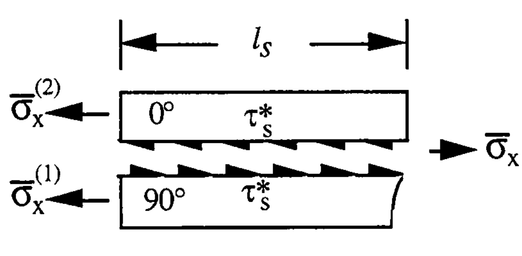

Figure 6.3 Force Balance Within the Slip Zone

These boundary conditions read:

$$\sigma_x^{(1)}(L-l_s)=\frac{\tau_s^* l_s}{h_1}$$
$$\sigma_x^{(2)}(L-l_s)=\frac{\bar{\sigma}_x\bar{h}}{h_2}-\frac{\tau_s^* l_s}{h_2} \qquad [6.3]$$

The solution within the contact region, $0 \le x < L-l_s$ will remain the same as that in Chapter 4, with modified boundary conditions of [6.3], governed by the identical differential equation given in [4.22] :

$$\tau''^{*}-\alpha_0^2\tau^{*}=0 \qquad [4.22]R$$

where $$\alpha_0^2=\frac{A_{55}}{\bar{h}}\left(\frac{1}{h_1 Q_{11}^{(1)}}+\frac{1}{h_2 Q_{11}^{(2)}}\right)$$

Note the symmetry condition $\tau^*(x=0)=0$ from Chapter 4 is still valid, and the solution to [4.22] remains:

$$\tau^*(x)=A_0\sinh(\alpha_0 x) \qquad [6.4]$$

Again, it is necessary to determine the constant A_0. However, in contrast to Chapter 4, boundary conditions [4.25] are now replaced by the expressions in [6.3]. Recall the constitutive relations for normal and shearing stresses given in equations [4.6] and [4.20]:

$$\bar{\sigma}_x^{(i)}=Q_{11}^{(i)}\bar{u}_i'+Q_{12}^{(i)}\bar{\varepsilon}_y$$
$$\bar{\sigma}_y^{(i)}=Q_{12}^{(i)}\bar{u}_i'+Q_{22}^{(i)}\bar{\varepsilon}_y \qquad [4.6]R$$

$$\tau^* = A_{55}\left(\frac{\bar{u}_2 - \bar{u}_1}{\bar{h}}\right) \qquad \text{where} \quad A_{55} = \frac{3\bar{h}C_{55}^{(1)}C_{55}^{(2)}}{h_1C_{55}^{(2)} + h_2C_{55}^{(1)}} \qquad [4.20]\text{R}$$

Using the same procedure as for the linear analysis without slip, differentiation of [4.20] with respect to x and substitution in [4.6], followed by employment of the boundary conditions in [6.3] yields the following result:

$$\tau'^*(L-l_s) = \frac{A_{55}}{\bar{h}}\left(\frac{\bar{\sigma}_x\bar{h}}{h_2Q_{11}^{(2)}} + \bar{\varepsilon}_y\left[\frac{Q_{12}^{(1)}}{Q_{11}^{(1)}} - \frac{Q_{12}^{(2)}}{Q_{11}^{(2)}}\right]\right) - \tau_s^* l_s \alpha_0^2 \qquad [6.5]$$

Differentiation of [6.4] with respect to x, evaluated at x=L-l_S, and comparison with [6.5] gives the following expression for A_0:

$$A_0 = k_1\left(k_3\bar{\sigma}_x + k_4\bar{\varepsilon}_y\right) - k_8 \qquad [6.6]$$

where

$$k_1 = A_{55}/\left(\bar{h}\,\alpha_0 Q_{11}^{(1)}Q_{11}^{(2)}\cosh(\alpha_0(L-l_s))\right)$$

$$k_3 = \frac{\bar{h}Q_{11}^{(1)}}{h_2}$$

$$k_4 = Q_{12}^{(1)}Q_{11}^{(2)} - Q_{12}^{(2)}Q_{11}^{(1)}$$

$$k_8 = \frac{\tau_s^* l_s \alpha_0}{\cosh(\alpha_0(L-l_s))}$$

It is interesting to point out that the constants, k_i, are the same as for the linear case if the parameter L is replaced by L-l_S. However, an additional term, k_8 appears in the current solution. With A_0 determined, integration of the equilibrium equations results in the following stress distribution for the linear slip solution within the region $\underline{0 \le x < L - l_s}$:

$$
\begin{aligned}
&\tau^*(x) = A_0 \sinh(\alpha_0 x) \\
&\bar{\sigma}_x^{(1)}(x) = \frac{\tau_s^* l_s}{h_1} + \frac{A_0}{h_1 \alpha_0}\left\{\cosh\left(\alpha_0 (L - l_s)\right) - \cosh\left(\alpha_0 x\right)\right\} \\
&\bar{\sigma}_x^{(2)}(x) = \frac{\bar{\sigma}_x \bar{h}}{h_2} - \frac{\bar{\sigma}_x^{(1)} h_1}{h_2}
\end{aligned}
\qquad [6.7]
$$

As expected, this stress distribution reduces to the linear solution without slip if the slip length, l_s is set equal zero.

Notice that the constant A_0 is now given in terms of the transverse strain $\bar{\varepsilon}_y$ as well as the newly introduced parameter, l_s. To evaluate these two unknowns it is necessary to employ equilibrium in the y-direction as in the linear solution without slip, together with numerical iteration needed to satisfy the condition given in [6.1]. Equilibrium in the y-direction is accomplished with equation [4.31]. However, since the stresses within the slip and contact regions are prescribed by distinct expressions it is necessary to split the integrals in [4.31] as shown below:

$$
\begin{aligned}
\bar{\sigma}_y \bar{h} L = h_1 &\int_0^{L-l_s} \bar{\sigma}_y^{(1)} dx + h_1 \int_{L-l_s}^{L} \bar{\sigma}_y^{(1)} dx \\
&+ h_2 \int_0^{L-l_s} \bar{\sigma}_y^{(2)} dx + h_2 \int_{L-l_s}^{L} \bar{\sigma}_y^{(2)} dx = 0
\end{aligned}
\qquad [6.8]
$$

Recalling equations [4.32], the transverse stresses $\bar{\sigma}_y^{(i)}$ can now be expressed in terms of the longitudinal stresses:

$$
\begin{aligned}
\bar{\sigma}_y^{(1)} &= C_1 \bar{\sigma}_x^{(1)} + C_2 \bar{\varepsilon}_y \\
\bar{\sigma}_y^{(2)} &= C_3 \bar{\sigma}_x^{(2)} + C_4 \bar{\varepsilon}_y
\end{aligned}
\qquad [4.32]\text{R}
$$

where

$$C_1 = Q_{12}^{(1)} / Q_{11}^{(1)}$$
$$C_2 = Q_{22}^{(1)} - \left(Q_{12}^{(1)}\right)^2 / Q_{11}^{(1)}$$
$$C_3 = Q_{12}^{(2)} / Q_{11}^{(2)}$$
$$C_4 = Q_{22}^{(2)} - \left(Q_{12}^{(2)}\right)^2 / Q_{11}^{(2)}$$

Upon substituting the longitudinal stresses from [6.2] and [6.7] into [4.32], and inserting this result in [6.8], the transverse strain $\bar{\varepsilon}_y$ can be expressed as follows:

$$\bar{\varepsilon}_y = \frac{\tau_s^*(C_3 - C_1)\left(Ll_s - \frac{l_s^2}{2}\right) - \bar{\sigma}_x\left(C_3\bar{h}L + \beta_1 k_1 k_3\right) + \beta_1 k_8}{\beta_1 k_1 k_4 + L(C_2 h_1 + C_4 h_2)} \qquad [6.9]$$

where $\beta_1 = \frac{(C_1 - C_3)}{\alpha_0}\left\{(L - l_s)\cosh(\alpha_0(L - l_s)) - \frac{\sinh(\alpha_0(L - l_s))}{\alpha_0}\right\}$

Note that, with the exception of l_S, all other terms in [6.9] are known. A comparison between the expressions for transverse strain in [6.9] and [4.33] indicate that when l_S is set equal to zero, the two expressions will be identical as expected.

As already mentioned, an iterative technique must be used to determine the slip zone length, l_S. This is accomplished by noting that by definition, at x=L-l_S, the interfacial shearing stress, $\tau^*(x = L - l_s)$ must equal the shear strength, τ_s^*. It is therefore possible to employ an iterative procedure similar to that used to find the position of the yield zone, x*, in Chapter 5. This procedure is outlined below:

(1) Select a value for the slip zone length, l_S.

(2) Calculate β_1, and $\bar{\varepsilon}_y$ from equations [6.9].

(3) Calculate A_0 from equation [6.6].

(4) Calculate $\tau^*(x = L - l_s)$ by using equation [6.7] and check to see if $\tau^*(x = L - l_s) = \tau_s^*$. If so, then l_s has been located, if not, it is necessary to perform another iteration by returning to step (1).

With the stress distributions in hand, the next step is to determine the global strain of the composite necessary construct the stress-strain curve. As before, the global strain of the cross-ply is still given by:

$$\bar{\varepsilon}_x = \frac{\bar{u}_2(L)}{L} \tag{4.34]R}$$

Employing the appropriate constitutive relation from [4.6] and splitting the integration of $\bar{u}_2'$ between the contact and slip regions, the following expression is obtained:

$$\bar{\varepsilon}_x = \frac{1}{L}\left\{\int_0^{L-l_s} \frac{\bar{\sigma}_x^{(2)} - Q_{12}^{(2)}\bar{\varepsilon}_y}{Q_{11}^{(2)}}dx + \int_{L-l_s}^{L} \frac{\bar{\sigma}_x^{(2)} - Q_{12}^{(2)}\bar{\varepsilon}_y}{Q_{11}^{(2)}}dx\right\} \tag{6.10]}$$

Substituting the expressions for $\bar{\sigma}_x^{(2)}(x)$ from equations [6.2] and [6.7] and carrying out the integration gives the following expression for the global strain for the linear slip solution:

$$\bar{\varepsilon}_x = \frac{1}{Q_{11}^{(2)}}\left\{\begin{aligned}&\frac{\bar{\sigma}_x \bar{h}}{h_2} - \frac{\tau_s^*}{h_2}\left(l_s - \frac{l_s^2}{2L}\right) - Q_{12}^{(2)}\bar{\varepsilon}_y - \\ &\frac{A_0}{h_2\alpha_0 L}\left[(L-l_s)\cosh(\alpha_0(L-l_s)) - \frac{\sinh(\alpha_0(L-l_s))}{\alpha_0}\right]\end{aligned}\right\} \tag{6.11]}$$

6.2 Bilinear Response Coupled with Interfacial Slip

When the bilinear response of the 0° plies and an interfacial slip between the 0° and 90° layers of the laminate are considered simultaneously, the location of the onset of the non-linear region, x^*, and the length of the slip zone, l_S, must be determined conjointly. Note that the location where $\overline{\sigma}_x^{(2)} = \sigma_0$ (x=x^*), may occur on the right or to the left of the location x=L-l_S, as indicated by x^* and x'^* respectively in Figure 6.4 below:

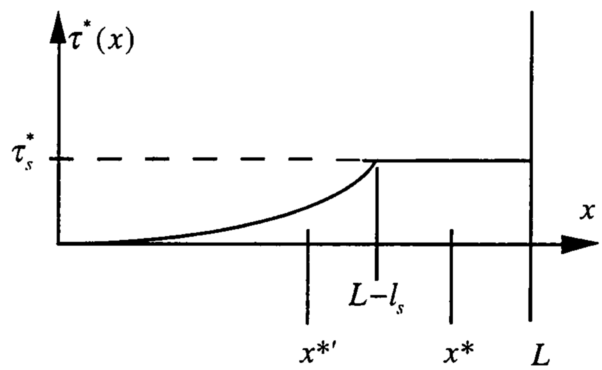

Figure 6.4 Interaction Between Yield and Slip Zones

As mentioned previously, determining the location of x^* in the bilinear case, and the length l_S in the presence of interfacial slip, require numerical iterative solutions even when considered separately. Obviously, the complexity is further increased when the slip and bilinearity occur simultaneously. In such a case it is not known *a priori* which phenomenon, interfacial slippage or yielding, occurs first. Additionally, relative positions of x^* and L-l_S may change with the amplitude of the applied stress, $\overline{\sigma}_x$ as well as with the crack spacing L. Thus, at one level of applied stress, L-l_S may exceed L-x* (slippage precedes yield), while at a later stages in the loading, the length of the region L-x* may become larger than L-l_S if the yield zone extends past the slip zone. This requires the generalization of distinct sets of solutions to account for each situation.

Essentially, the iterative solution must simultaneously determine two roots for the two foregoing locations. Then, based on the relative location of x^* and $L\text{-}l_S$, the appropriate solution for the corresponding stress distributions must be determined .

A third case of the combined bilinear and slip analysis occurs when the yield zone extends over the complete domain $0 \le x \le L$, and the location x^* is effectively located at the origin, x=0. This situation resembles the third case of bilinear solution without slippage depicted in Figure 5.2. However, for the current circumstance the presence of the slip zone must also be taken into account, adding to the complexity of the solution.

To categorize the distinct sub-cases of bilinear response of the 0° plies coupled with slip at the 0°/90° interface, the following terminology will be employed:

"Case I" : The slip zone exceeds the yield zone, i.e. $L\text{-}l_S < x^*$.

"Case II" : The yield zone exceeds the slip zone, i.e. $L\text{-}l_S > x^*$.

"Case III" : Yielding over the entire domain, i.e. x^*=0, with slippage over the region $L-l_s \le x \le L$.

6.2.1 Bilinear Response Coupled with Interlaminar Slip, Case I

In this case, the bilinear response of the 0° plies occurs over a distance $L\text{-}x^*$ which is smaller than the slip range, $L\text{-}l_S$ as shown in Figure 6.5 below:

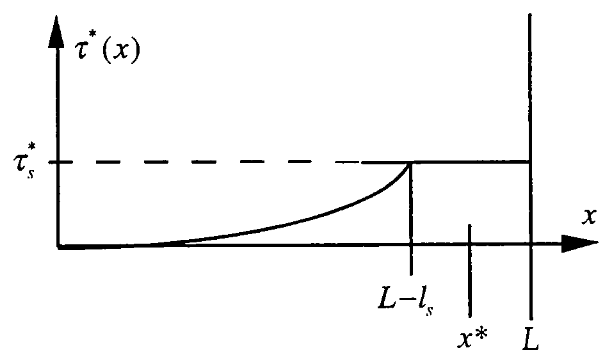

Figure 6.5 Shearing Stress Distribution for Combined Bilinear Response and Interfacial Slip, Case I

This circumstance requires the derivation of three distinct solutions for the regions $0 \le x < L - l_s$, $L - l_s \le x < x^*$, and $x^* \le x \le L$.

To begin, consider the region, $0 \le x < L - l_s$. Since $x^* > L - l_s$, the response of the 0° plies is linear in this range. Consequently the boundary conditions at $x = L - l_s$ given in equations [6.3] still hold, and the solution for the region $\underline{0 \le x < L - l_s}$ can be expressed by the same form as in [6.7], namely:

$$
\begin{aligned}
&\tau^*(x) = A_0 \sinh(\alpha_0 x) \\
&\bar{\sigma}_x^{(1)}(x) = \frac{\tau_s^* l_s}{h_1} + \frac{A_0}{h_1 \alpha_0}\left\{\cosh\left(\alpha_0 (L - l_s)\right) - \cosh\left(\alpha_0 x\right)\right\} \qquad [6.12] \\
&\bar{\sigma}_x^{(2)}(x) = \frac{\bar{\sigma}_x \bar{h}}{h_2} - \frac{\bar{\sigma}_x^{(1)} h_1}{h_2}
\end{aligned}
$$

where

$$
\begin{aligned}
&A_0 = k_1\left(k_3 \bar{\sigma}_x + k_4 \bar{\varepsilon}_y\right) - k_8 \\
&k_1 = A_{55} / \left(\bar{h}\, \alpha_0 Q_{11}^{(1)} Q_{11}^{(2)} \cosh(\alpha_0 (L - l_s))\right) \\
&k_3 = \frac{\bar{h} Q_{11}^{(1)}}{h_2} \\
&k_4 = Q_{12}^{(1)} Q_{11}^{(2)} - Q_{12}^{(2)} Q_{11}^{(1)} \\
&k_8 = \frac{\tau_s^* l_s \alpha_0}{\cosh(\alpha_0 (L - l_s))}
\end{aligned}
$$

It should be realized that the constant A_0 contains the yet unknown parameter l_s, which needs to be determined. Nevertheless, it is important to notice that although equations [6.12] and [6.7] have identical forms, the actual values of l_s and hence A_0 in [6.12] will differ from those in [6.7] since their values will be influenced by the non linearity that occurs in the subsequent regions beyond $0 \le x < L - l_s$.

Consider next the region $L - l_s \le x < x^*$. Since this range falls within the slip zone, the interfacial shearing stress is given by, τ_s^*. The normal stresses, $\bar{\sigma}_x^{(i)}$ are obtained by integrating the equilibrium equations of [4.5] and employing the following boundary conditions at $x=x^*$:

$$\bar{\sigma}_x^{(2)}(x=x^*)=\sigma_0\ ,\ \bar{\sigma}_x^{(1)}(x=x^*)=\frac{\bar{\sigma}_x\bar{h}-\sigma_0 h_2}{h_1} \qquad [6.13]$$

Consequently, the stress distribution in the region $\underline{L-l_s \le x < x^*}$ is given by:

$$\begin{aligned}
&\tau^*(x)=\tau_s^* \\
&\bar{\sigma}_x^{(1)}(x)=\frac{\tau_s^*(x^*-x)}{h_1}+\frac{\bar{\sigma}_x\bar{h}-\sigma_0 h_2}{h_1} \\
&\bar{\sigma}_x^{(2)}(x)=\sigma_0-\frac{\tau_s^*(x^*-x)}{h_2}
\end{aligned} \qquad [6.14]$$

Turning to the third region, $x^* \le x \le L$, the interfacial shearing remains τ_s^*, and the normal stresses are found by integrating equations [4.5] with the familiar boundary conditions at $x=L$:

$$\begin{aligned}
&\sigma_x^{(1)}(x=L)=0 \\
&\sigma_x^{(2)}(x=L)=\frac{\bar{\sigma}_x\bar{h}}{h_2}
\end{aligned} \qquad [4.25]\text{R}$$

Consequently, the stress distributions within the region $\underline{x^* \le x \le L}$ are given by:

$$\begin{aligned}
&\tau^*(x)=\tau_s^* \\
&\bar{\sigma}_x^{(1)}(x)=\frac{\tau_s^*(L-x)}{h_1} \\
&\bar{\sigma}_x^{(2)}(x)=\frac{\bar{\sigma}_x\bar{h}}{h_2}-\frac{\tau_s^*(L-x)}{h_2}
\end{aligned} \qquad [6.15]$$

However, recall from the definition of x*:

$$\overline{\sigma}_x^{(2)}(x=x^*)=\sigma_0$$

Hence, substitution in the third equation of [6.15] yields:

$$x^*=\frac{\sigma_0 h_2-\overline{\sigma}_x\overline{h}}{\tau_s^*}+L \qquad [6.16]$$

Since all terms on the right side of [6.16] are known, the location of x^* is determined from equilibrium, independent of l_S. This results in a substantial simplification of the remaining analysis for the Case I solution.

At this stage, the stress distributions within the aforementioned three regions are given in equations [6.12], [6.14] and [6.15]. As mentioned earlier, the constant A_0 is still given in terms of the transverse strain, $\overline{\varepsilon}_y$ and the slip zone length l_S, which remain to be determined. Employing equilibrium in the y-direction will result in an expression for $\overline{\varepsilon}_y$ in terms of l_S as well as various material constants. To determine l_S and complete the solution, it is necessary to recall the condition, $\tau^*(x=L-l_s)=\tau_s^*$, and employ an iterative numerical method.

To satisfy transverse equilibrium, condition [4.31] must be split over three regions as shown below:

$$\begin{aligned}\overline{\sigma}_y\overline{h}L&=h_1\left[\int_0^{L-l_s}\overline{\sigma}_y^{(1)}dx+\int_{L-l_s}^{x^*}\overline{\sigma}_y^{(1)}dx+\int_{x^*}^{L}\overline{\sigma}_y^{(1)}dx\right]\\&+h_2\left[\int_0^{L-l_s}\overline{\sigma}_y^{(2)}dx+\int_{L-l_s}^{x^*}\overline{\sigma}_y^{(2)}dx+\int_{x^*}^{L}\overline{\sigma}_y^{(2)}dx\right]=0\end{aligned} \qquad [6.17]$$

As shown in Chapter 5, the constitutive relations given in [5.2] can be employed to relate lateral to longitudinal stresses as follows:

$$
\begin{aligned}
&\bar{\sigma}_y^{(1)} = C_1\bar{\sigma}_x^{(1)} + C_2\bar{\varepsilon}_y \\
&\bar{\sigma}_y^{(2)} = C_3\bar{\sigma}_x^{(2)} + C_4\bar{\varepsilon}_y \qquad (0 \le x < x^*) \\
&\bar{\sigma}_y^{(2)} = C_5\bar{\sigma}_x^{(2)} + C_6\bar{\varepsilon}_y - C_7 \quad (x^* \le x \le L)
\end{aligned}
\qquad [5.21]\text{R}
$$

where

$$
\begin{aligned}
C_1 &= Q_{12}^{(1)} / Q_{11}^{(1)} \\
C_2 &= Q_{22}^{(1)} - \left(Q_{12}^{(1)}\right)^2 / Q_{11}^{(1)} \\
C_3 &= Q_{12}^{(2)} / Q_{11}^{(2)} \\
C_4 &= Q_{22}^{(2)} - \left(Q_{12}^{(2)}\right)^2 / Q_{11}^{(2)} \\
C_5 &= Q_{12}^{(2)} / \tilde{Q}_{11}^{(2)} \\
C_6 &= Q_{22}^{(2)} - \left(Q_{12}^{(2)}\right)^2 / \tilde{Q}_{11}^{(2)} \\
C_7 &= Q_{12}^{(2)}\hat{\sigma} / \tilde{Q}_{11}^{(2)}
\end{aligned}
$$

The integration in [6.17] can be carried out using the appropriate distributions of $\bar{\sigma}_x^{(i)}$ from equations [6.12], [6.14] and [6.15]. Straightforward, albeit tedious manipulations give:

$$
\bar{\varepsilon}_y = \frac{\left\{\begin{aligned}
&h_2C_7(L-x^*) - (C_3-C_1)\left[\frac{k_8\beta_1}{\alpha_0} + h_2\sigma_0(x^*-L+l_s)\right] \\
&-\bar{\sigma}_x\left[\frac{k_1k_3\beta_1}{\alpha_0}(C_1-C_3) + C_1\bar{h}(x^*-L+l_s) + C_3\bar{h}(L-l_s) + C_5\bar{h}(L-x^*)\right] \\
&-\tau_s^*\left[(C_1-C_3)\left(l_s(L-l_s) + \frac{(x^*-L+l_s)^2}{2}\right) + (C_1-C_5)\frac{(L-x^*)^2}{2}\right]
\end{aligned}\right\}}{\left\{\dfrac{k_1k_4\beta_1}{\alpha_0}(C_1-C_3) + h_1C_2L + h_2C_4x^* + h_2C_6(L-x^*)\right\}} \qquad [6.18]
$$

where $\beta_1 = (L-l_s)\cosh\left(\alpha_0(L-l_s)\right) - \sinh\left(\alpha_0(L-l_s)\right)/\alpha_0$

Notice that the constants k_i carry over from equation [6.6] and the transverse strain is given in terms of known constants, with the exception of the yet unknown slip zone length, l_s. To determine l_s it is necessary to employ the same type of iterative procedure as was used in section 6.1 for the linear slip solution. The procedure is outlined below:

(1) Calculate x^* from equation [6.16].

(2) Select a trial value for the slip zone length, l_s, consistent with $x^* > L-l_s$.

(3) Calculate β_1, and $\bar{\varepsilon}_y$ from equations [6.18].

(4) Calculate A_0 from equation [6.12].

(5) Calculate $\tau^*(x = L - l_s)$ using equation [6.12] and check to see if $\tau^*(x = L - l_s) = \tau_s^*$. If so, then l_s has been located, if not, it is necessary to perform another iteration by returning to step (1).

The global strain that corresponds to the present solution is obtained by integration of the constitutive relations over three regions considered herein. Employing [5.2] the global strain is then found to be:

$$\bar{\varepsilon}_x = \frac{1}{L}\left[\int_0^{L-l_s} \frac{\bar{\sigma}_x^{(2)} - Q_{12}^{(2)}\bar{\varepsilon}_y}{Q_{11}^{(2)}}dx + \int_{L-l_s}^{x^*} \frac{\bar{\sigma}_x^{(2)} - Q_{12}^{(2)}\bar{\varepsilon}_y}{Q_{11}^{(2)}}dx + \int_{x^*}^{L} \frac{\bar{\sigma}_x^{(2)} - Q_{12}^{(2)}\bar{\varepsilon}_y - \hat{\sigma}}{\tilde{Q}_{11}^{(2)}}dx\right] \qquad [6.19]$$

Upon substituting the appropriate stress distributions, and carrying out the integration, the final result reads:

$$\bar{\varepsilon}_x = \frac{1}{LQ_{11}^{(2)}h_2}\left\{\begin{aligned}&\left(\bar{\sigma}_x\bar{h} - \tau_s^* l_s - Q_{12}^{(2)}\bar{\varepsilon}_y h_2\right)(L-l_s) - \frac{A_0\beta_1 h_2}{\alpha_0}\\ &+h_2\left(x^* - L + l_s\right)\left(\sigma_0 - Q_{12}^{(2)}\bar{\varepsilon}_y\right) - \frac{\tau_s^*}{2}\left(x^* - L + l_s\right)^2\end{aligned}\right\} \qquad [6.20]$$
$$+\frac{1}{L\tilde{Q}_{11}^{(2)}h_2}\left\{\left(\bar{\sigma}_x\bar{h} - Q_{12}^{(2)}\bar{\varepsilon}_y h_2 - \hat{\sigma}h_2\right)(L - x^*) - \frac{\tau_s^*}{2}(L - x^*)^2\right\}$$

6.2.2 Bilinear Response Coupled with Interlaminar Slip, Case II

For this case the region of bilinear response of the 0° plies extends beyond the interfacial slip zone i.e. $x^* < L- l_s$ as depicted in Figure 6.5 below:

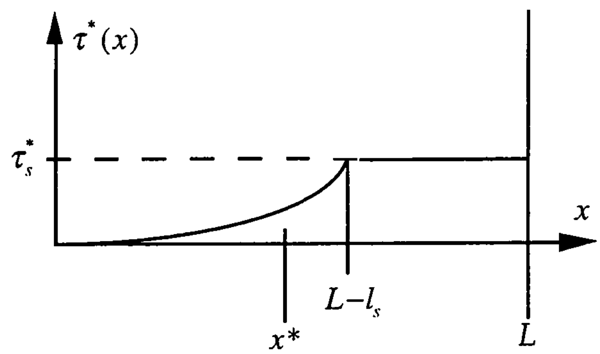

Figure 6.6 Shearing Stress Distribution for Combined Bilinear Response and Interfacial Slip, Case II

As in Case I it is necessary to construct three solutions for the stress distributions within three distinct regions. In this case these regions consist of $0 \le x < x^*$, $x^* \le x < L-l_s$, and $L-l_s \le x \le L$.

Referring to Figure 6.6, the innermost region, $0 \le x < x^*$, is governed by linear response and is bounded at $x=x^*$ by a region where bilinear behavior occurs without slip. Hence, the boundary conditions given in [5.5iii] and [5.5iv] hold. Consequently, the derivation in Chapter 5 remains valid , leading to expressions that are formally identical to those in equations [5.11]. Thus for the region, $\underline{0 \le x < x^*}$ we have:

$$\tau^*(x) = A_0 \sinh(\alpha_0 x)$$
$$\bar{\sigma}_x^{(1)} = \frac{\bar{\sigma}_x \bar{h}}{h_1} - \frac{\sigma_0 h_2}{h_1} + \frac{A_0}{h_1 \alpha_0}\left(\cosh(\alpha_0 x^*) - \cosh(\alpha_0 x)\right) \qquad [6.21]$$
$$\bar{\sigma}_x^{(2)} = \frac{\bar{\sigma}_x \bar{h}}{h_2} - \frac{\bar{\sigma}_x^{(1)} h_1}{h_2}$$

where $$A_0 = k_1\left(k_2 - k_3\bar{\sigma}_x + k_4\bar{\varepsilon}_y\right)$$

$$k_1 = \frac{A_{55}}{\bar{h}\alpha_0 Q_{11}^{(1)} Q_{11}^{(2)} \cosh(\alpha_0 x^*)}$$

$$k_2 = \sigma_0\left(Q_{11}^{(1)} + \frac{h_2}{h_1} Q_{11}^{(2)}\right)$$

$$k_3 = \frac{\bar{h} Q_{11}^{(2)}}{h_1}$$

$$k_4 = \left(Q_{12}^{(1)} Q_{11}^{(2)} - Q_{12}^{(2)} Q_{11}^{(1)}\right)$$

As noted in Section 6.2.1, it should be emphasized that in spite of the identical forms of equations [6.21] and [5.11], the actual values of A_0 and x^* for the current case will differ from those in Chapter 5 since they depend on the solution over the entire region $0 \le x \le L$.

Turning to the region $x^* \le x < L - l_s$, it is noted that the solution in this range can be constructed similarly to the approach used to arrive at equations [5.12] through [5.20], with the exception that the boundary conditions [4.25] at $x=L$ must be replaced by appropriate conditions at $x=L-l_S$. Then in accordance with [5.12], the general solution for the interfacial shearing stress for $x^* \le x < L - l_s$ is given by:

$$\tau^*(x) = A_1 \sinh(\alpha_1 x) + B_1 \cosh(\alpha_1 x) \qquad [6.22]$$

The condition of continuity of the interfacial shearing stress at $x=x^*$ is still maintained as in Chapter 5, namely:

$$\tau^*(x^*+) = \tau^*(x^*-) \qquad [5.5v]R$$

However, in the present case it is necessary to recognize the presence of the slip zone which begins at $x=L-l_S$. Consequently, the appropriate boundary conditions are again given as:

$$\bar{\sigma}_x^{(1)}(x=L-l_s)=\frac{\tau_s^* l_s}{h_1}$$
$$\bar{\sigma}_x^{(2)}(x=L-l_s)=\frac{\bar{\sigma}_x \bar{h}}{h_2}-\frac{\tau_s^* l_s}{h_2} \qquad [6.3]R$$

Enforcing the continuity of shearing stresses at x^* as indicated in [5.5v], the expressions for the shearing stresses from [6.21] and [6.22] give the following result:

$$A_1 \sinh(\alpha_1 x^*)+B_1 \cosh(\alpha_1 x^*)=A_o \sinh(\alpha_0 x^*)$$

Which in view of [6.21] can be rewritten as :

$$A_1 \sinh(\alpha_1 x^*)+B_1 \cosh(\alpha_1 x^*)=k_1(k_2-k_3\bar{\sigma}_x+k_4\bar{\varepsilon}_y)\sinh(\alpha_0 x^*) \qquad [6.23]$$

Recall the stress-strain relations,

$$\begin{aligned}
&\bar{\sigma}_x^{(1)}=Q_{11}^{(1)}\bar{u}_1'+Q_{12}^{(1)}\bar{\varepsilon}_y && \\
&\bar{\sigma}_y^{(i)}=Q_{12}^{(i)}\bar{u}_i'+Q_{22}^{(i)}\bar{\varepsilon}_y && (0\le x\le L) \qquad [5.2R]\\
&\bar{\sigma}_x^{(2)}=Q_{11}^{(2)}\bar{u}_2'+Q_{12}^{(2)}\bar{\varepsilon}_y && (0\le x< x^*)\\
&\bar{\sigma}_x^{(2)}=\tilde{Q}_{11}^{(2)}\bar{u}_2'+Q_{12}^{(2)}\bar{\varepsilon}_y+\hat{\sigma} && (x^*\le x\le L)
\end{aligned}$$

where $\hat{\sigma}=\sigma_0\left(1-\frac{\tilde{Q}_{11}^{(2)}}{Q_{11}^{(2)}}\right)$

and relation [4.20] that remains valid up to $x=L-l_S$, the edge of the contact zone:

$$\tau^* = A_{55}\left(\frac{\bar{u}_2 - \bar{u}_1}{\bar{h}}\right) \qquad [4.20]R$$

Differentiation of [4.20] and evaluation at $x=L\text{-}l_S$ yields:

$$\tau'^*(L-l_s)=A_{55}\left(\frac{\bar{u}_2'(L-l_s)-\bar{u}_1'(L-l_s)}{\bar{h}}\right) \qquad [6.24]$$

Note that equation [6.24] now plays the same role as [4.26] in Chapter 4. Then utilizing [5.2] yields:

$$\begin{aligned}\bar{u}_1'(L-l_s)&=\frac{1}{Q_{11}^{(1)}}\left(\bar{\sigma}_x^{(1)}(L-l_s)-Q_{12}^{(1)}\bar{\varepsilon}_y\right)\\ \bar{u}_2'(L-l_s)&=\frac{1}{\tilde{Q}_{11}^{(2)}}\left(\bar{\sigma}_x^{(2)}(L-l_s)-Q_{12}^{(2)}\bar{\varepsilon}_y-\hat{\sigma}\right)\end{aligned} \qquad [6.25]$$

Substituting [6.25] into [6.24] along with the boundary conditions in [6.3] then gives:

$$\tau'^*(L-l_s)=\frac{A_{55}}{\bar{h}}\left\{\frac{\bar{\sigma}_x\bar{h}}{\tilde{Q}_{11}^{(2)}h_2}+\bar{\varepsilon}_y\left(\frac{Q_{12}^{(1)}}{Q_{11}^{(1)}}-\frac{Q_{12}^{(2)}}{\tilde{Q}_{11}^{(2)}}\right)-\frac{\hat{\sigma}}{\tilde{Q}_{11}^{(2)}}\right\}-\tau_s^* l_s\alpha_1^2 \qquad [6.26]$$

Comparing this last result with [6.22] evaluated at $x=L\text{-}l_S$, we obtain:

$$A_1\alpha_1\cosh\left(\alpha_1(L-l_s)\right)+B_1\alpha_1\sinh\left(\alpha_1(L-l_s)\right)=k_5\bar{\sigma}_x+k_6\bar{\varepsilon}_y-k_7 \qquad [6.27]$$

where

$$\begin{aligned}k_5&=\frac{A_{55}}{h_2\tilde{Q}_{11}^{(2)}}\\ k_6&=\frac{A_{55}}{\bar{h}}\left(\frac{Q_{12}^{(1)}}{Q_{11}^{(1)}}-\frac{Q_{12}^{(2)}}{\tilde{Q}_{11}^{(2)}}\right)\\ k_7&=\frac{A_{55}\hat{\sigma}}{\bar{h}\tilde{Q}_{11}^{(2)}}+\tau_s^* l_s\alpha_1^2\end{aligned}$$

It should be noted now that [6.23] and [6.27] constitute a pair of linear algebraic equations for A_1 and B_1 which, upon inversion, can be arranged in matrix form as follows:

$$\begin{Bmatrix} A_1 \\ B_1 \end{Bmatrix} = \frac{1}{D}\begin{bmatrix} \cosh(\alpha_1 x^*) & -\alpha_1 \sinh(\alpha_1 (L-l_s)) \\ -\sinh(\alpha_1 x^*) & \alpha_1 \cosh(\alpha_1 (L-l_s)) \end{bmatrix}\begin{Bmatrix} k_5\bar{\sigma}_x + k_6\bar{\varepsilon}_y - k_7 \\ A_0 \sinh(\alpha_0 x^*) \end{Bmatrix} \qquad [6.28]$$

$$\text{where} \qquad D = \alpha_1 \cosh(\alpha_1 (L-l_s-x^*))$$

Comparison of [6.28] with [5.19] shows that the two expressions will be equal when l_s=0 in [6.28], which demonstrates that [5.19] is indeed a limiting case of the more general result obtained in [6.28].

It is important to observe that at this stage the constants, A_1 and B_1 contain the three yet undetermined quantities, namely, $x^*, \bar{\varepsilon}_y$ and l_s. These three unknowns are exactly matched by three boundary conditions. The first of these is the requirement that the lateral loading, N_y=0, leads to a condition of transverse equilibrium, while the remaining two conditions are given by:

$$\begin{aligned} &\bar{\sigma}_x^{(2)}(x=x^*) = \sigma_0 \\ &\tau^*(x=L-l_s) = \tau_s^* \end{aligned} \qquad [6.29]$$

Employment of [6.22] along with equilibrium equations in [4.5] and the boundary conditions of [6.3] yields the following expressions for the stress distributions within the interval $\underline{x^* \le x < L-l_s}$:

$$\begin{aligned} &\tau^*(x) = A_1 \sinh(\alpha_1 x) + B_1 \cosh(\alpha_1 x) \\ &\bar{\sigma}_x^{(1)}(x) = \frac{\tau_s^* l_s}{h_1} + \frac{1}{h_1\alpha_1}\begin{Bmatrix} A_1[\cosh(\alpha_1(L-l_s)) - \cosh(\alpha_1 x)] \\ +B_1[\sinh(\alpha_1(L-l_s)) - \sinh(\alpha_1 x)] \end{Bmatrix} \\ &\bar{\sigma}_x^{(2)}(x) = \frac{\bar{\sigma}_x \bar{h}}{h_2} - \frac{h_1 \bar{\sigma}_x^{(1)}(x)}{h_2} \end{aligned} \qquad [6.30]$$

Finally, in the region $L-l_s \leq x \leq L$ the interfacial shearing stress distribution is prescribed by the value of the interfacial shear strength, τ_s^*, and the normal stress distributions, $\bar{\sigma}_x^{(i)}$ in the 0° and 90° plies are then determined from the equilibrium equations of [4.5] along with the familiar boundary conditions at the location of the transverse crack:

$$\begin{aligned}
&\bar{\sigma}_x^{(1)}(x=L)=0 \\
&\bar{\sigma}_x^{(2)}(x=L)=\frac{\bar{\sigma}_x \bar{h}}{h_2}
\end{aligned} \qquad [4.25]R$$

Consequently, in the region $\underline{L-l_s \leq x \leq L}$ the stress distributions are given by:

$$\begin{aligned}
&\tau^*(x)=\tau_s^* \\
&\bar{\sigma}_x^{(1)}(x)=\frac{\tau_s^*(L-x)}{h_1} \\
&\bar{\sigma}_x^{(2)}(x)=\frac{\bar{\sigma}_x \bar{h}}{h_2}-\frac{\tau_s^*(L-x)}{h_2}
\end{aligned} \qquad [6.31]$$

With the stress distributions over $0 \leq x \leq L$ expressed in equations [6.21], [6.30] and [6.31], it is now possible to determine the constants A_1 and B_1 in terms of the unknown parameters, namely, x^*, $\bar{\varepsilon}_y$ and l_S.

The condition of transverse equilibrium given in [4.31] still applies. Appropriately splitting the integrations over the three regions for the current solution, the following expression is obtained:

$$\begin{aligned}
\bar{\sigma}_y \bar{h} L = h_1 &\left[\int_0^{x^*} \bar{\sigma}_y^{(1)} dx + \int_{x^*}^{L-l_s} \bar{\sigma}_y^{(1)} dx + \int_{L-l_s}^{L} \bar{\sigma}_y^{(1)} dx \right] \\
+h_2 &\left[\int_0^{x^*} \bar{\sigma}_y^{(2)} dx + \int_{x^*}^{L-l_s} \bar{\sigma}_y^{(2)} dx + \int_{L-l_s}^{L} \bar{\sigma}_y^{(2)} dx \right] = 0
\end{aligned} \qquad [6.32]$$

The integrations indicated in [6.32] are carried out after expressing the transverse stresses, $\bar{\sigma}_y^{(i)}$, in terms of the axial stresses, $\bar{\sigma}_x^{(i)}$ in analogy to equation [5.21]. Further manipulations yield:

$$\bar{\varepsilon}_y = \frac{\begin{array}{c} C_7 h_2 (L-x^*) - h_1 (C_1 - C_5)(\beta_9 + \beta_{10}) - h_1 \beta_6 (C_1 - C_3) \\ -\bar{\sigma}_x \left\{ h_1 \beta_4 (C_1 - C_3) + h_1 \beta_7 (C_1 - C_5) + C_3 \bar{h} x^* + C_5 \bar{h} (L - x^*) \right\} \end{array}}{\left\{ h_1 \beta_5 (C_1 - C_3) + h_1 \beta_8 (C_1 - C_5) + h_1 C_2 L + h_2 C_4 x^* + h_2 C_6 (L - x^*) \right\}} \qquad [6.33]$$

where

$$\beta_1 = x^* \cosh(\alpha_0 x^*) - \sinh(\alpha_0 x^*)/\alpha_0$$
$$\beta_2 = (L - l_s - x^*) \cosh(\alpha_1 (L - l_s)) - \sinh(\alpha_1 (L - l_s))/\alpha_1 + \sinh(\alpha_1 x^*)/\alpha_1$$
$$\beta_3 = (L - l_s - x^*) \sinh(\alpha_1 (L - l_s)) - \cosh(\alpha_1 (L - l_s))/\alpha_1 + \cosh(\alpha_1 x^*)/\alpha_1$$

$$\beta_4 = \frac{\bar{h} x^*}{h_1} - \frac{k_1 k_3 \beta_1}{h_1 \alpha_0} \qquad \beta_7 = \frac{\gamma_1 \beta_2 + \gamma_4 \beta_3}{h_1 \alpha_1}$$
$$\beta_5 = \frac{k_1 k_4 \beta_1}{h_1 \alpha_0} \qquad \beta_8 = \frac{\gamma_2 \beta_2 + \gamma_5 \beta_3}{h_1 \alpha_1}$$
$$\beta_6 = \frac{k_1 k_2 \beta_1}{h_1 \alpha_0} - \frac{\sigma_0 h_2 x^*}{h_1} \qquad \beta_9 = \frac{\gamma_3 \beta_2 + \gamma_6 \beta_3}{h_1 \alpha_1} + \frac{\tau_s^* l_s (L - l_s - x^*)}{h_1}$$
$$\beta_{10} = \frac{\tau_s^* l_s^2}{2 h_1}$$

and

$$\begin{Bmatrix} \gamma_1 \\ \gamma_2 \\ \gamma_3 \end{Bmatrix} = \frac{1}{D} \begin{bmatrix} k_5 & k_1 k_3 \alpha_1 \\ k_6 & -k_1 k_4 \alpha_1 \\ -k_7 & -k_1 k_2 \alpha_1 \end{bmatrix} \begin{Bmatrix} \cosh(\alpha_1 x^*) \\ \sinh(\alpha_1 (L - l_s)) \sinh(\alpha_0 x^*) \end{Bmatrix}$$

$$\begin{Bmatrix} \gamma_4 \\ \gamma_5 \\ \gamma_6 \end{Bmatrix} = \frac{1}{D} \begin{bmatrix} -k_5 & -k_1 k_3 \alpha_1 \\ -k_6 & k_1 k_4 \alpha_1 \\ k_7 & k_1 k_2 \alpha_1 \end{bmatrix} \begin{Bmatrix} \sinh(\alpha_1 x^*) \\ \cosh(\alpha_1 (L - l_s)) \sinh(\alpha_0 x^*) \end{Bmatrix}$$

Note that the constants k_1-k_4 carry over from the definition of A_0 in equation [6.21], while k_5-k_7 and D are given in [6.27] and [6.28] respectively.

With the transverse strain, $\bar{\varepsilon}_y$ expressed in terms x^* and l_s, according to [6.33], the problem reduces to determining x^* and l_s simultaneously employing a numerical iterative scheme. The procedure is outlined below:

Step (1) Guess an initial slip zone length, l_s.

Step (2) Guess an x^* location, (note: $x^*<L-l_s$ by definition).

Step (3) Employing [6.30], check if the first condition of [6.29] is satisfied, i.e. $\bar{\sigma}_x^{(2)}(x=x^*)=\sigma_0$. If so, then x^* for the current l_s is valid. If not repeat the procedure starting again at step (2).

step (4) Employing [6.30], check if the second condition of [6.29] is satisfied, i.e. $\tau^*(x=L-l_s)=\tau_s^*$.

If so, then x^* and l_s have been located. If not then repeat the procedure starting at step (1).

It should be pointed out that this iterative scheme consists of a double root locating algorithm, first selecting trial values for the slip zone length, l_s, in the outer loop of the procedure and then the location of x^* is determined for each value of l_s within the inner loop .

With the solution thus available, it is now possible to calculate the global strain, $\bar{\varepsilon}_x$. Employing [5.2] the following result is obtained:

$$\bar{\varepsilon}_x=\frac{1}{L}\left[\int_0^{x^*}\frac{\bar{\sigma}_x^{(2)}-Q_{12}^{(2)}\bar{\varepsilon}_y}{Q_{11}^{(2)}}dx+\int_{x^*}^{L-l_s}\frac{\bar{\sigma}_x^{(2)}-Q_{12}^{(2)}\bar{\varepsilon}_y-\hat{\sigma}}{\tilde{Q}_{11}^{(2)}}dx+\int_{L-l_s}^{L}\frac{\bar{\sigma}_x^{(2)}-Q_{12}^{(2)}\bar{\varepsilon}_y-\hat{\sigma}}{\tilde{Q}_{11}^{(2)}}dx\right] \qquad [6.34]$$

These integrals can be evaluated in a straightforward manner after substituting the stress distributions for the three regions from equations [6.21], [6.30], and [6.31]. The global strain for the combined bilinear response and interfacial slip, Case II is then found to be:

$$\bar{\varepsilon}_x = \frac{\bar{u}_2(L)}{L} = \frac{1}{Q_{11}^{(2)}L}\left\{\frac{\bar{\sigma}_x \bar{h} x^*}{h_2} - \frac{h_1}{h_2}\left(\bar{\sigma}_x\beta_4 + \bar{\varepsilon}_y\beta_5 + \beta_6\right) - Q_{12}^{(2)}\bar{\varepsilon}_y x^*\right\}$$
$$+\frac{1}{\tilde{Q}_{11}^{(2)}L}\left\{\frac{\bar{\sigma}_x\bar{h}(L-x^*)}{h_2} - \frac{h_1}{h_2}\left(\bar{\sigma}_x\beta_7 + \bar{\varepsilon}_y\beta_8 + \beta_9\right) - \left(Q_{12}^{(2)}\bar{\varepsilon}_y + \hat{\sigma}\right)(L-x^*) - \frac{h_1}{h_2}\beta_{10}\right\} \qquad [6.35]$$

6.2.3 Bilinear Response Coupled with Interlaminar Slip, Case III

This case represents a limiting circumstance of Case II, when the region of bilinear response of the 0° plies extends completely to the origin, i.e., $x^*=0$. The slip zone, l_s, however is still located within $0 \le x \le L$.

The analysis for this case resembles the circumstance of linear behavior with slip, since it does not necessitate the consideration of two sets of constitutive relations for the response of the 0° plies. However, it remains necessary to construct two solutions within the contact and slip regions, namely, $0 \le x < L-l_s$ and $L-l_s \le x \le L$.

For the region, $\underline{0 \le x < L-l_s}$, the stress distributions are determined similarly to the linear slip analysis, however since the reduced modulus of the 0° plies applies in the present case, it is necessary to use the replacements $Q_{11}^{(2)} \to \tilde{Q}_{11}^{(2)}$, and $\alpha_0 \to \alpha_1$. Thus in analogy with [6.7], the stress distributions are given by:

$$\tau^*(x) = A_0\sinh(\alpha_1 x)$$
$$\bar{\sigma}_x^{(1)}(x) = \frac{\tau_s^* l_s}{h_1} + \frac{A_0}{h_1\alpha_1}\left\{\cosh\left(\alpha_1(L-l_s)\right) - \cosh\left(\alpha_1 x\right)\right\} \qquad [6.36]$$
$$\bar{\sigma}_x^{(2)}(x) = \frac{\bar{\sigma}_x\bar{h}}{h_2} - \frac{\bar{\sigma}_x^{(1)}h_1}{h_2}$$

where

$$A_0 = k_1(k_2\bar{\sigma}_x + k_3\bar{\varepsilon}_y - k_4) - k_8$$

and

$$k_1 = A_{55} / \left(\bar{h}\,\alpha_1 Q_{11}^{(1)} \tilde{Q}_{11}^{(2)} \cosh\left(\alpha_1 (L-l_s)\right)\right)$$
$$k_2 = \frac{\bar{h} Q_{11}^{(1)}}{h_2}$$
$$k_3 = Q_{12}^{(1)} \tilde{Q}_{11}^{(2)} - Q_{12}^{(2)} Q_{11}^{(1)}$$
$$k_4 = Q_{11}^{(1)} \hat{\sigma}$$
$$k_8 = \frac{\tau_s^* l_s \alpha_1}{\cosh\left(\alpha_1 (L-l_s)\right)}$$

$$\bar{\varepsilon}_y = \frac{h_2 C_7 L - C_5 \bar{\sigma}_x \bar{h} L + (C_5 - C_1)\left(k_1 k_2 \beta_1 \bar{\sigma}_x - k_1 k_4 \beta_1 - k_8 \beta_1 + \tau_s^* l_s (L-l_s) + \frac{\tau_s^* l_s^2}{2}\right)}{L\left(h_1 C_2 + h_2 C_6\right) + \left(C_1 - C_5\right) k_1 k_3 \beta_1}$$

$$\beta_1 = \frac{1}{\alpha_1}\left\{(L-l_s)\cosh\left(\alpha_1 (L-l_s)\right) - \sinh\left(\alpha_1 (L-l_s)\right)/\alpha_1\right\}$$

It should be noted once again, that although the solution procedure is the same as for the linear slip case, the constants k_i, Ao have been redefined for the current solution.

Turning to the slip region, $L-l_s \le x \le L$, the solution has an identical form as in the linear case expressed in equations [6.2]. Therefore, for $\underline{L-l_s \le x \le L}$ we have:

$$\tau^*(x) = \tau_s^*$$
$$\sigma_x^{(1)}(x) = \frac{\tau_s^*(L-x)}{h_1} \qquad [6.37]$$
$$\sigma_x^{(2)}(x) = \frac{\bar{\sigma}_x \bar{h}}{h_2} - \frac{\tau_s^*(L-x)}{h_2}$$

Similar to previous cases, the average normal strain is found to be:

$$\bar{\varepsilon}_x = \frac{1}{L}\int_0^{L-l_s} \frac{\bar{\sigma}_x^{(2)} - Q_{12}^{(2)} \bar{\varepsilon}_y - \hat{\sigma}}{\tilde{Q}_{11}^{(2)}} dx + \frac{1}{L}\int_{L-l_s}^{L} \frac{\bar{\sigma}_x^{(2)} - Q_{12}^{(2)} \bar{\varepsilon}_y - \hat{\sigma}}{\tilde{Q}_{11}^{(2)}} dx \qquad [6.38]$$

Substituting the expressions for $\bar{\sigma}_x^{(2)}$ from [6.36] and [6.37] and carrying out the integrations, the global strain for Case III becomes:

$$\bar{\varepsilon}_x = \frac{1}{\tilde{Q}_{11}^{(2)}} \left\{ \begin{array}{l} \dfrac{\bar{\sigma}_x \bar{h}}{h_2} + \dfrac{\tau_s^* l_s}{2h_2 L}(l_s - 2L) - \left(Q_{12}^{(2)}\bar{\varepsilon}_y + \hat{\sigma}\right) \\ - \dfrac{A_0}{h_2\alpha_1 L}\left[(L-l_s)\cosh(\alpha_1(L-l_s)) - \dfrac{\sinh(\alpha_1(L-l_s))}{\alpha_1}\right] \end{array} \right\} \qquad [6.39]$$

6.3 Special Considerations Concerning the Progression of the Slip Zone

Sections 6.1 and 6.2 contain the formulations for all possible cases of interfacial slippage coupled with bilinear behavior of the 0° plies. These solutions suffice when considering a fixed geometry with a specific half crack spacing, say L. However, recall that it is necessary to consider two crack geometries with half crack spacings of L and $L/2$ at each applied stress, $\bar{\sigma}_x$, in order to compare available energy levels for crack growth. Two such geometries are depicted in Figure 6.7 below:

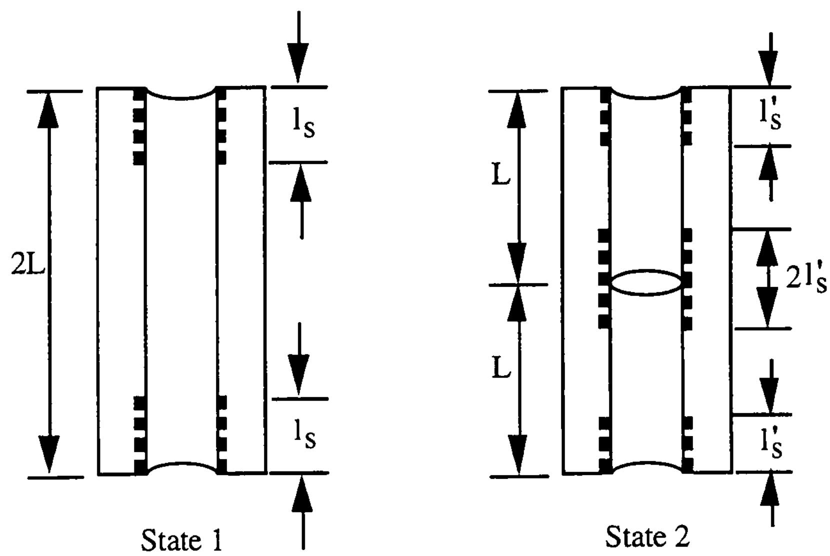

Figure 6.7 Crack Density and Slip Zone Progression

It should be realized, that the current model considers that the introduction of new transverse cracks are accompanied by slip zones with lengths equal to that in the previous crack geometry. Although this assumption is an inherent limitation to the model, the alternative approach would be to calculate the growth of every individual set of slip zones for all of the transverse cracks as they form progressively. Such an analysis would become intractable because it will no longer involve slip regions of equal lengths, thereby incurring the loss of symmetry about $x=0$.

It turns out that as the two foregoing geometries are considered, it may be possible to have a slip zone length for a crack spacing of $L/2$ which is shorter than that for spacing L, as sketched in Figure 6.7, with $l'_S < l_S$. This circumstance cannot be handled in the context of the present model, which considers two states with fully established transverse cracks that span the entire width of the specimen, but does not address the details of the transition between states 1 and 2. Therefore, although the situation where $l'_S < l_S$ may occur in reality, it will be discarded in the present analysis in order to retain tractability. When such a circumstance is nevertheless predicted by the current analysis, the resulting value of $l'_S < l_S$ will be modified to read : $l'_S = l_S$. This modification implies that for a crack spacing of $L/2$, a given value of $\bar{\sigma}_x$ will correspond to a prescribed value of l_S. In the context of the previous analysis, this circumstance implies an over specified boundary value problem whose solution, though simpler since the slip zone length is now known, requires a modified approach.

6.3.1 Modified Linear Response Coupled with Interlaminar Slip

Recall from section 6.1 the stress distributions for the linear slip solution. For the region $0 \le x < L - l_s$ the interfacial shearing stress was given as:

$$\tau^*(x) = A_0 \sinh(\alpha_0 x) \qquad [6.7]R$$

And we had the boundary condition:

$$\tau^*(x = L - l_s) = \tau_s^* \qquad [6.1]R$$

However, since by hypothesis the value of l_s is considered to be known, it is possible to solve for A_0 immediately from [6.1] and [6.7]:

$$A_0 = \frac{\tau_s^*}{\sinh\left(\alpha_0 (L - l_s)\right)} \qquad [6.40]$$

The stress distributions in this modified case will retain the same form as in section 6.1. Specifically equations [6.2] and [6.7] will apply within the respective regions $0 \le x < L - l_s$ and $L - l_s \le x \le L$. Additionally it should be noted that the calculation of global strain for this modified case will remain the same as that given in section 6.1, upon employment of the modified value of A_0 given in equation [6.40].

6.3.2 Modified Bilinear Response Coupled with Interfacial Slip, Case I

In this case, the necessary modification is accomplished by a simple adjustment of the analysis of section 6.2.1. Since the slip length, l_s is again known by hypothesis, the constant A_0 is once again given by [6.40]. The remainder of the solution will then retain the forms given in section 6.2.1, employing the modified value for A_0, for the stress distributions for the three regions given in equations [6.12], [6.14] and [6.15].

6.3.3 Modified Bilinear Response Coupled with Interfacial Slip, Case II

In this case, the hypothesis that l_S is prescribed will result in a more complicated modification than in sections 6.3.1 and 6.3.2. The reason for the additional complexity is due to the fact the condition in [6.1] will influence the solutions in the adjacent regions $0 \le x < x^*$ and $L - l_s \le x \le L$. It should be noted that the formulation of this solution closely parallels that of section 6.2.2.

The form of the modified solution in the region $\underline{0 \le x < x^*}$ remains unchanged, since boundary condition [6.1] applies to a location outside this region. Consequently, the stress distribution is still given by:

$$\begin{aligned} &\tau^*(x) = A_0 \sinh(\alpha_0 x) \\ &\bar{\sigma}_x^{(1)} = \frac{\bar{\sigma}_x \bar{h}}{h_1} - \frac{\sigma_0 h_2}{h_1} + \frac{A_0}{h_1 \alpha_0}\left(\cosh(\alpha_0 x^*) - \cosh(\alpha_0 x)\right) \qquad \text{[6.21]R} \\ &\bar{\sigma}_x^{(2)} = \frac{\bar{\sigma}_x \bar{h}}{h_2} - \frac{\bar{\sigma}_x^{(1)} h_1}{h_2} \end{aligned}$$

Turning to the region $x^* \le x < L - l_s$, we note that the form of the solution given in [6.30] as well as the boundary conditions stated in [5.5v], and [6.3] remain valid. However, since the slip zone length is now assumed to be known, it is necessary to include the condition given in [6.1]. Summarizing these conditions, we then have:

$$\tau^*(x^*+) = \tau^*(x^*-) \qquad \text{[5.5v]R}$$

$$\begin{aligned} &\bar{\sigma}_x^{(1)}(x = L - l_s) = \frac{\tau_s^* l_s}{h_2} \\ &\bar{\sigma}_x^{(2)}(x = L - l_s) = \frac{\bar{\sigma}_x \bar{h}}{h_2} - \frac{\tau_s^* l_s}{h_2} \end{aligned} \qquad \text{[6.3]R}$$

$$\tau^{*}(x = L - l_s) = \tau_s^{*} \qquad [6.1]\text{R}$$

Recall that in view of [6.23] we had :

$$A_1 \sinh(\alpha_1 x^*) + B_1 \cosh(\alpha_1 x^*) = A_o \sinh(\alpha_0 x^*) \qquad [6.23]\text{R}$$

Employing [6.1] gives:

$$A_1 \sinh(\alpha_1 (L - l_s)) + B_1 \cosh(\alpha_1 (L - l_s)) = \tau_s^{*} \qquad [6.41]$$

Upon inversion, these last two expressions can then be arranged matrix form to read:

$$\begin{Bmatrix} A_1 \\ B_1 \end{Bmatrix} = \frac{1}{D} \begin{bmatrix} \cosh(\alpha_1 x^*) & -\cosh(\alpha_1 (L - l_s)) \\ -\sinh(\alpha_1 x^*) & \sinh(\alpha_1 (L - l_s)) \end{bmatrix} \begin{Bmatrix} \tau_s^{*} \\ A_0 \sinh(\alpha_0 x^*) \end{Bmatrix} \qquad [6.42]$$

where $\qquad D = \sinh(\alpha_1 (L - l_s - x^*))$

Note that equation [6.42] is analogous to [6.28], with the constants A_1 and B_1 once again given in terms of the parameters x*, $\bar{\varepsilon}_y$, and l_s, however the parameter l_s is now presumed known. The stress distribution for this region, $(x^* \leq x < L - l_s)$, which is still give by [6.30], reads:

$$\tau^{*}(x) = A_1 \sinh(\alpha_1 x) + B_1 \cosh(\alpha_1 x)$$

$$\bar{\sigma}_x^{(1)}(x) = \frac{\tau_s^{*} l_s}{h_1} + \frac{1}{h_1 \alpha_1} \begin{Bmatrix} A_1 [\cosh(\alpha_1 (L - l_s)) - \cosh(\alpha_1 x)] \\ + B_1 [\sinh(\alpha_1 (L - l_s)) - \sinh(\alpha_1 x)] \end{Bmatrix} \qquad [6.30]\text{R}$$

$$\bar{\sigma}_x^{(2)}(x) = \frac{\bar{\sigma}_x \bar{h}}{h_2} - \frac{h_1 \bar{\sigma}_x^{(1)}(x)}{h_2}$$

Now the modified expressions for A_1 and B_1 are given in [6.42] (instead of [6.28] in section 6.2.2).

Finally, within the region, $\underline{L-l_s \le x \le L}$, the expressions for the stress distributions can be taken directly from section 6.2.2, namely:

$$\tau^*(x)=\tau_s^*$$
$$\bar{\sigma}_x^{(1)}(x)=\frac{\tau_s^*(L-x)}{h_1} \qquad [6.31]R$$
$$\bar{\sigma}_x^{(2)}(x)=\frac{\bar{\sigma}_x\bar{h}}{h_2}-\frac{\tau_s^*(L-x)}{h_2}$$

As in the previous solution for Case II, it remains necessary to determine the unknown parameters x^* and $\bar{\varepsilon}_y$ that are needed to compute the constants A_1 and B_1. This is accomplished, as before by first employing equilibrium in the transverse direction, resulting in an expression for the transverse strain, $\bar{\varepsilon}_y$ in terms of x^*:

$$\bar{\varepsilon}_y=\frac{\begin{array}{c}C_7h_2(L-x^*)-h_1(C_1-C_5)(\beta_9+\beta_{10})-h_1\beta_6(C_1-C_3)\\ -\bar{\sigma}_x\left\{h_1\beta_4(C_1-C_3)+h_1\beta_7(C_1-C_5)+C_3\bar{h}x^*+C_5\bar{h}(L-x^*)\right\}\end{array}}{\left\{h_1\beta_5(C_1-C_3)+h_1\beta_8(C_1-C_5)+h_1C_2L+h_2C_4x^*+h_2C_6(L-x^*)\right\}} \qquad [6.33]R$$

where

$$\beta_1=x^*\cosh(\alpha_0x^*)-\sinh(\alpha_0x^*)/\alpha_0$$
$$\beta_2=(L-l_s-x^*)\cosh(\alpha_1(L-l_s))-\sinh(\alpha_1(L-l_s))/\alpha_1+\sinh(\alpha_1x^*)/\alpha_1$$
$$\beta_3=(L-l_s-x^*)\sinh(\alpha_1(L-l_s))-\cosh(\alpha_1(L-l_s))/\alpha_1+\cosh(\alpha_1x^*)/\alpha_1$$

$$\beta_4=\frac{\bar{h}x^*}{h_1}-\frac{k_1k_3\beta_1}{h_1\alpha_0}$$
$$\beta_5=\frac{k_1k_4\beta_1}{h_1\alpha_0}$$
$$\beta_6=\frac{k_1k_2\beta_1}{h_1\alpha_0}-\frac{\sigma_0h_2x^*}{h_1}$$

$$\beta_7=\frac{\gamma_1\beta_2+\gamma_4\beta_3}{h_1\alpha_1}$$
$$\beta_8=\frac{\gamma_2\beta_2+\gamma_5\beta_3}{h_1\alpha_1}$$
$$\beta_9=\frac{\gamma_3\beta_2+\gamma_6\beta_3}{h_1\alpha_1}+\frac{\tau_s^*l_s(L-l_s-x^*)}{h_1}$$
$$\beta_{10}=\frac{\tau_s^*l_s^2}{2h_1}$$

These expressions are the same as in section 6.2.2, however, in the present case the constants γ_i will differ from those listed in 6.2.2 and now read:

$$\begin{Bmatrix}\gamma_1\\ \gamma_2\\ \gamma_3\end{Bmatrix}=\frac{1}{D}\begin{bmatrix}0 & k_1k_3\\ 0 & -k_1k_4\\ 1 & -k_1k_2\end{bmatrix}\begin{Bmatrix}\tau_s^*\cosh(\alpha_1 x^*)\\ \cosh(\alpha_1(L-l_s))\sinh(\alpha_0 x^*)\end{Bmatrix}$$

$$\begin{Bmatrix}\gamma_4\\ \gamma_5\\ \gamma_6\end{Bmatrix}=\frac{1}{D}\begin{bmatrix}0 & -k_1k_3\\ 0 & k_1k_4\\ -1 & k_1k_2\end{bmatrix}\begin{Bmatrix}\tau_s^*\sinh(\alpha_1 x^*)\\ \sinh(\alpha_1(L-l_s))\sinh(\alpha_0 x^*)\end{Bmatrix}$$

$$D=\sinh(\alpha_1(L-l_s-x^*))$$

In summary, the modifications to due to the assumption that l_S is prescribed do not change the forms of the solutions expressed in section 6.2.2, but require adjustments in the various constants listed therein.

It should also be noted that since the slip length l_S is assumed known, it is no longer necessary to use a nested root finding scheme to determine the slip and yield zone lengths as in section 6.2.2. A single iterative procedure will suffice to determine the location of x^*, which is the only parameter that needs to be determined.

6.3.4 Modified Bilinear Response Coupled with Interfacial Slip, Case III

The procedure in this circumstance closely resembles the modifications employed in 6.3.1 for the linear case. The stress distributions and the global strain calculations will be the same as derived in section 6.2.3 for an unknown l_S, with the exception that the constant A_0 is now given by :

$$A_0 = \frac{\tau_s^*}{\sinh\left(\alpha_1(L-l_s)\right)} \qquad [6.40]R$$

Subsequently, the complete modification for this case is accomplished by employing the foregoing expression for A_0 in the expressions given in section 6.2.3.

6.4 Summary of Solutions and Order of Occurrence

It may be helpful at this point to summarize the results for the various solutions developed for the cases with and without interfacial slip between the 0° and 90° ply groups. The following list is arranged in the typical order of damage initiation and progression, as it occurs in the cross-ply ceramic laminate under monotonically increasing applied stress, $\overline{\sigma}_x$.

(1) Linear Analysis Without Slip: The results of this case remain valid at relatively low levels of applied stress, when the interfacial shearing stress is below the interfacial shearing strength, $\tau^*(x) < \tau_s^*$, and the stresses $\overline{\sigma}_x^{(2)}$ in the 0° plies are below the yield stress, σ_0, of the 0° plies over the entire range, $0 \le x \le L$. This solution is given in Chapter 4.

2) Linear Solution with Slip : As the applied stress, $\overline{\sigma}_x$, increases, the maximum value of the interfacial shearing stress attains the level of τ_s^* over a region $L - l_s \le x \le L$. Since the maximum value of $\tau^*(x)$ occurs in the vicinity of the transverse crack located at $x=L$, the slip zone emanates from the crack location and extends inwardly with each increase of applied stress (see Figure 6.2). If the stresses, $\overline{\sigma}_x^{(2)}$ remain below σ_0, there is no need to address the non-linearity of the 0° plies. Locating the length of the slip zone, l_s requires a single iterative operation. This solution is given in Section 6.2.1.

(3) Bilinear Solution with Slip, Case I : Upon further increase in the applied stress, the slip zone extends further inward from the crack location at $x=L$ while the stresses in the 0° plies continue to increase until they reach, and then exceed, the "yield stress", σ_0. Referring to the normal stress distribution shown in Figure 6.2, it can be seen that the axial stress in the 0° plies has a maximal value at the crack face ($x=L$), hence the onset of yielding will initiate at this location. At this stage, the non-linearity of the 0° plies must be considered. Due to the relative magnitudes of τ_s^* and σ_0, it turns out that the location of x^*, where $\bar{\sigma}_x^{(2)}(x^*)=\sigma_0$ is located inside the slip region. Since the axial stresses within the slip zone are linear functions of x, as discussed in section 6.2.2, the location of x^* is obtainable in a straightforward manner. In this case the slip zone length, l_s, can be determined through a single iterative procedure.

(4) Bilinear Solution with Slip, Case II: Additional increases in applied stress, $\bar{\sigma}_x$, result in further growth of both the slip and yield zones. At a certain stage, the extent of the yield zone may exceed the length of the slip zone as depicted in Figure 6.6. Specifically, we then have $x^* < L-l_s$. The details of this solution, given in section 6.2.2 reveal that the determination of the slip zone length l_s along with the yield location x^* requires the employment of a nested simultaneous iterative procedure.

(5) Bilinear Solution with Slip, Case III: In this circumstance the non-linear response of the 0° plies occurs over the entire domain, $0 \leq x \leq L$, while the slip region is confined to the region $L-l_s \leq x \leq L$. The solution resembles the linear analysis with slippage, however the reduced modulus of the 0° plies must be employed for all x. The slip zone length for this case is again determined by means of a single iterative procedure.

6.5 Energy Calculations for Linear and Bilinear Stress-Strain Response with Interlaminar Slip

As mentioned at the beginning of this chapter, the mismatch in the average displacement between the 0° and 90° plies within the slip zone gives rise to a dissipative energy term. The energy is caused solely by the frictional forces associated with the slippage between the 0° and 90° ply groups, resulting in a reduction of the available energy for transverse crack formation.

However, it should be noted that any of the preceding solutions which included interfacial slip, have implicitly incorporated the discontinuity in displacements over the slip zone at the 0°/90° interface. Consequently, the evaluation of the complementary energy, U^*, which involves volume integrals, accounts for the presence of the aforementioned dissipative term. Hence, the expressions for U^*, given in equations [4.40] and [4.41] remain valid in the presence of slip as well. Namely:

$$U_\sigma^*(L) = 4h_1 \int_0^L \int_0^{\sigma_x^{(1)}} \tilde{\varepsilon}_x^{(1)}\left(\tilde{\sigma}_x^{(1)}\right) d\tilde{\sigma}_x^{(1)} dx + 4h_2 \int_0^L \int_0^{\sigma_x^{(2)}} \tilde{\varepsilon}_x^{(2)}\left(\tilde{\sigma}_x^{(2)}\right) d\tilde{\sigma}_x^{(2)} dx \qquad [4.40]\text{R}$$

$$U_\tau^*(L) = 4\int_0^L \int_0^{h_1} \int_0^{\tau_{xz}^{(1)}} \tilde{\gamma}_{xz}^{(1)}\left(\tilde{\tau}_{xz}^{(1)}\right) d\tilde{\tau}_{xz}^{(1)} dz dx + 4\int_0^L \int_{h_1}^{\bar{h}} \int_0^{\tau_{xz}^{(2)}} \tilde{\gamma}_{xz}^{(2)}\left(\tilde{\tau}_{xz}^{(2)}\right) d\tilde{\tau}_{xz}^{(2)} dz dx \qquad [4.41]\text{R}$$

And as before:

$$U^* = U_\sigma^* + U_\tau^* \qquad [4.42]\text{R}$$

In spite of the formal validity of the preceding expressions, it is necessary to exercise care to split the above integrals among the appropriate ranges of x, with due consideration for the proper stress distributions that change within the distinct regions. In this context it is helpful to recall the constitutive equations that account for the bilinear response of the 0° plies. From Chapter 5 we have:

$$\begin{aligned}\bar{\sigma}_x^{(1)} &= Q_{11}^{(1)}\bar{u}_1' + Q_{12}^{(1)}\bar{\varepsilon}_y \\ \bar{\sigma}_y^{(i)} &= Q_{12}^{(i)}\bar{u}_i' + Q_{22}^{(i)}\bar{\varepsilon}_y\end{aligned} \qquad (0 \le x \le L)$$

$$\begin{aligned}\bar{\sigma}_x^{(2)} &= Q_{11}^{(2)}\bar{u}_2' + Q_{12}^{(2)}\bar{\varepsilon}_y && (0 \le x \le L) \\ \bar{\sigma}_x^{(2)} &= \tilde{Q}_{11}^{(2)}\bar{u}_2' + Q_{12}^{(2)}\bar{\varepsilon}_y + \hat{\sigma} && (x^* \le x \le L)\end{aligned} \qquad [5.2R]$$

where

$$\hat{\sigma} = \sigma_0\left(1 - \frac{\tilde{Q}_{11}^{(2)}}{Q_{11}^{(2)}}\right)$$

6.5.1 Energy Calculations for Linear Response with Interlaminar Slip

In this case there are different stress distributions on the two regions, $0 \le x < L - l_s$ and $L - l_s \le x \le L$ as shown in Figure 6.2. This requires splitting the integrals of [4.40] and [4.41] over these regions to carry out the integrations with respect to x. However, since the response of the 0° plies is assumed linear for all x in this circumstance, the inner integration with respect to $\tilde{\sigma}_x^{(i)}$ in [4.40] can be carried out directly, leading to:

$$\begin{aligned}U_\sigma^*(L) = {} & \frac{4h_1}{Q_{11}^{(1)}}\int_0^{L-l_s}\left(\frac{\left(\bar{\sigma}_x^{(1)}\right)^2}{2} - \bar{\sigma}_x^{(1)}Q_{12}^{(1)}\bar{\varepsilon}_y\right)dx + \frac{4h_1}{Q_{11}^{(1)}}\int_{L-l_s}^{L}\left(\frac{\left(\bar{\sigma}_x^{(1)}\right)^2}{2} - \bar{\sigma}_x^{(1)}Q_{12}^{(1)}\bar{\varepsilon}_y\right)dx \\ & + \frac{4h_2}{Q_{11}^{(2)}}\int_0^{L-l_s}\left(\frac{\left(\bar{\sigma}_x^{(2)}\right)^2}{2} - \bar{\sigma}_x^{(2)}Q_{12}^{(2)}\bar{\varepsilon}_y\right)dx + \frac{4h_2}{Q_{11}^{(2)}}\int_{L-l_s}^{L}\left(\frac{\left(\bar{\sigma}_x^{(2)}\right)^2}{2} - \bar{\sigma}_x^{(2)}Q_{12}^{(2)}\bar{\varepsilon}_y\right)dx\end{aligned} \qquad [6.43]$$

The expressions for the stress distributions of [6.43] are then given in equations [6.2] and [6.7].

Turning to the energy contribution of the shearing stresses U_τ^* to the total complementary energy U^*, it is possible to employ the expressions given in Chapter 4 for the linear case without slip. The only difference, in view of the presence of slip, occurs due to the necessity to split the integrations in [4.41] between the slip and contact regions. Upon performing the integrations, we obtain:

$$U_\tau^* = \frac{2}{3}\left\{A_0^2\left(\frac{\sinh\left(2\alpha_0(L-l_s)\right)}{4\alpha_0} - \frac{L-l_s}{2}\right) + \left(\tau_s^*\right)^2 l_s\right\}\left\{\frac{h_1}{C_{55}^{(1)}} + \frac{h_2}{C_{55}^{(2)}}\right\} \qquad [6.44]$$

As noted earlier, the total complementary energy available for transverse crack formation is still given as:

$$U^* = U_\sigma^* + U_\tau^* \qquad [4.42]\mathrm{R}$$

6.5.2 Energy Calculations for Bilinear Response with Interlaminar Slip, Case I

The contribution of the axial stresses to the complementary energy resembles that expressed in section 5.5.1 in the absence of interfacial slip, namely:

$$I_1 = \frac{4h_1}{Q_{11}^{(1)}}\left\{\int_0^{x^*}\left(\frac{\left(\bar{\sigma}_x^{(1)}\right)^2}{2} - \bar{\sigma}_x^{(1)}Q_{12}^{(1)}\bar{\varepsilon}_y\right)dx + \int_{x^*}^{L}\left(\frac{\left(\bar{\sigma}_x^{(1)}\right)^2}{2} - \bar{\sigma}_x^{(1)}Q_{12}^{(1)}\bar{\varepsilon}_y\right)dx\right\} \qquad [5.31]\mathrm{R}$$

$$I_2=\frac{4h_2}{Q_{11}^{(2)}}\int_0^{x^*}\left(\frac{\left(\bar{\sigma}_x^{(2)}\right)^2}{2}-\bar{\sigma}_x^{(2)}\bar{\varepsilon}_y Q_{12}^{(2)}\right)dx+\frac{4h_2}{\tilde{Q}_{11}^{(2)}}\int_{x^*}^{L}\left(\frac{\left(\bar{\sigma}_x^{(2)}\right)^2}{2}-\bar{\sigma}_x^{(2)}\left(\bar{\varepsilon}_y Q_{12}^{(2)}+\hat{\sigma}\right)\right)dx$$
$$+4h_2(L-x^*)\left\{\frac{1}{Q_{11}^{(2)}}\left(\frac{\sigma_0^2}{2}-\sigma_0\bar{\varepsilon}_y Q_{12}^{(2)}\right)+\frac{1}{\tilde{Q}_{11}^{(2)}}\left(\sigma_0(\bar{\varepsilon}_y Q_{12}^{(2)}+\hat{\sigma})-\frac{\sigma_0^2}{2}\right)\right\} \qquad [5.34]R$$

where $\qquad U_\sigma^*=I_1+I_2$

The only modification required due to the presence of interfacial slip is the necessity to further split the ranges of integration to account for the distinct solutions listed in equations [6.12], [6.14] and [6.15]. Then expressions [5.31] and [5.34] can be recast in the following form:

$$I_1=\frac{4h_1}{Q_{11}^{(1)}}\int_0^{L-l_s}\left(\frac{\left(\bar{\sigma}_x^{(1)}\right)^2}{2}-\bar{\sigma}_x^{(1)}Q_{12}^{(1)}\bar{\varepsilon}_y\right)dx+\frac{4h_1}{Q_{11}^{(1)}}\int_{L-l_s}^{x^*}\left(\frac{\left(\bar{\sigma}_x^{(1)}\right)^2}{2}-\bar{\sigma}_x^{(1)}Q_{12}^{(1)}\bar{\varepsilon}_y\right)dx$$
$$+\frac{4h_1}{Q_{11}^{(1)}}\int_{x^*}^{L}\left(\frac{\left(\bar{\sigma}_x^{(1)}\right)^2}{2}-\bar{\sigma}_x^{(1)}Q_{12}^{(1)}\bar{\varepsilon}_y\right)dx \qquad [6.45]$$

$$I_2=\frac{4h_2}{Q_{11}^{(2)}}\int_0^{L-l_s}\left(\frac{\left(\bar{\sigma}_x^{(2)}\right)^2}{2}-\bar{\sigma}_x^{(2)}\bar{\varepsilon}_y Q_{12}^{(2)}\right)dx+\frac{4h_2}{Q_{11}^{(2)}}\int_{L-l_s}^{x^*}\left(\frac{\left(\bar{\sigma}_x^{(2)}\right)^2}{2}-\bar{\sigma}_x^{(2)}\bar{\varepsilon}_y Q_{12}^{(2)}\right)dx$$
$$+\frac{4h_2}{\tilde{Q}_{11}^{(2)}}\int_{x^*}^{L}\left(\frac{\left(\bar{\sigma}_x^{(2)}\right)^2}{2}-\bar{\sigma}_x^{(2)}\left(\bar{\varepsilon}_y Q_{12}^{(2)}+\hat{\sigma}\right)\right)dx \qquad [6.46]$$
$$+4h_2(L-x^*)\left\{\frac{1}{Q_{11}^{(2)}}\left(\frac{\sigma_0^2}{2}-\sigma_0\bar{\varepsilon}_y Q_{12}^{(2)}\right)+\frac{1}{\tilde{Q}_{11}^{(2)}}\left(\sigma_0(\bar{\varepsilon}_y Q_{12}^{(2)}+\hat{\sigma})-\frac{\sigma_0^2}{2}\right)\right\}$$

The energy contribution from the shearing stresses for this case is calculated according to the same procedure as for the linear slip solution. It should be noted that since the shear response is assumed linear, and is uncoupled from the non-linear response of the

0° plies, the integrations can be carried out without regard to the location, x^*, and it is only necessary to split the integrals at $x=L-l_s$. Consequently, it is not surprising that the result is given by a form that is identical to that obtained for the linear slip case, namely:

$$U_\tau^* = \frac{2}{3}\left\{A_0^2\left(\frac{\sinh(2\alpha_0(L-l_s))}{4\alpha_0}-\frac{L-l_s}{2}\right)+\left(\tau_s^*\right)^2 l_s\right\}\left\{\frac{h_1}{C_{55}^{(1)}}+\frac{h_2}{C_{55}^{(2)}}\right\} \qquad [6.44]R$$

6.5.3 Energy Calculations for Bilinear Response with Interlaminar Slip, Case II

For this case, the calculation of the contribution of the axial and shearing stresses to the complementary energy, U^*, are analogous to the two previous cases. Employing the general equations for the complementary energy due to axial stresses (equation [4.40]) results in the following expressions:

$$\begin{aligned} I_1 &= \frac{4h_1}{Q_{11}^{(1)}}\int_0^{x^*}\left(\frac{\left(\bar{\sigma}_x^{(1)}\right)^2}{2}-\bar{\sigma}_x^{(1)}Q_{12}^{(1)}\bar{\varepsilon}_y\right)dx+\frac{4h_1}{Q_{11}^{(1)}}\int_{x^*}^{L-l_s}\left(\frac{\left(\bar{\sigma}_x^{(1)}\right)^2}{2}-\bar{\sigma}_x^{(1)}Q_{12}^{(1)}\bar{\varepsilon}_y\right)dx \\ &+\frac{4h_1}{Q_{11}^{(1)}}\int_{L-l_s}^{L}\left(\frac{\left(\bar{\sigma}_x^{(1)}\right)^2}{2}-\bar{\sigma}_x^{(1)}Q_{12}^{(1)}\bar{\varepsilon}_y\right)dx \end{aligned} \qquad [6.47]$$

$$\begin{aligned} I_2 &= \frac{4h_2}{Q_{11}^{(2)}}\int_0^{x^*}\left(\frac{\left(\bar{\sigma}_x^{(2)}\right)^2}{2}-\bar{\sigma}_x^{(2)}\bar{\varepsilon}_y Q_{12}^{(2)}\right)dx+\frac{4h_2}{\tilde{Q}_{11}^{(2)}}\int_{x^*}^{L-l_s}\left(\frac{\left(\bar{\sigma}_x^{(2)}\right)^2}{2}-\bar{\sigma}_x^{(2)}\left(\bar{\varepsilon}_y Q_{12}^{(2)}+\hat{\sigma}\right)\right)dx \\ &+\frac{4h_2}{\tilde{Q}_{11}^{(2)}}\int_{L-l_s}^{L}\left(\frac{\left(\bar{\sigma}_x^{(2)}\right)^2}{2}-\bar{\sigma}_x^{(2)}\left(\bar{\varepsilon}_y Q_{12}^{(2)}+\hat{\sigma}\right)\right)dx \\ &+4h_2(L-x^*)\left\{\frac{1}{Q_{11}^{(2)}}\left(\frac{\sigma_0^2}{2}-\sigma_0\bar{\varepsilon}_y Q_{12}^{(2)}\right)+\frac{1}{\tilde{Q}_{11}^{(2)}}\left(\sigma_0(\bar{\varepsilon}_y Q_{12}^{(2)}+\hat{\sigma})-\frac{\sigma_0^2}{2}\right)\right\} \end{aligned} \qquad [6.48]$$

Note that the integration with respect to x, along with the constitutive relations from [5.2], was divided among the three ranges consistent with the stress distributions given in equations [6.21], [6.30] and [6.31], respectively. Obviously the sum of these last two expressions constitute the total complementary energy from the axial stresses, namely, $U_\sigma^* = I_1 + I_2$.

The contribution due to shearing stresses for this case also follows the previously established procedures. Recall that in this case, $\tau^*(x)$ consists of both $\sinh(\alpha_1 x)$ and $\cosh(\alpha_1 x)$ terms, as shown in [6.30]. Consequently, the integrations leading to U_τ^* are somewhat more complex yielding the following expression:

$$U_\tau^* = \frac{2}{3}\left\{\begin{array}{l} A_0^2\left(\dfrac{\sinh(2\alpha_0(L-l_s))}{4\alpha_0} - \dfrac{x^*}{2}\right) + \dfrac{(A_1^2+B_1^2)}{4\alpha_1}\left[\sinh(2\alpha_1(L-l_s)) - \sinh(2\alpha_1 x^*)\right] \\ + \dfrac{(B_1^2-A_1^2)(L-l_s-x^*)}{2} + \dfrac{A_1 B_1}{2\alpha_1}\left[\cosh(2\alpha_1(L-l_s)) - \cosh(2\alpha_1 x^*)\right] + (\tau_s^*)^2 l_s \end{array}\right\} \quad [6.49]$$

$$\times \left\{\frac{h_1}{C_{55}^{(1)}} + \frac{h_2}{C_{55}^{(2)}}\right\}$$

6.5.4 Energy Calculations for Bilinear Response with Interlaminar Slip, Case III

In this case the energy due to axial stresses is given by the same expression as in [5.40] in the absence of slip, except that in the present case, it is necessary once again to split the integrations between the slip and contact regions and employ the stress distributions in [6.36] and [6.37] appropriately. We then have:

$$U_\sigma^* = \frac{4h_1}{Q_{11}^{(1)}}\int_0^{L-l_s}\left(\frac{(\bar{\sigma}_x^{(1)})^2}{2} - \bar{\sigma}_x^{(1)}\bar{\varepsilon}_y Q_{12}^{(1)}\right)dx + \frac{4h_1}{Q_{11}^{(1)}}\int_{L-l_s}^{L}\left(\frac{(\bar{\sigma}_x^{(1)})^2}{2} - \bar{\sigma}_x^{(1)}\bar{\varepsilon}_y Q_{12}^{(1)}\right)dx$$

$$\frac{4h_2}{\tilde{Q}_{11}^{(2)}}\int_0^{L-l_s}\left(\frac{(\bar{\sigma}_x^{(2)})^2}{2} - \bar{\sigma}_x^{(2)}(\bar{\varepsilon}_y Q_{12}^{(2)} + \hat{\sigma})\right)dx + \frac{4h_2}{\tilde{Q}_{11}^{(2)}}\int_{L-l_s}^{L}\left(\frac{(\bar{\sigma}_x^{(2)})^2}{2} - \bar{\sigma}_x^{(2)}(\bar{\varepsilon}_y Q_{12}^{(2)} + \hat{\sigma})\right)dx \quad [6.50]$$

$$+4h_2 L\left\{\frac{\sigma_0^2}{2}\left(\frac{1}{Q_{11}^{(2)}} - \frac{1}{\tilde{Q}_{11}^{(2)}}\right) + \sigma_0\left(\frac{\bar{\varepsilon}_y Q_{12}^{(2)} + \hat{\sigma}}{\tilde{Q}_{11}^{(2)}} - \frac{\bar{\varepsilon}_y Q_{12}^{(2)}}{Q_{11}^{(2)}}\right)\right\}$$

The complementary energy attributable to shearing stresses in this case is given by an expression that resembles equation [6.44] for the linear slip solution. However, in this circumstance, it is necessary to account for the reduced stiffness of the 0° plies by replacing α_0 with α_1 to obtain:

$$U_\tau^* = \frac{2}{3}\left\{ A_0^2\left(\frac{\sinh\left(2\alpha_1(L-l_s)\right)}{4\alpha_1} - \frac{L-l_s}{2} \right) + \left(\tau_s^*\right)^2 l_s \right\}\left\{ \frac{h_1}{C_{55}^{(1)}} + \frac{h_2}{C_{55}^{(2)}} \right\} \qquad [6.51]$$

This concludes the derivations for the various sub-cases of the slip solutions. Though the implementation of these results is fairly straightforward, it is obvious from the preceding analysis that there are numerous details that need to be addressed. To examine these details in turn, the logic and development of a computer program written by the author, which incorporates the numerous results presented in this chapter, will be presented. Additionally, specific case studies to examine the effects of input parameters such as fracture toughness, interfacial shearing strength, and specimen geometry on the response of the ceramic matrix cross-ply composite will be presented. Correlations will be made between the predicted response and laboratory data to assess the validity of the analytical model.

CHAPTER 7

MODEL IMPLEMENTATION AND CASE STUDIES

As mentioned previously, a computer program was written to implement the solutions derived in Chapters 4-6. A number of case studies were then conducted to evaluate the effect of the material parameters J_{IC} and τ_s^* on the predicted stress-strain response and damage progression of the ceramic cross-ply laminate. Predicted and experimental results were compared for both $[0_2/90_2]_s$ and $[0_2/90_4]_s$ laminates.

The computer program was written in THINK C version 7.0 for the Apple Macintosh Computer. With the exception of some Macintosh specific graphic routines, this code should be easily portable to any platform with an ANSI C compiler, albeit real-time viewing of stress distributions would need to be disabled, or rewritten for the specific system. The bulk of the code and all accompanying algorithms associated with the mechanical analysis were developed by the author, while several specific utility subroutines concerned with vectors/arrays and dynamic memory allocation were supplied through a numerical package included with reference [66]. The complete program consists of approximately 1500 lines of code listed in Appendix E.

7.1 Computer Algorithms

Although brief procedures to implement the analysis were given for each section in Chapters 4-6, at this stage a more comprehensive outline of the computer program is required to describe the manner by which the various solutions were implemented. The algorithm for the main program segment is outlined in Figure 7.1 below. Note that subscripts within the flowchart diagrams are omitted to maintain consistency with the actual program code given in Appendix E.

At the start of the program, material properties are specified, together with initial and final applied stress levels and a prescribed stress increment. For each increment of applied stress $\bar{\sigma}_x$, two complete solutions are computed, for the current and subdivided crack spacings (Since a quarter volume element is employed, multiples of the initial half crack spacings L_0 and $L_0/2$ will be used throughout this discussion). These calculations take place within the subroutine "stresscalc", where the stress distributions, strains, and complementary energy are determined.

Main Program

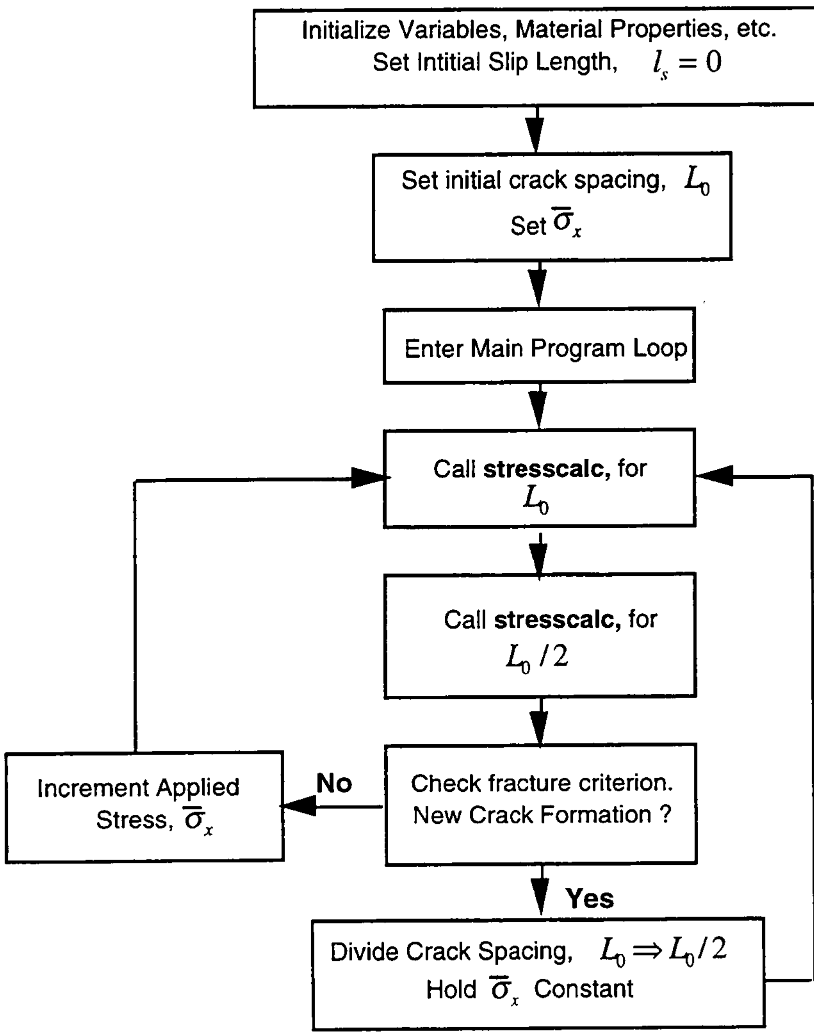

Figure 7.1 Main Program Flowchart

The levels of complementary energy for the two crack spacings are computed in "stresscalc" and then returned to the main program. The fracture criterion is then employed to determine if it is necessary to update the crack spacing. If the criterion is satisfied, the crack spacing is divided, while the applied stress, $\overline{\sigma}_x$, is held constant for the next pass through the loop with the updated crack spacings. If the energy criterion is not satisfied, the applied stress is incremented. This process is repeated until the prescribed final stress level is reached.

As might be expected, "stresscalc" is a key subroutine within the program. This subroutine contains all the necessary decision making algorithms to determine the appropriate solution type corresponding to the applied stress level and crack spacing, namely, the appropriate combination of linear, bilinear and slip effects. The first part of this subroutine evaluates the stress $\overline{\sigma}_x^{(2)}$ in the outer, 0° plies, at $x=L$ to determine if the solution will be linear or bilinear as shown in Figure 7.2 below:

Subroutine "stresscalc"

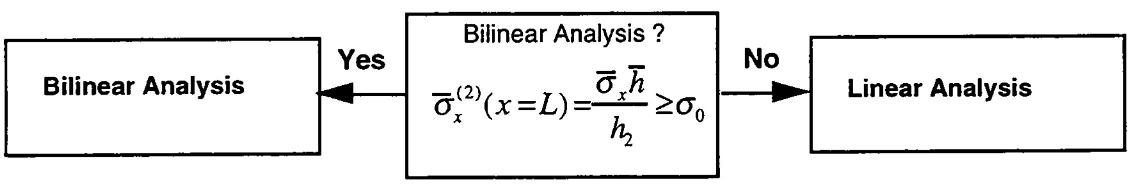

Figure 7.2 Entry Point to Subroutine "stresscalc"

If it turns out linear analysis applies, the program executes the steps outlined in the flowchart given in Figure 7.3. The first step in the linear analysis determines if there is interfacial slip between the 0° and 90° plies. The iterative subroutine "GetLsLinear" returns a trial slip length, "lsnew". A check is then made to see if the trial slip length, "lsnew" is greater than the previous slip length (recall the modified analysis of Chapter 6). If the slip length, l_S has grown, it is set equal "lsnew", and the calculations for the transverse strain, axial strain, stress distributions and complementary energy are carried out in accordance with section 6.1. On the other hand, if the trial slip length, "lsnew" decreases, it is discarded and the modified analysis of section 6.3.1 is utilized with the previous slip length. At this point all parameters (in either case) are written to an output file, and the value for the complementary energy is returned to the main program. Finally, it should be noted that if the slip length is found to be zero, this circumstance reduces to the case of linear response without slip.

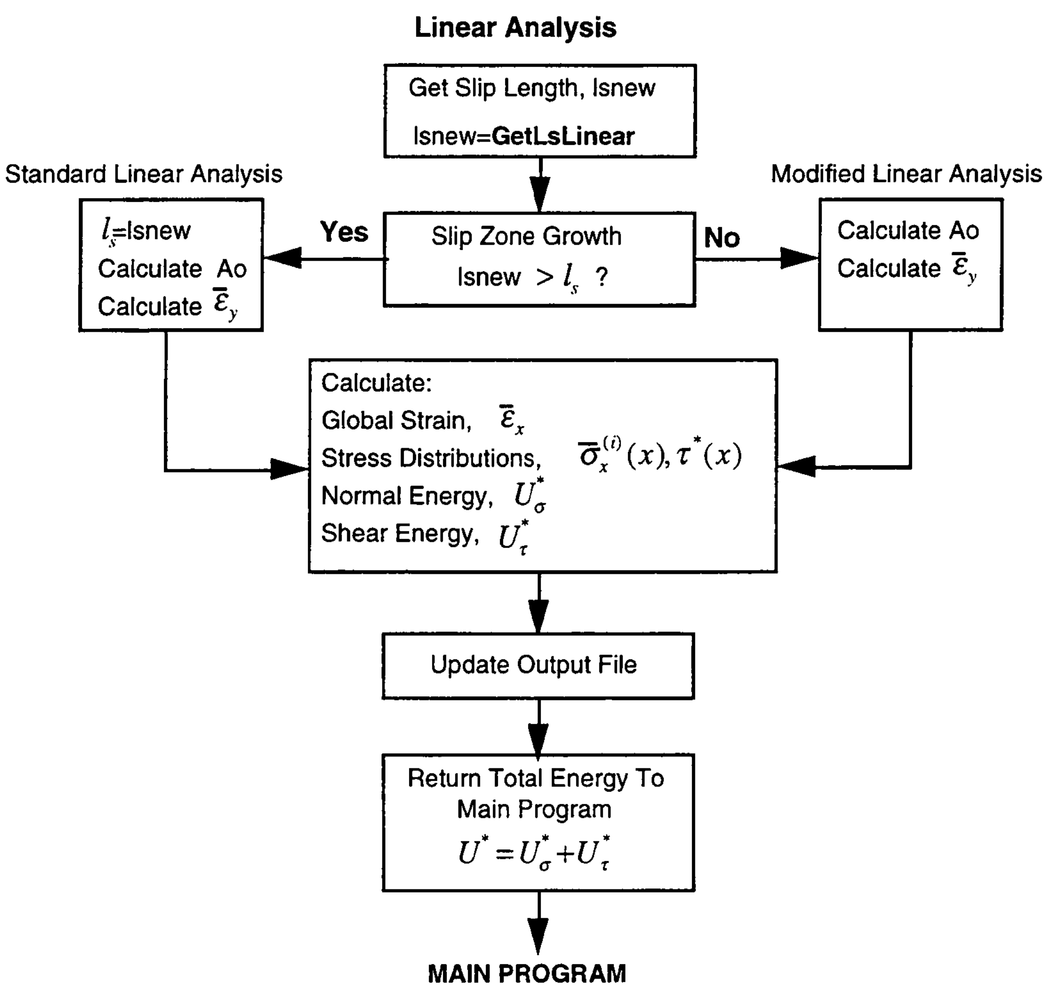

Figure 7.3 Linear Analysis Flowchart for the Subroutine "stresscalc"

Referring to Figure 7.2, if it is determined that $\overline{\sigma}_x^{(2)}(x = L)$ has reached the level of σ_0, routines for the bilinear analysis apply. The algorithms for the bilinear analysis are outlined in Figure 7.4 below.

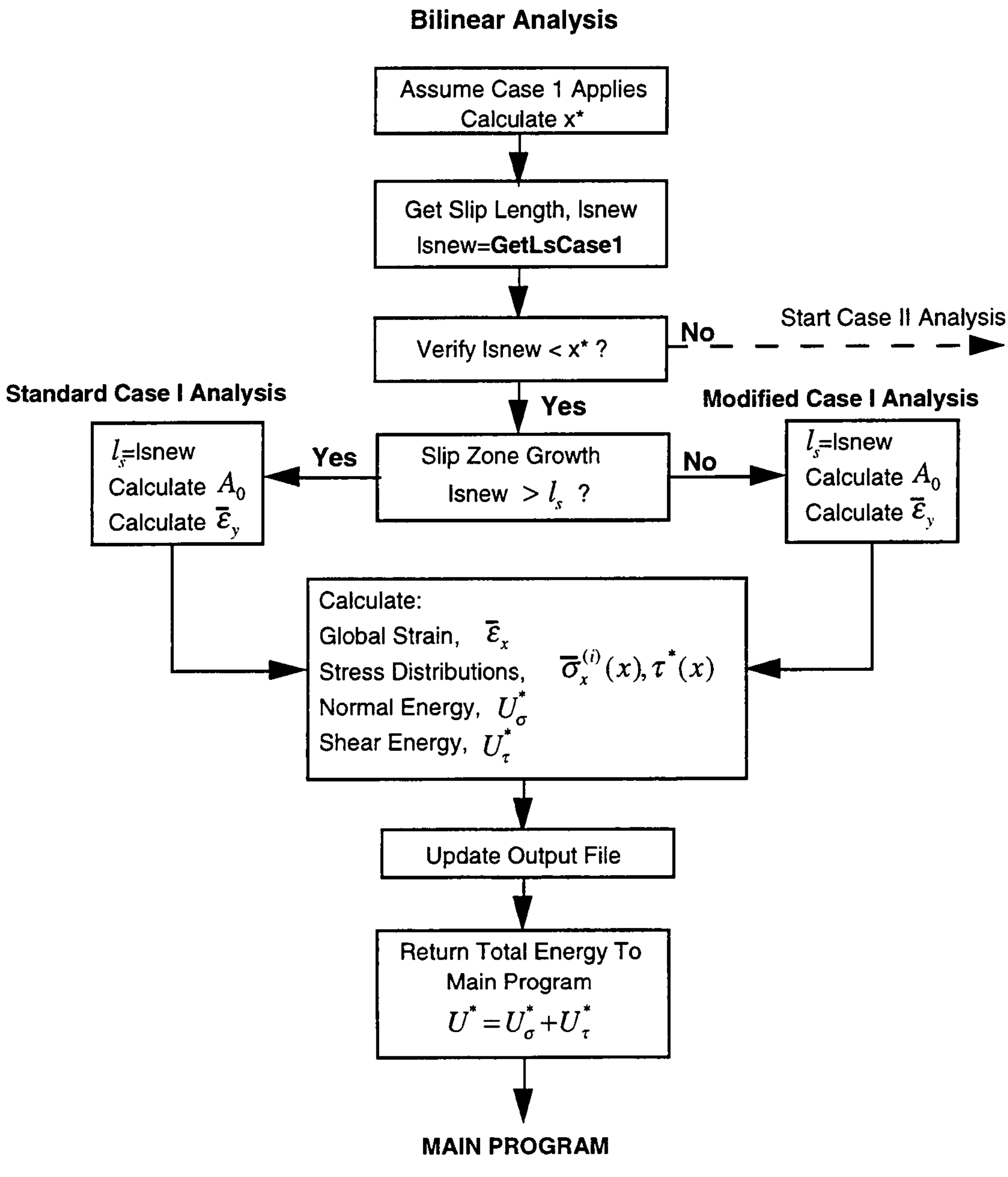

Figure 7.4 Bilinear Analysis, Case I of the Subroutine "stresscalc"

At the start of these routines, it is assumed that the Case I of the bilinear analysis with slip as detailed in section 6.2.1 applies. Recall from section 6.2.1 that we have a closed form expression for x^* given in equation [6.16], but need to employ an iterative scheme to determine the slip length, l_S. A trial slip length, "lsnew" is then determined in the subroutine, "GetLsCase1" and compared with x^*. If "lsnew" is greater than L-x^*, the assumption of using a Case I slip solution is correct, and we can proceed with the steps outlined in Figure 7.3. Otherwise, it is necessary to consider the Case II slip solution. The rest of the Case I algorithm is carried out similarly to the linear algorithm of Figure 7.3 described earlier.

As the applied stress, $\bar{\sigma}_x$, is increased during the Case I solution, the growing yield zone may eventually exceed the length of the slip zone. In this circumstance, the Case II slip solution derived in section 6.2.2 applies. The algorithm is given in Figure 7.5 below.

The first step for the Case II algorithm is to obtain x^* along with the trial slip length, "lsnew" simultaneously in the subroutine "GetLsCase2". As before, a check is made to determine if the slip zone has grown, and the standard or modified routines are then employed accordingly. Note for this case, it is also necessary to iteratively recalculate x^* for the modified solution employing the subroutine "GetXstarCase2mod". Additionally, in both the standard and modified cases, it is necessary to check if the yield zone has extended over the entire region $0 \leq x \leq L$, i.e. $x^*=0$. If this occurs, Case II no longer applies, and we must consider the Case III bilinear slip solution.

The flowchart for Case III is given in Figure 7.6. In this case, the procedure to implement the solutions is similar to the linear case outlined in Figure 7.2. Of course, the specific subroutines for this algorithm will be different from the linear case since they now correspond to the analysis of section 6.2.3, for Case III.

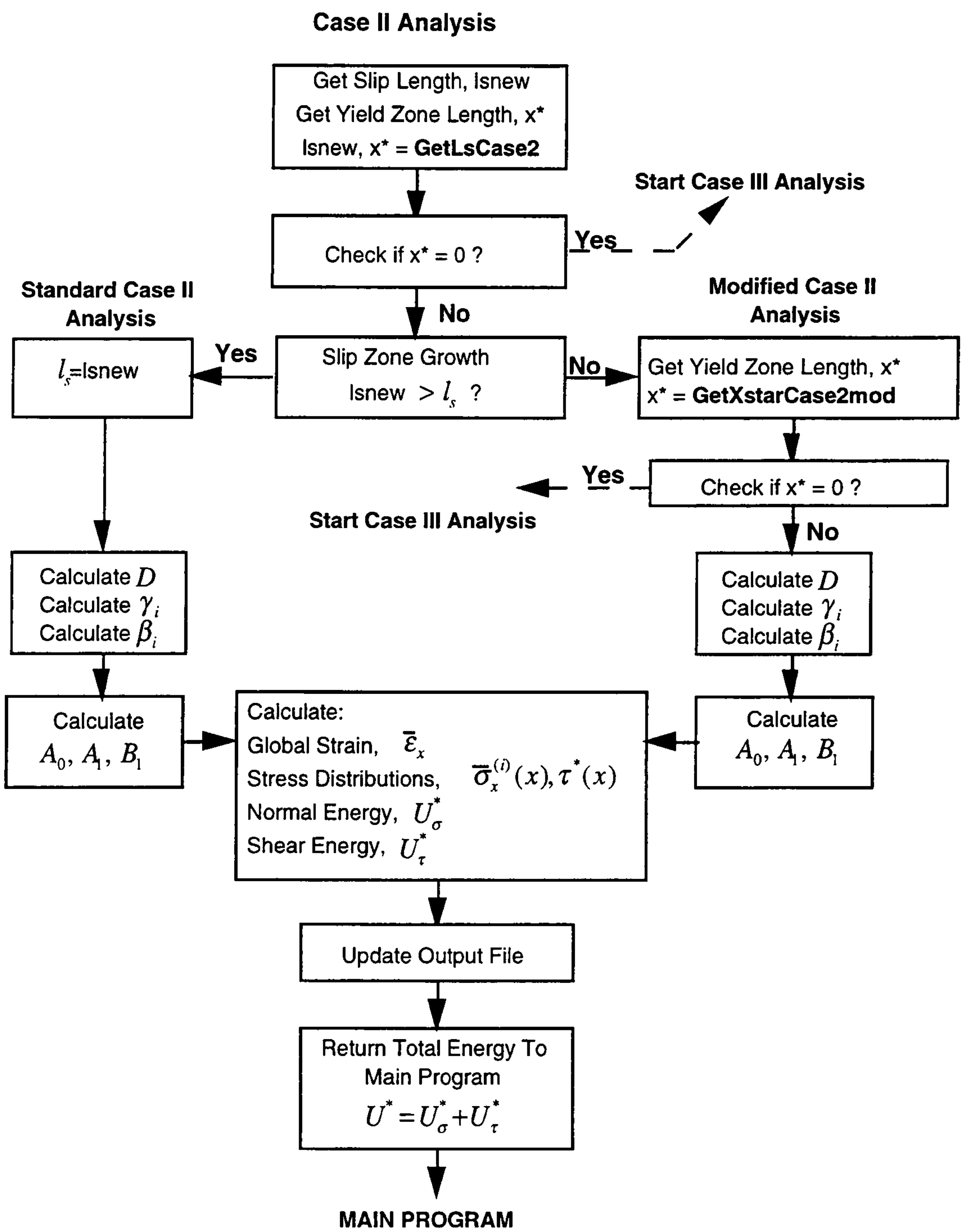

Figure 7.5 Bilinear Analysis, Case II of the Subroutine "stresscalc"

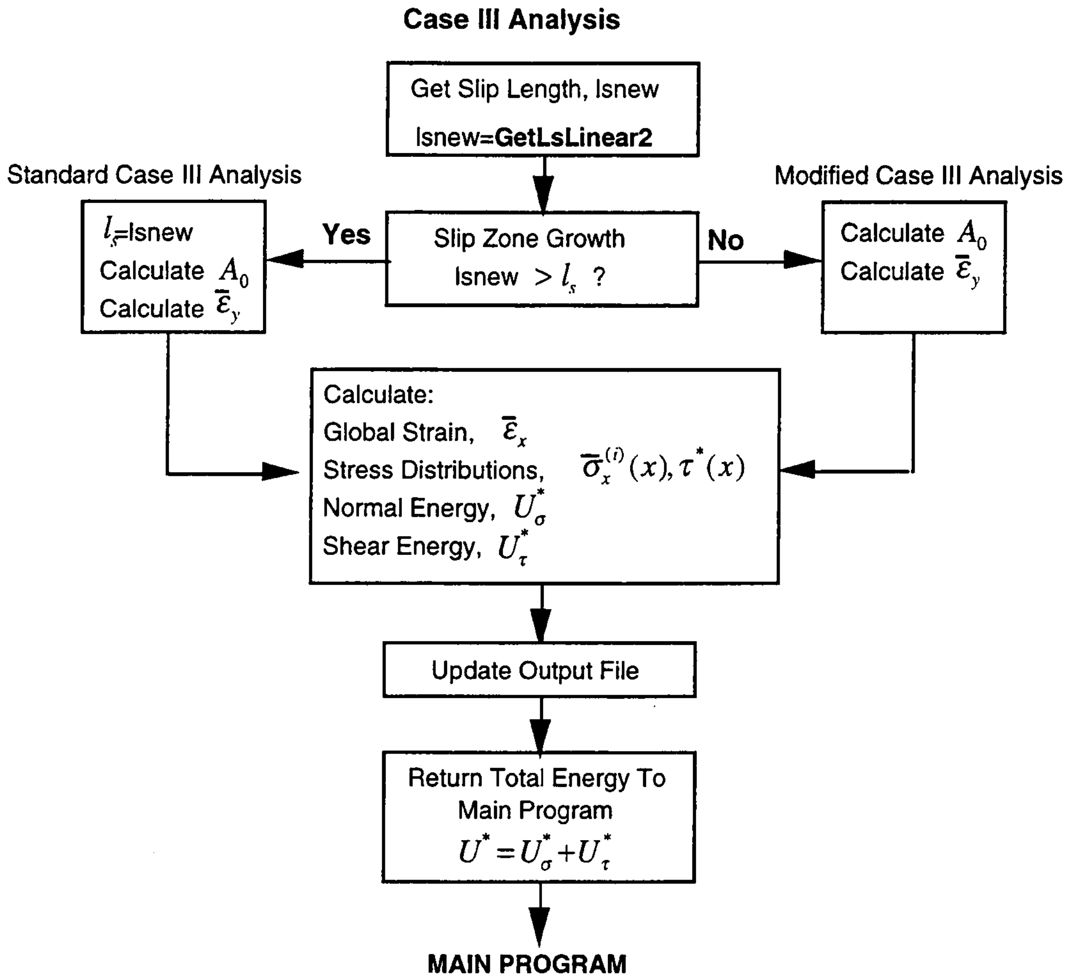

Figure 7.6 Bilinear Analysis, Case III of the Subroutine "stresscalc"

7.2 Case Studies

A total of 24 case studies were conducted for the $[0_2/90_2]_s$ and $[0_2/90_4]_s$ lay-ups to examine the influence of the fracture toughness, J_{IC} and the interfacial shear strength, τ_s^* on the stress-strain response and crack density accumulation. The material properties and dimensions corresponding to these lay-ups are given below. The stiffness values are given in GPa, while the yield stress, σ_0 has units of MPa. Specimen thickness and initial crack spacing are given in millimeters, and the larger thickness, $h_1 = 0.8$ applies to the $[0_2/90_4]_s$ laminate. We employed:

$$Q_{11}^{(1)} = Q_{22}^{(2)} = 110 \qquad C_{55}^{(1)} = 52 \qquad 2L_0 = 25$$

$$Q_{11}^{(2)} = Q_{22}^{(1)} = 120 \qquad C_{55}^{(2)} = 37 \qquad h_1 = 0.4,\ 0.8$$

$$Q_{12}^{(1)} = Q_{12}^{(1)} = 30 \qquad \sigma_0 = 200 \qquad h_2 = 0.4$$

The case studies conducted for the $[0_2/90_2]_s$ lay-up are listed in Table 7.1 below:

Table 7.1 Case Study Parameters for the $[0_2/90_2]_s$ Laminate

Case Study Number	J_{IC} [J/m^2]	τ_s^* [MPa]
1	15	35
2	15	45
3	15	55
4	12	35
5	12	45
6	12	55
7	20	35
8	20	45
9	20	55
10	30	35
11	30	45
12	30	55

Since the fracture toughness of the matrix material was reported to be approximately 25 J/m^2 by Budianski *et. al* [7], J_{IC}=15 J/m^2 was chosen as a reasonable starting point for these studies in view of the weak fiber-matrix interface. The interfacial shear strength was found experimentally to be about 35 MPa. However, there is reason to believe that it may be higher as mentioned in Chapter 3, consequently, the interfacial shear strength was varied between 35 and 55 MPa for each prescribed fracture toughness value. The resulting predictions stress-strain response and crack densities for J_{IC}=15 J/m^2 are given in Figures 7.7 (a) and (b).

The results in Figure 7.7(a) and (b) reveal that increasing τ_s^* postpones the onset of transverse matrix cracking. Since transverse cracking leads to reduced specimen stiffness, it would be reasonable to expect that each increase in τ_s^* should result in a raising of the stress-strain curve. However in Figure 7.7(a), it can be seen that the curve for case 3 unexpectedly terminates at a higer stress level than case 2. This apparent contradiction can be explained if we consider that the length of the slip zone, l_s, which is governed by the shear strength, also influences the overall stiffness of the laminate. A larger slip zone will result in a more compliant specimen, if all other factors are equivalent. Therefore, since the crack densities for cases 2 and 3 are the same as observed from Figure 7.7, and the larger value of τ_s^* for case 3 results in a shorter slip zone, the laminate has a corresponding higher overall stiffness. Hence, an increase in τ_s^* has two contradictory effects on the stiffness of the laminate since it affects both the extent of the interfacial slippage and the density of transverse cracks. Overall, the predictions for the stress-strain response and crack density in Figures 7(a) and 7(b) are reasonably close to the experimental results for cases 2 and 3.

The results for J_{IC}=12 J/m^2 are given in Figures 7.8. The lowering of the fracture toughness yields a somewhat better correlation between the experimental data and the predicted stress-strain response. However, the predicted level of the crack density at saturation for case 6 exceeds the experimental results by about 25 percent. It is interesting to note that since the saturation crack densities for cases 4, 5 and 6 differ for J_{IC}=12, the stress-strain curves no longer cross over each other as they did for J_{IC}=15.

Additional case studies for J_{IC} =20 and 30 J/m^2 were also conducted to demonstrate the increase in laminate stiffness with fracture toughness. These results are shown in Figures 7.9 and 7.10. Note that the choice of J_{IC}=30 J/m^2 is unrealistic since it is larger than the fracture toughness of the matrix material (25 J/m^2). However employing J_{IC}=30 J/m^2 illustrates the sensitivity of the stress-strain predictions to fracture toughness.

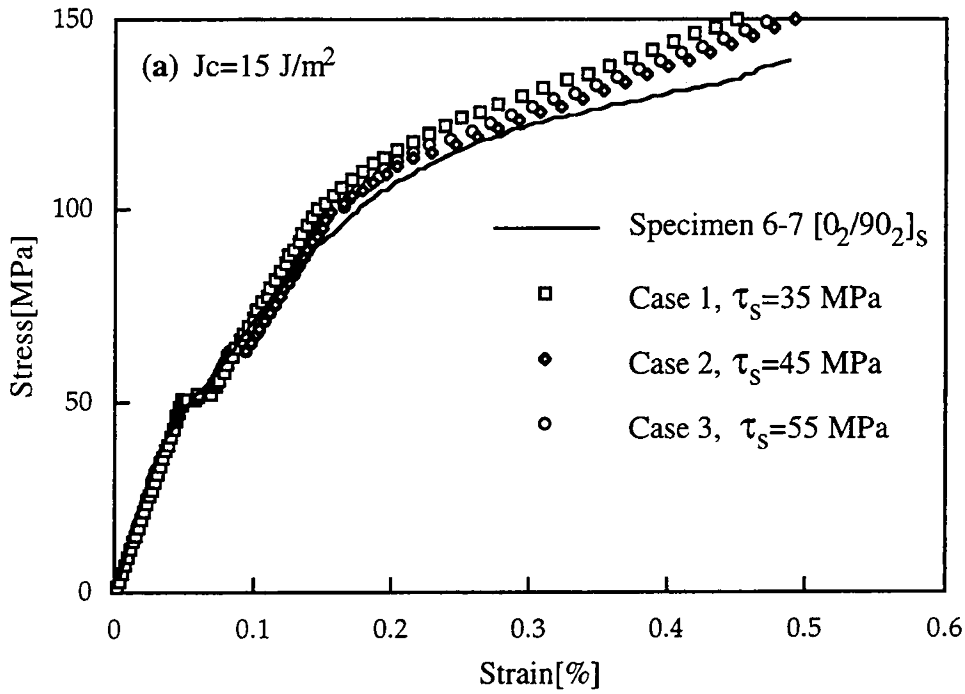

(a) Stress-Strain Response

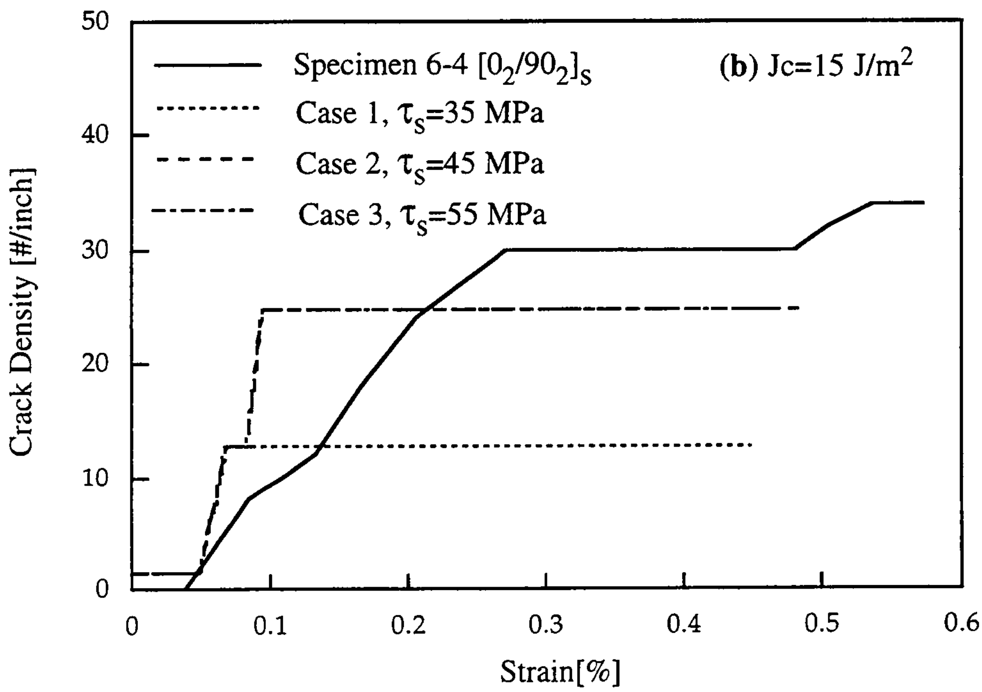

(b) Transverse Crack Density

Figure 7.7 Response of a $[0_2/90_2]_s$ Laminate for Bilinear Slip Analyses Case Studies, J_{IC}=15 J/m^2

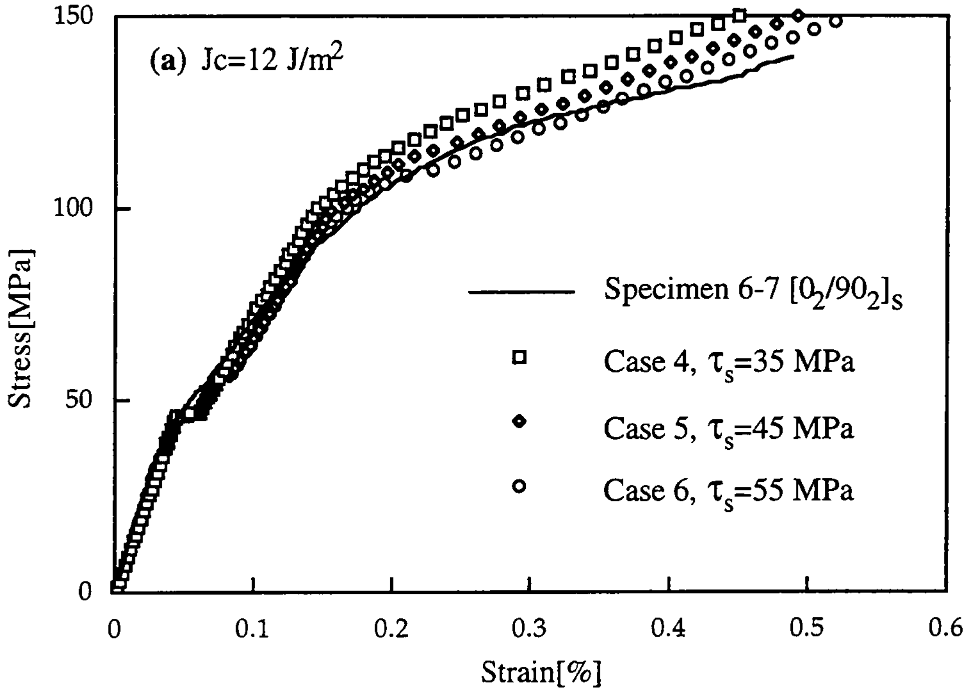

(a) Stress-Strain Response

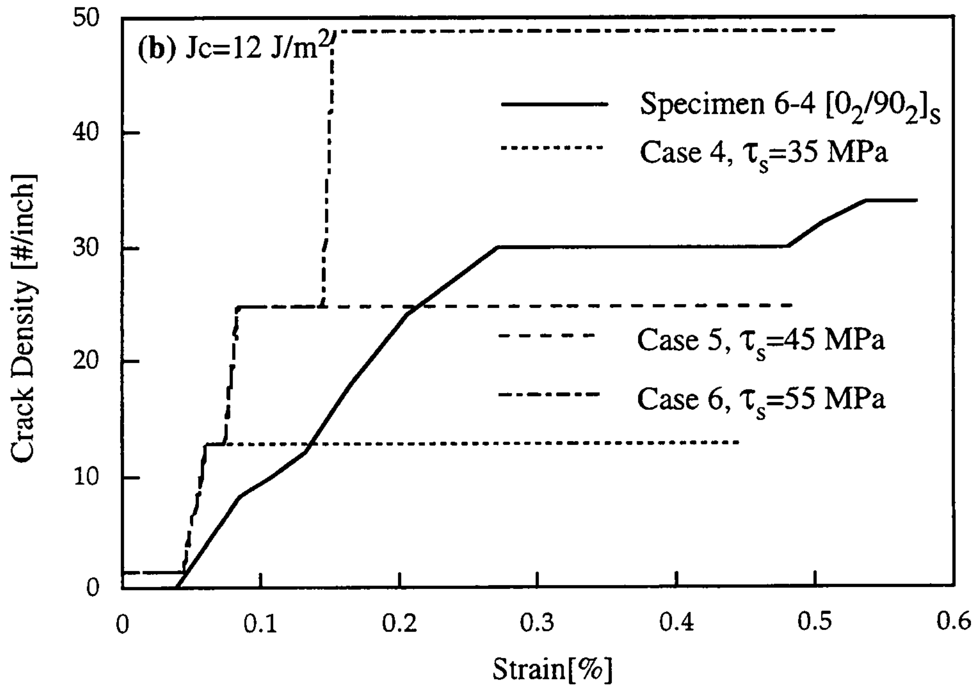

(b) Transverse Crack Density

Figure 7.8 Response of a $[0_2/90_2]_S$ Laminate for Bilinear Slip Analyses Case Studies, J_{IC}=12 J/m^2

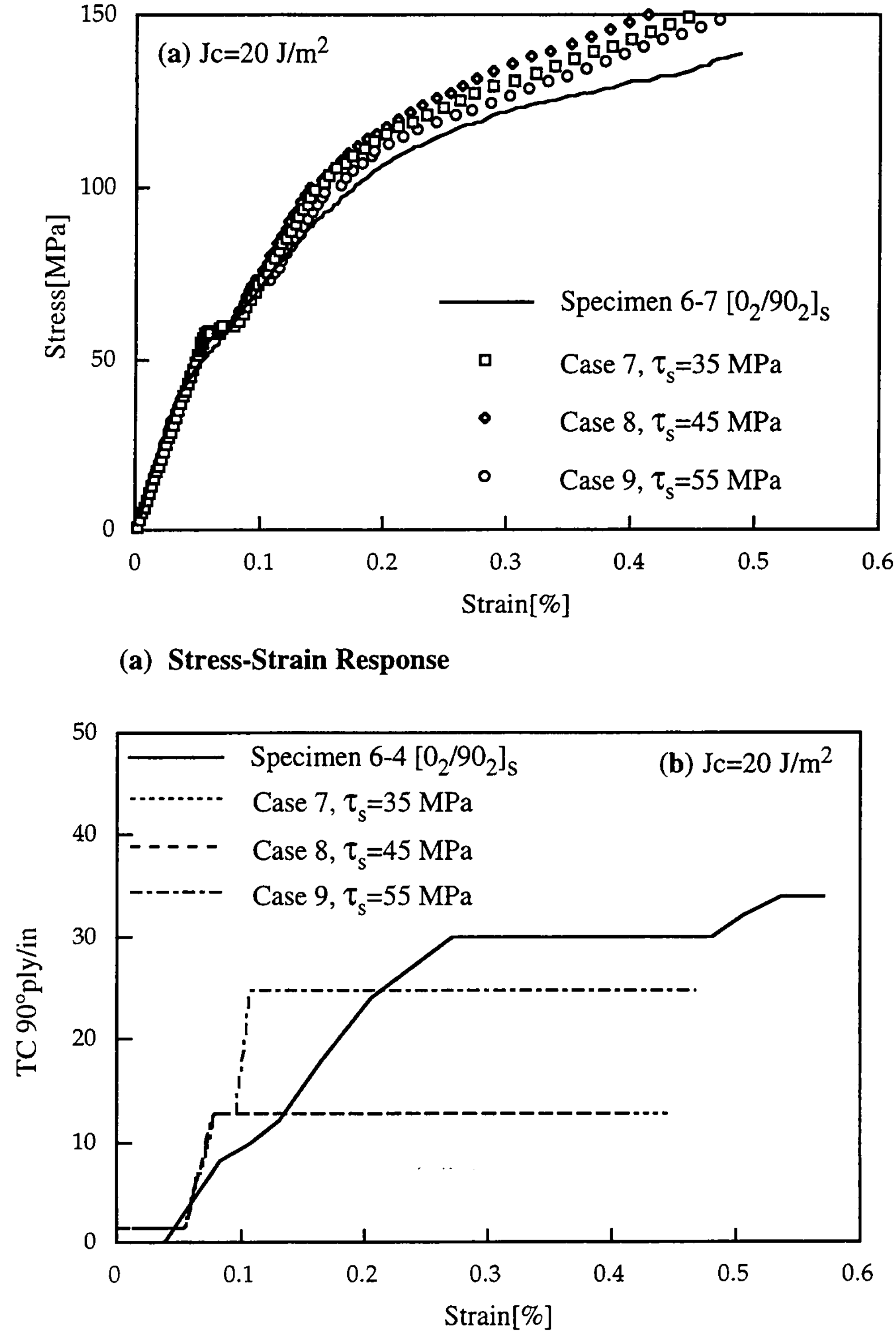

(a) **Stress-Strain Response**

(b) **Transverse Crack Density**

Figure 7.9 Response of a $[0_2/90_2]_S$ Laminate for Bilinear Slip Analyses Case Studies, J_{IC}=20 J/m^2

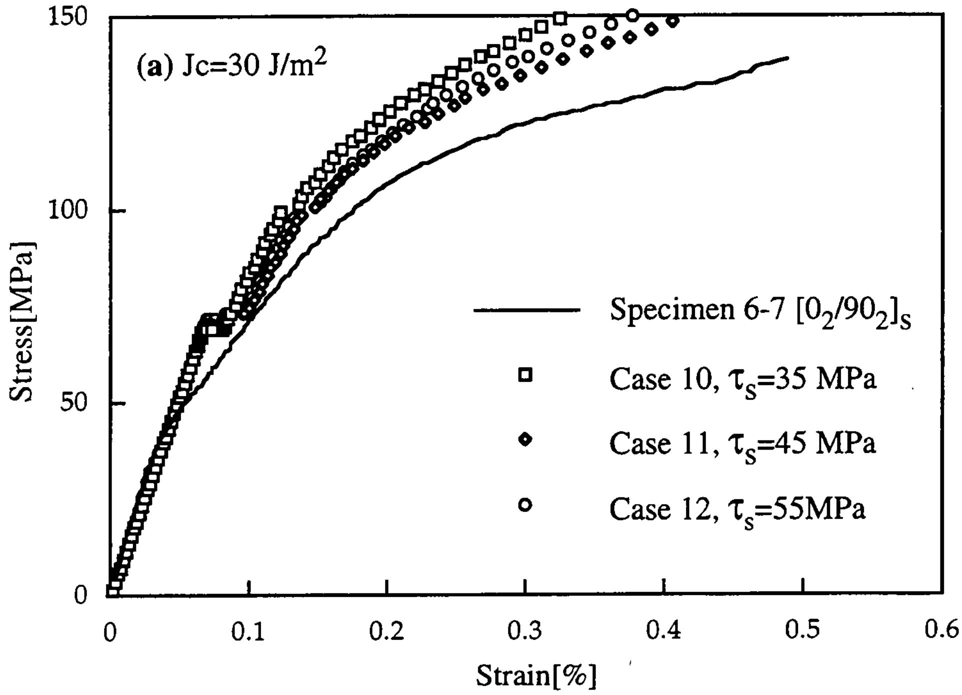

(a) Stress-Strain Response

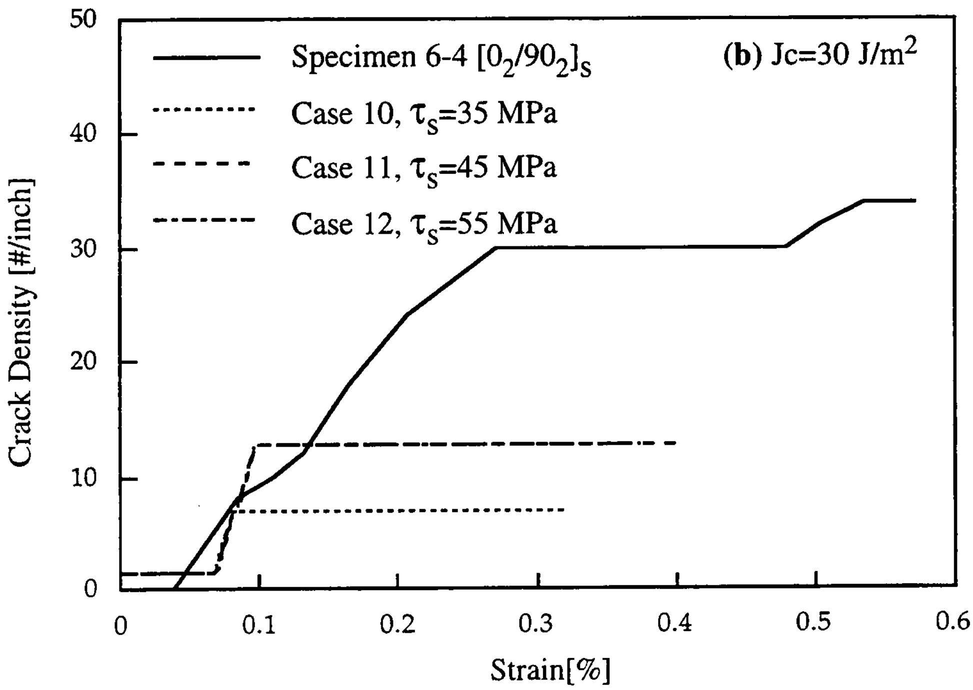

(b) Transverse Crack Density

Figure 7.10 Response of a $[0_2/90_2]_S$ Laminate for Bilinear Slip Analyses Case Studies, J_{IC}=30 J/m^2

The additional series of case studies conducted for the $[0_2/90_4]_s$ laminate includes the ranges of J_{IC} and τ_s^* listed in Table 7.1 below:

Table 7.2 Case Study Parameters for the $[0_2/90_4]_s$ Laminate

Case Study Number	J_{IC} [J/m^2]	τ_s^* [MPa]
13	15	35
14	15	45
15	15	55
16	12	35
17	12	45
18	12	55
19	20	35
20	20	45
21	20	55
22	30	35
23	30	45
24	30	55

The results for this lay-up are plotted in Figures 7.11-7.14. Figures 7.11 show good correlation between the experimental and predicted stress-strain response as well as transverse crack density. Similarly to the $[0_2/90_2]_s$ laminate, the best agreement between the experimental and predicted results are obtained for an interfacial shearing strength of τ_s^*=55 MPa. Although this value exceeds the experimentally observed level of 35 MPa, this not surprising in view of the aforementioned limitations of the experimental approach employed to measure τ_s^*. Turning to Figures 7.12-7.14, it is noted an increase in the fracture toughness delays the onset of transverse cracking and enhances the overall stiffness of the laminate. These observations are consistent with the results obtained for the $[0_2/90_2]_s$ laminate.

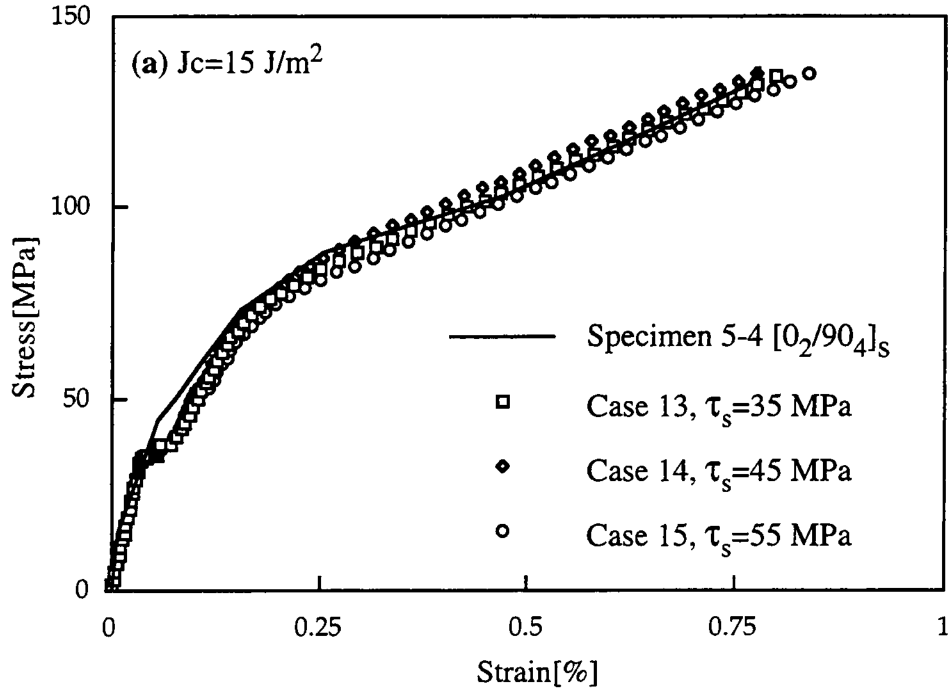

(a) Stress-Strain Response

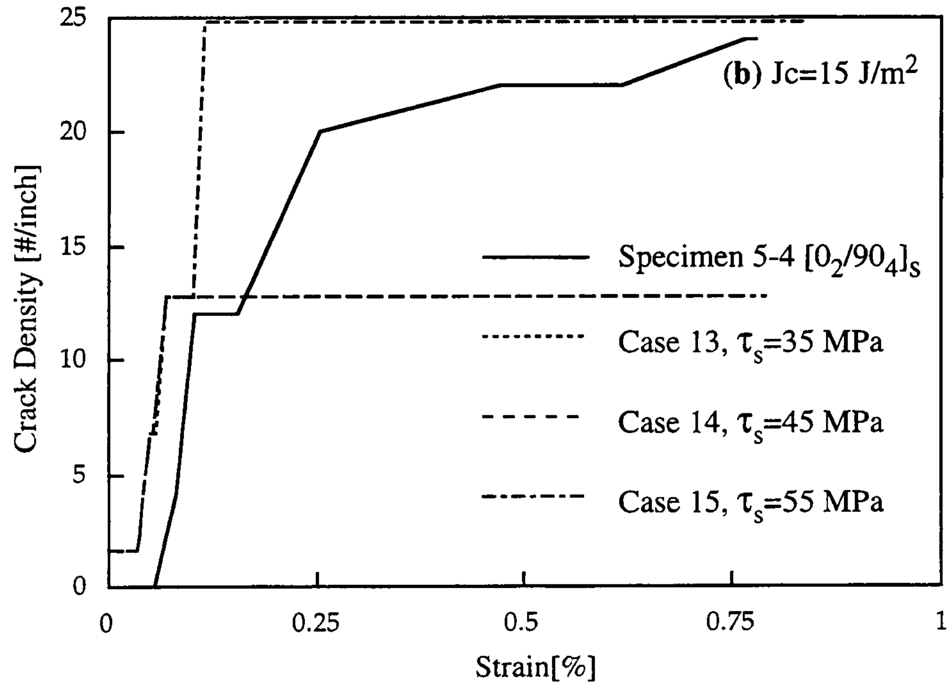

(b) Transverse Crack Density

Figure 7.11 Response of a $[0_2/90_4]_S$ Laminate for Bilinear Slip Analyses Case Studies, J_{IC}=15 J/m^2

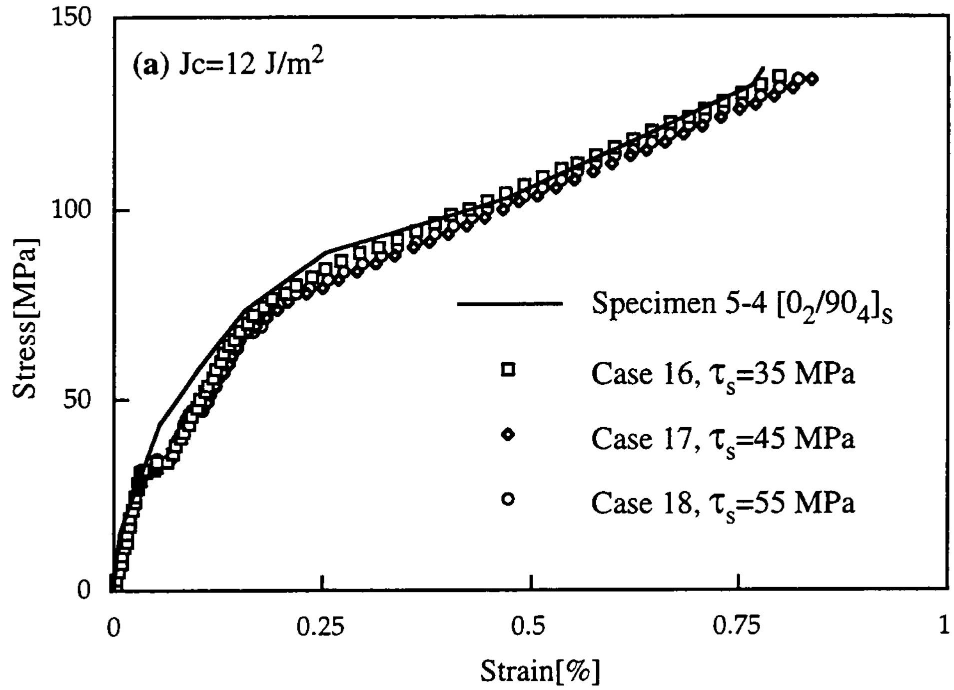

(a) Stress-Strain Response

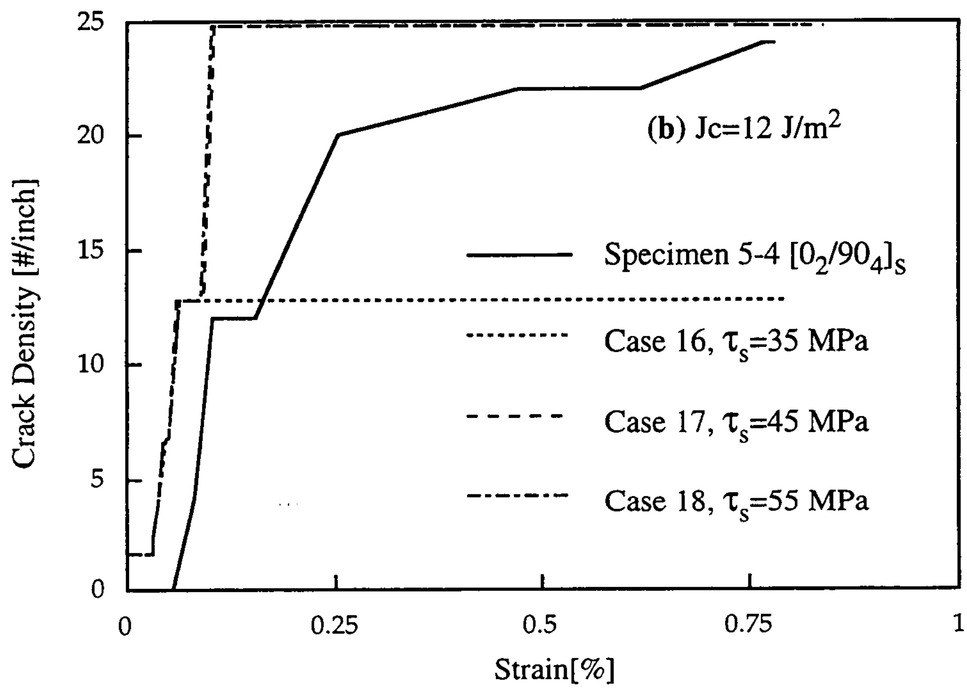

(b)Transverse Crack Density

Figure 7.12 Response of a $[0_2/90_4]_S$ Laminate for Bilinear Slip Analyses Case Studies, J_{IC}=12 J/m^2

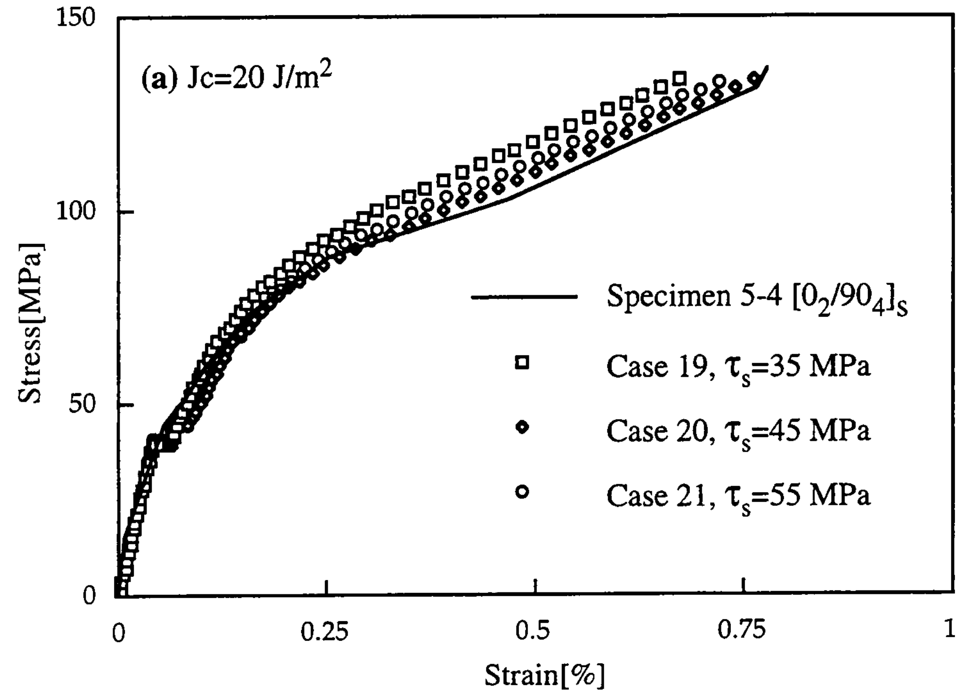

(a) Stress-Strain Response

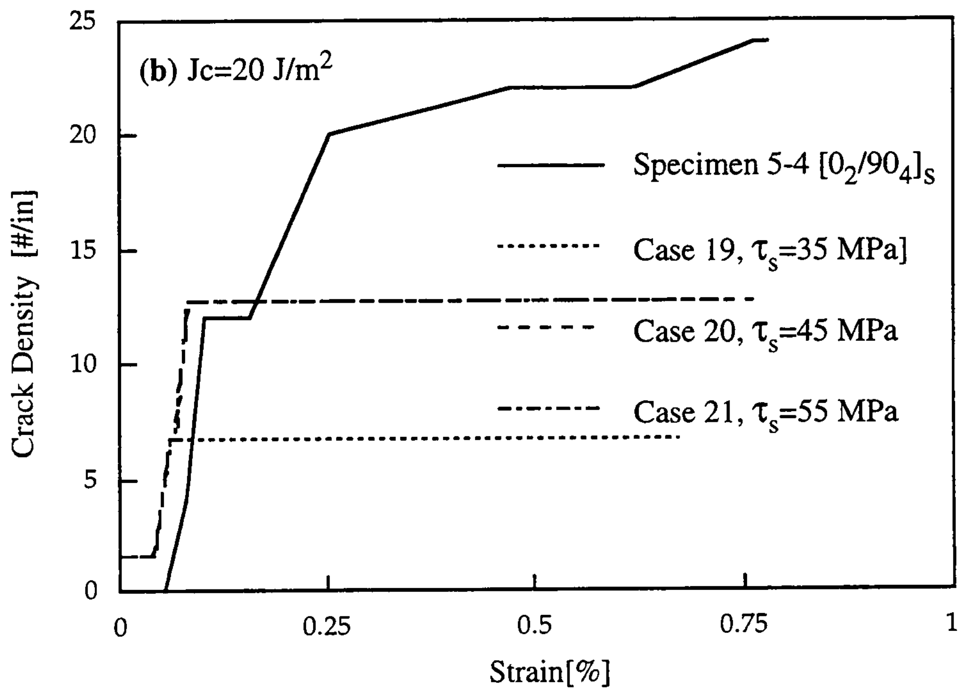

(b) Transverse Crack Density

Figure 7.13 Response of a $[0_2/90_4]_S$ Laminate for Bilinear Slip Analyses Case Studies, J_{IC}=20 J/m^2

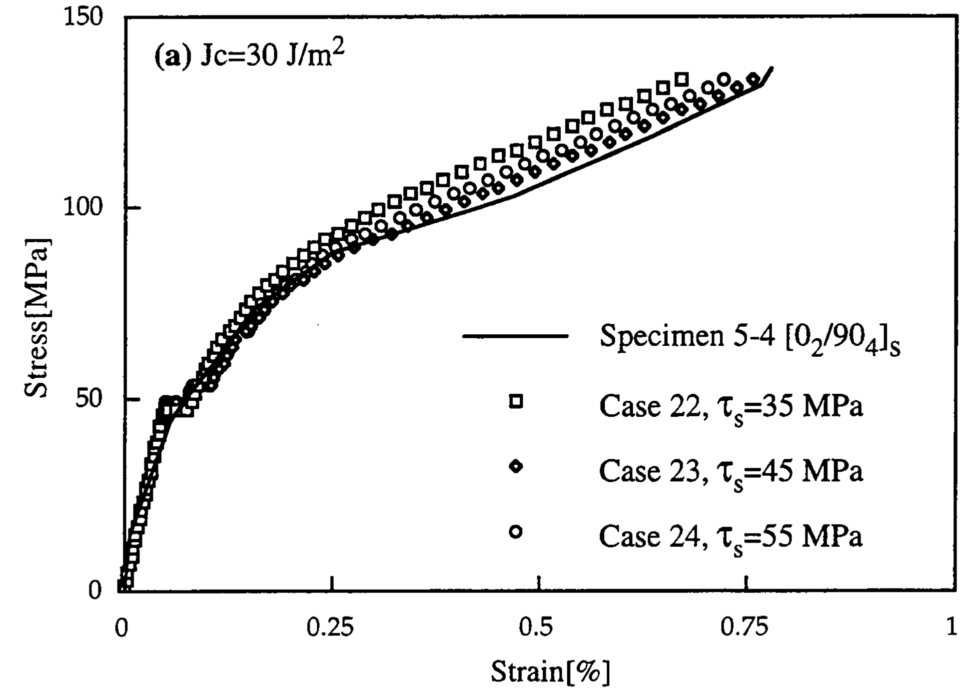

(a) Stress-Strain Response

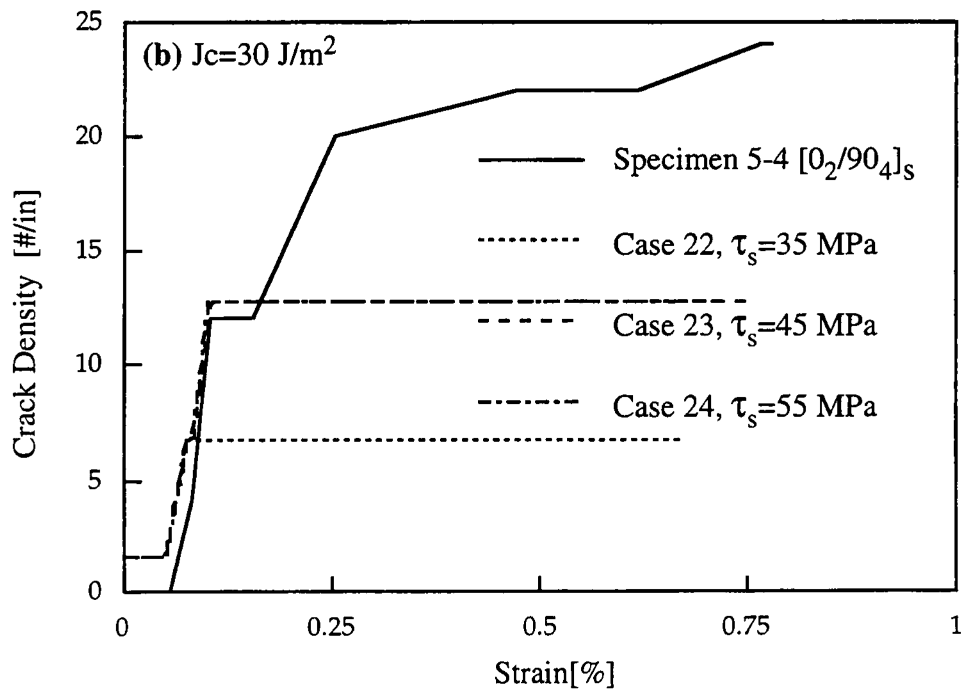

(b) Transverse Crack Density

Figure 7.14 Response of a $[0_2/90_4]_S$ Laminate for Bilinear Slip Analyses Case Studies, J_{IC}=30 J/m^2

CHAPTER 8

SUMMARY AND CONCLUSIONS

8.1 Summary

The primary goals of this research were to develop a comprehensive analytical model to predict the stress-strain behavior of ceramic cross-ply laminates along with a mechanical test program to provide material properties, damage observations, and laminate stress-strain data for correlations with the predictions from the model. These goals were achieved through the development of a shear-lag type analysis which predicts both the evolution of damage associated with this material system, along with the resultant stress-strain response. Additionally, mechanical testing was conducted to characterize material response and generate the data required as input to the model.

8.1.1 Mechanical Testing Program

As shown in Table 3.1, a total of ten tensile tests were conducted for the ceramic matrix cross-ply specimen. Stress-strain response and laminate strength was measured for each of these tests. Seven of these tests include detailed studies of the initiation and accumulation of transverse crack density with monotonically increasing applied stress. The stress-strain data is plotted in Figure 3.2 and Appendix A. Stress levels for transverse crack initiation in the 90° ply groups along with saturation density are summarized in Table 3.1, while crack density accumulation measurements are given in Figure 3.5 and Appendix A. Selected photographs of microscopic examinations of transverse cracking are presented in Figure 3.4 and Appendix B.

As mentioned previously, information concerning the interfacial shearing strength for ceramic matrix cross-ply material was non-existent. Therefore, a test fixture was designed and built which provided interfacial shear failure between the 0° and 90° ply groups of the cross-ply specimens. The details of this fixture are discussed in Chapter 3. A total of nineteen "mini-shear" tests were conducted to examine the progression of interfacial failure and measure the interfacial shear strength. The results of these tests are summarized in Table 3.2. This work resulted in an experimental measurement for a lower bound estimate of the interfacial shearing strength. Micrographs for several "mini-shear" specimens depicting interfacial damage initiation leading to ply separation are shown in Figure 3.9 and Appendix D.

8.1.2 Predictive Shear-Lag Analysis

A comprehensive model to predict the evolution of damage along with the associated stress-strain behavior of the ceramic matrix cross-ply laminate has been developed. Specific features of the model include transverse matrix cracking within the 90° plies along with interfacial slippage between the 0° and 90° ply groups. Additionally this model incorporates the non-linear behavior of the 0° plies. Transverse matrix crack progression in the 90° plies is predicted by means of an energy criterion that accounts for both the material non-linearity of the 0° plies and the dissipative effects of interfacial slip between the 0° and 90° ply groups. Interfacial slip-zone lengths are determined by considerations of shearing strength at the 0°/90° interface. Since damage and "yielding" evolves in a sequential manner with applied stress, it was necessary to construct individual solutions to account for all combinations of damage and material non-linearity. These solutions are summarized below:

(1) Linear analysis without interfacial slip : A linear solution that considers matrix crack progression is outlined in Chapter 4.

(2) Bilinear Analysis : Two more solutions that consider matrix cracking along with bilinear response of the 0° plies is given in Chapter 5.

(3) Analysis involving Interlaminar Slip : Seven solutions that account for all combinations of linear and bilinear response of the 0° plies along with matrix cracking and interlaminar slip are developed in Chapter 6.

These solutions were incorporated in a computer program to evaluate the damage state and the associated stress-strain response of the laminate with applied stress. This program is outlined in Chapter 7. Twenty four case studies for $[0_2/90_2]_s$ and $[0_2/90_4]_s$ laminates were conducted to study the effects of input parameters and correlate results with experimental data.

8.2 Conclusions

The aforementioned material properties, laminate response characteristics, and damage observations not available in current publications have been determined. Specifically, the following conclusions concerning the $[0_2/90_2]_s$ and $[0_2/90_4]_s$ lay-ups are presented :

(1) Laminate stress-strain response was found to be highly non-linear, but reproducible for a given loading rate as shown in Figure 3.2 and Appendix A.

(2) It is possible to accurately measure transverse crack initiation and progression under monotonically increasing applied stress. Although these measurements contain inherent scatter, primarily due to the random nature of brittle fracture, the general sequence of matrix cracking in both the 0° and 90° plies was found to develop in a consistent manner.

(3) Careful inspection of matrix cracking provides evidence of shear-lag type behavior between the 0° and 90° ply groups. This is observed by noting that at the locations where a transverse crack in the 90° approaches the 0° plies, there occurs a clustering of closely spaced matrix cracks in the 0° plies. This suggests a region of increased axial stress in the 0° plies as the load carried by the cracked 90° plies is transferred to the 0° plies through shear at the interface. This phenomenon is shown in Figure 3.4 and in Appendix B.

(4) Slippage between the 0° and 90° ply groups can be observed in the vicinity where a transverse crack in the 90° impinges upon the 0°/90° interface. This is most noticeable as the transverse cracks in the 90° ply group "open" under applied stress, resulting in a disparity in displacement between the 0° and 90° ply groups.

(5) A lower bound estimate of the interfacial shearing strength between the 0° and 90° plies was obtained. Additionally this investigation presents a new testing procedure to measure the interlaminar shearing strength of cross-ply laminates.

Turning to the results of the predictive shear-lag model, the following conclusions can be made:

(1) The linear analysis presented in Chapter 4 along with the energy criterion for transverse crack progression predicts the laminate stress-strain response fairly well at lower applied

stress levels. However, the model significantly underestimates the "global" strain of the laminate beyond that point as shown in Figure 4.10. Nevertheless, this analysis demonstrates the usefulness of the shear-lag approach as a basis for a more a comprehensive model.

(2) In Chapter 5, the linear analysis of Chapter 4 was modified by introducing a bilinear constitutive relation for the 0° ply groups, resulting in a significant improvement in stress-strain response (Figures 5.3-5.5). This consequence illustrates that it is essential to account for the non-linear stress-strain response of the 0° plies to realistically model this laminate. In contrast to the satisfactory prediction for the stress-strain response, the predicted saturation crack density with this model turned out to be 2-4 times larger than the experimental results. Increasing the fracture toughness value, even to unrealistically high levels, provides only modest improvements between predicted and experimental crack densities. It should be noted that these results were consistent for both the $[0_2/90_2]_s$ and $[0_2/90_4]_s$ laminates.

(3) The introduction of interlaminar slip along with bilinear response of the 0° plies results in good correlations between experimental data and model predictions for both stress-strain response and saturation crack density. The results from the parametric studies in Chapter 7 show that both interfacial shearing strength and fracture toughness have significant effects on the predicted results. An increase in the fracture toughness delays the onset of transverse matrix cracking, resulting in higher laminate stiffness. On the other hand, it was observed that the interfacial shearing strength plays a dual role in the laminate response. Lower interlaminar strength will be accompanied by longer slip zones and higher levels of dissipative energy. This circumstance reduces the amount of available

energy for transverse cracking leading to a increased laminate stiffness, resulting in a trend that is similar to that of increasing fracture toughness. However, longer slip zones will also result in increased laminate strain. Hence, the interaction between interfacial shearing strength and fracture toughness must be considered in full detail to evaluate the effects of these material properties on laminate response. Overall, the best predictions were obtained with J_{IC}=12 /m^2 and τ_s^*= 55 MPa for both the $[0_2/90_2]_s$ and $[0_2/90_4]_s$ laminates.

BIBLIOGRAPHY

[1] Aveston, J., Cooper, G. A., and Kelly, A., "Single and Multiple Fracture", The Properties of Fibre Composites, Conference Proceedings, National Physical Laboratory, IPC Science and Technology Press Ltd., (1971), pp. 15-26.

[2] Aveston, J., and Kelly, A., "The Theory of Multiple Fracture of Fibrous Composites", Journal of Materials Science 8 (1973), pp. 352-362.

[3] Bhatt, R. T. and Phillips, R. E., "Laminate Behavior for SiC Fiber-Reinforced Reaction-Bonded Silicon Nitride Matrix Composites", NASA Technical Memorandum 101350. (Oct. 1988).

[4] Budiansky, B., Hutchchinson, J. W. and Evans, A. G., "Matrix Fracture in Fiber-Reinforced Ceramics", Journal of Mechanics and Physics of Solids, 35 (1986), pp. 167-189.

[5] Budiansky, B., "On the Theoretical Toughness and Strength of Ceramic Composites", To be published in Proceedings of IUTAM Symposium on Fracture of Brittle Disordered Materials: Concrete, Rock, Ceramics, (1993) Brisbane.

[6] Budiansky, B., and Cui, Y. L., "On the Tensile Strength of a Fiber-Reinforced Ceramic Composite Containing a Crack -Like Flaw", J. Mech. Phys. Solids Vol. 42, No. 1, pp. 1-19, 1994.

[7] Budiansky, B., Evans, A. G., and Hutchchinson, J. W., "Fiber-Matrix Debonding Effects On the Cracking In Aligned-Fiber Ceramic Composites", MECH-233, Harvard University, Division of Applied Sciences, (1994) Cambridge MA.

[8] Chan, K. S., He, M. Y., and Hutchchinson, J. W., "Cracking and Stress Redistribution in Ceramic Layered Composites", Materials Science and Engineering, A167, (1993), pp. 57-64.

[9] Cui, Y. L.,"On the Strength of Fiber-Reinforced Ceramic Composites Containing an Elliptical Hole", MECH-217, Harvard University, Division of Applied Sciences, (1993) Cambridge MA.

[10] Cui, Y. L., and Budiansky, B., "Steady-State Matrix Cracking of Ceramics Reinforced by Aligned Fibers and Transforming Particles", J. Mech. Phys. Solids Vol. 41, No. 4, (1993) pp. 615-630.

[11] He, M. Y., Wu, B. -X., and Evans, A G.,"Inelastic Strains Due To Matrix Cracking In Unidirectional Fiber Reinforced Composites", MECH-222, Harvard University, Division of Applied Sciences, (1993) Cambridge MA.

[12] Kuo, Wen-Shyong and Chou, Tsu-Wei, "Mechanical Behaviors of Ceramic Matrix Composites with Matrix Cracking and Fiber Debonding", 5th Japan-US Conference on Composites, Tokyo, Japan, June 1990.

[13] Lu, T. J., and Hutchchinson, J. W.,"Effect of Matrix Cracking and Interface Sliding On the Thermal Expansion of Fiber-Reinforced Composites", MECH-231, Harvard University, Division of Applied Sciences, (1994) Cambridge MA.

[14] Cao, H. C., "Tensile Tests of Ceramic Matrix Composites : Theory and Experiment", Journal of the American Ceramic Society 73, No. 7, (1990), pp. 2091-2094.

[15] Chulya, A., Geyekenyesi, J. P., and Bhatt, R. T., "Mechanical Behavior of Fiber Reinforced SiC/RBSN Ceramic Matrix Composites: Theory and Experiments", NASA Technical Memorandum 103688, (1991).

[16] Daniel, I. M., Anastassopoulos, G. and Lee, J. W., "Experimental Micromechanics of Brittle Matrix Composites." In "Micromechanics : Experimental Techniques." ASME, AMD-Vol. 102 (1989) pp. 133-146.

[17] Daniel, I. M., Anastassopoulos, G. and Lee, J. W., "Failure Mechanisms and Interfacial Shear Strength in Brittle-Matrix Composites", ASME AD-Vol.29/AMD-Vol. 146 Advances in Experimental Mechanics and Biomeimetics, (1992), pp. 57-69.

[18] Weitsman, Y. J. and Zhu, H.," Failure Progression in Unidirectionally Reinforced Ceramic Composites", ASME, AMD-Vol. 150/AD-Vol. 32, Damage Mechanics in Composites, (1992), pp. 155-179.

[19] Weitsman, Y. J. and Zhu, H., "Multi-Fracture of Ceramic Composites", J. Mech. Phys. Solids Vol. 41, No. 2, (1993), pp. 351-388.

[20] Zhu, H. and Weitsman, Y. J., "The progression of Failure Mechanisms in Unidirectionally Reinforced Ceramic Composites", J. Mech. Phys. Solids Vol. 42, No. 10, (1994), pp. 1601-1632.

[21] Baaklini, G. Y., and Bhatt, R. T., "Failure Analysis of SiC/RSBN Composite Using X-Ray Monitoring", 4th HITEMP, NASA CD-91-56650, pp 73.1-73.16.

[22] Davidson, D. L., Rousseau, C. Q. and Campbell, J. B., "The Micromechanics of Ambient Temperature Cyclic Loading Fatigue in a Composite of CAS Glass Ceramic Reinforced with Nicalon Fibers", submitted to Acta Metall for review. (11-91)

[23] Larsen, C. G., "Ceramics Tensile Grip", Thermal and Mechanical Behavior of Metal Matrix and Ceramic Matrix Composites, ASTM STP 1080, (1990), pp. 235-246 .

[24] Nardone, V. C. and Prewo, K. M., "Tensile Performance of Carbon-Fibre-Reinforced Glass", Journal of Materials Science 23 (1988), pp. 168-180.

[25] Prewo, K. M. and Brennan, J. J., "High-Strength Silicon Carbide Fibre-Reinforced Glass-Matrix Composites", Journal of Materials Science 15 (1980), pp. 463-468.

[26] Prewo, K. M. and Brennan, J. J., "Silicon Carbide Yarn Reinforced Glass Matrix Composites", Journal of Materials Science 17 (1982), pp. 1201-1206.

[27] Prewo, K. M., "Tension and Flexural Strength of Silicon Carbide Fiber Reinforced Glass-Ceramics", Journal of Materials Science 21 (1986), pp. 3590-3600.

[28] Prewo, K. M., "Fatigue and Stress Rupture of Silicon Carbide Fiber Reinforced Glass-Ceramics", Journal of Materials Science 22 (1987), pp. 2695-2701.

[29] Walter, M. E., An Experimental Investigation of Damage Evolution in a Ceramic Matrix Composite", Journal of Engineering Materials and Technology, Vol. 117, Jan. (1995), pp. 101-108.

[30] Evans, A. G., "Perspective on the Development of High-Toughness Ceramics", Journal of the American Ceramic Society 73, No. 2, (1990), pp. 187-206.

[31] Hillig, W. B., "Strength and Toughness of Ceramic Matrix Composites", Am. Rev. Mater. Sci. 17 (1987), pp. 341-383.

[32] Schioler, L. J. and Stiglich, J. J. Jr., "Ceramic Matrix Composites: A Literature Review", Ceramic Bulletin 65 No. 2 (1986), pp. 289-292.

[33] Nuismer, R. J. and Tan, S. C., "Constitutive Relations of a Cracked Composite Lamina", Journal of Composite Materials, Vol. 22 - April (1988), pp. 306-321.

[34] Tan, S. C. and Nuismer, R. J., "A Theory for Progressive Matrix Cracking in Composite Laminates", Journal of Composite Materials, Vol. 23 - October (1989), pp. 1029-1047.

[35] Lee, J. -W., and Daniel, I. M., "Progressive Transverse Cracking of Crossply Laminates", Journal of Composite Materials, Vol. 24 - November (1990), pp. 1225-1243.

[36] Xia, Z. C., Carr, R. R. and Hutchinson, J. W., "Transverse Matrix Cracking In Fiber-Reinforced Brittle Matrix, Cross-Ply Laminates", Acta metall. mater. Vol. 41, No. 8, pp. 2365-2376, (1993).

[37] Xia, Z. C., Carr, R. R. and Hutchinson, J. W., " Matrix Cracking of Cross-Ply Ceramic Composites", MECH-218, Harvard University, Division of Applied Sciences, (1993) Cambridge MA.

[38] Daniel, I. M. "Failure Mechanisms and Damage Evolution in Crossply Ceramic Matrix Composites, International Journal of Solids and Structures, to be published. McCormick School of Engineering and Applied Science, Northwestern University. (Recd, 1-95).

[39] Karandikar, P. and Chou, Tsu-Wei, "Characterization and Modeling of Microcracking and Elastic Moduli Changes in Nicalon-CAS Composites", Composite Science and Tech., to be published. Center for Composite Materials and Material Science Program, University of Delaware. (Recd 5-92.)

[40] Kuo, Wen-Shyong and Chou, Tsu-Wei, "Modeling of Damage in Ceramic Matrix Cross-Ply Composites", AMD-Vol 142/MD-Vol. 34, Damage Mechanics and Localization, ASME (1992), pp. 97-107.

[41] Kuo, Wen-Shyong and Chou, Tsu-Wei, "Multiple Cracking of Unidirectional and Cross-Ply Ceramic Matrix Composites", Center For Composite Materials and Dept. of Mechanical Engineering, University of Delaware, Newark DE. To be published.

[42] Pryce, A. W. and Smith, P. A., "Matrix Cracking in Ceramic Matrix Composites Under Quasi-Static Tensile Loading", Proceedings of the Eighth International Conference on Composite Materials (ICCM/8), Jujy 15-19, (1991), pp. 24-A-1 - 24-A-10.

[43] Brennan, J. J., and Prewo, K. M., "Silicon Carbide Fibre Reinforced Glass-Ceramic Matrix Composites Exhibiting High Strength and Toughness", Journal of Materials Science 17, (1982), pp. 2371-2383.

[44] Kim, R. Y., "Experimental Observation of Progressive Damage in SiC/Glass-Ceramic Composites", ACSS Proceedings of the 16th Annual Conference on Composites and Advanced Ceramics Material, Vol 13, #7-8 (1992), pp. 281-300.

[45] Rousseau, C. Q., "Monotonic and Cyclic Behavior of a Silicon Carbide/Calcium-Aluminosilicate Ceramic Composite", Thermal and Mechanical Behavior of Metal Matrix and Ceramic Matrix Composites, (ASTM STP 1080), pp. 136-151.

[46] Ballarini, R. and Ahmed, S., "Finite Element Modeling of Frictionally Restrained Composite Interfaces", Lewis Research Ctr, Grant NAG3-8956, Contract Report 182281, (1989).

[47] Bright, J. D., Shetty, D. K., Griffin, C. W. and Limaye, S. Y., "Interfacial Bonding and Friction in Silicon Carbide (Filament)-Reinforced Ceramic- and Glass-Matrix Composites", J. Am. Ceram. Soc., 72, [5], (1989), pp. 746-753.

[48] Charalambides, P. G., and Evans, A. G., "Debonding Properties of Residually Stresses Brittle-Matrix Composites", J. Am. Ceram. Soc., 72, [10], (1989), pp. 1891-1898.

[49] Deshmukh, U. V., and Coyle, T. W., "Determination of the Interface Strength in Glass-SiC Composites via Single Fiber Tensile Testing", Ceramic Engineering Science Proceedings 9 (1988), No. 7-8, pp. 627-634.

[50] Erdogan, F. and Joseph, P. F., "Toughening of Ceramics Through Crack Bridging by Ductile Particles", J. AM. Ceram. Soc., 72 [2], pp. 262-270, (1989).

[51] Hsueh, C. -H., "Some Considerations of Evaluation of Interfacial Frictional Stress from the Indentation Technique for Fibre-Reinforced Ceramic Composites", Journal of Materials Science Letters 8 (1989), pp. 739-742.

[52] Hsueh, C. -H., "Evaluation of Interfacial Shear Strength, Residual Clamping Stress and Coefficient of Friction for Fiber-Reinforced Ceramic Composites", Acta metall. mater., Vol. 38, No. 3, (1990), pp. 403-409.

[53] Kerans, R. J., Hay, R. S., and Pagano, N. J., "The Role of the Fiber-Matrix Interface in Ceramic Composites", American Ceramic Society Bulletin 68 (1989), No. 2, pp. 429-442.

[54] Kimber, A. C. and Keer, J. G., "On the Theoretical Average Spacing in Brittle Matrix Composites Containing Continuous Aligned Fibres", Journal of Materials Science Letters 1 (1982), pp. 353-354.

[55] Lu, M. -C., and Hsueh, C. -H, "Effects of Friction in Ceramic Coating/Fiber Composites", Journal of Composite Materials, Vol. 24 - June (1990), pp. 572-593.

[56] Marshall, D. B., "An Indentation Method for Measuring Matrix-Fiber Frictional Stresses in Ceramic Composites", Communications of the American Ceramic Society, December (1984), pp. C259-260.

[57] Marshall, D. B., "Interfaces in Ceramic Matrix Composites", Materials Science Research 21 (Ceramic Microstructures 1986). New York and London: Plenum Press (1987).

[58] Phillips, D. C., "Interfacial Bonding and the Toughness of Carbon Fibre Reinforced Glass and Glass-Ceramics", Journal of Materials Science 9 (1974), 1847-1854.

[59] Singh, R. N., "Fiber-Matrix Interfacial Characteristics In a Fiber-Reinforced Ceramic Matrix Composite", Ceram. Eng. Sci. Proc. 10[7-8], (1989), pp. 883-893.

[60] Wu, C. C., Bender, B. A., and Jesson, T. L., "Shear Test and Shear Strength of Ceramic Composites", Proceeding of the Seventeenth Annual Conference on Composites and Advanced Materials. American Ceramic Society, Vol 14, No. 7-8, (1993), pp. 198-205.

[61] Anderson, T. L., "Fracture Mechanics, Fundamentals and Applications", CRC Press, Boca Raton, FL (1991).

[62] Burden, R. L. and Faires, J. D., "Numerical Analysis, 5th Edition", PWS Publishing Co., Boston, MA (1993).

[63] Ewalds, H. L. and Wanhill, R. J. H., "Fracture Mechanics", Edward Arnold (Publishers) Ltd., Baltimore, MD (1985).

[64] Kanninen, M. F. and Popelar, C. H., "Advanced Fracture Mechanics", Oxford University Press, New York, NY (1985).

[65] Kincaid, D. and Cheney, W.,"Numerical Analysis : Mathematics of Scientific Computing", Brooks/Cole Publishing Co., Belmont, CA (1990).

[66] Press, W. H., Teukosky, S. A., Vetterling, W. T., and Plannery, B. P. "Numerical Recipes in C", Cambridge University Press, New York, NY (1992).

APPENDICES

APPENDIX A

CERAMIC CROSS-PLY LAMINATE STRESS-STRAIN CURVES AND CRACK DENSITY DATA

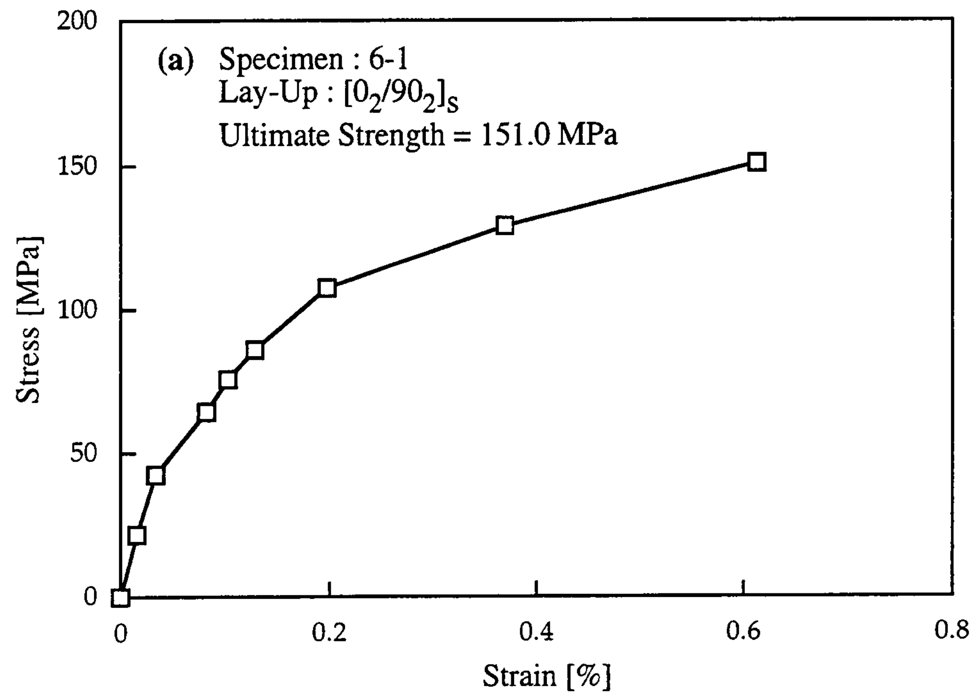

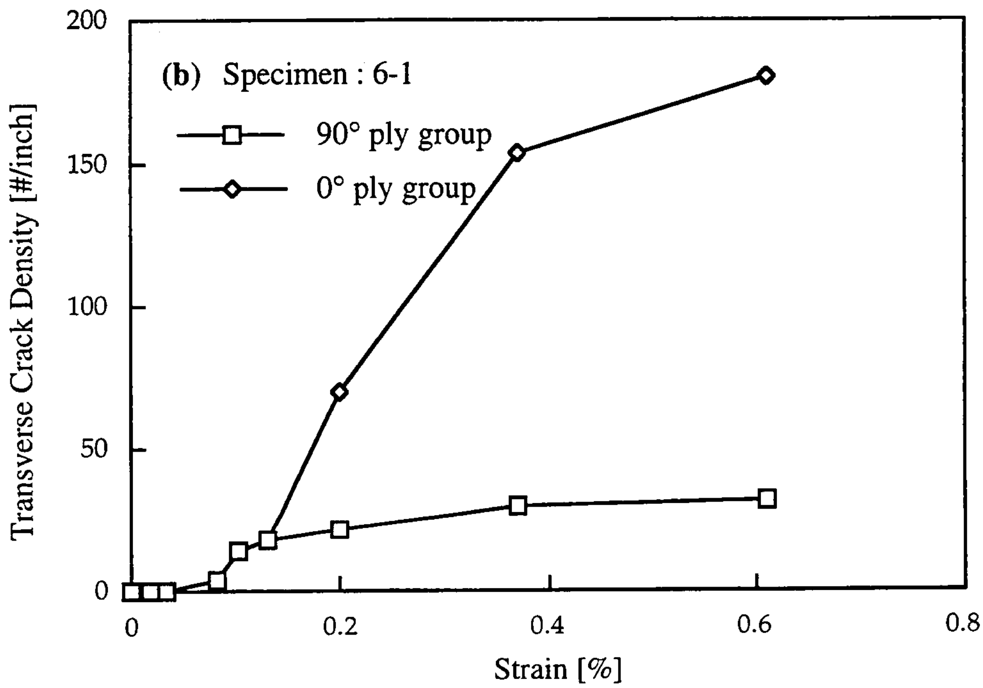

Figure A1. Axial Test Results for Specimen 6.1, Lay-Up : $[0_2/90_2]_S$
(a) Stress/Strain Behavior
(b) Crack Densities in the 0° and 90° Plies vs. Strain

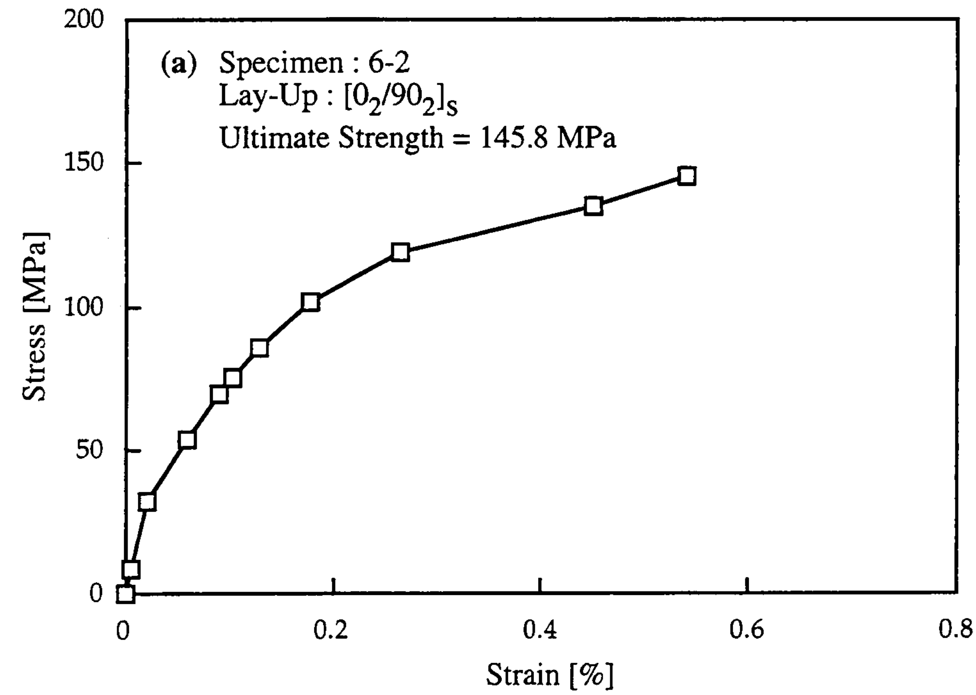

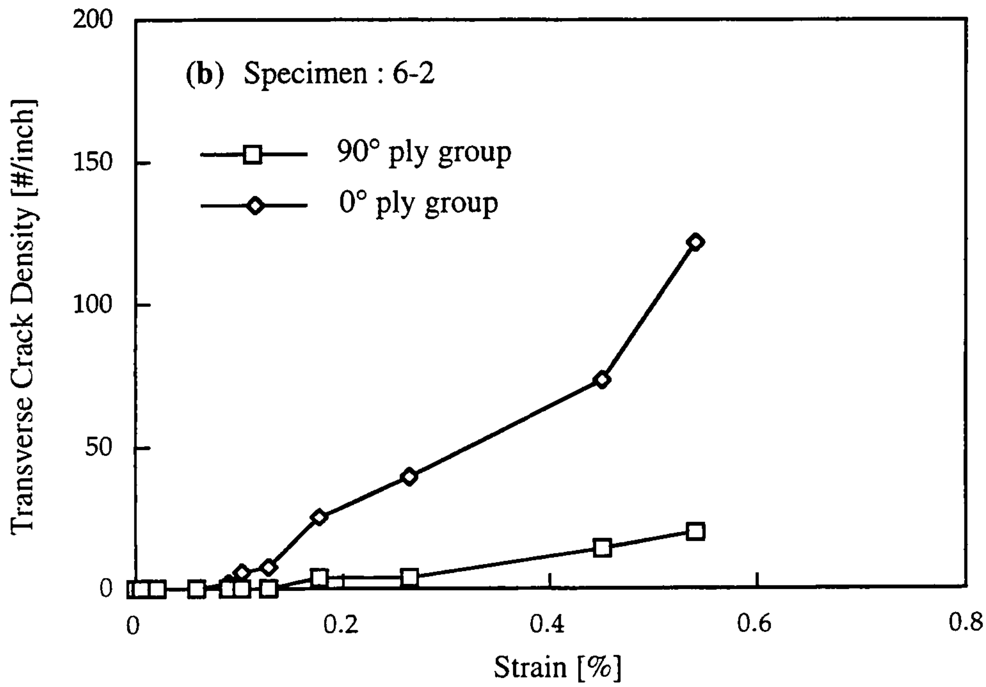

Figure A2. Axial Test Results for Specimen 6.2, Lay-Up : $[0_2/90_2]_S$
(a) Stress/Strain Behavior
(b) Crack Densities in the 0° and 90° Plies vs. Strain

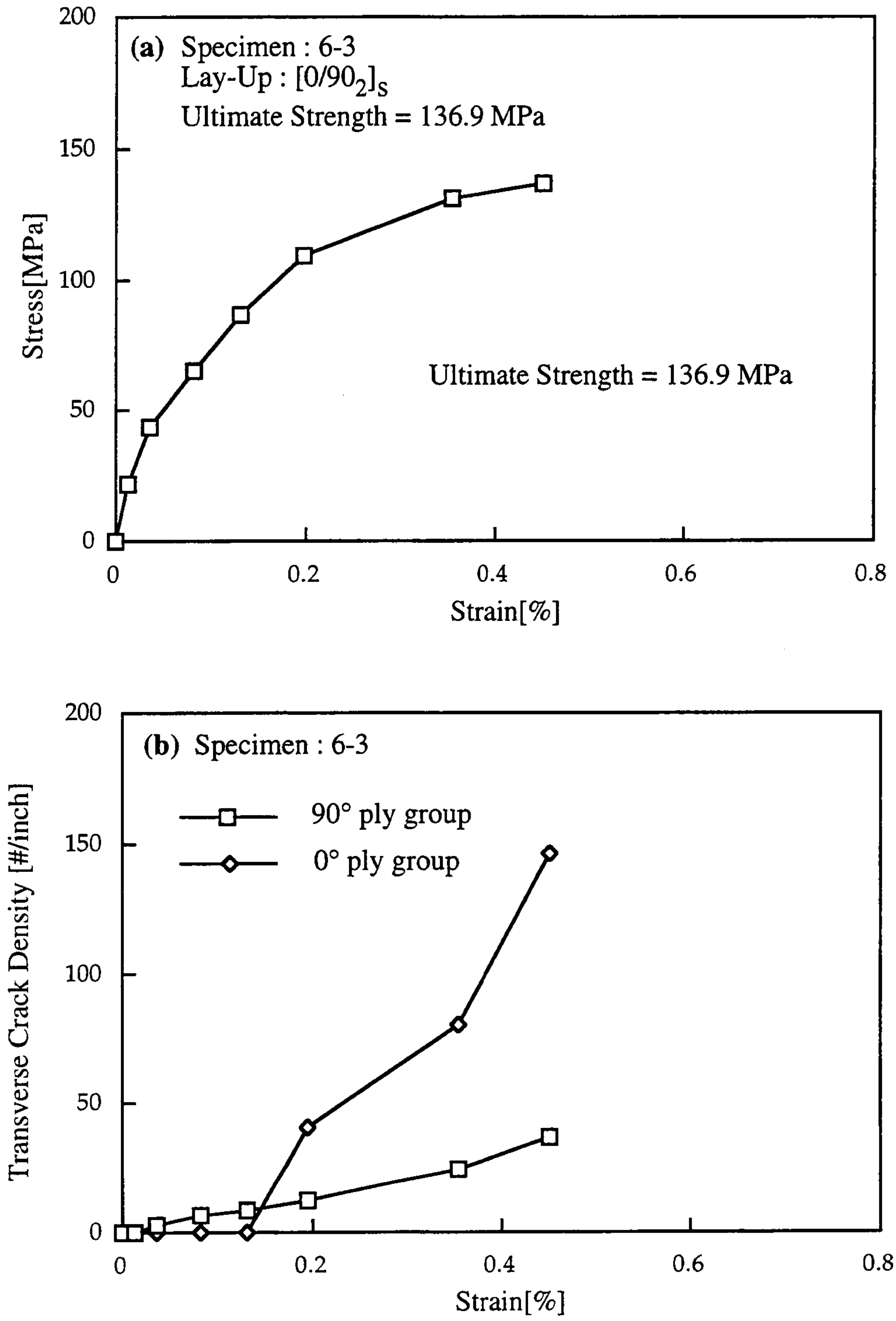

Figure A3. Axial Test Results for Specimen 6.3, Lay-Up : $[0_2/90_2]_S$
(a) Stress/Strain Behavior
(b) Crack Densities in the 0° and 90° Plies vs. Strain

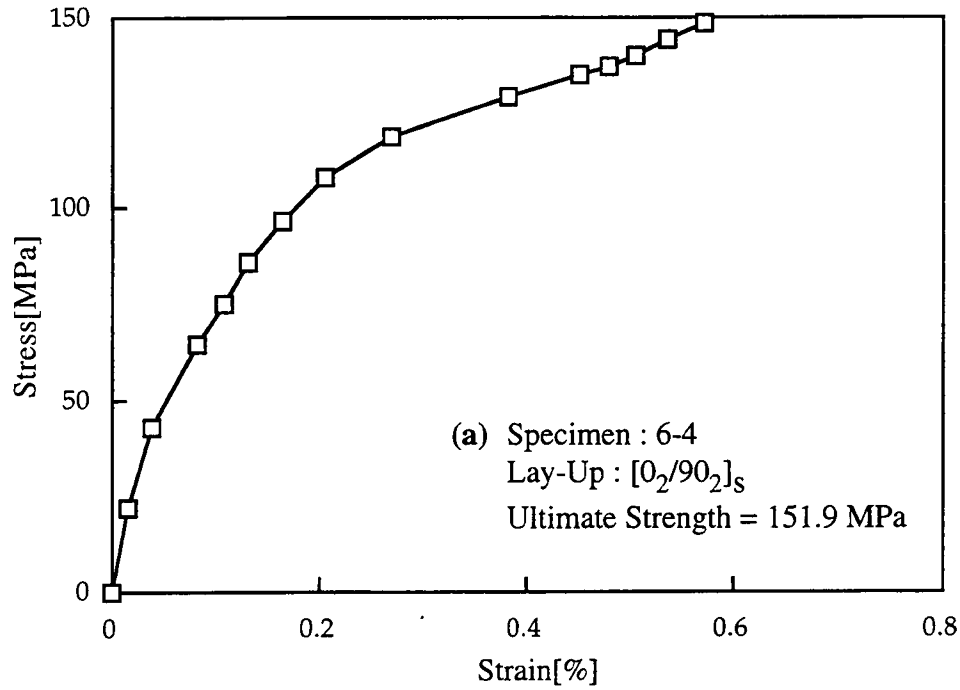

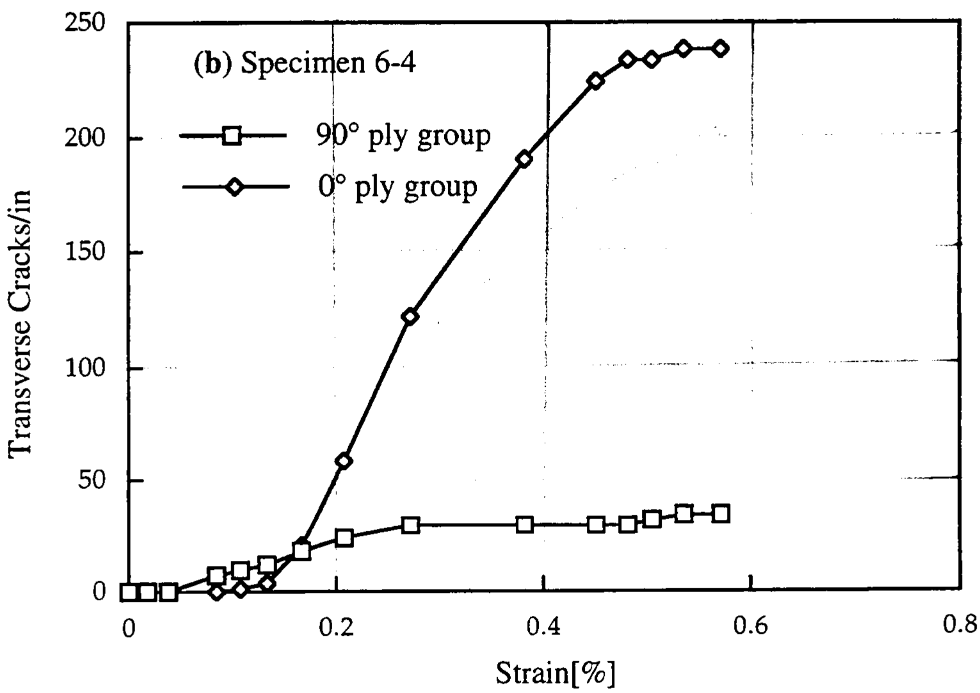

Figure A4. **Axial Test Results for Specimen 6.4, Lay-Up : $[0_2/90_2]_S$**
(a) Stress/Strain Behavior
(b) Crack Densities in the 0° and 90° Plies vs. Strain

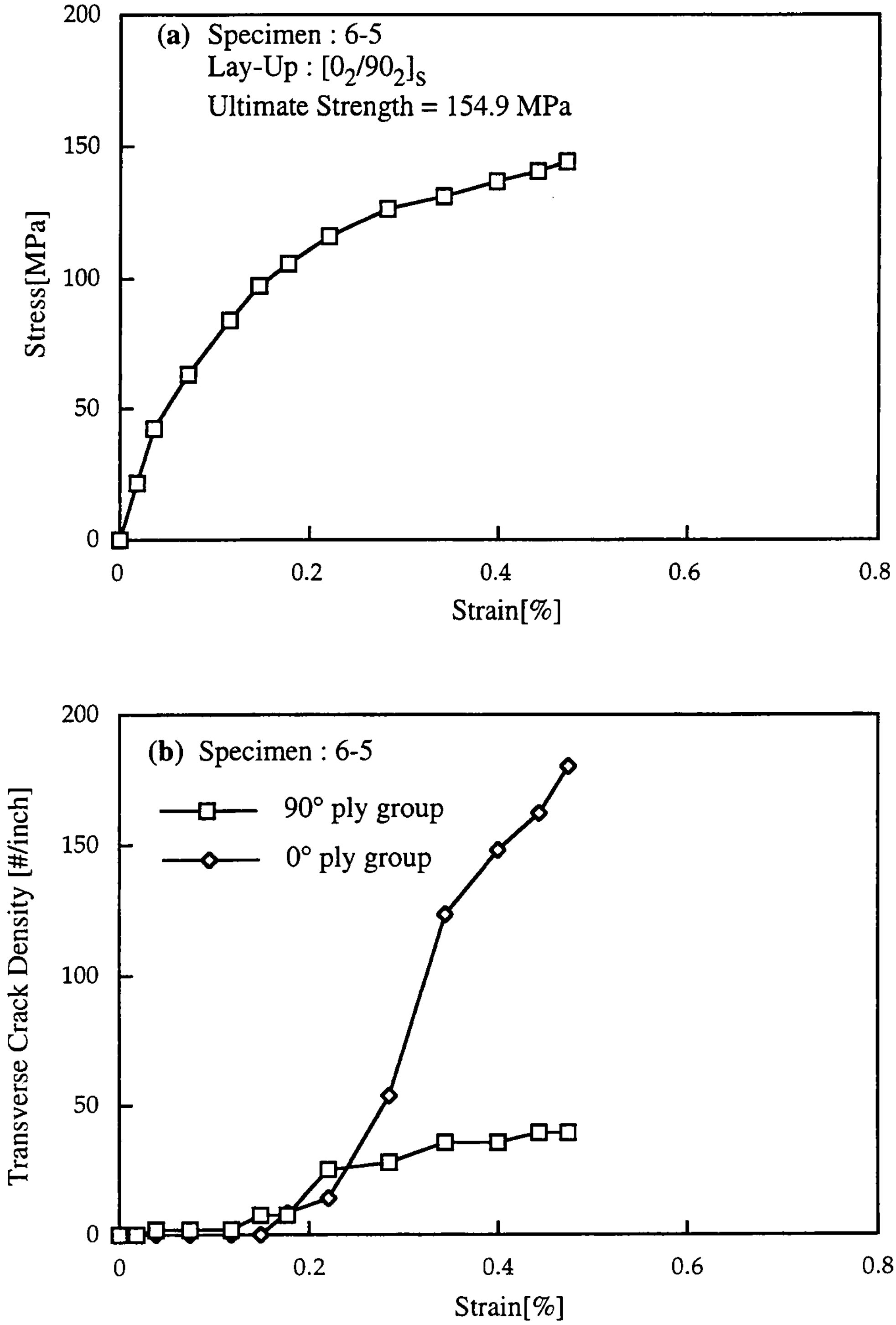

Figure A5. Axial Test Results for Specimen 6.5, Lay-Up : $[0_2/90_2]_S$
(a) Stress/Strain Behavior
(b) Crack Densities in 0° and 90° Plies vs. Strain

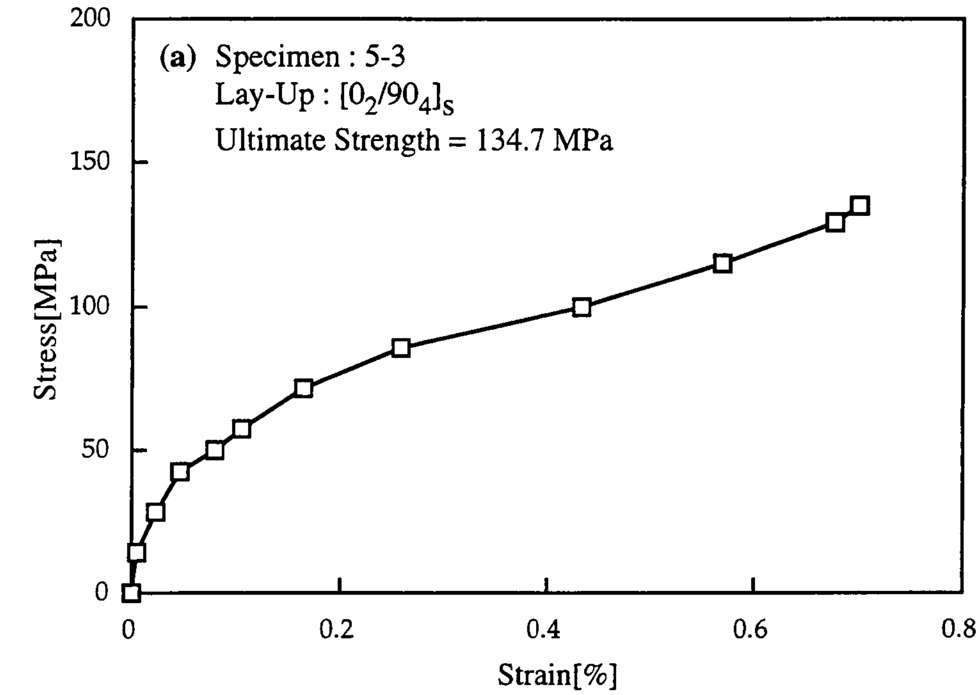

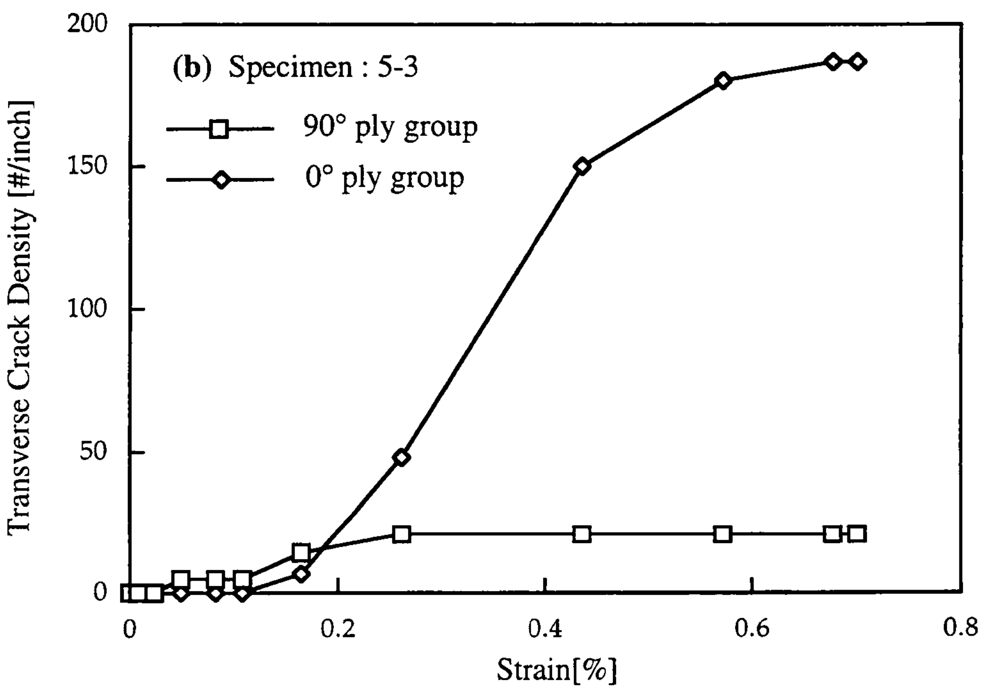

Figure A6. Axial Test Results for Specimen 5.3, Lay-Up : $[0_2/90_4]_S$
(a) Stress/Strain Behavior
(b) Crack Densities in the 0° and 90° Plies vs. Strain

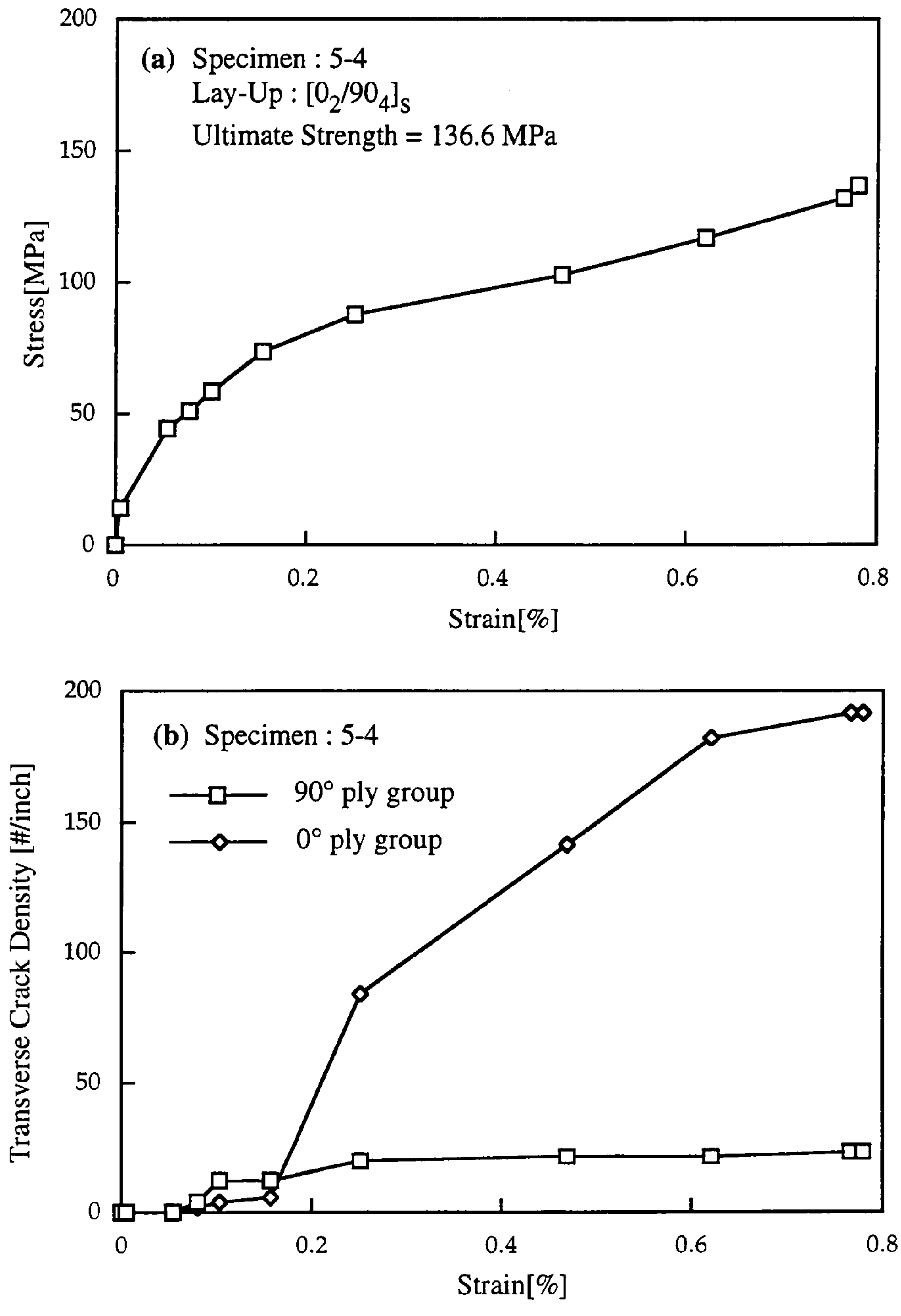

Figure A7. **Axial Test Results for Specimen 5.4, Lay-Up : $[0_2/90_4]_S$**
(a) Stress/Strain Behavior
(b) Crack Densities in 0° and 90° Plies vs. Strain

APPENDIX B

EXAMPLES OF MATRIX CRACK PROGRESSION IN THE 0° AND 90° PLIES OF CROSS-PLY CERAMIC LAMINATES UNDER MONOTONICALLY INCREASING LOAD

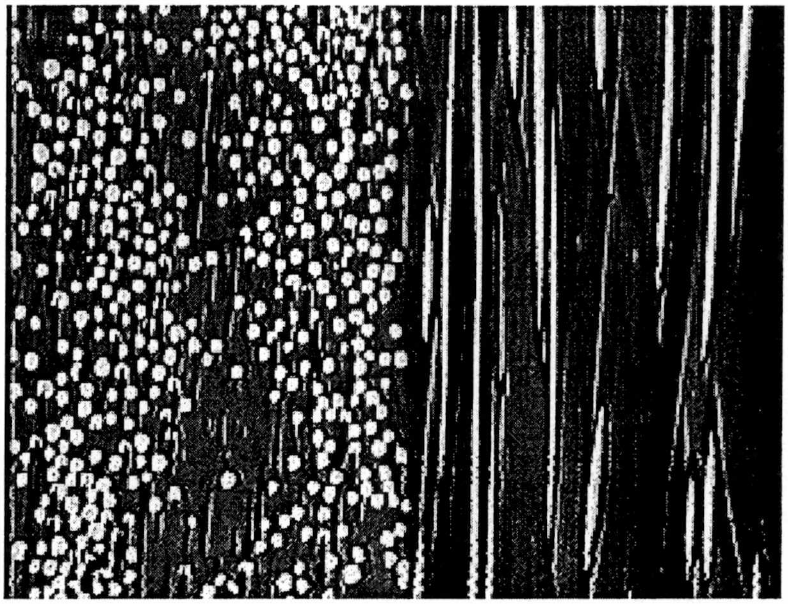

(a) Transverse Crack Initiation in the 90° Plies, $\sigma/\sigma_{ult} = 0.41$

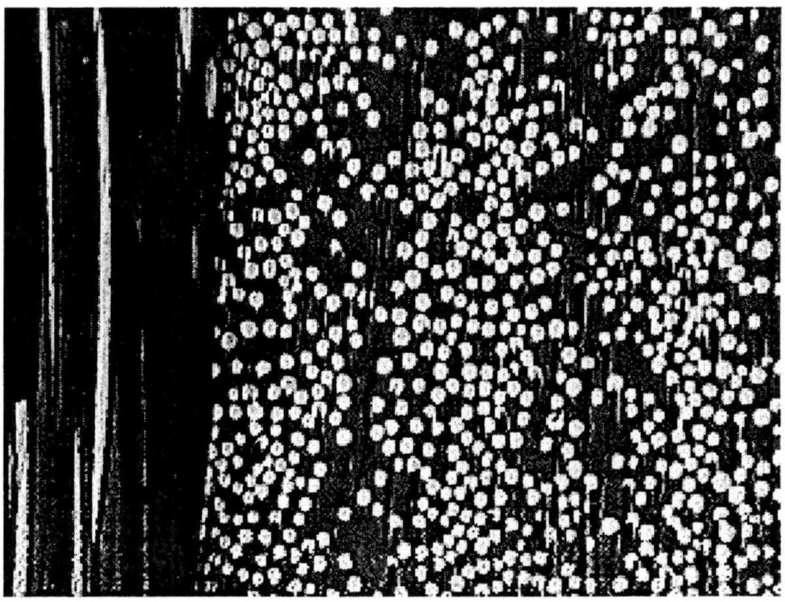

(b) Additional Transverse Cracking in the 90° Plies, $\sigma/\sigma_{ult} = 0.48$

Figure B1. Transverse Crack Progression in a $[0_2/90_2]_s$ Ceramic Matrix Composite

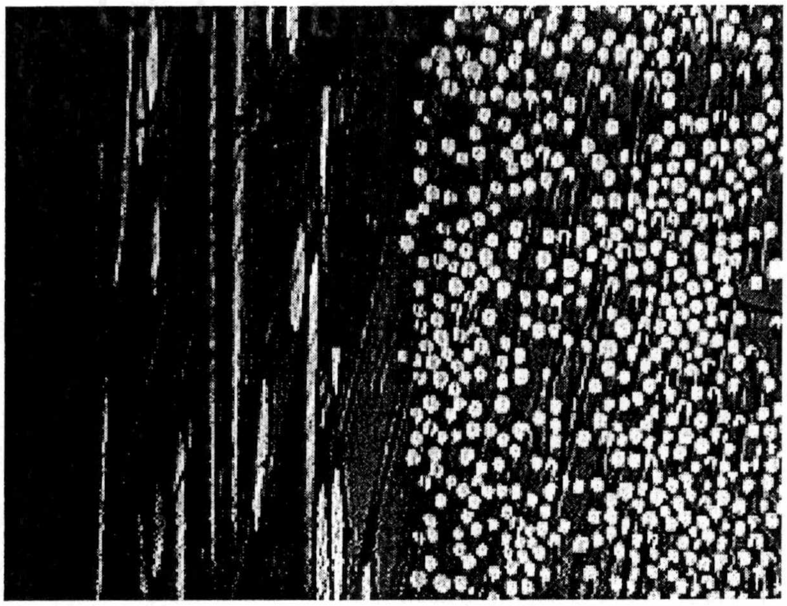

(c) Transverse Crack Initiation in the 0° Plies, $\sigma/\sigma_{ult} = 0.68$

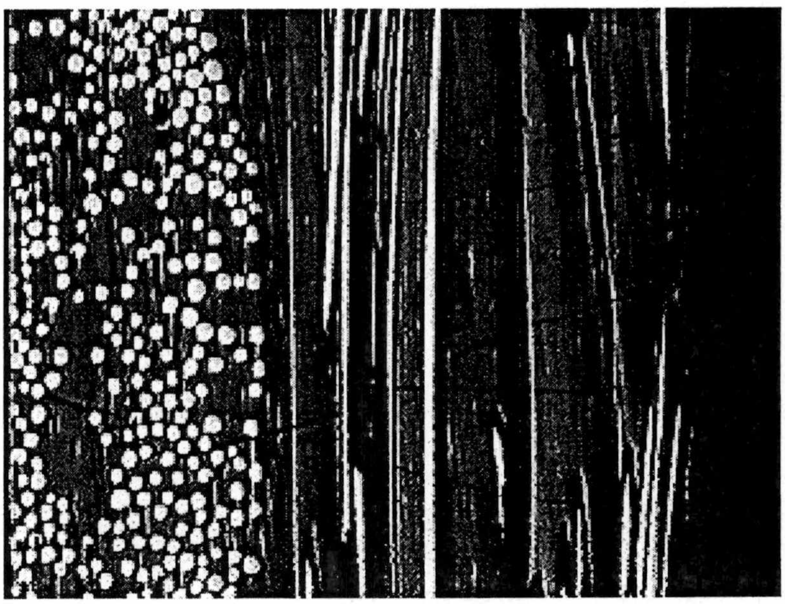

(d) Matrix Crack Progression in the 0° Plies, $\sigma/\sigma_{ult} = 0.82$

Figure B1. Continued

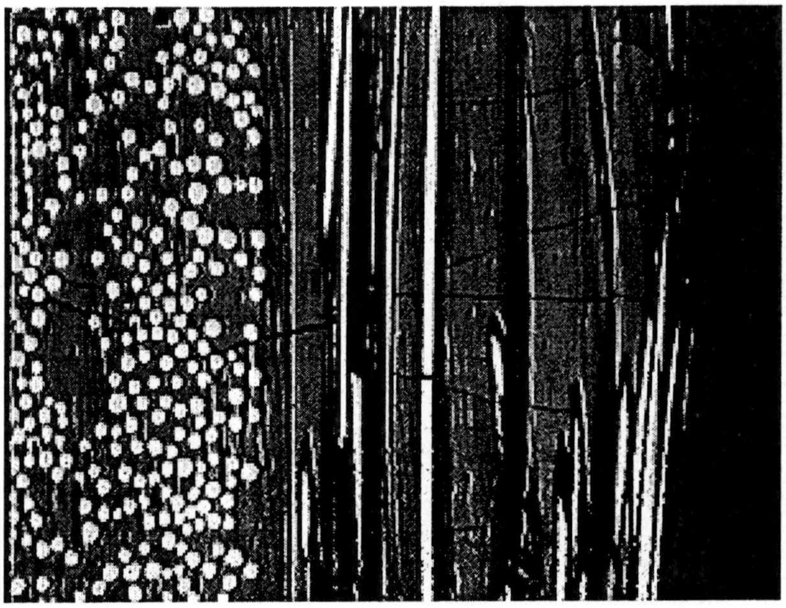

(e) Matrix Cracks Open in the 0° and 90° Plies, $\sigma/\sigma_{ult} = 0.95$

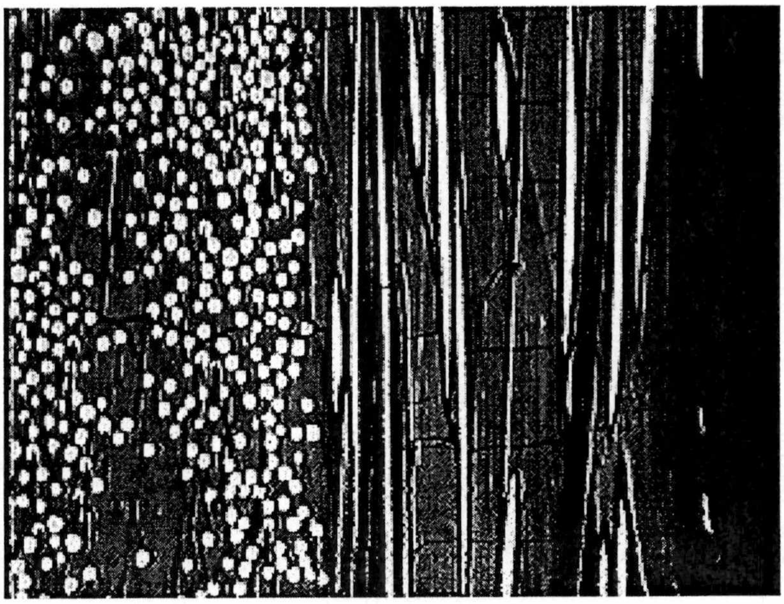

(f) Damage State Prior to Failure, $\sigma/\sigma_{ult} = 0.95$

Figure B1. Continued

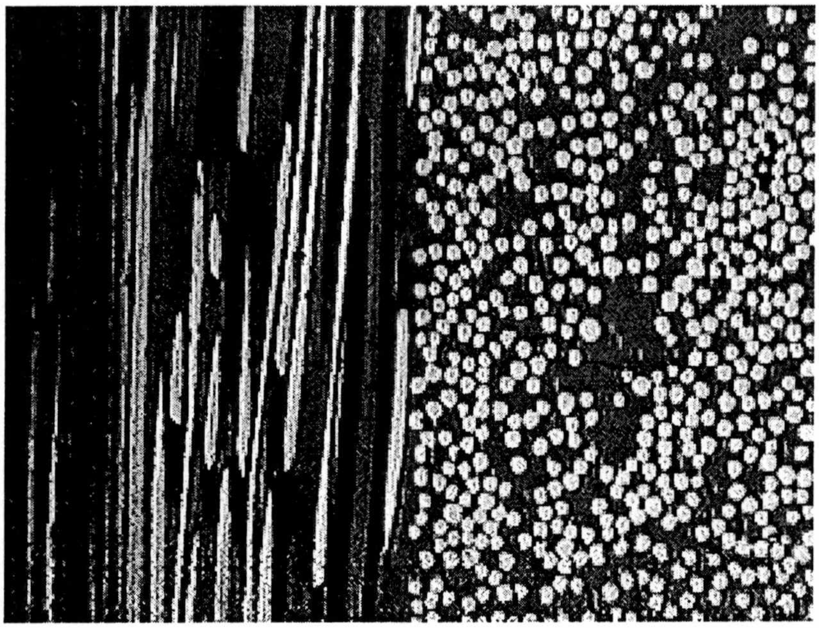

(a) Transverse Crack Initiation in the 90° Plies, $\sigma/\sigma_{ult} = 0.37$

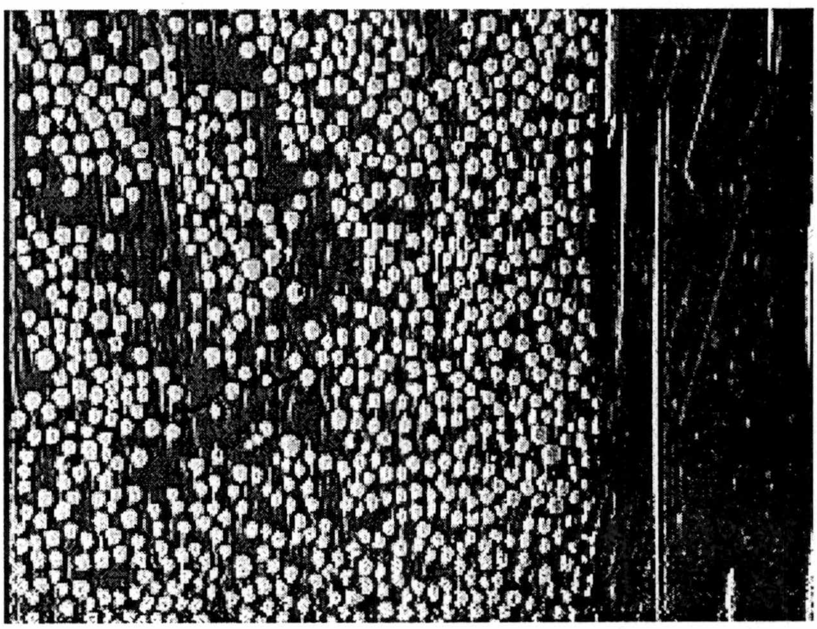

(b) Matrix Crack Progression in the 0° Plies, $\sigma/\sigma_{ult} = 0.64$

Figure B2. Transverse Crack Progression in a $[0_2/90_4]_s$ Ceramic Matrix Composite

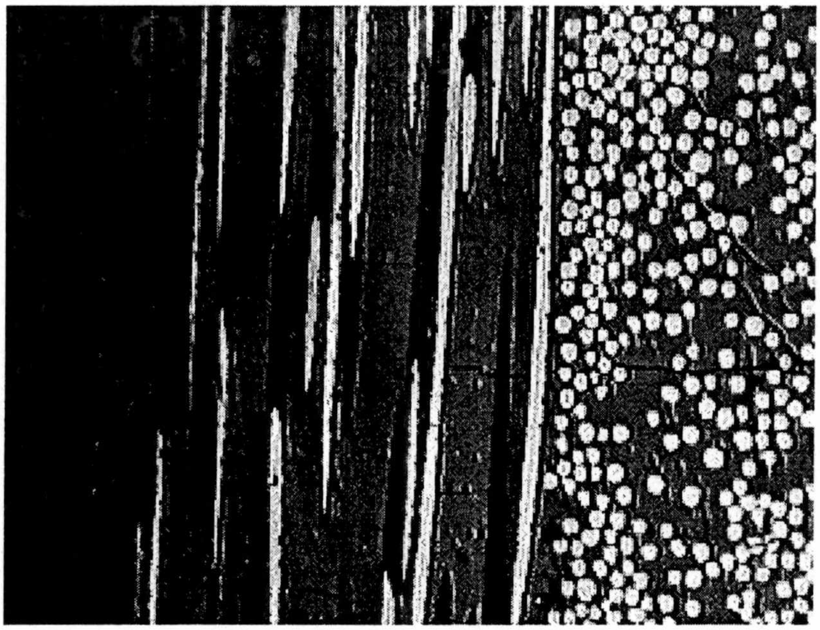

(c) Matrix Crack Branching in the 90° Plies, $\sigma/\sigma_{ult} = 0.75$

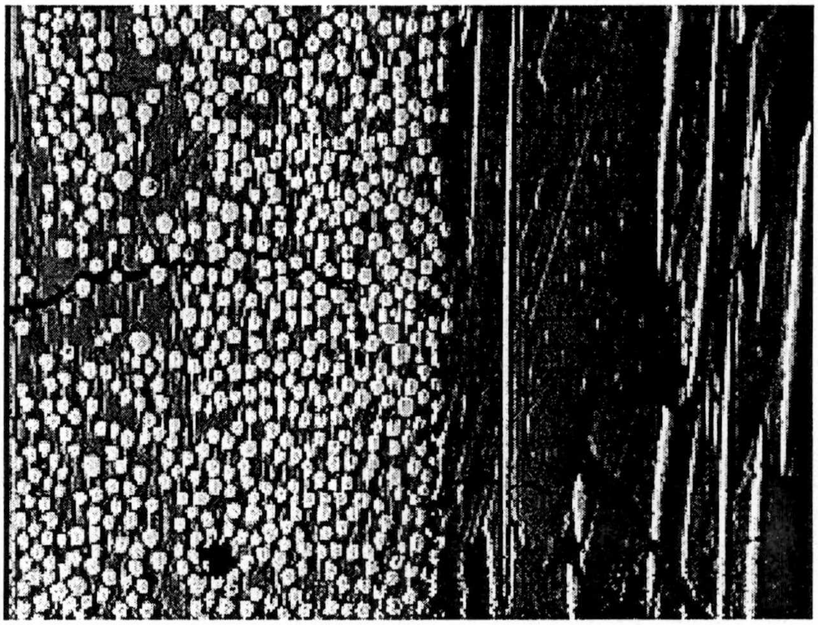

(d) Matrix Crack Opening in the 0° and 90° Plies, $\sigma/\sigma_{ult} = 0.97$

Figure B2. Continued

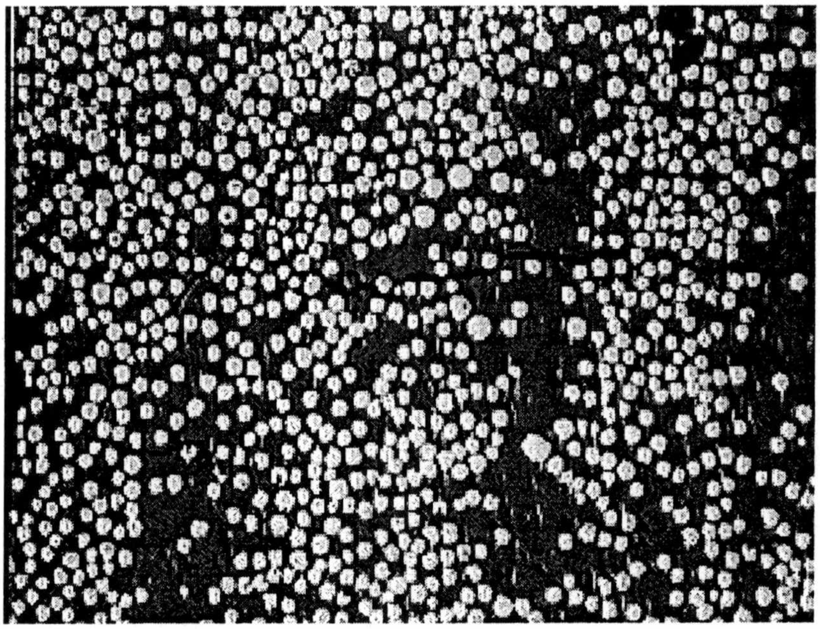

(e) Details of Matrix Cracks Opening in the 90° Plies, $\sigma/\sigma_{ult} = 0.97$

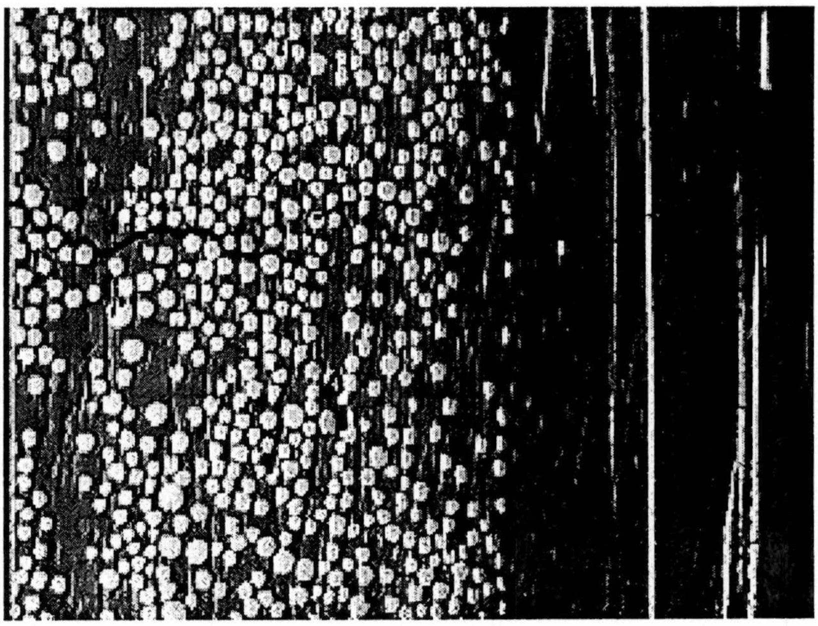

(f) Damage State Prior to Failure, $\sigma/\sigma_{ult} = 0.97$

Figure B2. Continued

APPENDIX C

MINI-SHEAR TEST LOAD-DISPLACEMENT CURVES

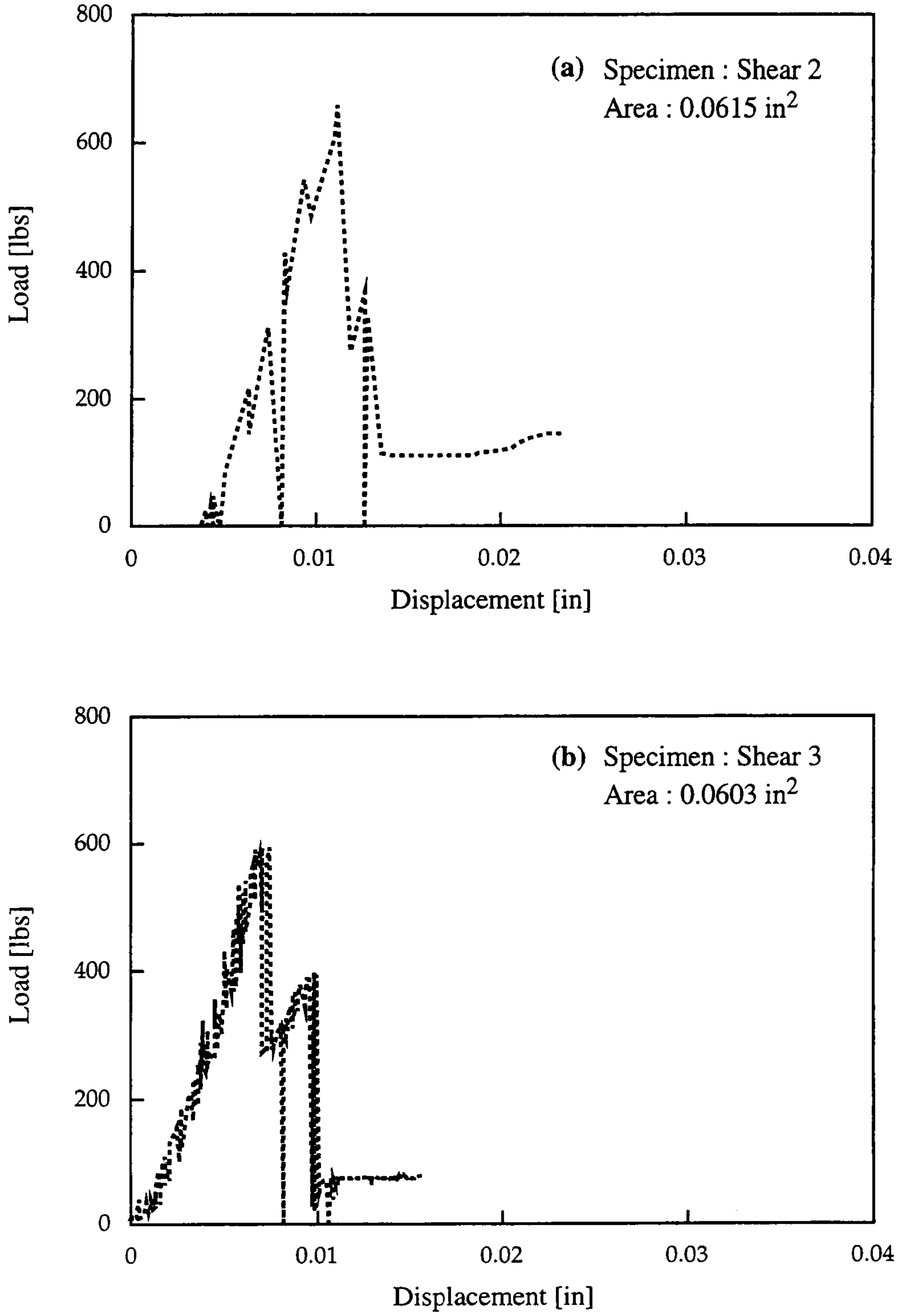

Figure C1. Mini-Shear Test Load Displacement Response for 0.25 Inch Axial Length Specimen Geometry.
(a) Specimen Shear 2, (b) Specimen Shear 3

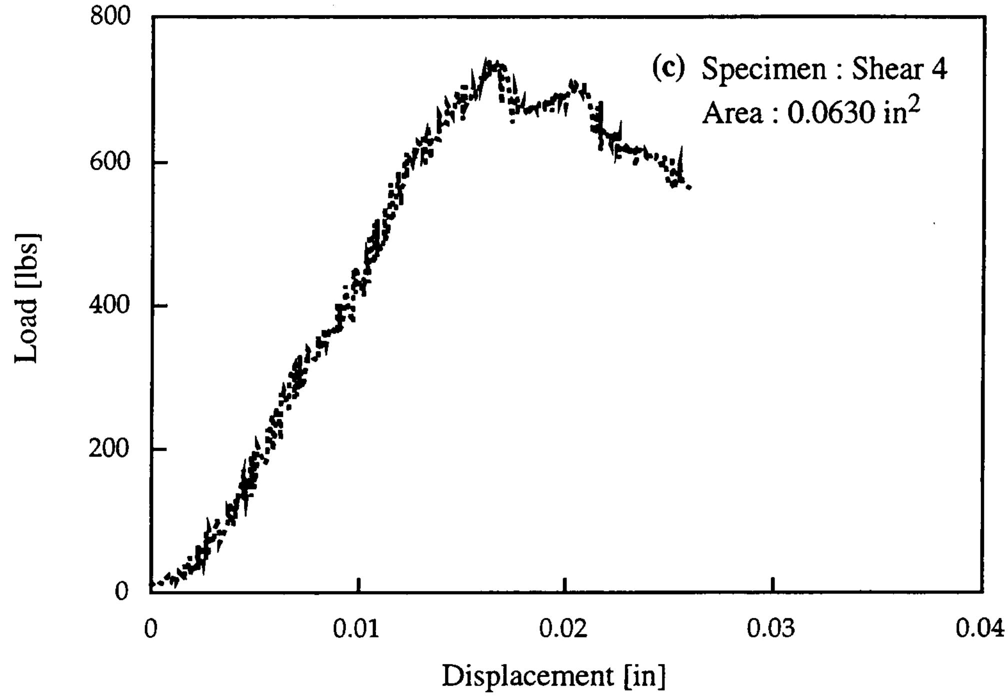

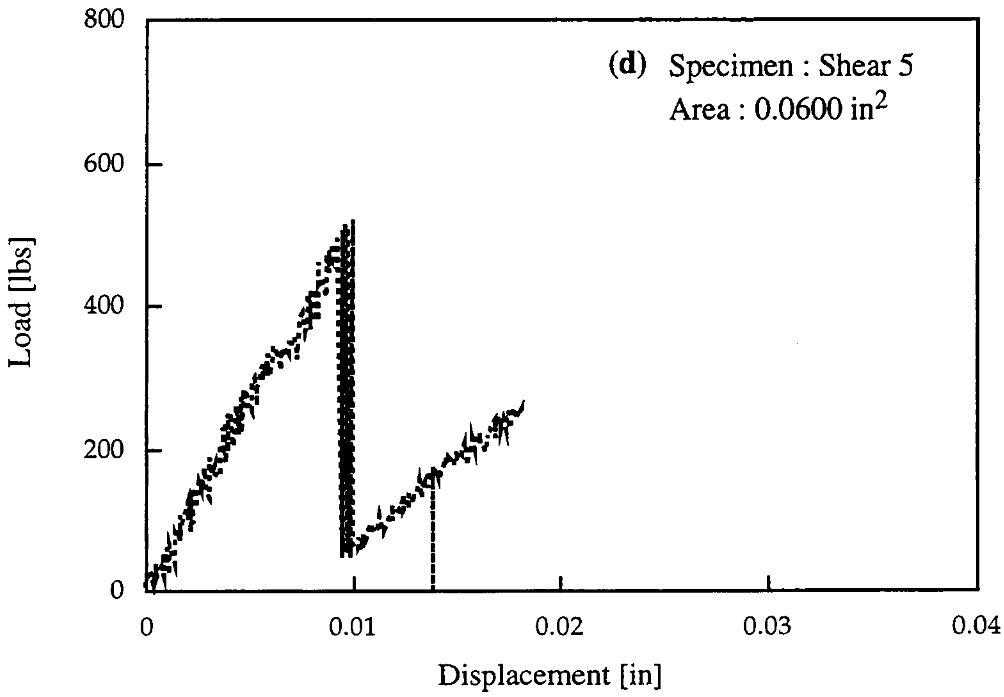

Figure C1. Continued, (c) Specimen Shear 4, (d) Specimen Shear 5

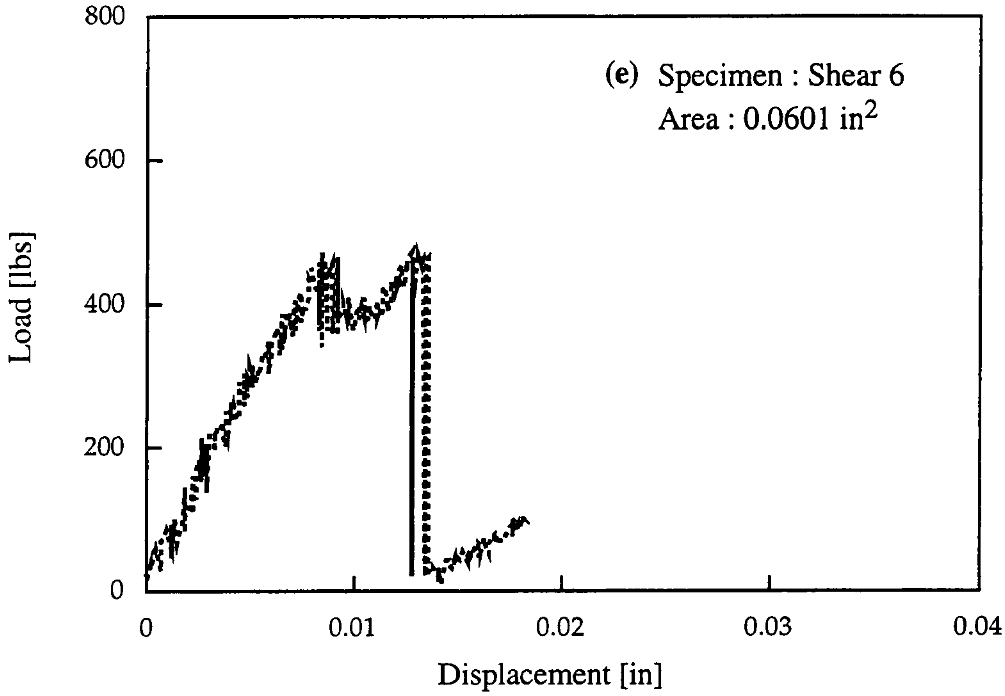

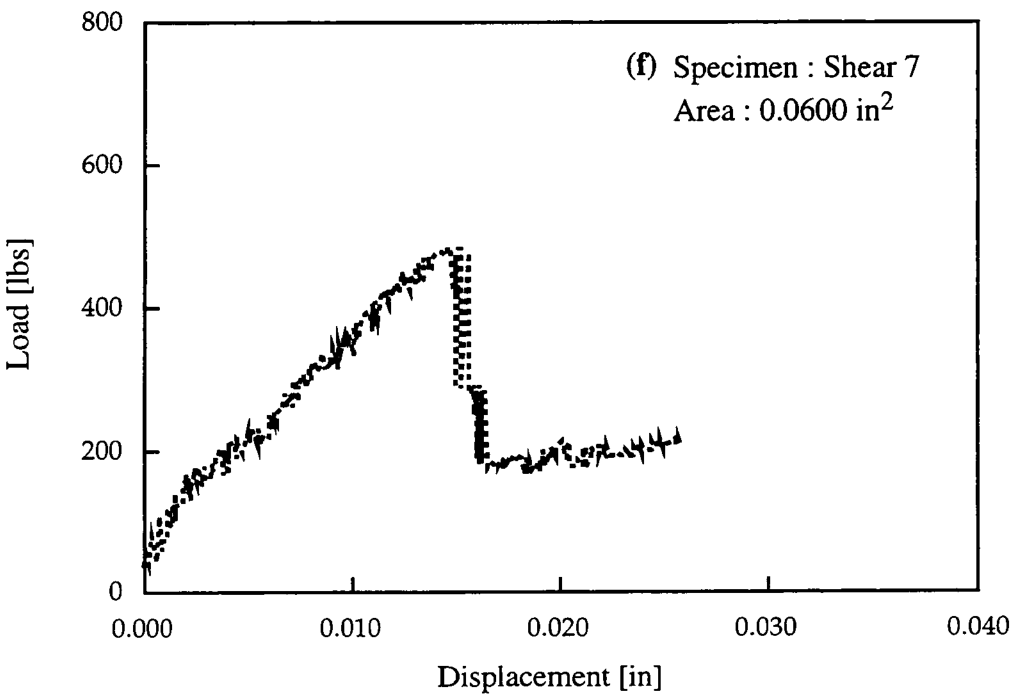

Figure C1. Continued, (e) Specimen Shear 6, (f) Specimen Shear 7

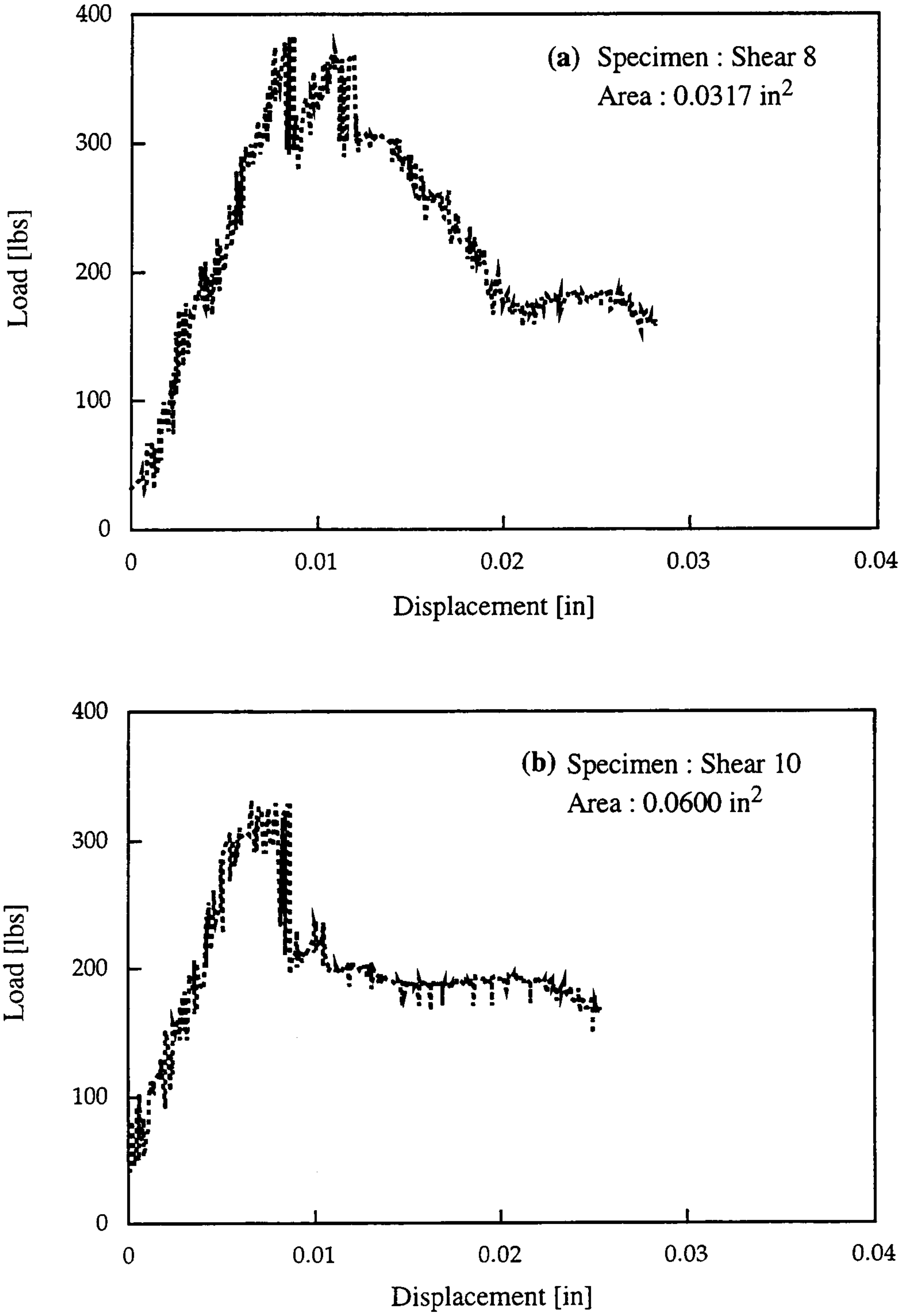

Figure C2. Mini-Shear Test Load Displacement Response for 0.125 Inch Axial Length Specimen Geometry. (a) Specimen Shear 8, (b) Specimen Shear 10

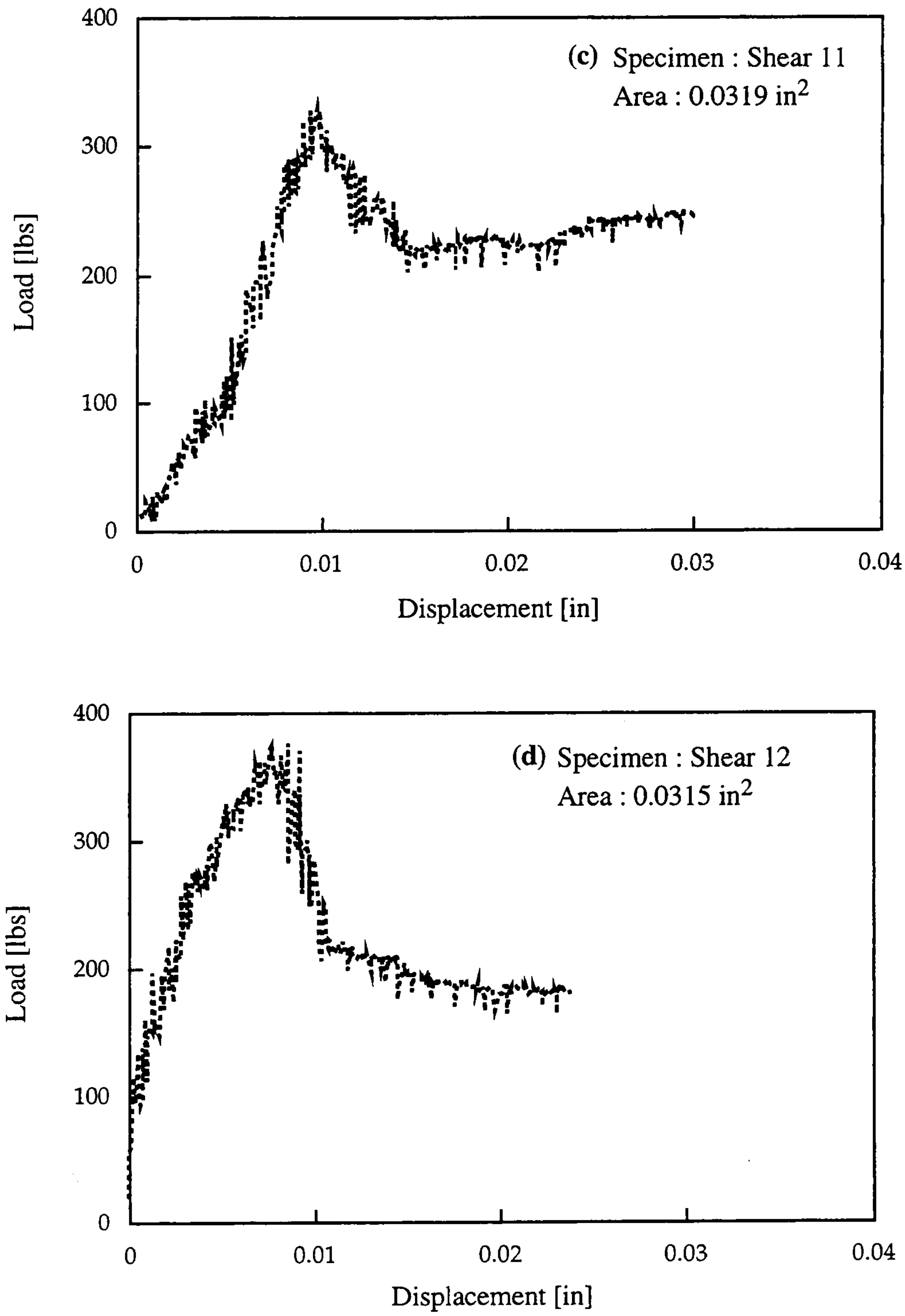

Figure C2. Continued, (c) Specimen Shear 11, (d) Specimen Shear 12

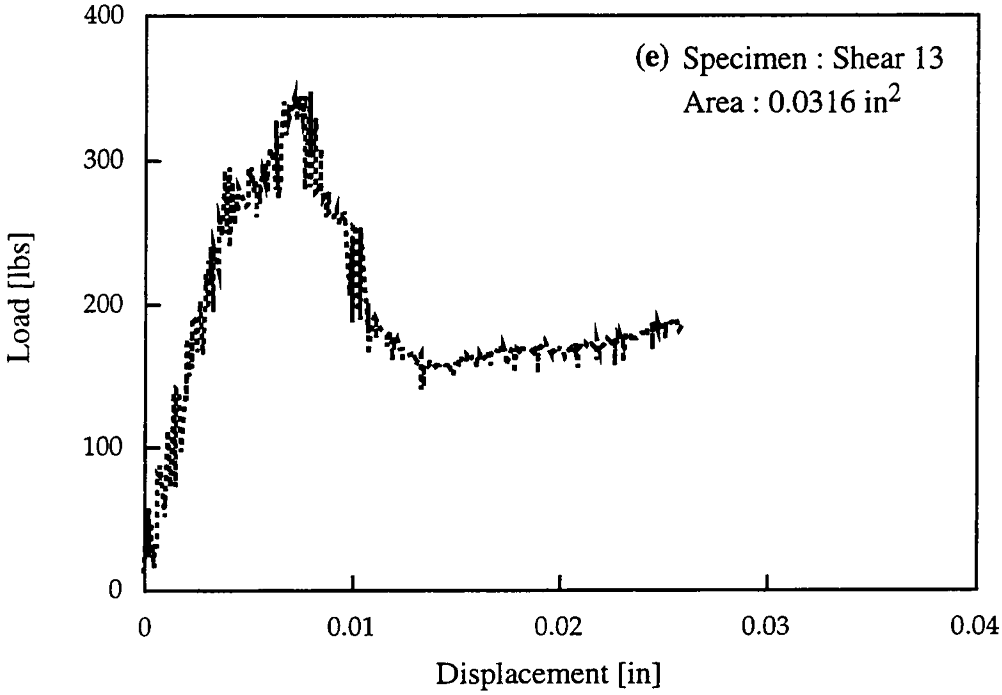

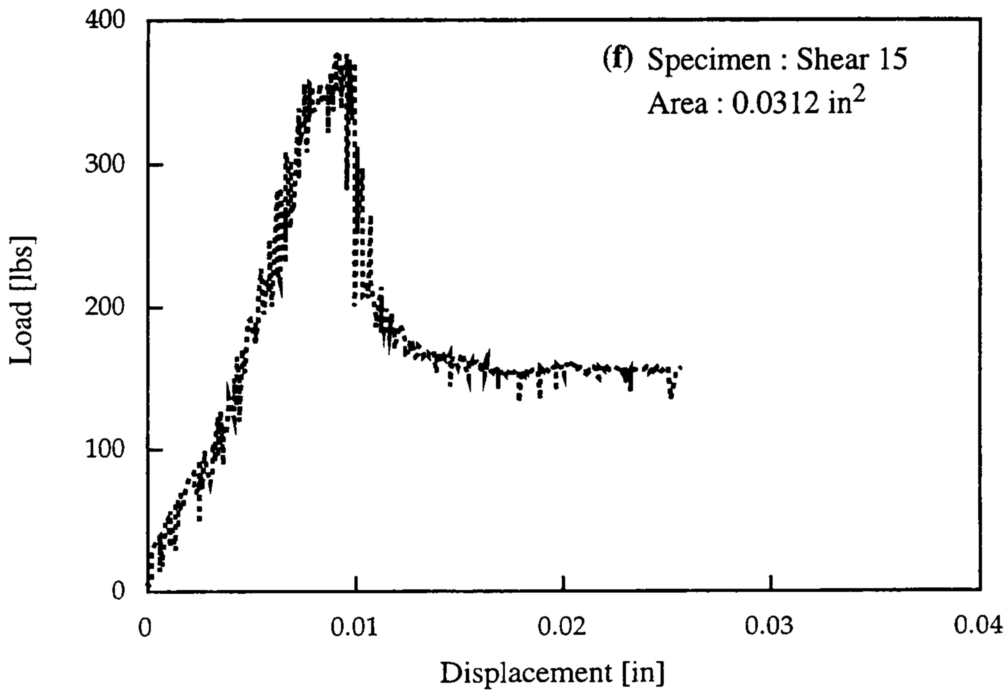

Figure C2. Continued, (e) Specimen Shear 13, (f) Specimen Shear 15

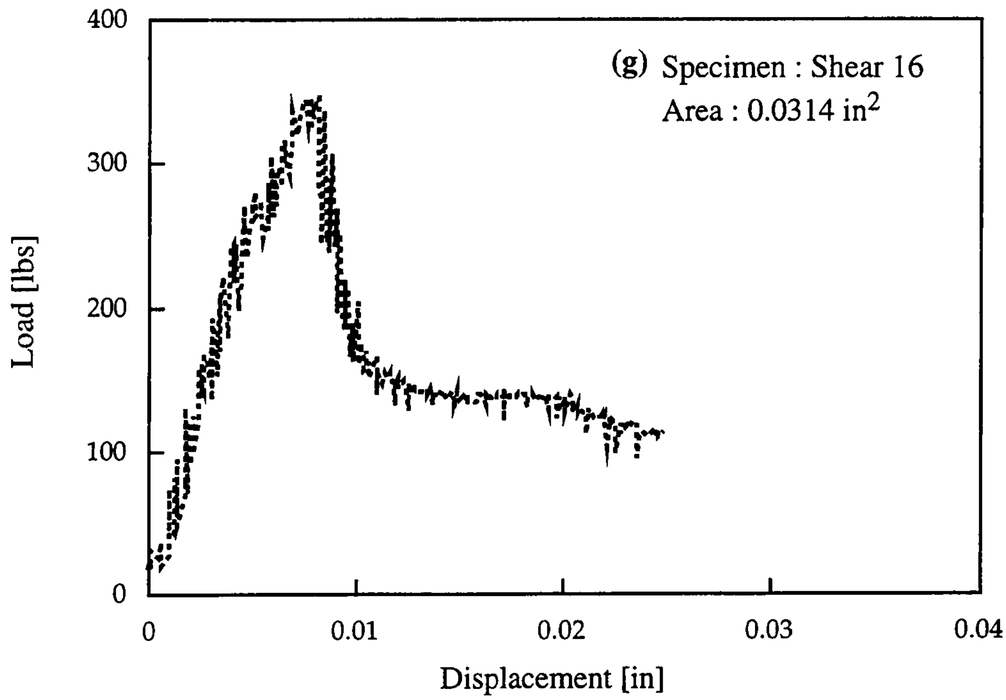

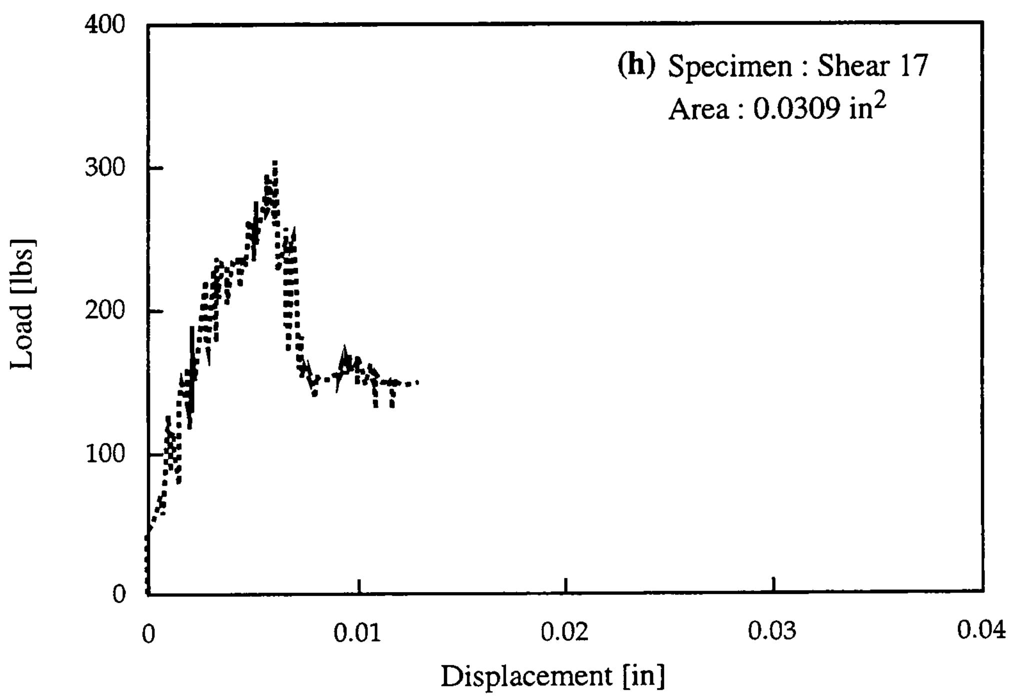

Figure C2. Continued, (g) Specimen Shear 16, (h) Specimen Shear 17

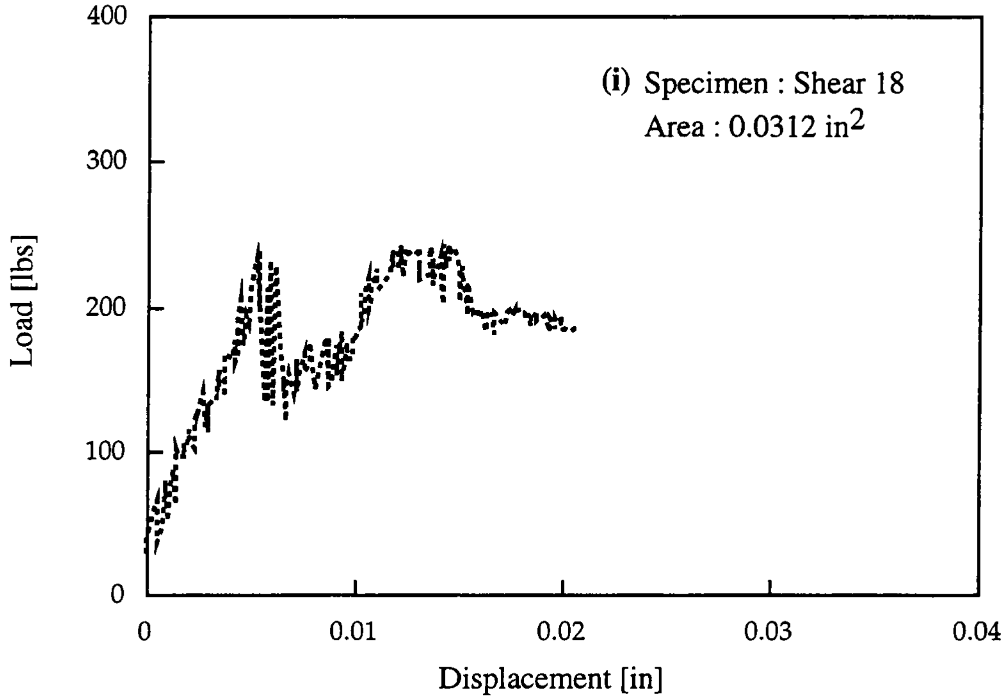

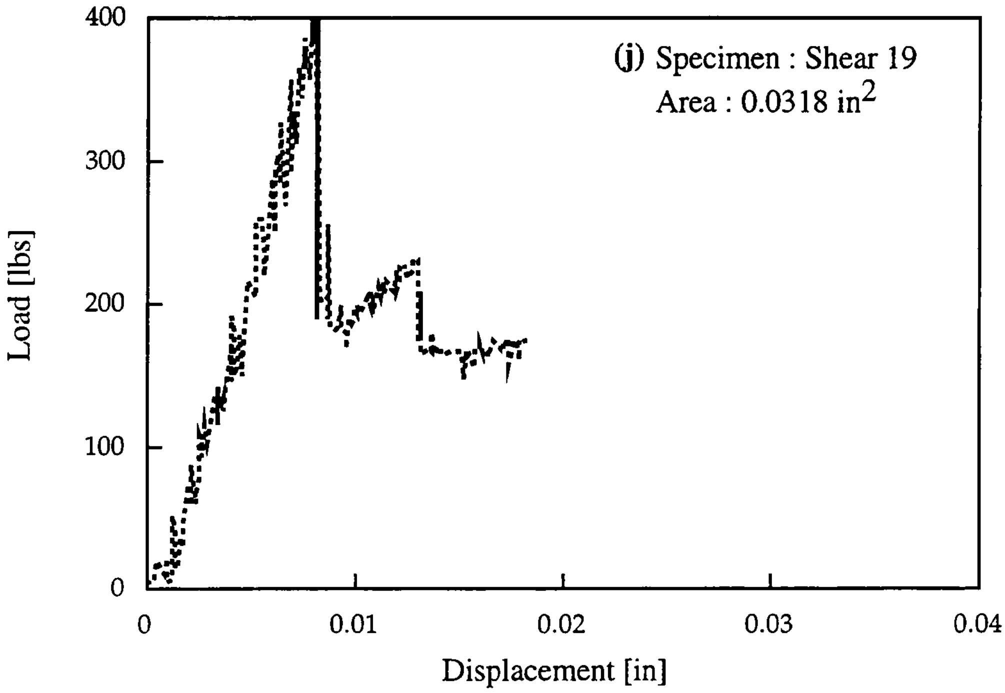

Figure C2. Continued, (i) Specimen Shear 18, (j) Specimen Shear 19

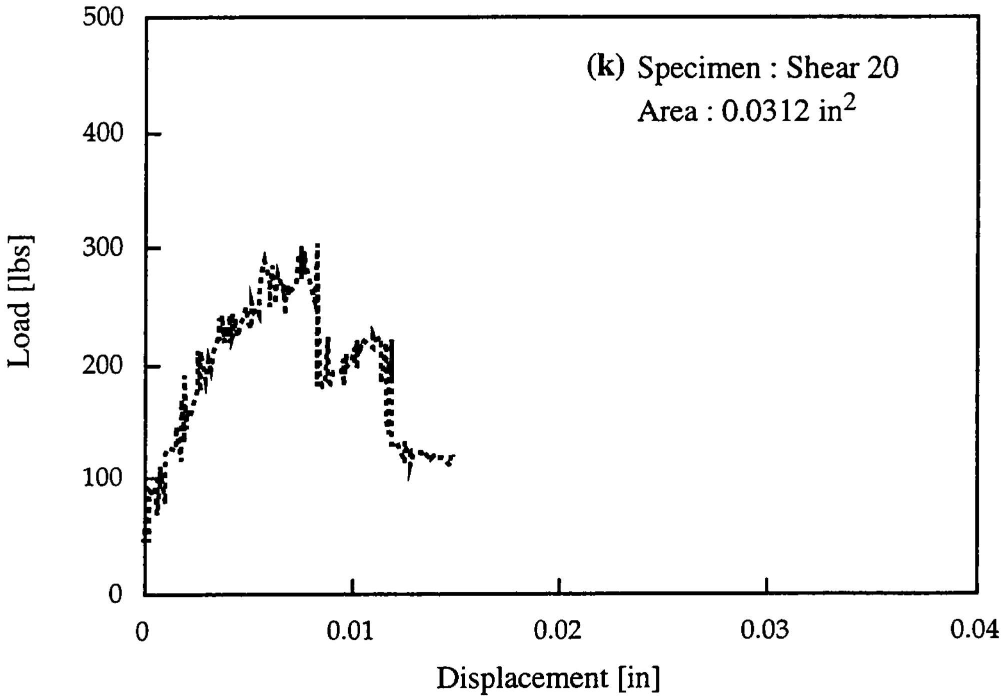

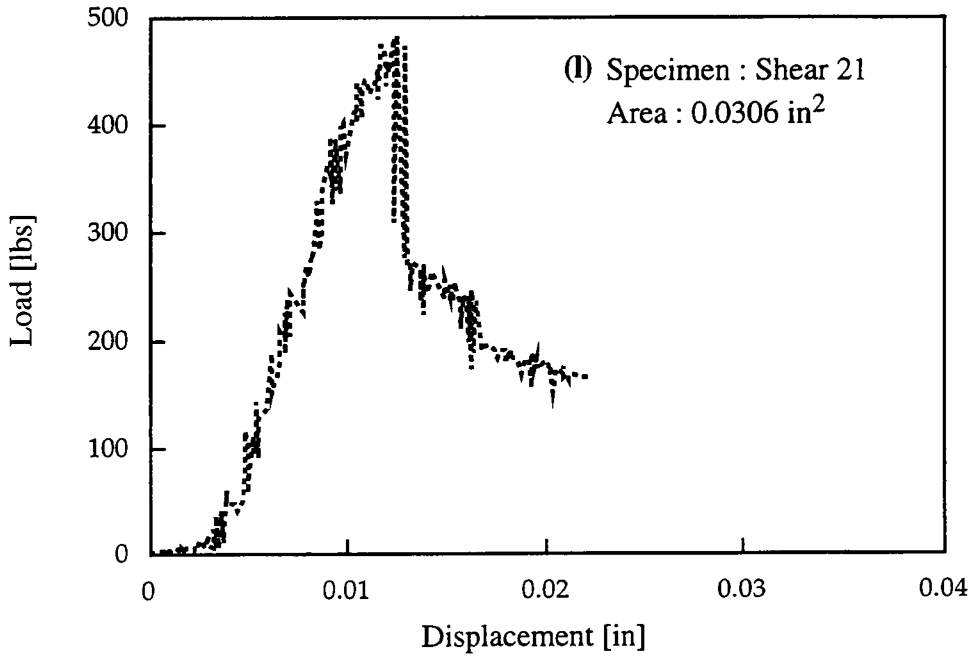

Figure C2. Continued, (k) Specimen Shear 20, (l) Specimen Shear 21

APPENDIX D

EXAMPLES OF INTERLAMINAR SHEAR FAILURE AS OBSERVED DURING THE MINI-SHEAR TESTS

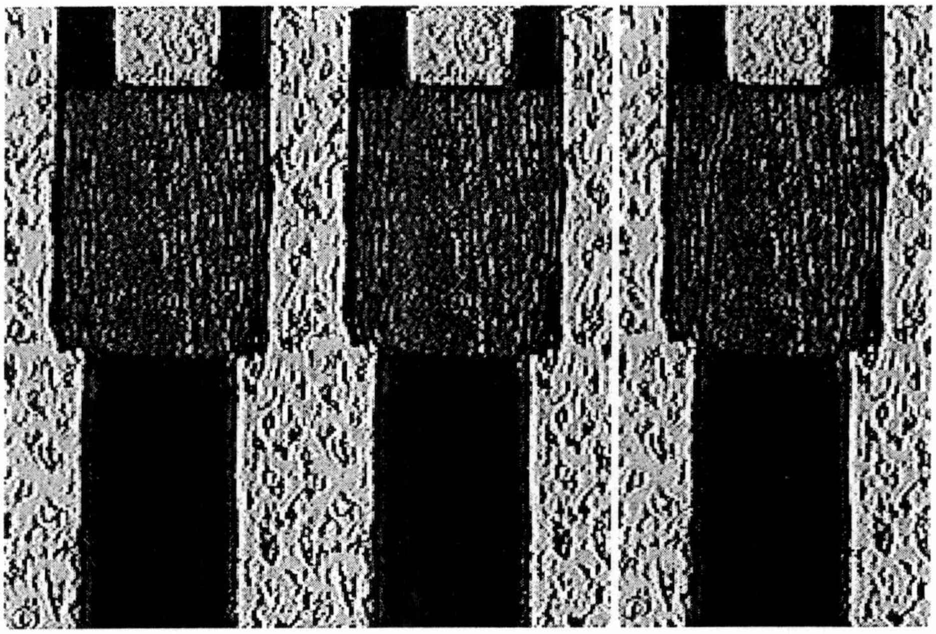

Figure D1. Shear Failure Sequence For Mini-Shear Specimen 10

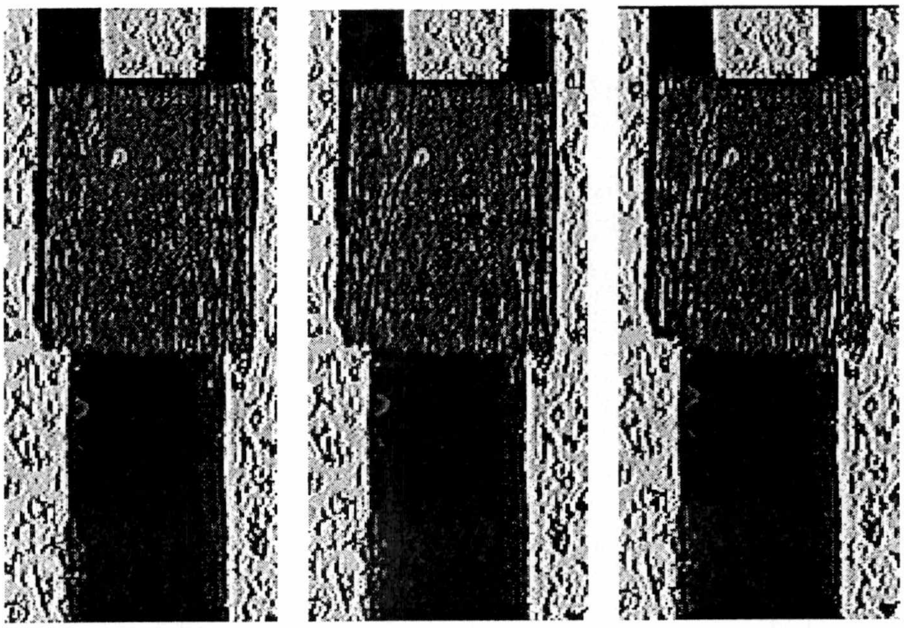

Figure D2. Shear Failure Sequence For Mini-Shear Specimen 11

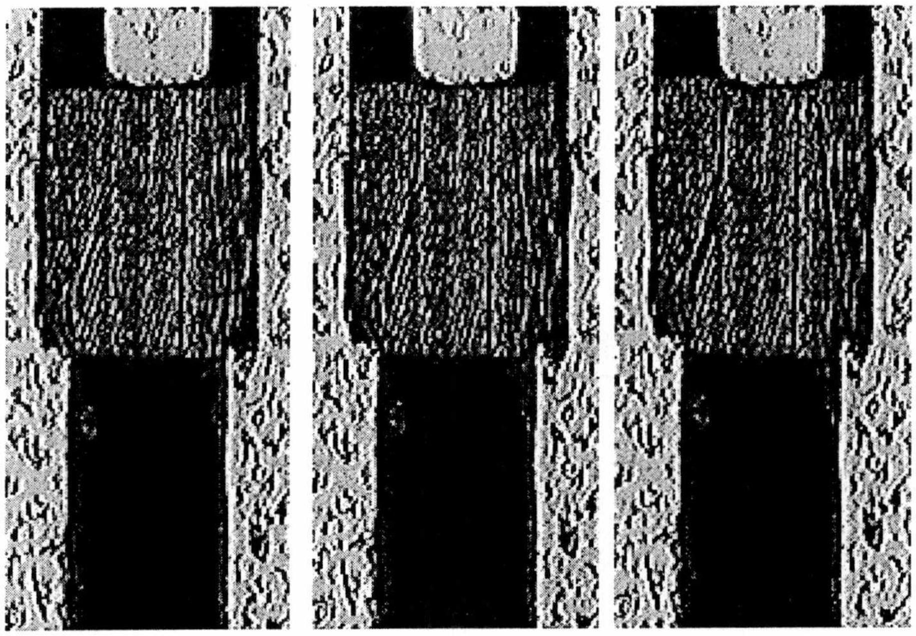

Figure D3. Shear Failure Sequence For Mini-Shear Specimen 13

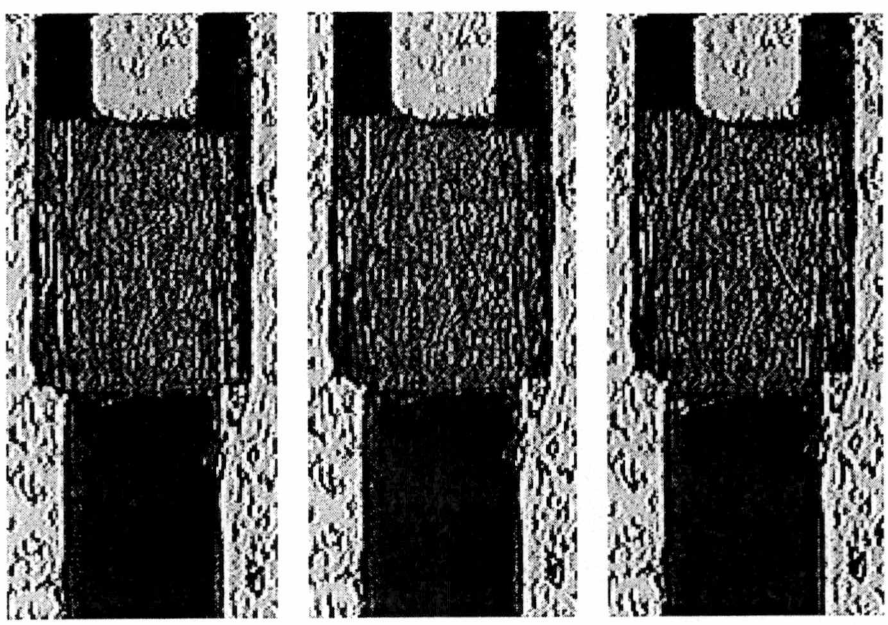

Figure D4. Shear Failure Sequence For Mini-Shear Specimen 16

APPENDIX E

COMPUTER PROGRAM SOURCE CODE

/* Basic Operation:

This program generates the stress-strain response curve along with the damage growth predictions as a function of applied stress. The output file is called "stress", and an additional file called "stress2" which contains only the data at the current crack spacing is also generated. These output files contain the following data in column type format:

Average applied stress [Mpa], sigxbar
Average global strain, epsxbar
Average transverse strain, epsybar
Crack Density [cracks/in], density
Slip zone location, [meters], l-ls
Normalized slip zone location, (l-ls)/l
Yield zone location [meters], x*
Normalized yield zone location, x*/l
Normal complementary energy [J], energy
Shear complementary energy [J], U1+U2
Total Energy [J], energy+U1+U2

The input information that must be supplied by the user and entered in the source code prior to compilation is listed below:

Beginning applied stress level [MPa], startstress
Final applied stress level [MPa], endstress
Stress increment [MPa], inc
Initial crack spacing [meters], Lo
Fracture toughness [J/m^2], Jic
Ply group thicknesses [meters], h1,h2
Moduli [GPa], Q1[i][j], Q2[i][j], C1[5][5],C2[5][5]
Reduced axial modulus ratio, E1=0.25*E0 where E0=Q2[1][1]
Interfacial shearing strength [MPa], Ts
Number of points to evaluate stress distributions at, Numpoints (usually 100-200 suffices)

This program requires no run-time input from the user. The program executes on the basis of the input parameters entered in the source code, and then generates the aforementioned output files. As the code executes, all printf statements are directed to a console window on the computer screen, (mainly for debugging purposes). This information is also "echoed" to a file called "echo" to archive the details of the computer run. Normalized plots of the stress distributions (stress vs. [x / crack spacing]) are drawn in a second pane below the console window, primarily for debugging purposes. The stress distribution data can also be displayed to the screen by removing the comment markers in the printf statements after the stress distribution loops (note: this severely affects execution time since there will be "numpoints" lines printed for each applied stress interval).

Finally, it should be realized that although this program is fully functional, run-time user input was excluded to minimize the size of the source code, and improve execution speed. This code could be employed as a basis for developing application software, however the author would like to be informed before any modifications are made to the code with the exception of input parameters.

Questions are welcome, please contact me, Don Erdman at ErdmanDL@ORNL.GOV

```
* /


#include     "ShearLagBiSlip.h"
FILE         *fpstress;
FILE         *fpstress2;
double       L0, k , density ,ls=0.0;

void main(void)                              //main program starts here
{
FILE         *fpecho;                        // output file pointers
FILE         *fpenergy;

double  state1,state2, Jvalue,l1,l2;         // energy for states 1 and 2, available energy, crack spacings
int     startstress , endstress;             // start and stop levels for the stress increment

double  sigxbar,last,l,Jic,inc;              // applied stress, last stress level, fracture toughness, stress increment

double  h1, h2, hbar;                        // specimen thickness
double  A55,alpha0, alpha1;                  // material constanst, see analysis
double  E0, E1,eps0,sigx0, sighat,energy;    // material constanst, see analysis

double  **C1,**C2 , *cc;                     //material constanst, see analysis
double  **Q1,**Q2;                           //material constanst, see analysis

console_options.left=5;                      // system console set-up for viewing data as generated
console_options.txFont=4;
console_options.nrows=15;
console_options.ncols=102;
cecho2file ("logfile",0,stdout);

fpenergy= fopen("Energy.out","w");           // open the output files
fpstress = fopen("Stress.out","w");
fpstress2 =fopen("Stress.out2","w");
                                             // the next 4 lines put headers on the output files, hence file content defined

fprintf(fpstress,"Stress [MPa] \t  Strain [] \t epsybar \t Crack Density[#/in] \t l-ls [m] \t ");
fprintf(fpstress, "(l-ls)/l  \t xstar[m] \t xstar/l \t energy \t shear energy\t total energy \n");

fprintf(fpstress2,"Stress [MPa] \t  Strain [] \t epsybar \t Crack Density[#/in] \t l-ls [m] \t ");
fprintf(fpstress2, "(l-ls)/l  \t xstar[m] \t xstar/l \t energy \t shear energy\t total energy \n");

WindowInit();                                // set up a mac graphics window for plotting stress distributions in real time


    cc=dvector(1,7);                         // allocate memory for vectors and arrays
    C1=dmatrix(1,6,1,6);
    C2=dmatrix(1,6,1,6);
    Q1=dmatrix(1,6,1,6);
    Q2=dmatrix(1,6,1,6);
    h2=0.4000/1000.0;                        // define the ply thickness
    h1=0.8000/1000.0;                        // define the ply thickness
    hbar=h1+h2;                              // define the specimen thickness
    Jic=30.0;                                // define the fracture toughness
    Jvalue=0;

    startstress=1.0;                         // define the 1st  applied stress level
    endstress=135.0;                         // define the last applied stress level
    inc=2.0;                                 // define the applied stress increment
    E0=120.0;                                // define the first modulus in o° plies
    sigx0=200.0/1000.0;                      // define the yield stress in o° plies
    eps0=sigx0/E0;                           // define the yield strain in o° plies
    E1=0.25*E0;                              // set the reduced modulus in 0° plies
    sighat = sigx0 - (E1 * eps0);            // see the def. in bilinear constitutive relation
```

```
    C2[5][5] =37.0;                                                      // define laminate moduli
    C1[5][5]  =52.0;
    Q2[1][1]=120.0;
    Q2[1][2]=30.0;
    Q2[2][2]=110.0;
    Q1[1][1]=110.0;
    Q1[1][2]=30.0;
    Q1[2][2]=120.0;

    cc[1]=Q1[1][2]  /  Q1[1][1];                                         // the Ci vector defined in bilinear analysis
    cc[2]=Q1[2][2]  -  (  (  Q1[1][2]  *  Q1[1][2]  )  /  Q1[1][1]  );
    cc[3]=Q2[1][2]  /  Q2[1][1];
    cc[4]=Q2[2][2]  -  (  (  Q2[1][2]  *  Q2[1][2]  )  /  Q2[1][1]  );
    cc[5]=Q2[1][2]/E1;
    cc[6]=Q2[2][2]  -  (  Q2[1][2]  *  Q2[1][2]  /  E1);
    cc[7]=sighat*Q2[1][2]/E1;

    A55 = 3*hbar*C1[5][5]*C2[5][5] / (h1* C2[5][5] + h2* C1[5][5] );   // material property def, see analysis
    alpha0=pow(A55/hbar*(1/(h2*E0)+1/(h1*Q1[1][1])),0.5);
    alpha1=pow(A55/hbar*(1/(h2*E1)+1/(h1*Q1[1][1])),0.5);
    printf("sighat=%+10.6f\n",sighat*1000);
    printf("alpha0=  %+10.6f\n",alpha0);
    printf("alpha1=  %+10.6f\n",alpha1);
    printf("A55=  %+10.6f\n",A55);
    printf("-----------------------------------\n");
    fprintf(fpenergy,"U*(L)   [J/m^2]  \t  2U*(L/2)  [J/m^2]  \t   J[J/m^2]  \t  Stress  [MPa]  \n");


        L0=0.00635*2;                                                    // set the initial crack spacing
        k=1;
        sigxbar=startstress;                                             // set applied stress
        while  (sigxbar<=endstress)                                      // start the main loop
        {                                                                // refer to flowchart in figure 7.1
            l1=L0/k;
            l2=L0/(k*2);
            density=(k+1)/(2.0*L0)*0.0254;                               // calculate crack density
            printf("\n  going  to  get  state1\n");
            state1=stresscalc(sigxbar,sigx0,sighat,l1,A55,alpha0,alpha1, E0 , E1, Q1, Q2,h1,h2,hbar,cc,C1,C2,1.0)*1E9;
            printf("end  of  state  1\n");
            printf("------------------------------------------\n");
            printf("going  to  get  state2\n");
            state2= stresscalc(sigxbar,sigx0,sighat,l2,A55,alpha0,alpha1, E0 , E1, Q1, Q2,h1,h2,hbar,cc,C1,C2,0.0)*1E9;
            printf("end  of  state  2\n");
            printf("------------------------------------------\n");
            Jvalue=(2*state2-state1)*1.0;
            printf("%f\t%f\t%f\t%f\n",state1,2*state2,Jvalue,sigxbar);
            fprintf(fpenergy,"%f\t%f\t%f\t%f\n",state1,2*state2,Jvalue,sigxbar);

            last=sigxbar;
            if  ((Jic-Jvalue)<=4.0)                                      // check fracture criterion
                {                                                        // change inc if approaching Jic
                sigxbar=sigxbar+0.5;
                }
            else
                {
                sigxbar=sigxbar+inc;
                }
            if(Jvalue>=Jic)
                {
                fprintf(fpenergy,"new  crack\n");
                 k=k*2;
                fprintf(fpenergy,"k=%f\n",k);
                fprintf(fpenergy,"NEW CRACK LENGTH, k=%f\n",k);
                Jvalue=0.0;
                sigxbar=last;
                }
        }
fclose(fpenergy);
```

```
fclose(fpstress);
fclose(fpstress2);
}                                                               // end of main program

//------------------------------This is the subroutine where we calculate the stresses-------------------------------

double      stresscalc(sigxbar,sigx0,sighat,l,A55,alpha0,alpha1, E0 , E1, Q1, Q2,h1,h2,hbar,cc,C1,C2,kick)
double      sigxbar, sigx0, sighat, l , A55, alpha0, alpha1, E0, E1,h1,h2,hbar,*cc,**C1,**C2;
double      **Q1, **Q2;
long        kick;
{
    long    numpoints , i ;                                     // number of points in stress distributions
    double  sigx2xstar, sigx2l,epsybar,epsxbar, xstar, energy,U1,U2;   // stress at x* and at 2L, average strains, energies
    double  *sigx1, *sigx2 ,*Tau, *x ,Taupriml;                 // stress ditribution vectors
    double  A0,A1,B1,D,Ts;                                      // stress distribution amplitudes
    double  *g,*k,*b,energylinear,lsnew,lsnew2;                 // constants for stress distributions
    double  *case2vector;x;                                     // vector for x* and lsnew in slip solution

    printf("\n\n In the stress loop, the Applied Stress = %+10.6f\n",sigxbar);

    Ts=55.0/1000.0;                                             // define interfacial shearing strength
    xstar=0.0;                                                  // yield location
    lsnew=0.0;                                                  // trial slip lengths set zero each pass through
    lsnew2=0.0;
    numpoints=100.0;                                            // define numpoints
    Tau=dvector(0,numpoints);                                   // set up the distributions vectors
    sigx1=dvector(0,numpoints);
    sigx2=dvector(0,numpoints);
    x=dvector(0,numpoints);                                     // x position vector
    k=dvector(1,8);                                             // alpha, beta and gamma vectors
    g=dvector(1,9);
    b=dvector(1,10);
    case2vector=dvector(0,1);

    sigx2l=sigxbar/1000.0*hbar/h2;                              // check if bilinear analysis
    printf("sigx2(L) = %+10.6f\n\n", sigx2l*1000);

        if ( sigx2l<=sigx0)                                     // start linear analysis
        {                                                       // see flowchart in figure 7.3
            //printf("Linear Analysis\n");
            lsnew=GetLsLinear(Ts,A55,l,sigxbar,alpha0,cc,Q1,Q2,hbar,h1,h2);
            //printf("lsnew=%e\n",lsnew);

            if (lsnew>=ls)                                      // regular linear solution
                {
                ls=lsnew;
                k[1]=A55/(hbar*alpha0*Q1[1][1]*Q2[1][1]*cosh(alpha0*(l-ls) ) );
                k[3]=hbar/h2*Q1[1][1];
                k[4]= Q1[1][2] * Q2[1][1] - Q1[1][1] * Q2[1][2] ;
                k[8]=Ts*ls*alpha0/(cosh(alpha0*(l-ls)));
                b[1]=( (l-ls)*cosh(alpha0*(l-ls)) - sinh(alpha0*(l-ls))/alpha0 )*(cc[1]-cc[3])/alpha0;
                epsybar=((cc[3]-cc[1])*Ts*(l*ls-ls*ls/2)-sigxbar/1000*(cc[3]*hbar*l+b[1]*k[1]*k[3])+b[1]*k[8])
                        /( l*(cc[2]*h1+cc[4]*h2) +k[1]*k[4]*b[1]);  // transverse strain calculation
                A0=k[1]*(k[3]*sigxbar/1000 + k[4]*epsybar)-k[8];    // shear amplitude
                }
            else .                                              // modified linear solution
                {
                k[1]=A55/(hbar*alpha0*Q1[1][1]*Q2[1][1]*cosh(alpha0*(l-ls) ) );
                k[3]=hbar/h2*Q1[1][1];
                k[4]= Q1[1][2] * Q2[1][1] - Q1[1][1] * Q2[1][2] ;
                k[8]=Ts*ls*alpha0/(cosh(alpha0*(l-ls)));
                b[1]=( (l-ls)*cosh(alpha0*(l-ls)) - sinh(alpha0*(l-ls))/alpha0 )*(cc[1]-cc[3])/alpha0;
                epsybar=((cc[3]-cc[1])*Ts*(l*ls-ls*ls/2)-sigxbar/1000*(cc[3]*hbar*l+b[1]*k[1]*k[3])+b[1]*k[8])
                        /( l*(cc[2]*h1+cc[4]*h2) +k[1]*k[4]*b[1]);  // transverse strain calculation
                A0=Ts/(sinh(alpha0*(l-ls)));                        // shear amplitude
                }
                                                                    // global strain
                epsxbar= 1/Q2[1][1]* ( sigxbar*hbar/(1000*h2)-Ts/h2*(ls-ls*ls/(2*l)) - Q2[1][2]*epsybar
```

```
        -A0/(h2*alpha0*l)*((l-ls)*cosh(alpha0*(l-ls))-sinh(alpha0*(l-ls))/alpha0));

        for (i=0; i<=numpoints; i++)                    // stress distributions as f(x)
            {
            x[i]=(double)i / numpoints * l;
            if (x[i]<= (l-ls))
                {
                Tau[i]=A0*sinh(alpha0*x[i]);
                sigx1[i]=Ts*ls/h1+A0/(alpha0*h1) * ( cosh(alpha0*(l-ls))- cosh(alpha0*x[i] ) );
                sigx2[i]=(hbar*sigxbar/1000-sigx1[i]*h1)/h2;
                }
            else
                {
                Tau[i]=Ts;
                sigx1[i]=Ts/h1*(l-x[i]);
                sigx2[i]=(hbar*sigxbar/1000-sigx1[i]*h1)/h2;
                }
            //printf (" %+10.6f\t%+10.6f\t%+10.6f\t%+10.6f\n", x[i]/l, Tau[i]*1000, sigx1[i]*1000,
            sigx2[i]*1000 );
            }

DrawPlot(numpoints,x,Tau,sigx1,sigx2,kick);                              //plot distributions on screen
energy=presimpson_linear(numpoints,x,sigx1,sigx2,h1,h2,Q1,Q2,E0,epsybar);  // calculate energies
U1=2*A0*A0*h1/ (6*C1[5][5] )*((sinh(2*alpha0*(l-ls)))/(4*alpha0)-(l-ls)/2) + 2*Ts*Ts*h1*ls/(6*C1[5][5] );
U2=2*A0*A0*h2/ (6*C2[5][5] )*((sinh(2*alpha0*(l-ls)))/(4*alpha0)-(l-ls)/2) + 2*Ts*Ts*h2*ls/(6*C2[5][5] );

}


if (sigx2l>sigx0)                                       // start bilinear cases
{                                                       // use flowchart figure 7.4

    printf("\nBilinear Analysis\n");
    xstar=(h2*sigx0-sigxbar/1000*hbar)/Ts+l;
    lsnew=GetLsCase1(l, alpha0, h1, h2, hbar, sigx2l, sigx0, Q1, Q2 , sighat, A55, cc,sigxbar,Ts);
    if (lsnew>=ls) ls=lsnew;

    if ((l-ls)< xstar)                                  // then we have bilinear case 1
        {
        //printf("\nCASE 1 ANALYSIS\n");
        lsnew=GetLsCase1(l, alpha0, h1, h2, hbar, sigx2l, sigx0, Q1, Q2 , sighat, A55, cc,sigxbar,Ts);
        if (lsnew>=ls) ls=lsnew;
        printf("lsnew from GetLsCase1=%e\n",lsnew);
        xstar=(sigx0*h2-sigxbar/1000*hbar)/Ts+l;
        //printf("xstar form case1 equation=%e\n",xstar);
        }
    else                                                // then we have bilinear case 2
        {
        //printf("\n CASE 2 ANALYSIS\n");
        case2vector=GetLsCase2( alpha0, alpha1, h1, h2, hbar, sigx0, Q1, Q2 , E0, E1,sighat,A55,cc,sigxbar,l,Ts);
        lsnew2=case2vector[0];
        xstar=case2vector[1];
        if (lsnew2>ls)
            {
            ls=lsnew2;                                  // check that the slip length grew
            //printf("found lsnew2>ls");
            }
        else
            {
            //printf("have to get alternate xstar for case 2\n");
            xstar=GetXstarCase2mod(ls,alpha0, alpha1, h1, h2, hbar, sigx0, Q1, Q2 , E0,
            E1,sighat,A55,cc,sigxbar,l,Ts);
            }
        }

    if (xstar!=0.0)
    {
        if ( (l-ls)< xstar)                             // bilinear slip, CASE 1
```

```
        {
        k[1]=A55/(alpha0*hbar*Q1[1][1]*Q2[1][1]*cosh(alpha0*(l-ls)));
        k[3]=hbar*Q1[1][1]/h2;
        k[4]=( Q2[1][1] * Q1[1][2] ) - ( Q2[1][2] * Q1[1][1] ) ;
        k[8]=Ts*ls*alpha0/cosh(alpha0*(l-ls));
        b[1]=(l-ls)*cosh(alpha0*(l-ls))-sinh(alpha0*(l-ls))/alpha0;

        xstar=(h2*sigx0-sigxbar/1000*hbar)/Ts+l;          // calaculate x* and transverse strain

epsybar=(h2*cc[7]*(l-xstar)-k[8]*b[1]/alpha0*(cc[3]-cc[1])-h2*sigx0*(xstar-l+ls)*(cc[3]-cc[1])-sigxbar/1000)*
        (k[1]*k[3]*b[1]/alpha0*(cc[1]-cc[3])+ cc[1]*hbar*(xstar-l+ls)+ cc[3]*hbar*(l-ls)+ cc[5]*hbar*(l-
        xstar))-Ts*( ls*(l-ls)*(cc[1]-cc[3])+pow((xstar-l+ls),2)/2*(cc[1]-cc[3])+(l-xstar)*(l-xstar)/2*(cc[1]-
        cc[5])))/(k[1]*k[4]*b[1]/alpha0 *(cc[1]-cc[3]) + h1*cc[2]*l +h2*cc[4]*xstar + h2*cc[6]*(l-xstar));

        A0 = k[1]*(k[3]*sigxbar/1000+k[4]*epsybar)-k[8];      // shear amplitude

        if ((ls>lsnew) && kick==0)                           // check that slip zone grew
            {
            A0=Ts/(sinh(alpha0*(l-ls)));
            epsybar=(h2*cc[7]*(l-xstar)-sigxbar/1000*hbar*(cc[5]*(l-xstar)+cc[3]*(l-ls)+cc[1]*(xstar-l+ls))
            - (cc[1]-cc[3])*(Ts*ls*(l-ls)+A0*b[1]/alpha0+Ts/2*pow((xstar-l+ls),2)-sigx0*h2*(xstar-l+ls))
            - (cc[1]-cc[5])*Ts/2*pow((l-xstar),2))/(h1*cc[2]*l+h2*cc[4]*xstar+h2*cc[6]*(l-xstar));
            printf("found that ls>lsnew\n");
            printf("case1 epsybar=%e\n",epsybar);
            }                                                // global strain

        epsxbar=1/(Q2[1][1]*l*h2)*((sigxbar*hbar/1000-Ts*ls-Q2[1][2]*epsybar*h2)*(l-ls)-
        A0/alpha0*b[1]*h2+ h2*(xstar-l+ls)*(sigx0-Q2[1][2]*epsybar) - Ts/2*pow((xstar
        l+ls),2))+1/(l*E1*h2)*((sigxbar*hbar/1000-Q2[1][2]*h2*epsybar-sighat*h2)*(l-xstar)-Ts*pow((l-
        xstar),2)/2 );

        for (i=0; i<=numpoints; i++)                        // stress distributions as f(x)
            {
            x[i]=(double)i / numpoints* l;

            if ( x[i] < (l-ls) )
                {
                Tau[i]=A0*sinh( alpha0 * x[i] );
                sigx2[i]=sigx2l-Ts*ls/h2-A0/(h2*alpha0) * ( cosh(alpha0*(l-ls)) - cosh(alpha0*x[i] ) );
                sigx1[i]=(sigxbar/1000*hbar-sigx2[i]*h2)/h1;
                }
            if ( (x[i] >= (l-ls)) && (x[i] < xstar) )
                {
                Tau[i]=Ts;
                sigx2[i]=sigx0-Ts*(xstar-x[i])/h2;
                sigx1[i]=(sigxbar/1000*hbar-sigx2[i]*h2)/h1;
                }
            if (x[i]>=xstar)
                {
                Tau[i]=Ts;
                sigx2[i]=sigx2l-Ts*(l-x[i])/h2;
                sigx1[i]=(sigxbar/1000*hbar-sigx2[i]*h2)/h1;
                }
    //printf (" %+10.6f\t%+10.6f\t%+10.6f\t%+10.6f\n",x[i]/l,Tau[i]*1000,sigx1[i]*1000,sigx2[i]*1000 );

            }                                                // energy calculations

    energy=presimpson(numpoints,xstar,x,sigx1,sigx2,h1,h2,Q1,Q2,sighat,sigx0,E0,E1,epsybar);
    U1=2*A0*A0*h1/(6*C1[5][5] )*((sinh(2*alpha0*(l-ls)))/(4*alpha0)-(l-ls)/2) + 2*Ts*Ts*h1*ls/(6*C1[5][5] );
    U2=2*A0*A0*h2/(6*C2[5][5] )*((sinh(2*alpha0*(l-ls)))/(4*alpha0)-(l-ls)/2) + 2*Ts*Ts*h2*ls/(6*C2[5][5] );

        }                                                    //end CASE 1

    if( (l-ls)>=xstar)                                       // start CASE 2 slip solution
        {
        printf("entered the case 2 stress calculation\n");

        k[1]=A55/(alpha0*hbar*Q1[1][1]*Q2[1][1]*cosh(alpha0*xstar));
```

```
        k[2]=sigx0*(  Q1[1][1]+h2/h1*Q2[1][1]  );
        k[3]=hbar/h1*Q2[1][1];
        k[4]=( Q2[1][1] * Q1[1][2] ) - ( Q2[1][2] * Q1[1][1] ) ;
        k[5]=A55/(h2*E1);
        k[6]=A55/hbar*(Q1[1][2] / Q1[1][1] - Q2[1][2] /E1);
        k[7]=sighat/E1*A55/hbar+Ts*ls*alpha1*alpha1;

    if ( (ls>lsnew2) && kick==0)                                // check slip length greww
        {
        //printf("went to alternate equations for g[i]\n");
        //pause();                                              // gamma vector
        D=sinh(alpha1*(l-ls-xstar) );
        g[1]=1/D*(   k[1]*k[3]*sinh(alpha0*xstar)*cosh(alpha1*(l-ls))  );
        g[2]=1/D*(  -k[1]*k[4]*sinh(alpha0*xstar)*cosh(alpha1*(l-ls))  );
        g[3]=1/D*(  Ts*cosh(alpha1*xstar)-k[1]*k[2]*sinh(alpha0*xstar)*cosh(alpha1*(l-ls))  );
        g[4]=1/D*(  -k[1]*k[3]*sinh(alpha0*xstar)*sinh(alpha1*(l-ls))  );
        g[5]=1/D*(   k[1]*k[4]*sinh(alpha0*xstar)*sinh(alpha1*(l-ls))  );
        g[6]=1/D*(  -Ts*sinh(alpha1*xstar)+k[1]*k[2]*sinh(alpha0*xstar)*sinh(alpha1*(l-ls))  );
        }
        else
        {                                                       // gamma vector
        D=alpha1*cosh( alpha1*(l-ls-xstar) );
        g[1]=1/D*(  k[5]*cosh(alpha1*xstar)+k[1]*k[3]*alpha1*sinh(alpha1*(l-ls))*sinh(alpha0*xstar)  );
        g[2]=1/D*(  k[6]*cosh(alpha1*xstar)-k[1]*k[4]*alpha1*sinh(alpha1*(l-ls))*sinh(alpha0*xstar)  );
        g[3]=1/D*(-k[7]*cosh(alpha1*xstar)-k[1]*k[2]*alpha1*sinh(alpha1*(l-ls))*sinh(alpha0*xstar)  );
        g[4]=1/D*(-k[5]*sinh(alpha1*xstar)-k[1]*k[3]*alpha1*sinh(alpha0*xstar)*cosh(alpha1*(l-ls))  );
        g[5]=1/D*(-k[6]*sinh(alpha1*xstar)+k[1]*k[4]*alpha1*sinh(alpha0*xstar)*cosh(alpha1*(l-ls))  );
        g[6]=1/D*(  k[7]*sinh(alpha1*xstar)+k[1]*k[2]*alpha1*sinh(alpha0*xstar)*cosh(alpha1*(l-ls))  );
        }
        b[1]=xstar*cosh(alpha0*xstar)-sinh(alpha0*xstar)/alpha0;     // beta vector
        b[2]=(l-ls-xstar)*cosh(alpha1*(l-ls))-sinh(alpha1*(l-ls))/alpha1+sinh(alpha1*xstar)/alpha1;
        b[3]=(l-ls-xstar)*sinh(alpha1*(l-ls))-cosh(alpha1*(l-ls))/alpha1+cosh(alpha1*xstar)/alpha1;
        b[4]=hbar*xstar/h1 - k[1]*k[3]*b[1] / (h1*alpha0);
        b[5]=k[1]*k[4]*b[1] / (h1*alpha0);
        b[6]=k[1]*k[2]*b[1] / (h1*alpha0) - sigx0*h2*xstar/h1;
        b[7]=( g[1]*b[2]+g[4]*b[3] ) / (h1* alpha1);
        b[8]=( g[2]*b[2]+g[5]*b[3] ) / (h1* alpha1);
        b[9]=( g[3]*b[2]+g[6]*b[3] ) / (h1* alpha1) + Ts*ls*(l-ls-xstar)/h1;
        b[10]=Ts*ls*ls/(2*h1);
                                                                // transverse strain
        epsybar  =(cc[7]*h2*(l-xstar)-h1*(cc[1]-cc[5])*(b[9]+b[10])-h1*b[6]*(cc[1]-cc[3])-
           sigxbar/1000.0)*
           ( h1*b[4] *(cc[1]-cc[3])+h1*b[7]*(cc[1] -cc[5]) + hbar*cc[3]*xstar+hbar*cc[5]*(l-xstar)))/
           ( h1*(b[5]*(cc[1]-cc[3])+b[8]*(cc[1]-cc[5]) +cc[2]*l ) + h2*(cc[4]*xstar + cc[6] * (l-xstar)));

        A0=k[1]*(k[2]-k[3]*sigxbar/1000+k[4]*epsybar);          // stress distribution amplitudes
        A1=sigxbar/1000*g[1]+epsybar*g[2]+g[3];
        B1=sigxbar/1000*g[4]+epsybar*g[5]+g[6];


        epsxbar=1/(Q2[1][1]*l)*(sigxbar/1000*hbar*xstar/h2-            // gloabl strain
        h1/h2*(sigxbar/1000*b[4]+epsybar*b[5]+b[6])-Q2[1][2]*epsybar*xstar)
        +1/(E1*l)*(sigxbar/1000*hbar*(l-xstar)/h2-h1/h2*(sigxbar/1000*b[7]+epsybar*b[8]+b[9]+b[10])
        -(Q2[1][2]*epsybar+sighat)*(l-xstar)  );

        for (i=0; i<=numpoints; i++)                            // stress distributions as f(x)
           {
           x[i]=(double)i / numpoints* l;
           if ( x[i] < xstar )
              {
                 Tau[i]=A0*sinh( alpha0 * x[i] );
                 sigx2[i]=sigx0-A0/(h2*alpha0) * ( cosh(alpha0*(l-ls)) - cosh(alpha0*x[i] ) );
                 sigx1[i]=(sigxbar/1000*hbar-sigx2[i]*h2)/h1;
              }
           if ( (x[i] >= xstar) && (x[i]< (l-ls)) )
              {
                 Tau[i]=A1*sinh(alpha1*x[i] )+B1*cosh(alpha1*x[i] );
                 sigx2[i]=sigxbar/1000*hbar/h2-Ts*ls/h2-1/(h2*alpha1)*
```

```
                    (
                    A1*(cosh(alpha1*(l-ls))-cosh(alpha1*x[i] )) +
                    B1*(sinh(alpha1*(l-ls))-sinh(alpha1*x[i] ))
                    );
                sigx1[i]=(sigxbar/1000*hbar-sigx2[i]*h2)/h1;
            }
        if ( x[i]>=(l-ls) )
            {
                Tau[i]=Ts;
                sigx2[i]=sigx2l-Ts*(l-x[i])/h2;
                sigx1[i]=(sigxbar/1000*hbar-sigx2[i]*h2)/h1;
            }
        //printf ("%+10.6f\t%+10.6f\t%+10.6f\t%+10.6f\t  %d\n", x[i]/l, Tau[i]*1000,
            sigx1[i]*1000,sigx2[i]*1000,region);
        }
                                                        // energy calculations
        energy=presimpson(numpoints,xstar,x,sigx1,sigx2,h1,h2,Q1,Q2,sighat,sigx0,E0,E1,epsybar);

        U1=2*h1/(6*C1[5][5])*(
        A0*A0*(sinh(2*alpha0*xstar)/(4*alpha0) - xstar/2) +
        (A1*A1+B1*B1)*( sinh(2*alpha1*(l-ls))/(4*alpha1)-sinh(2*alpha1*xstar)/(4*alpha1) )
        + (B1*B1-A1*A1)*(l-ls-xstar)/2
        + A1*B1/(2*alpha1) * (cosh(2*alpha1*(l-ls))-cosh(2*alpha1*xstar))+Ts*Ts*ls);

        U2=2*h2/(6*C2[5][5])*(
        A0*A0*(sinh(2*alpha0*xstar)/(4*alpha0) - xstar/2) +
        (A1*A1+B1*B1)*( sinh(2*alpha1*(l-ls))/(4*alpha1)-sinh(2*alpha1*xstar)/(4*alpha1) )
        + (B1*B1-A1*A1)*(l-ls-xstar)/2
        + A1*B1/(2*alpha1) * (cosh(2*alpha1*(l-ls)) -cosh(2*alpha1*xstar))+Ts*Ts*ls);


    }                                                   // end of CASE 2

    DrawPlot(numpoints,x,Tau,sigx1,sigx2,kick);         // plot stress distributions to screen

}                                                       // end of CASES 1 and 2 ie end of xstar != 0.0

if (xstar==0.0)                                         // CASE 3 where the stress is > sigx0 for all x.
  {
  printf ("\nLinear Analysis with reduced modulus\n");
  lsnew=GetLsLinear2(Ts,A55,l,sigxbar,sighat,alpha1,cc,Q1,Q2,E1,hbar,h1,h2);
  if (lsnew>=ls)
    {                                                   // check if slip length grew
    ls=lsnew;
    k[1]=A55/(hbar*alpha1*Q1[1][1]*E1*cosh(alpha1*(l-ls)));
    k[2]=hbar*Q1[1][1]/h2;
    k[3]=Q1[1][2]*E1 - Q2[1][2]*Q1[1][1];
    k[4]=sighat*Q1[1][1];
    k[8]=Ts*ls*alpha1;
    b[1]=1/alpha1*( (l-ls)*cosh(alpha1*(l-ls))-sinh(alpha1*(l-ls))/alpha1);
    epsybar = ( h2*cc[7]*l - cc[5]*hbar*l *sigxbar/1000 + (cc[5]-cc[1]) *
    ( k[1]*k[2]*b[1]*sigxbar/1000 -k[1]*b[1]*k[4]-b[1]*k[8] +Ts*ls*(l-ls)+Ts*ls*ls/2) )
    / ( l*( h1*cc[2] +h2*cc[6] )+(cc[1]-cc[5])* k[1]*k[3]*b[1] );
    A0=k[1]*( k[2]*sigxbar/1000 +k[3]*epsybar-k[4] ) - k[8];
    }
  else
    {
    k[1]=A55/(hbar*alpha1*Q1[1][1]*E1*cosh(alpha1*(l-ls)));
    k[2]=hbar*Q1[1][1]/h2;
    k[3]=Q1[1][2]*E1 - Q2[1][2]*Q1[1][1];
    k[4]=sighat*Q1[1][1];
    k[8]=Ts*ls*alpha1/cosh(alpha1*(l-ls));
    b[1]=1/alpha1*( (l-ls)*cosh(alpha1*(l-ls))-sinh(alpha1*(l-ls))/alpha1);
    epsybar = ( h2*cc[7]*l - cc[5]*hbar*l *sigxbar/1000 + (cc[5]-cc[1]) *
    ( k[1]*k[2]*b[1]*sigxbar/1000 -k[1]*b[1]*k[4]-b[1]*k[8] +Ts*ls*(l-ls)+Ts*ls*ls/2) )
    / ( l*( h1*cc[2] +h2*cc[6] )+(cc[1]-cc[5])* k[1]*k[3]*b[1] );
    A0=Ts/(sinh(alpha1*(l-ls)));
    }
```

```
                                                                    // global strain

        epsxbar=1/(E1*l)*(sigxbar/1000*hbar*l/h2-A0/(h2*alpha1)*(  (l-ls)*cosh(alpha1*(l-ls))-
              sinh(alpha1*(l-ls))/alpha1)  +Ts*ls/(2*h2)*(ls-2*l)  -  epsybar*Q2[1][2]*l-sighat*l);

        for (i=0; i<=numpoints; i++)                                // stress distributions as f(x)
            {
            x[i]=(double)i / numpoints * l;
            if (x[i]<=  (l-ls))
                {
                Tau[i]=A0*sinh(alpha0*x[i]);
                sigx1[i]=Ts*ls/h1+A0/(alpha1*h1) * ( cosh(alpha1*(l-ls))- cosh(alpha1*x[i] ) );
                sigx2[i]=(hbar*sigxbar/1000-sigx1[i]*h1)/h2;
                }
            else
                {
                Tau[i]=Ts;
                sigx1[i]=Ts/h1*(l-x[i]);
                sigx2[i]=(hbar*sigxbar/1000-sigx1[i]*h1)/h2;
                }
        //printf  ("%+10.6f\t%+10.6f\t%+10.6f\t%+10.6f\n",  x[i]/l,Tau[i]*1000,  sigx1[i]*1000,sigx2[i]*1000  );
            }

        DrawPlot(numpoints,x,Tau,sigx1,sigx2,kick);                // plot distributions to screen
                                                                   // calculate energies

        U1=2*A0*A0*h1/  (6*C1[5][5]  )*((sinh(2*alpha1*(l-ls)))/(4*alpha1)-(l-ls)/2)  +
            2*Ts*Ts*h1*ls/(6*C1[5][5]  );
        U2=2*A0*A0*h2/  (6*C2[5][5]  )*((sinh(2*alpha1*(l-ls)))/(4*alpha1)-(l-ls)/2)  +
            2*Ts*Ts*h2*ls/(6*C2[5][5]  );
        energy=presimpson_linear1(numpoints,x,sigx1,sigx2,h1,h2,Q1,Q2,E0,E1,sighat,sigx0,epsybar);
        }
    }
  //THE FOLLOWING LINES WRITE THE DATA TO THE OUTPUT FILE FOR STRESS-STARIN CURVE CONSTRUCTION

  printf("\n sigxbar=%f \t epsxbar=%e \t epsybar=%e \t  density=%f  \nl-ls=%e \t xstar=%e \n\n",
        sigxbar,epsxbar,epsybar, density,l-ls,xstar);
  fprintf(fpstress,"%f \t %e \t %e \t %f \t %e \t %e \t %e \t %f \t %f \t %f \t %f \n",sigxbar,epsxbar*100,epsybar,
        density*0.75,l,(l-ls)/l,xstar,xstar/l,energy*1e9,(U1+U2)*1e9,(U1+U2+energy)*1e9);

  if  (kick==0)  fprintf(fpstress,"\n");
  if  (kick==1)  fprintf(fpstress2,"%f \t %e \t %e \t %e \t %f \t %e \t %e \t %f \t %f \t %f \t %f
              \n",sigxbar,epsxbar*100,epsybar,
              density*0.75,l,(l-ls)/l,xstar,xstar/l,energy*1e9,(U1+U2)*1e9,(U1+U2+energy)*1e9);

free_dvector(Tau,0,numpoints);              //Free up the memory, eliminate the vectors and matrices
free_dvector(sigx1,0,numpoints);
free_dvector(sigx2,0,numpoints);
free_dvector(x,0,numpoints);
free_dvector(k,1,8);
free_dvector(g,1,9);
free_dvector(b,1,10);
free_dvector(case2vector,1,2);
energy=(U1+U2)+energy;                                  //calculate the total available energy
printf("total energy from stresses=%f\n",energy*1e9);
if ((l/2-ls)<0.0) energy =0.0;
printf("returned energy=%f\n",energy*1e9);
return(2*energy/(2*h1));                                //return the energy to the mian program
}

//-----------------------------Root solver to get xstar , bi-linear slip solution , CASE2 mod---------------------------
//-----this is when ls is is known and we still need to iterate on x star,  ie it's then a single root solver---------------

double  GetXstarCase2mod(lstrial,alpha0, alpha1, h1, h2, hbar, sigx0, Q1, Q2 , E0, E1,sighat,A55,cc,sigxbar,l,Ts)
double  lstrial,alpha0, alpha1, h1, h2, hbar, sigx0, **Q1, **Q2, E0, E1, sighat, A55,*cc,sigxbar,l,Ts;
{
  double     u=sigx0,v,w,a,b,c,e,x,eps,xstar;
  long       M=100;
```

```
    int         k,i=0;
    a=0;
    b=l;
    eps= 0.0000001;

printf ("Started the GetXstarCase2mod routine\n");

while( (i<=100)  && (u>=sigx0) )            //just a little loop to get a first guess at the root
{
xstar=(l)*(1-(double)i/100);
u=BilinearStressSlipCase2mod(xstar,lstrial,alpha0, alpha1, h1, h2, hbar, sigx0, Q1, Q2 , E0, E1,sighat,A55,cc,sigxbar,l,Ts);
//printf("x/l=%f  sigx2=%f\n",xstar/l  ,u*1000);
i++;
}

u=BilinearStressSlipCase2mod(xstar,lstrial,alpha0,alpha1,h1,h2,hbar,sigx0, Q1,Q2,E0,E1,sighat,A55,cc,sigxbar,l,Ts)-sigx0;
v=BilinearStressSlipCase2mod(b,lstrial, alpha0, alpha1, h1, h2, hbar, sigx0, Q1, Q2 , E0, E1,sighat,A55,cc,sigxbar,l,Ts)-sigx0;

printf("\nbisection routine GetXstarCase2mod\n");
//printf("u=%f\n",u);
//printf("v=%f\n",v);
//pause();
e=b-a;

if ( (u*v) > 0.0 )
{
    printf("no  root\n");
    return (0);          // no root!!!
}
for(k=1; k<= M ; k++)
    {
    e=e/2.0;                              // get an xstar value  ls=c
    c=a+e;
    w=BilinearStressSlipCase2mod(c,lstrial, alpha0, alpha1, h1, h2, hbar, sigx0, Q1, Q2 , E0, E1,sighat,A55,cc,sigxbar,l,Ts)-
sigx0;
    //printf ("k=%d \t c=%f \t w=%e \t e=%e\n",k,c,w[1],e);
    if ( fabs(w)<eps || e< 0.0000001)
        {
        w=c;
        return(w);                        // convirged on a root
        }
    if ( w*u< 0.0 )
        {
        b=c;
        v=w;
        }
    else
        {
        a=c;
        u=w;
        }
    }

}

//------------------Just evaluates the value of sigx2 to the right of xstar for case2mod----------------
//------------------This is for the case II solution returns normal stress to find xstar-------------------

double BilinearStressSlipCase2mod(xstar,lstrial, alpha0, alpha1, h1, h2, hbar, sigx0, Q1, Q2 , E0,
E1,sighat,A55,cc,sigxbar,l,Ts)
double lstrial,xstar, alpha0, alpha1, h1, h2, hbar,sigx0, **Q1, **Q2, E0 , E1, sighat,A55,*cc,sigxbar,l,Ts;
{
double A0,A1,B1,D, epsybar;
double *k,*g,*b,sigx2xstar;
long        i;
            k=dvector(1,4);
            g=dvector(1,6);
            b=dvector(1,10);
```

```
		k[1]=A55/(alpha0*hbar*Q1[1][1]*Q2[1][1]*cosh(alpha0*xstar));
		k[2]=sigx0*(  Q1[1][1]+h2/h1*Q2[1][1]  );
		k[3]=hbar/h1*Q2[1][1];
		k[4]=( Q2[1][1] * Q1[1][2] ) - ( Q2[1][2] * Q1[1][1] ) ;

		D=sinh(alpha1*(l-lstrial-xstar) );
		g[1]=1/D*(    k[1]*k[3]*sinh(alpha0*xstar)*cosh(alpha1*(l-lstrial))  );
		g[2]=1/D*(  -k[1]*k[4]*sinh(alpha0*xstar)*cosh(alpha1*(l-lstrial))  );
		g[3]=1/D*(  Ts*cosh(alpha1*xstar)-k[1]*k[2]*sinh(alpha0*xstar)*cosh(alpha1*(l-lstrial))  );
		g[4]=1/D*(  -k[1]*k[3]*sinh(alpha0*xstar)*sinh(alpha1*(l-lstrial))  );
		g[5]=1/D*(    k[1]*k[4]*sinh(alpha0*xstar)*sinh(alpha1*(l-lstrial))  );
		g[6]=1/D*(  -Ts*sinh(alpha1*xstar)+k[1]*k[2]*sinh(alpha0*xstar)*sinh(alpha1*(l-lstrial))  );

		b[1]=xstar*cosh(alpha0*xstar)-sinh(alpha0*xstar)/alpha0;
		b[2]=(l-lstrial-xstar)*cosh(alpha1*(l-lstrial))-sinh(alpha1*(l-lstrial))/alpha1+sinh(alpha1*xstar)/alpha1;
		b[3]=(l-lstrial-xstar)*sinh(alpha1*(l-lstrial))-cosh(alpha1*(l-lstrial))/alpha1+cosh(alpha1*xstar)/alpha1;
		b[4]=hbar*xstar/h1  -  k[1]*k[3]*b[1]  /  (h1*alpha0);
		b[5]=k[1]*k[4]*b[1]  /  (h1*alpha0);
		b[6]=k[1]*k[2]*b[1]  /  (h1*alpha0)  -  sigx0*h2*xstar/h1;
		b[7]=(  g[1]*b[2]+g[4]*b[3]  )  /  (h1*  alpha1);
		b[8]=(  g[2]*b[2]+g[5]*b[3]  )  /  (h1*  alpha1);
		b[9]=(  g[3]*b[2]+g[6]*b[3]  )  /  (h1*  alpha1)  +  Ts*lstrial*(l-lstrial-xstar)/h1;
		b[10]=Ts*lstrial*lstrial/(2*h1);

		epsybar  =(cc[7]*h2*(l-xstar)-  h1*(cc[1]-cc[5])*(b[9]+b[10])  -  h1*b[6]*(cc[1]-cc[3])  -
			(sigxbar/1000.0)*
			(  h1*b[4]  *(cc[1]-cc[3])+h1*b[7]*(cc[1]  -cc[5])  +  hbar*cc[3]*xstar+hbar*cc[5]*(l-xstar)))/
			(  h1*(b[5]*(cc[1]-cc[3])+  b[8]*(cc[1]-cc[5])  +cc[2]*l  )  +  h2*(cc[4]*xstar  +  cc[6]  *  (l-xstar)));

		A0=k[1]*(k[2]-k[3]*sigxbar/1000+k[4]*epsybar);
		A1=sigxbar/1000*g[1]+epsybar*g[2]+g[3];
		B1=sigxbar/1000*g[4]+epsybar*g[5]+g[6];

		sigx2xstar=sigxbar/1000*hbar/h2-Ts*lstrial/h2-1/(h2*alpha1)*
				(
				A1*(cosh(alpha1*(l-lstrial))-cosh(alpha1*xstar))  +
				B1*(sinh(alpha1*(l-lstrial))-sinh(alpha1*xstar))
				);
free_dvector(k,1,4);
free_dvector(g,1,6);
free_dvector(b,1,10);
return (sigx2xstar);
}


//subroutines shearlagbislipsubs.c

#define	FREE_ARG char*
#define	NR_END			1
#define	kBaseResID		128
#define	kMoveToFront		(WindowPtr) -1L
#define	kRandomUpperLimit	32768

#include	"ShearLagBiSlip.h"

extern	double ls;

//---------------------------------Root solver to get ls for the bi-linear slip solution CASE 3-----------------------------------
//---------------------for the case where the stresses are greater than sigx0 over the whole domain---------

double  GetLsLinear2(Ts,A55,l,sigxbar,sighat,alpha1,cc,Q1,Q2,E1,hbar,h1,h2)
double  Ts,A55,l, sigxbar,sighat,alpha1,*cc, **Q1,**Q2, hbar, h1, h2,E1;
{
	double	u=Ts,v,w,a,b,c,e,x,eps;
	long	M=100;
	int	k,i=0;
	a=0;
```

```
    b=l;
    eps= 0.0000001;

//printf("Pre-scan for a root in the GetLsLinear2 routine\n");
while( (i<=25)) //&& ( (u-Ts)>=0.0) )
    {
    x=(double)i*l/25;
    u=EvalTauLinSlip2(x,Ts,A55,l,sigxbar,sighat,alpha1,cc,Q1,Q2,E1,hbar,h1,h2);
    //printf("x/l=%f  \t  u=%f\n",x/l,u);
    i++;
    }
b=x;

u=EvalTauLinSlip2(a,Ts,A55,l,sigxbar,sighat,alpha1,cc,Q1,Q2,E1,hbar,h1,h2)-Ts;
v=EvalTauLinSlip2(b,Ts,A55,l,sigxbar,sighat,alpha1,cc,Q1,Q2,E1,hbar,h1,h2)-Ts;
e=b-a;

if ( (u*v) >= 0.0 )
{
    //printf("no root in GetLsLinear2 \n");
    return (0);            // no root!!!
}
for(k=1; k<= M ; k++)
    {
    e=e/2.0;
    c=a+e;
    w=EvalTauLinSlip2(c,Ts,A55,l,sigxbar,sighat,alpha1,cc,Q1,Q2,E1,hbar,h1,h2)-Ts;
    //printf ("k=%d \t c=%f \t w=%e \t e=%e\n",k,c,w,e);
    if ( fabs(w)<eps || e< 0.0000001)
        {
        w=c;
        return(w);        // convirged on a root
        }
    if ( w*u < 0.0 )
        {
        b=c;
        v=w;
        }
    else
        {
        a=c;
        u=w;
        }
    }
}


//----------------------------Evaluates the expression for T*(x) for the linear slip solution-----------------------------------
//----------------------------for the case where the stresses are greater than sigx0 over the whole domain--------------------
double  EvalTauLinSlip2(lstrial,Ts,A55,l,sigxbar,sighat,alpha1,cc,Q1,Q2,E1,hbar,h1,h2)
double  lstrial,Ts,A55,sigxbar,sighat,l,hbar,h1,h2,**Q1,**Q2,E1,*cc,alpha1;
{
        double  A0,*b,epsybar,Tau,*k;


            k=dvector(1,8);
            b=dvector(1,8);

            k[1]=A55/(hbar*alpha1*Q1[1][1]*E1*cosh(alpha1*(l-lstrial)));
            k[2]=hbar*Q1[1][1]/h2;
            k[3]=Q1[1][2]*E1  -  Q2[1][2]*Q1[1][1];
            k[4]=sighat*Q1[1][1];
            k[8]=Ts*lstrial*alpha1/cosh(alpha1*(l-lstrial));

            b[1]=1/alpha1*(  (l-lstrial)*cosh(alpha1*(l-lstrial))-sinh(alpha1*(l-lstrial))/alpha1);

            epsybar =  ( h2*cc[7]*l - cc[5]*hbar*l *sigxbar/1000 + (cc[5]-cc[1]) *
```

```
                ( k[1]*k[2]*b[1]*sigxbar/1000  -k[1]*b[1]*k[4]-b[1]*k[8]  +Ts*lstrial*(l-lstrial)+Ts*lstrial*lstrial/2) )
                / ( l*( h1*cc[2] +h2*cc[6] )+(cc[1]-cc[5])* k[1]*k[3]*b[1] );
        A0=k[1]*( k[2]*sigxbar/1000 +k[3]*epsybar - k[4] )-k[8];
        Tau=A0 * sinh(alpha1*(l-lstrial));
free_dvector(k,1,8);
free_dvector(b,1,8);
return(Tau);
}


//---------------------------------Root solver to get ls, bi-linear slip solution , CASE1----------------------------------
double  GetLsCase1(l, alpha0, h1, h2, hbar, sigx2l, sigx0, Q1, Q2 , sighat, A55, cc,sigxbar,Ts)
double  l, alpha0, h1, h2, hbar,sigx2l,sigx0, **Q1, **Q2, sighat, A55,*cc,sigxbar,Ts;
{
    double      u=Ts,v,w,a,b,c,e,x,eps;
    long        M=100;
    int     k,i=0;
    a=0;
    b=l;
    eps= 0.0000001;

    while( (i<=25) && ( (u-Ts)>=0.0) )
    {
        x=(double)i/25*l;
        u=BilinearStressSlipCase1(x, alpha0, h1, h2, hbar, sigx0, Q1, Q2,sighat,A55,cc,sigxbar,l,Ts);
        //printf("x/l=%f  \t  u=%f\n",x/l,u);
        i++;
    }
b=x;
u=BilinearStressSlipCase1(a, alpha0, h1, h2, hbar, sigx0, Q1, Q2,sighat,A55,cc,sigxbar,l,Ts)-Ts;
v=BilinearStressSlipCase1(b, alpha0, h1, h2, hbar, sigx0, Q1, Q2,sighat,A55,cc,sigxbar,l,Ts)-Ts;
e=b-a;

//printf("\n  u=%f\n",u);
//printf("  v=%f\n",v);

if ( (u*v) > 0.0 )
{
    //printf("\n no root in GetLsCase1\n");
    return (0);         // no root!!!
}
for(k=1; k<= M ; k++)
    {
    e=e/2.0;
    c=a+e;
    w=BilinearStressSlipCase1(c, alpha0, h1, h2, hbar, sigx0, Q1, Q2,sighat,A55,cc,sigxbar,l,Ts)-Ts;
    //printf ("k=%d \t c=%f \t w=%e \t e=%e\n",k,c,w,e);
    if ( fabs(w)<eps || e< 0.0000001)
        {
        w=c;
        return(w);      // convirged on a root
        }
    if ( w*u < 0.0 )
        {
        b=c;
        v=w;
        }
    else
        {
        a=c;
        u=w;
        }
    }
}

//-------------------------------Just evaluates the value of Tau to the left of slip zone---------------------------------
//---------------------------------------this is for the CASE I solution-----------------------------------------------
```

```
double  BilinearStressSlipCase1(lstrial, alpha0, h1, h2, hbar, sigx0, Q1, Q2,sighat,A55,cc,sigxbar,l,Ts)
double  lstrial,alpha0, h1, h2, hbar,sigx0, **Q1, **Q2, sighat,A55,*cc,sigxbar,l,Ts;
{
double  A0, epsybar;
double  *k,*b,Taus , xstar;
long        i;
            k=dvector(1,8);
            b=dvector(1,10);

                xstar=(sigx0*h2-sigxbar/1000*hbar)/Ts + l;
                k[1]=A55/(alpha0*hbar*Q1[1][1]*Q2[1][1]*cosh(alpha0*(l-lstrial)));
                k[3]=hbar*Q1[1][1]/h2;
                k[4]=( Q2[1][1] * Q1[1][2] ) - ( Q2[1][2] * Q1[1][1] ) ;
                k[8]=Ts*lstrial*alpha0/cosh(alpha0*(l-lstrial));

                b[1]=(l-lstrial)*cosh(alpha0*(l-lstrial))-sinh(alpha0*(l-lstrial))/alpha0;

                epsybar=(h2*cc[7]*(l-xstar)-k[8]*b[1]/alpha0*(cc[3]-cc[1])-h2*sigx0*(xstar-l+lstrial)*(cc[3]-cc[1])  -
                        (sigxbar/1000.0)*(k[1]*k[3]*b[1]/alpha0*(cc[1]-cc[3])  +  cc[1]*hbar*(xstar-l+lstrial)  +
                        cc[3]*hbar*(l-lstrial)  +  cc[5]*hbar*(l-xstar))
                         -Ts*(  lstrial*(l-lstrial)*(cc[1]-cc[3])+pow((xstar-l+lstrial),2)/2*(cc[1]  -cc[3])  +pow((l-
                        xstar),2)/2*(cc[1]-cc[5])))/(k[1]*k[4]*b[1]/alpha0*(cc[1]-cc[3])  +  h1*cc[2]*l  +h2*cc[4]*xstar
                        *h2*cc[6]*(l-xstar));

                //printf("epsybar=%e\n",epsybar);

                A0=k[1]*(k[3]*sigxbar/1000+k[4]*epsybar)-k[8];
                //printf("A0=%e\n",A0);
                Taus=A0*sinh(alpha0*(l-lstrial));

free_dvector(k,1,8);
free_dvector(b,1,10);
return (Taus);
}


//---------------------------------Root solver to get ls , bi-linear slip solution , CASE2---------------------

double*     GetLsCase2(alpha0, alpha1, h1, h2, hbar, sigx0, Q1, Q2 , E0, E1,sighat,A55,cc,sigxbar,l,Ts)
double              alpha0, alpha1, h1, h2, hbar,sigx0, **Q1, **Q2, E0,E1,sighat, A55,*cc,sigxbar,l,Ts;
{
    double      u=Ts,v,w,a,b,c,e,x,eps,xstar,lsnew2;
    long        M=100;
    int     k,i=0;
    double  case2vector[1];
    a=0;                        // used to be set to zero
    b=l;
    eps= 0.0000001;

while( (i<=25) &&  (u-Ts)>=0.0 )
    {
        x=(double)i/25*l ;
        xstar=GetXstarCase2(x,alpha0, alpha1, h1, h2, hbar, sigx0, Q1, Q2 , E0, E1,sighat,A55,cc,sigxbar,l,Ts);
        u=BilinearTausSlipCase2(x, alpha0, alpha1, h1, h2, hbar, sigx0, Q1, Q2 , E0, E1,sighat,A55,cc,sigxbar,l,Ts,xstar);
            if ((i==0) && (u<Ts))
                {
                lsnew2=0.0;
                xstar=0.0;
                printf("stuck in the prescan for GetLsCase2\n");
                //pause();
                case2vector[0]=lsnew2;
                case2vector[1]=xstar;
                return(case2vector);
                }
        //printf("\n This is from prescan in GetLsCase2, x/l=%f \t u=%f\n\n",x/l,u);
        i++;
    }
```

```
b=x;
                                    // get an xstar value for ls=a;

//printf("going to get an xstar value for lstrial=ls in GetLsCase2\n");
xstar=GetXstarCase2(a,alpha0, alpha1, h1, h2, hbar, sigx0, Q1, Q2 , E0, E1,sighat,A55,cc,sigxbar,l,Ts);
//printf("returned  xstar=%f\n",xstar);

//printf("going to get an lsnew2 value for lstrial=ls in GetLsCase2\n");
u=BilinearTausSlipCase2(a, alpha0, alpha1, h1, h2, hbar, sigx0, Q1, Q2 , E0, E1,sighat,A55,cc,sigxbar,l,Ts,xstar)-Ts;

                                    // get an xstar value for ls=b;

//printf("going to get an xstar value for lstrial=l in GetLsCase2\n");
xstar=GetXstarCase2(b,alpha0, alpha1, h1, h2, hbar, sigx0, Q1, Q2 , E0, E1,sighat,A55,cc,sigxbar,l,Ts);
//printf("returned  xstar=%f\n",xstar);

//printf("going to get an lsnew2 value for lstrial=l in GetLsCase2\n");
v=BilinearTausSlipCase2(b, alpha0, alpha1, h1, h2, hbar, sigx0, Q1, Q2 , E0, E1,sighat,A55,cc,sigxbar,l,Ts,xstar)-Ts;

//printf("\nStart the actual GetLsCase2 root solver\n");
//printf("u=%f\n",u);
//printf("v=%f\n",v);
//pause();
e=b-a;

if ( (u*v) > 0.0 )
{
   //printf("no  root\n");
   case2vector[0]=0.0;          // no root!!!
   case2vector[1]=0.0;
}
for(k=1; k<= M ; k++)
   {
   e=e/2.0;
   c=a+e;

   xstar=GetXstarCase2(c,alpha0, alpha1, h1, h2, hbar, sigx0, Q1, Q2 , E0, E1,sighat,A55,cc,sigxbar,l,Ts);
   w=BilinearTausSlipCase2(c, alpha0, alpha1, h1, h2, hbar, sigx0, Q1, Q2 , E0, E1,sighat,A55,cc,sigxbar,l,Ts,xstar)-Ts;

   //printf ("k=%d \t c=%f \t w=%e \t e=%e\n",k,c,w[1],e);
   if ( fabs(w)<eps || e< 0.0000001)
      {
      w=c;
      lsnew2=c;
      case2vector[0]=lsnew2;
      case2vector[1]=xstar;
      printf("ready to return from getLsCase2\n");
      printf("lsnew2=%e\n",lsnew2);
      printf("xstar=%e\n",xstar);
      printf("case2vector[0]=%e\n",case2vector[0]);
      printf("case2vector[1]=%e\n",case2vector[1]);
      //pause();
      return(case2vector);        // convirged on a root
      }
   if ( w*u< 0.0 )
      {
      b=c;
      v=w;
      }
   else
      {
      a=c;
      u=w;
      }
   }

}
```

```
//------------------Just evaluates the value of sigx2 to the right of xstar-------------------------------
//------------------This is for the case ll solution returns Taus stress to find ls--------------------

double  BilinearTausSlipCase2(lstrial, alpha0, alpha1, h1, h2, hbar, sigx0, Q1, Q2 , E0, E1,sighat,A55,cc,sigxbar,l,Ts,xstar)
double  lstrial, alpha0, alpha1, h1, h2, hbar,sigx0, **Q1, **Q2, E0 , E1, sighat,A55,*cc,sigxbar,l,Ts,xstar;
{
double  A1,B1,D, epsybar;
double  *k,*g,*b,Taus;
long        i;
            k=dvector(1,8);
            g=dvector(1,6);
            b=dvector(1,10);

                k[1]=A55/(alpha0*hbar*Q1[1][1]*Q2[1][1]*cosh(alpha0*xstar));
                k[2]=sigx0*(  Q1[1][1]+h2/h1*Q2[1][1]  );
                k[3]=hbar/h1*Q2[1][1];
                k[4]=( Q2[1][1] * Q1[1][2] ) - ( Q2[1][2] * Q1[1][1] ) ;
                k[5]=A55/(h2*E1);
                k[6]=A55/hbar*(Q1[1][2]  /  Q1[1][1]  -  Q2[1][2]  /E1);
                k[7]=sighat/E1*A55/hbar+Ts*lstrial*alpha1;

                //for  (i=1;i<=8;i++)  printf("k[%d]=%e\n",i,k[i]);

                D=alpha1*cosh( alpha1*(l-lstrial-xstar) );

                //printf("D=%e\n",D);

                g[1]=1/D*(  k[5]*cosh(alpha1*xstar)+k[1]*k[3]*alpha1*sinh(alpha1*(l-lstrial))*sinh(alpha0*xstar)  );
                g[2]=1/D*(  k[6]*cosh(alpha1*xstar)-k[1]*k[4]*alpha1*sinh(alpha1*(l-lstrial))*sinh(alpha0*xstar)  );
                g[3]=1/D*(-k[7]*cosh(alpha1*xstar)-k[1]*k[2]*alpha1*sinh(alpha1*(l-lstrial))*sinh(alpha0*xstar)  );
                g[4]=1/D*(-k[5]*sinh(alpha1*xstar)-k[1]*k[3]*alpha1*sinh(alpha0*xstar)*cosh(alpha1*(l-lstrial))  );
                g[5]=1/D*(-k[6]*sinh(alpha1*xstar)+k[1]*k[4]*alpha1*sinh(alpha0*xstar)*cosh(alpha1*(l-lstrial))  );
                g[6]=1/D*(  k[7]*sinh(alpha1*xstar)+k[1]*k[2]*alpha1*sinh(alpha0*xstar)*cosh(alpha1*(l-lstrial))  );

                //for  (i=1;i<=6;i++)  printf  ("g[%d]=%e\n",i,g[i]);

                b[1]=xstar*cosh(alpha0*xstar)-sinh(alpha0*xstar)/alpha0;
                b[2]=(l-lstrial-xstar)*cosh(alpha1*(l-lstrial))-sinh(alpha1*(l-lstrial))/alpha1+sinh(alpha1*xstar)/alpha1;
                b[3]=(l-lstrial-xstar)*sinh(alpha1*(l-lstrial))-cosh(alpha1*(l-lstrial))/alpha1+cosh(alpha1*xstar)/alpha1;
                b[4]=hbar*xstar/h1  -  k[1]*k[3]*b[1]  /  (h1*alpha0);
                b[5]=k[1]*k[4]*b[1]  /  (h1*alpha0);
                b[6]=k[1]*k[2]*b[1]  /  (h1*alpha0)  -  sigx0*h2*xstar/h1;
                b[7]=(  g[1]*b[2]+g[4]*b[3]  )  /  (h1*  alpha1);
                b[8]=(  g[2]*b[2]+g[5]*b[3]  )  /  (h1*  alpha1);
                b[9]=(  g[3]*b[2]+g[6]*b[3]  )  /  (h1*  alpha1)  +  Ts*lstrial*(l-lstrial-xstar)/h1;
                b[10]=Ts*lstrial*lstrial/(2*h1);

                //for  (i=1;i<=9;i++)  printf  ("b[%d]=%e\n",i,b[i]);

                epsybar =      (cc[7]*h2*(l-xstar)     -  h1*(cc[1]-cc[5])*(b[9]+b[10])  -  h1*b[6]*(cc[1]-cc[3])
                            -(sigxbar/1000.0)*(  h1*b[4]  *(cc[1]-cc[3])+h1*b[7]*(cc[1]  -cc[5])  +
                            hbar*cc[3]*xstar+hbar*cc[5]*(l-xstar)))/
                (h1*(b[5]*(cc[1]-cc[3])+  b[8]*(cc[1]-cc[5])  +cc[2]*l  )  +  h2*(cc[4]*xstar  +  cc[6]  *  (l-xstar)));

                //printf("epsybar=%e\n",epsybar);

                A1=sigxbar/1000*g[1]+epsybar*g[2]+g[3];
                B1=sigxbar/1000*g[4]+epsybar*g[5]+g[6];

                //printf("A1=%e\n",A1);
                //printf("B1=%e\n",B1);

                Taus=A1*sinh(alpha1*(l-lstrial))+B1*cosh(alpha1*(l-lstrial));

free_dvector(k,1,8);
free_dvector(g,1,6);
free_dvector(b,1,10);
return (Taus);
```

```
}

//----------------------------Root solver to get xstar , bi-linear slip solution , CASE2---------------------------

double GetXstarCase2(lstrial,alpha0, alpha1, h1, h2, hbar, sigx0, Q1, Q2 , E0, E1,sighat,A55,cc,sigxbar,l,Ts)
double lstrial,alpha0, alpha1, h1, h2, hbar, sigx0, **Q1, **Q2, E0, E1, sighat, A55,*cc,sigxbar,l,Ts;
{
    double      u=sigx0,v,w,a,b,c,e,x,eps,xstar;
    long        M=100;
    int      k,i=0;
    a=0;
    b=l;
    eps= 0.0000001;

while( (i<=25)  && (u>=sigx0) )             //just a little loop to get a first guess at the root
{
xstar=(l)*(1-(double)i/25);
u=BilinearStressSlipCase2(xstar,lstrial,alpha0, alpha1, h1, h2, hbar, sigx0, Q1, Q2 , E0, E1,sighat,A55,cc,sigxbar,l,Ts);
i++;
}
//printf ("that was the pre-scan for GetXstarCase2\n");

u=BilinearStressSlipCase2(xstar,lstrial,alpha0, alpha1, h1, h2, hbar, sigx0, Q1, Q2 , E0, E1,sighat,A55,cc,sigxbar,l,Ts)-sigx0;

v=BilinearStressSlipCase2(b,lstrial, alpha0, alpha1, h1, h2, hbar, sigx0, Q1, Q2 , E0, E1,sighat,A55,cc,sigxbar,l,Ts)-sigx0;
e=b-a;

//printf("\nbisection routine  GetXstarCase2\n");
//printf("u=%f\n",u);
//printf("v=%f\n",v);

if ( (u*v) > 0.0 )
{
    //printf("no  root  in  GetXstarCase2\n");
    return (0);                   // no root!!!
}
for(k=1; k<= M ; k++)
    {
    e=e/2.0;
    c=a+e;                                  // get an xstar value  ls=c
    w=BilinearStressSlipCase2(c,lstrial, alpha0, alpha1, h1, h2, hbar, sigx0, Q1, Q2 , E0, E1,sighat,A55,cc,sigxbar,l,Ts)-sigx0;
    //printf ("k=%d \t c=%f \t w=%e \t e=%e\n",k,c,w[1],e);
    if ( fabs(w)<eps || e< 0.0000001)
        {
        w=c;
        return(w);        // convirged on a root
        }
    if ( w*u< 0.0 )
        {
        b=c;
        v=w;
        }
    else
        {
        a=c;
        u=w;
        }
    }

}

//-------------------Just evaluates the value of sigx2 to the right of xstar-------------------------------
//-------------------This is for the case II solution returns normal stress to find xstar--------------------

double BilinearStressSlipCase2(xstar,lstrial, alpha0, alpha1, h1, h2, hbar, sigx0, Q1, Q2 , E0, E1,sighat,A55,cc,sigxbar,l,Ts)
double lstrial,xstar, alpha0, alpha1, h1, h2, hbar,sigx0, **Q1, **Q2, E0 , E1, sighat,A55,*cc,sigxbar,l,Ts;
{
```

```
double  A0,A1,B1,D, epsybar;
double  *k,*g,*b,sigx2xstar;
long        i;
            k=dvector(1,8);
            g=dvector(1,6);
            b=dvector(1,10);

                k[1]=A55/(alpha0*hbar*Q1[1][1]*Q2[1][1]*cosh(alpha0*xstar));
                k[2]=sigx0*( Q1[1][1]+h2/h1*Q2[1][1] );
                k[3]=hbar/h1*Q2[1][1];
                k[4]=( Q2[1][1] * Q1[1][2] ) - ( Q2[1][2] * Q1[1][1] ) ;
                k[5]=A55/(h2*E1);
                k[6]=A55/hbar*(Q1[1][2] / Q1[1][1] - Q2[1][2] /E1);
                k[7]=sighat/E1*A55/hbar+Ts*lstrial*alpha1*alpha1;

                D=alpha1*cosh( alpha1*(l-lstrial-xstar) );

                g[1]=1/D*( k[5]*cosh(alpha1*xstar)+k[1]*k[3]*alpha1*sinh(alpha1*(l-lstrial))*sinh(alpha0*xstar) );
                g[2]=1/D*( k[6]*cosh(alpha1*xstar)-k[1]*k[4]*alpha1*sinh(alpha1*(l-lstrial))*sinh(alpha0*xstar) );
                g[3]=1/D*(-k[7]*cosh(alpha1*xstar)-k[1]*k[2]*alpha1*sinh(alpha1*(l-lstrial))*sinh(alpha0*xstar) );
                g[4]=1/D*(-k[5]*sinh(alpha1*xstar)-k[1]*k[3]*alpha1*sinh(alpha0*xstar)*cosh(alpha1*(l-lstrial)) );
                g[5]=1/D*(-k[6]*sinh(alpha1*xstar)+k[1]*k[4]*alpha1*sinh(alpha0*xstar)*cosh(alpha1*(l-lstrial)) );
                g[6]=1/D*( k[7]*sinh(alpha1*xstar)+k[1]*k[2]*alpha1*sinh(alpha0*xstar)*cosh(alpha1*(l-lstrial)) );

                b[1]=xstar*cosh(alpha0*xstar)-sinh(alpha0*xstar)/alpha0;
                b[2]=(l-lstrial-xstar)*cosh(alpha1*(l-lstrial))-sinh(alpha1*(l-lstrial))/alpha1+sinh(alpha1*xstar)/alpha1;
                b[3]=(l-lstrial-xstar)*sinh(alpha1*(l-lstrial))-cosh(alpha1*(l-lstrial))/alpha1+cosh(alpha1*xstar)/alpha1;
                b[4]=hbar*xstar/h1 - k[1]*k[3]*b[1] / (h1*alpha0);
                b[5]=k[1]*k[4]*b[1] / (h1*alpha0);
                b[6]=k[1]*k[2]*b[1] / (h1*alpha0) - sigx0*h2*xstar/h1;
                b[7]=( g[1]*b[2]+g[4]*b[3] ) / (h1* alpha1);
                b[8]=( g[2]*b[2]+g[5]*b[3] ) / (h1* alpha1);
                b[9]=( g[3]*b[2]+g[6]*b[3] ) / (h1* alpha1) + Ts*lstrial*(l-lstrial-xstar)/h1;
                b[10]=Ts*lstrial*lstrial/(2*h1);

                epsybar =(cc[7]*h2*(l-xstar)- h1*(cc[1]-cc[5])*(b[9]+b[10]) - h1*b[6]*(cc[1]-cc[3]) -
                        (sigxbar/1000.0)*
                        ( h1*b[4] *(cc[1]-cc[3])+h1*b[7]*(cc[1] -cc[5]) + hbar*cc[3]*xstar+hbar*cc[5]*(l-xstar)))/
                        ( h1*(b[5]*(cc[1]-cc[3])+ b[8]*(cc[1]-cc[5]) +cc[2]*l ) + h2*(cc[4]*xstar + cc[6] * (l-xstar)));

                A0=k[1]*(k[2]-k[3]*sigxbar/1000+k[4]*epsybar);
                A1=sigxbar/1000*g[1]+epsybar*g[2]+g[3];
                B1=sigxbar/1000*g[4]+epsybar*g[5]+g[6];

                sigx2xstar=sigxbar/1000*hbar/h2-Ts*lstrial/h2-1/(h2*alpha1)*
                                (
                                A1*(cosh(alpha1*(l-lstrial))-cosh(alpha1*xstar)) +
                                B1*(sinh(alpha1*(l-lstrial))-sinh(alpha1*xstar))
                                );
free_dvector(k,1,8);
free_dvector(g,1,6);
free_dvector(b,1,10);
return (sigx2xstar);
}


//----------------------------Evaluates the expression for T*(x) for the linear slip solution----------------------------------

double  EvalTauLinSlip(lstrial,Ts,A55,l,sigxbar,alpha0,cc,Q1,Q2,hbar,h1,h2)
double  lstrial,Ts,A55,sigxbar,l,hbar,h1,h2,**Q1,**Q2,*cc,alpha0;
{
        double  A0,b1,k1,k3,k4,k8,epsybar,Tau;

            k1=A55/(hbar*alpha0*Q1[1][1]*Q2[1][1]*cosh(alpha0*(l-lstrial) ) );
            k3=hbar/h2*Q1[1][1];
            k4= Q1[1][2] * Q2[1][1] - Q1[1][1] * Q2[1][2] ;
            k8=Ts*lstrial*alpha0/(cosh(alpha0*(l-lstrial)));
            b1=( (l-lstrial)*cosh(alpha0*(l-lstrial)) - sinh(alpha0*(l-lstrial))/alpha0 )*(cc[1]-cc[3])/alpha0;
```

```
		epsybar=(  (cc[3]-cc[1])*Ts*(l*lstrial-lstrial*lstrial/2)-sigxbar/1000*(cc[3]*hbar*l+b1*k1*k3)+b1*k8  )
				/ ( l*(cc[2]*h1+cc[4]*h2) +k1*k4*b1) ;
		A0=k1*( k3*sigxbar/1000 + k4*epsybar)-k8;
		Tau=A0 * sinh(alpha0*(l-lstrial));
return(Tau);
}


//--------------------------------Root solver to get ls for the linear slip solution---------------------------------

double GetLsLinear(Ts,A55,l,sigxbar,alpha0,cc,Q1,Q2,hbar,h1,h2)
double Ts,A55,l, sigxbar,alpha0,*cc, **Q1,**Q2, hbar, h1, h2;
{
	double	u=Ts,v,w,a,b,c,e,x,eps;
	long	M=100;
	int	k,i=0;
	a=0;
	b=l;
	eps= 0.0000001;

//printf("Pre-scan for a root in the GetLsLinear routine\n");
while( (i<=25) && ( (u-Ts)>=0.0) )
	{
	x=(double)i*l/25;
	u=EvalTauLinSlip(x,Ts,A55,l,sigxbar,alpha0,cc,Q1,Q2,hbar,h1,h2);
	//printf("x/l=%f  \t  u=%f\n",x/l,u);
	i++;
	}
b=x;

u=EvalTauLinSlip(a,Ts,A55,l,sigxbar,alpha0,cc,Q1,Q2,hbar,h1,h2)-Ts;
v=EvalTauLinSlip(b,Ts,A55,l,sigxbar,alpha0,cc,Q1,Q2,hbar,h1,h2)-Ts;
e=b-a;

//printf("bisection routine for the linear slip solution\n");
//printf("u=%f\n",u);
//printf("v=%f\n",v);
//pause();

if ( (u*v) >= 0.0 )
{
	printf("no root in GetLsLinear \n");
	return (0);		// no root!!!
}
for(k=1; k<= M ; k++)
	{
	e=e/2.0;
	c=a+e;
	w=EvalTauLinSlip(c,Ts,A55,l,sigxbar,alpha0,cc,Q1,Q2,hbar,h1,h2)-Ts;
	//printf ("k=%d \t c=%f \t w=%e \t e=%e\n",k,c,w,e);
	if ( fabs(w)<eps || e< 0.0000001)
		{
		w=c;
		return(w);		// convirged on a root
		}
	if ( w*u < 0.0 )
		{
		b=c;
		v=w;
		}
	else
		{
		a=c;
		u=w;
		}
	}
}
```

```
/*----------------------------Gets the stress vectors set up for the integration----------------------------*/
/*-----------------------------------(this is for the linear case)----------------------------------------*/
double      presimpson_linear(numpoints,x,sigx1,sigx2,h1,h2,Q1,Q2,E0,epsybar)
long        numpoints;
double  h1,h2,E0,epsybar;
double  *sigx1,*sigx2,*x,**Q1,**Q2;
{
    int i;
    double *f,value;
    f=dvector(0,numpoints);

    //printf("\n started into the presimpson_linear routine\n");

    for (i=0; i<=numpoints; i++)                    // set up the data to integrate sigx1 and sigx2
    {

    f[i]=2*h2/Q2[1][1]*( pow(sigx2[i],2)/2 - Q2[1][2]*epsybar*sigx2[i] ) +
            2*h1/Q1[1][1]*( pow(sigx1[i],2)/2 - Q1[1][2]*epsybar*sigx1[i] );

    }
    value=simpson(numpoints,x,f);
    free_dvector(f,0,numpoints);
    return(value);
}

/*----------------------------Gets the stress vectors set up for the integration----------------------------*/
//-----------------------------(this is for the linear case above the yield point)---------------------------

double      presimpson_linear1(numpoints,x,sigx1,sigx2,h1,h2,Q1,Q2,E0,E1,sighat,sigx0,epsybar)
long        numpoints;
double  h1,h2,E0,E1,sighat,sigx0,epsybar;
double  *sigx1,*sigx2,*x,**Q1,**Q2;
{
    int i;
    double *f,value;
    f=dvector(0,numpoints);
    for (i=0; i<=numpoints; i++)                    // set up the data to integrate sigx1 and sigx2
    {
    f[i] = 2*h2/E1*( pow(sigx2[i],2)/2-sigx2[i]*(sighat+Q2[1][2]*epsybar ) ) +
        2*h1/Q1[1][1]*( pow(sigx1[i],2)/2 - Q1[1][2]*sigx1[i]*epsybar);
    }
    value=simpson(numpoints,x,f);
    value=value+2*h2*x[numpoints]*(
    sigx0*sigx0/2*( 1/Q2[1][1]-1/E1 ) + sigx0*( (Q2[1][2]*epsybar+sighat)/E1-Q2[1][2]*epsybar/Q2[1][1] )
                        );
    free_dvector(f,0,numpoints);
    return(value);
}


/*----------------------------Gets the stress vectors set up for the integration----------------------------*/
/*----------------------------(this is for the bi-linear case)---------------------------------------------*/

double      presimpson(numpoints,xstar,x,sigx1,sigx2,h1,h2,Q1,Q2,sighat,sigx0,E0,E1,epsybar)
long        numpoints;
double  xstar,h1,h2,sighat,sigx0,E0,E1,epsybar;
double  *sigx1,*sigx2,*x,**Q1,**Q2;
{
    int     i;
    double  *f,*f1,value,value1;

    f=dvector(0,numpoints);
    f1=dvector(0,numpoints);

    // printf("\n started into the presimpson routine\n");

    for (i=0; i<=numpoints; i++)                            // set up the data to integrate sigx1
```

```
    {
    f[i]=( sigx1[i] )*( sigx1[i] )/2 - epsybar*Q1[1][2]*sigx1[i];
    }
    value=(2*h1/Q1[1][1])*simpson(numpoints,x,f);

    for(i=0;i<=numpoints;i++)                          // set up the data to integrate sigx2
    {
        if (x[i]<xstar)
        {
        f1[i]=2*h2/E0* ( pow(sigx2[i],2)/2 - Q2[1][2]*sigx2[i]*epsybar);
        }
        if(x[i]>=xstar)
        {
        f1[i]=2*h2/E1* ( pow(sigx2[i],2)/2 - sigx2[i]*(Q2[1][2]*epsybar+sighat));
        }
    }

     value1= simpson(numpoints, x, f1 ) + 2*h2*(x[numpoints]-xstar)* (
            (pow(sigx0,2)/2-Q2[1][2]*sigx0*epsybar)/Q2[1][1] +
            (sigx0*(Q2[1][2]*epsybar+sighat) - pow(sigx0,2)/2) /E1) ;

    // pause();

    free_dvector(f,0,numpoints);
    free_dvector(f1,0,numpoints);
    return(value+value1);

}
//------------------------------------------Makes the stress plots (Mac Only)----------------------------------------------
void        DrawPlot (numpoints,x,Tau,sigx1,sigx2,kick)
double      *x, *Tau,*sigx1,*sigx2;
long        kick;
long        numpoints;
{
int         i;
double      max,min;
short       xpt,y1pt,y2pt,y3pt;


    max=min=0.0;
    for (i=0; i<=numpoints; i++)                 /*find the max and mins of the stress vectors*/
        {
        if (sigx1[i] > max) max = sigx1[i];
        if (sigx2[i] > max) max= sigx2[i];
        if (Tau[i] > max) max =Tau[i];
        if (sigx1[i] < min) min= sigx1[i];
        if (sigx2[i] < min) min= sigx2[i];
        if (Tau[i] < min) min=Tau[i];
        }

        MoveTo(20,200);
    for (i=0; i<=numpoints; i++)
        {
        xpt=(short)(x[i]/x[numpoints]*540+20);
        y1pt=200-(short)(Tau[i]/fabs(max-min)*180);
        LineTo(xpt,y1pt);
        }
        MoveTo(20,200);
    for (i=0; i<=numpoints; i++)
        {
        xpt=(short)(x[i]/x[numpoints]*540+20);
        y1pt=200-(short)(sigx1[i]/fabs(max-min)*180);
        LineTo(xpt,y1pt);
        }
        MoveTo(20,200);
    for (i=0; i<=numpoints; i++)
        {
```

```
        xpt=(short)(x[i]/x[numpoints]*540+20);
        y1pt=200-(short)(sigx2[i]/fabs(max-min)*180);
        LineTo(xpt,y1pt);
        }
        MoveTo(20,200);
}


void WindowInit ( void )
{
WindowPtr  window;
int           i;

     window = GetNewWindow ( kBaseResID , nil , kMoveToFront );
     if  ( window == nil )
      {
      SysBeep (10);
      ExitToShell();
      }
     ShowWindow ( window);
     SetPort ( window );

     MoveTo(20,20);                              //draw the frame
     LineTo(560,20);
     LineTo(560,200);
     LineTo(20,200);
     LineTo(20,20);

     for  (i=80;  i<=560;  i=i+60)                  // draw the gridlines
         {
         MoveTo(i,200);
         LineTo(i,20);
         }
     MoveTo(20,20);
}


/*-----------------------------Numerical  Errors-----------------------------------*/
void   nrerror(error_text)
char  error_text[];
{
     void exit();
     fprintf(stderr,"Numerical Recipes run-time error...\n");
     fprintf(stderr,"%s\n",error_text);
     fprintf(stderr,"...now exiting to system...\n");
     exit(1);
}

/*-----------------------------Simple  Pause  Routine-----------------------------------*/

void pause(void)
{
char a;
a='\0';

printf("\n <hit return to continue> \n");
while  (a=='\0')  a=getchar();
}

/*-----------------------------Set  Up  Double  Vector-----------------------------------*/

double *dvector(long nl, long nh)
{
     double *v;

     v=(double  *)malloc((size_t)  ((nh-nl+1+NR_END)*sizeof(double)));
     if (!v) nrerror("allocation failure in dvector()");
     return v-nl+NR_END;
```

```
}

void free_dvector(double *v, long nl, long nh)
{
    free((FREE_ARG) (v+nl-NR_END));
}


/*------------------------------Set Up Double Matrix-----------------------------------*/

double **dmatrix(nrl,nrh,ncl,nch)
long     nrl,nrh,ncl,nch;
{
    int i;
    double **m;

    m=(double **) malloc((unsigned) (nrh-nrl+1)*sizeof(double*));
    if (!m) nrerror("allocation failure 1 in dmatrix()");
    m -= nrl;

    for(i=nrl;i<=nrh;i++) {
        m[i]=(double *) malloc((unsigned) (nch-ncl+1)*sizeof(double));
        if (!m[i]) nrerror("allocation failure 2 in dmatrix()");
        m[i] -= ncl;
    }
    return m;
}

void free_dmatrix(m,nrl,nrh,ncl,nch)
double **m;
long     nrl,nrh,ncl,nch;
{
    int i;

    for(i=nrh;i>=nrl;i--) free((char*) (m[i]+ncl));
    free((char*) (m+nrl));
}

//------------------------------------------simple simpsons rule-------------------------------------------
double simpson(n,x,f)
long       n;
double *f, *x;
{
int     i,j;
double       h,sum;

    sum=0.0;

    // printf("\nentered simpsons rule\n");
    //  printf("x[o]=%f\n",x[0]);
      //printf("x[n]=%f\n",x[n]);
    // pause();

    h=(x[n]-x[0])/n;
    for (j=1;j<= (n-1) ; j++)
    {
        sum=sum+f[j];
        //printf("x[%d] = %f\n", j , x[j] );
    }
    sum=h/2 * ( f[0]+f[n]+2*sum );

    return (sum);
}

//header file for shearlagbislip.c program

#include <stdio.h>
#include <string.h>
```

```
#include <stdlib.h>
#include <ctype.h>
#include <math.h>
#include <console.h>

double      *dvector(long, long );
double      **dmatrix(long,long,long,long);
void        free_dmatrix(double**,long,long,long,long);
void        free_dvector(double*,long,long);
void        nrerror();
void        pause(void);
void        WindowInit (void);
void        DrawPlot (long,double*,double*,double*,double*,long);


double  simpson(long,double*,double*);

double  stresscalc(double,double,double,double,double,double,double, double ,
        double,double**,double**,double,double,double,double*,double**,double**,long);

double  presimpson(long,double,double*,double*,double*,double,double,double**,double**,double,double,double,double,double);
double  presimpson_linear(long,double*,double*,double*,double,double,double**,double**,double,double);
double  presimpson_linear1(long,double*,double*,double*,double,double,double**,double**,
        double,double,double,double,double);

double  GetLsLinear(double,double,double,double,double,double*,double**,double**,double,double,double);
double  GetLsLinear2(double,double,double,double,double,double,double*,double**,double**,double,double,double,double);
double  BilinearStressSlipCase1(double,double, double, double, double, double, double**, double**,
        double,double,double*,double,double,double);

double  BilinearStressSlipCase2( double,double, double, double, double, double, double, double, double**, double**,
        double, double,double,double,double*,double,double,double);

double  BilinearStressSlipCase2mod( double,double, double, double, double, double, double, double, double**, double**,
        double, double,double,double,double*,double,double,double);

double  EvalTauLinSlip(double,double,double,double,double,double,double*,double**,double**,double,double,double);
double  EvalTauLinSlip2(double,double,double,double,double,double,double,double*,double**,double**,double,
        double,double,double)    ;

double  BilinearTausSlipCase2(double, double, double, double, double, double, double, double**, double**,
        double, double,double,double,double*,double,double,double,double);

double  GetLsCase1(double, double, double, double, double, double, double, double**, double**,
        double, double, double*,double,double);

double  *GetLsCase2(double, double, double, double, double, double, double**, double**,
        double, double,double,double,double*,double,double,double);

double  GetXstarCase2(double,double, double, double, double, double, double, double**, double** ,
        double, double,double,double,double*,double,double,double);

double  GetXstarCase2mod(double,double, double, double, double, double, double, double**, double** ,
        double, double,double,double,double*,double,double,double);

double  GetXstarCase2mod(double,double, double, double, double, double, double, double**, double** ,
        double, double,double,double,double*,double,double,double);
```

VITA

Donald L. Erdman III was born in Allentown, Pennsylvania on October 9, 1962. He attended the Allentown public school system for grades K-5, then St. Thomas Moore School for grades 6-8. He then completed grades 9-12 at Southern Lehigh High School in Center Valley, Pennsylvania , while attending Lehigh County Vocational Technical School in Schnecksville, Pennsylvania, training in Electrical Construction. He entered Lehigh County Community College, Schnecksville, Pennsylvania in 1981 and received the Associate in Science in Electronics Technology and then the Associate in Arts in Pre-Engineering. In 1985 he transferred to Drexel University in Philadelphia Pennsylvania, and graduated with the Bachelor of Science in Mechanical Engineering in 1989 and then the Master of Science in Mechanical Engineering in 1991. During his tenure at Drexel University, he worked with Dr. Jonathan Awerbuch at the Composite Materials Laboratory as an undergraduate cooperative education student, and then as a graduate research assistant. In 1991 he entered the doctorate program in the Engineering Science and Mechanics Department at the University of Tennessee, Knoxville, with Dr. Y. J. Weitsman as principal advisor. The doctoral degree was granted in December 1995.